Conference on

ENVIRONMENTAL EFFECTS ON ANTENNA PERFORMANCE

Proceedings, Vol. I

Edited by James R. Wait

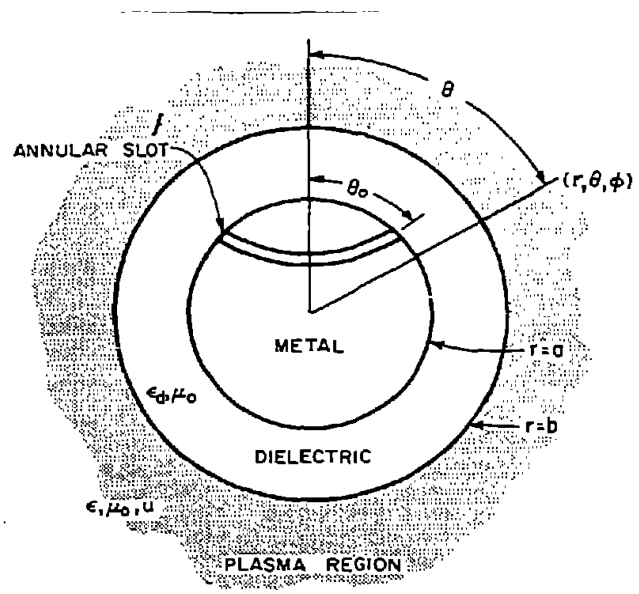

Boulder, Colorado

July 14-18, 1969

FOREWORD

This volume contains concise versions of most of the papers presented at the Conference on Environmental Effects on Antenna Performance. The papers as printed here were reproduced from the manuscripts supplied by the authors. Editing on the submitted material was relatively light, although many of the manuscripts required at least some revision. As editor, I should like to thank the members of the advisory board for their assistance and, in particular, I am grateful to the conference secretary, Mrs. Eileen Brackett, for her diligence in assembling the papers and readying the material for the printer.

Volume II will be issued at a later date and it will contain papers and other relevant material which were not available when Volume I went to press.

James R. Wait

Additional copies of this volume will be available at $3.00 from the Clearinghouse for Federal Scientific and Technical Information, Sills Building, 5285 Port Royal Road, Springfield, Virginia 22151.

CONFERENCE ON ENVIRONMENTAL EFFECTS ON ANTENNA PERFORMANCE

Boulder, Colorado - July 14-18, 1969

PROCEEDINGS - Vol. I

Sponsors: Institute for Telecommunication Sciences (Environmental Science Services Administration); Cooperative Institute for Research in Environmental Sciences (ESSA); Air Force Cambridge Research Laboratories; Department of Electrical Engineering (University of Colorado); Denver-Boulder Chapter of the IEEE Group on Antennas and Propagation.

Advisory Board: P. Blacksmith, R. Cohen, H. V. Cottony, W. Flock, R. C. Kirby, M. T. Ma, S. W. Maley, R. J. Papa, R. V. Row, C. J. Sletten, W. J. Surtees, W. F. Utlaut

Chairman: J. R. Wait - Secretary: Mrs. Eileen Brackett

Registration Facilities: R. D. Hunsucker and D. C. Chang

Auditorium and Projection Facilities: H. V. Cottony and R. H. Ott

Place: ESSA Radio Building Auditorium

Time allotted for presentation is indicated in minutes after each title; also indicated is the page number where paper (if available) appears in this volume.

Monday, July 14th - 8:30 a.m.

Introductory Remarks: Dr. G. S. Benton, Director, ESSA Research Labs., C. J. Sletten, AFCRL, and R. C. Kirby, ITS/ESSA

Session I - Electromagnetic Theory - Chairman, Professor J. R. Wait (ESSA Research Labs., and CIRES)

Monday, July 14th - 1:30 p. m.

Session II - Boundary Value Problems - Chairman, Prof. L. B. Felsen (Brooklyn Polytechnic Institute)

Prolate spheroidal and linear antennas in lossy media (20); R. J. Lytle

Metallic and dielectric antennas in conducting media (20); G. Franceschetti, O. Bucci, E. Corti, and G. Latmiral [pg. 33]

Radiation from a semi-infinite dielectric-coated spherically tipped perfectly conducting cone (20); R. Chatterjee [pg. 38]

Electromagnetic coupling of horizontal loops over a stratified ground (15); H. Kurss [pg. 42]

Quasi-static fields of subsurface horizontal electric antennas(20); P. R. Bannister [pg. 45]

Magnetic field excited by a long horizontal wire antenna near the earth's surface (20); D. B. Large and L. Ball [pg. 50]

Numerical analysis of aircraft antennas (15); E. K. Miller, J. B. Morton, G. M. Pjerrou, and B. J. Maxum [pg. 55]

Tuesday, July 15th - 8:30 a. m.

Session III - Influence of Homogeneous Half Space - Chairman, Professor M. Kharadly (Univ. of British Columbia)

Finite tubular antenna above a conducting half-space (15); D. C. Chang [pg. 59]

EM propagation over a constant impedance plane (10); R. J. King [pg. 64]

On the surface impedance concept (10); R. J. King [pg. 66]

The impedance of a finite horizontal antenna above ground (15); W. J. Surtees [pg. 68]

Impedance of a finite-length insulated dipole in dissipative media (15); C. K. H. Tsao and J. R. deBettencourt [pg. 72]

Distributed shunt admittance of horizontal dipole over lossy ground (15); C. K. H. Tsao [pg. 77]

The linear antenna in a piecewise homogeneous environment(15); D. V. Otto [pg. 81]

Characteristics of the ground wave attenuation function for highly inductive surfaces (15); D. B. Ross [pg. 85]

Impedance of a Hertzian dipole over a conducting half-space (15); J. R. Wait [pg. 89]

Tuesday, July 15th - 1:30 p.m.

Session IV - Ground Screen Effects - Chairman, Dr. W. F. Utlaut (ESSA)

Radial wire ground systems for vertical monopole antennas(20); S. W. Maley [pg. 196]
Effect of the ground screen on the field radiated from a monopole(15); W. J. Surtees [pg. 95]
Numerical studies of the effects of nonplanar local terrain and ground screens (15); R. V. Row and D. M. Cunnold
Radiation of a monopole antenna on the base of a conical structure (15); G. A. Thiele, M. Travieso-Diaz, H. S. Jones [pg. 99]
Current distribution on a finite length dipole in the presence of ground screens (15); V. R. Arens, U. R. Embry, D. L. Motte
Reflection of waves of arbitrary polarization from a rectangular mesh ground screen (15); G. A. Otteni [pg. 103]
Some design considerations for HF antenna ground screens (15); T. Kaliszewski [pg. 201]
Measured patterns of HF antennas and correlation with surrounding terrain (15); D. R. McCoy, R. D. Wengenroth, and J. J. Simons

Wednesday, July 16th - 8:30 a.m.

Session V - Antennas in Plasma - A - Chairman, Dr. J. Galejs (Sylvania)

Radiation by a VHF dipole-type antenna imbedded in its plasma sheath (20); R. V. DeVore and R. Caldecott
Current distribution and input admittance of a cylindrical antenna in a gyrotropic medium (15); H. S. Lu and K. K. Mei [pg. 108]
Numerical solution of dipole radiation in a compressible plasma with a vacuum sheath surrounding the antenna (20); S. H. Lin and K. K. Mei [pg. 112]
Plane wave synthesis of plasma coated aperture admittance and radiation pattern (20); H. Hodara and D. Damlamayan [pg. 117]
Effects of electron acoustic waves on a dipole RF magneto-plasma probe (20); H. Oya
Radiation characteristics of a slotted ground plane into a two-fluid compressible plasma (20); K. R. Cook and R. B. Buchanan [pg. 122]
Studies of VLF radiation patterns of a dipole immersed in a lossy magnetoplasma (20); D. P. GiaRusso and J. E. Bergeson [pg. 127]
Some features of electroacoustic waves excited by linear antennas in hot plasma(15); V. L. Talekar [pg. 132]
Linear antenna in anisotropic medium(15); P. Meyer [pg. 136]

Wednesday, July 16th - 1:30 p.m.

Session VI - Antennas in Plasma-B - Chairman, Prof. R.E. Collin, (Case Western Reserve University)

Boundary and transition problems for antennas in warm plasmas(20); J. P. Lafon

Studies of antenna-induced ionization problems(20); W. C. Taylor, J. B. Chown, and T. Morita [pg. 139]

Behavior of strong field electromagnetic waves in anisotropic plasmas (20); M. P. Bachynski and B. W. Gibbs [pg. 145]

The Trailblazer II reentry antenna test program(20); J. L. Poirier, W. Rotman, D. Hayes, and J. Lennon [pg. 151]

Single and multislot antennas in an inhomogeneous reentry plasma environment (20); K. E. Golden and G. E. Stewart [pg. 156]

Ionospheric antenna impedance probe (15); E. K. Miller, H. F. Schulte, and J. W. Kuiper [pg. 161]

How to determine ELF/VLF transmitting antenna performance in the ionosphere(20); J. P. Leiphart

On the transient response of an antenna and the time decrease of Alouette spikes (15); P. Graff [pg. 165]

Thursday, July 17th - 8:30 a.m.

Session VII - Related Environmental Aspects - Chairman, Dr. C. J. Sletten (AFCRL)

Dipole radiation in the lunar environment (20); R. J. Phillips [pg.169]

VLF transmitting antennas using fast wave dipoles (15); E. W. Seeley [pg. 174]

Ground-wave propagation across strips and islands on a flat earth (10); R. J. King and W. L. Tsukamoto [pg. 179]

Some considerations on ground-wave propagation across coastlines and islands (15); R. K. Rosich [pg. 181]

VLF ground-based measurements on stratified antarctic media (20); G. E. Webber and I. C. Peden

Effective ground conductivity measurement at radio frequencies using small loop antennas (15); W. L. Taylor [pg. 186]

Phase measurements of electromagnetic field components (20); P. Cornille [pg. 190]

Thursday, July 17th - 1:30 p.m.

Session VIII - Round Table Discussion on: Design techniques for pattern control by ground screens - Moderator, Dr. R. V. Row (Sylvania)

(Sessions IX and X, on Friday, are reserved for late informal papers.

COMPLEX RAYS AND THE LOCAL PROPERTIES OF RADIATION IN LOSSY MEDIA*

H. L. Bertoni, L. B. Felsen and A. Hessel

Polytechnic Institute of Brooklyn
Electrophysics Department
Farmingdale, N. Y. 11735

Abstract

The ray-optical description of radiation in lossy, inhomogeneous media, is, in general, in terms of complex rays. To clarify the physical significance of such a description, the local environment responsible for the fields at an observation point is found for a particular example and related to the complex ray reaching the observation point.

1. Introduction

At sufficiently high frequencies, propagation and scattering phenomena in piecewise homogeneous or inhomogeneous, lossless media can be described in terms of rays. The rays define real trajectories along which the fields and energy propagate, in that the ray fields are influenced primarily by the enviornment in the immediated vicinity of the ray. This local property of ray fields makes ray optics a powerful tool for analysis of high frequency radiation and scattering.

When an inhomogeneous or piecewise homogeneous medium contains loss, the ray paths for fields traversing regions of varying loss tangent lie in complex space (Furutsu, 1952; Seekler and Keller, 1959: Budden and Jull, 1964) (ray paths for fields traversing a homogeneous, lossy medium are real). In the case of complex rays, the definition of a local environment primarily responsible for the fields at a given observation point is not evident. To clarify the location and extent of the local environment, the fields transmitted across a planar interface between a lossless and a lossy half-space are considered. The local environment appropriate to an arbitrary observation point is found and is related to the parameters of the complex ray reaching this point. This knowledge of the local properties of the field should prove useful in the study of radiation and scattering in lossy configurations not amenable to rigorous analysis.

* This work was supported in part by the University Science Development Program of the National Science Foundation under Grant Number GU-1557 to the Polytechnic Institute of Brooklyn.

2. Determination of the Local Environment

In order to define the local environment that primarily influence the fields transmitted to a given observation point across a planar interface between a lossless and a lossy half-space, an idealized "window", which transmits the fields essentially over a limited range, is inserted in the lossy medium in a plane parallel to the interface at a distance h below the observation point (see fig. 1). The center of the window is placed so that for minimum

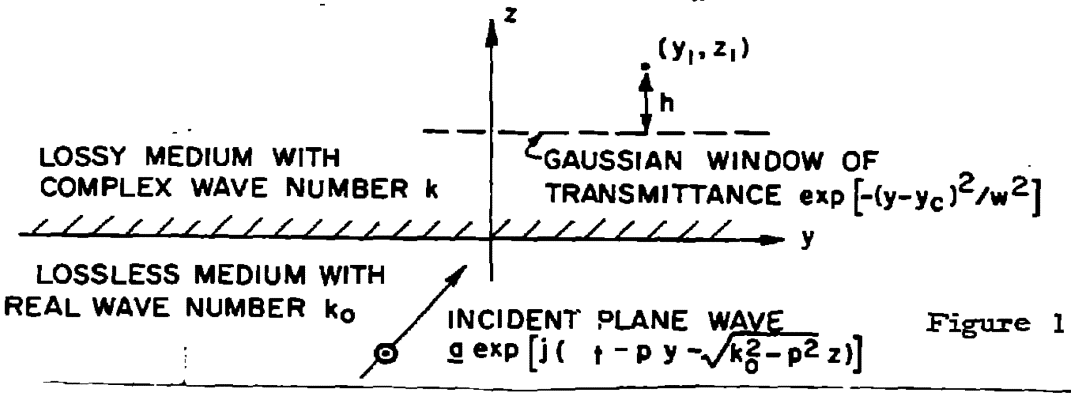

Figure 1

window size, the field at the observation point approximates the fields occurring in the absence of the window to within some fixed accuracy. By the above process, one determines the area in the plane whose illumination is principally responsible for the field at the observation point. In the lossless case, this area comprises the first few Fresnel zones which are centered about the intersection of the plane and the ray reaching the observation point. If several distinct field types contribute to the observation point, the local environment associated with each field type could be found in a similar way.

For simplicity, a two-dimensional problem is considered wherein a plane wave is incident at an angle in the y-z plane from the lossless medium. Sampling of this canonical incident field with an appropriate window, which is assumed uniform along x, the relation between the local environments and the complex rays is determined. To limit diffraction effects, which in the case of a lossy half-space can be exponentially stronger than the transmitted fields, the transmittance of the window should be analytic. The Gaussian function $\exp[-(y-y_c)^2/W^2]$, centered at y_c, is used here.

If $\underline{E}_t$ is the field at the observation point (y_1, z_1) of fig. 1 when no window is present, then the field $\underline{E}_g$ at the observation point when a "wide" Gaussian window is inserted is given approximately by

$$\underline{E}_g \approx \underline{E}_t \left\{ 1 + \frac{1}{W^2} \left[jh \frac{k^2}{q^3} - (y_c - y_{cm} - jd)^2 \right] \right\}, \qquad (1)$$

where p is the wavenumber along y of the incident plane wave, k is the complex wavenumber of the lossy medium, $q=\sqrt{k^2-p^2}$, $y_{cm}=y_1-h\mathrm{Re}(p/q)$ and $d=-h\mathrm{Im}(p/q)$. In order that, for minimum width, $\underline{E}_g$ approximate $\underline{E}_t$ to within some fixed percentage error, the window location y_c should minimize the magnitude of the square bracketed term in (1). However, taking the window location as $y_c=y_{cm}$ provides a simple, frequency independent center for the local environment and can be interpreted in terms of complex rays. The displacement of the actual minimum of the square bracketed term in (1) from y_{cm} is less than the minimum half-width W of the window for which $\underline{E}_g$ even crudely approximate $\underline{E}_t$.

For $y_c=y_{cm}$, $\underline{E}_g$ differs from $\underline{E}_t$ by less than some relative amount $2\alpha^2<1$ if $\alpha^2>h|k^2/q^3|/W^2$ and $\alpha^2>d^2/W^2$. Thus, if W is larger than the greater of $(1/\alpha)\sqrt{h|k^2/q^3|}$ and $|d|/\alpha$, then $|\underline{E}_g-\underline{E}_t|/|\underline{E}_t|<2\alpha^2$. The half-width W so chosen delineates the region about y_{cm} in the $z=z_1-k$ plane whose illumination is principally responsible for the fields at (y_1, z_1).

For a lossless medium (k real), y_{cm} is the intersection, with the plane, of the ray illuminating (y_1, z_1) and $d=0$, so that the Fresnel criterion $W>(1/\alpha)\sqrt{hk^2/q^3}$ determines W. The principal effect of loss on W is to impose a condition, linear in h, that must be satisfied in addition to the Fresnel criterion. For $h<|k^2/q^3|/[\mathrm{Im}(p/q)]^2$, the half-width is determined by the condition $W>(1/\alpha)\sqrt{h|k^2/q^3|}$ while for h greater than this value, W is determined by $W>|d|/\alpha$.

3. Relation to Complex Rays

If the medium for $z>0$ is lossless, the fields at (y_1, z_1) can be interpreted in terms of real rays. In this case, the incident plane wave is viewed as being composed of a family of rays parallel to the direction of propagation of the plane wave. These rays are refracted at the interface and one of them illuminates (y_1, z_1). The equation of the path of this ray is $(y_1-y)=h(p/q)$, where y is the intercept of the ray with any plane $z=z_1-h>0$.

For the case of a lossy medium (k complex), the foregoing ray equation still describes the path of the ray illuminating (y_1, z_1). However, since q is now complex, except for normal incidence the ray intersects the $z=z_1-h$ plane at a complex point. In particular, y is complex at $z=0$, thus requiring the extension of the family of rays representing the incident plane wave to include rays lying in complex space. In fig. 2, the complex ray is plotted for $p>0$.

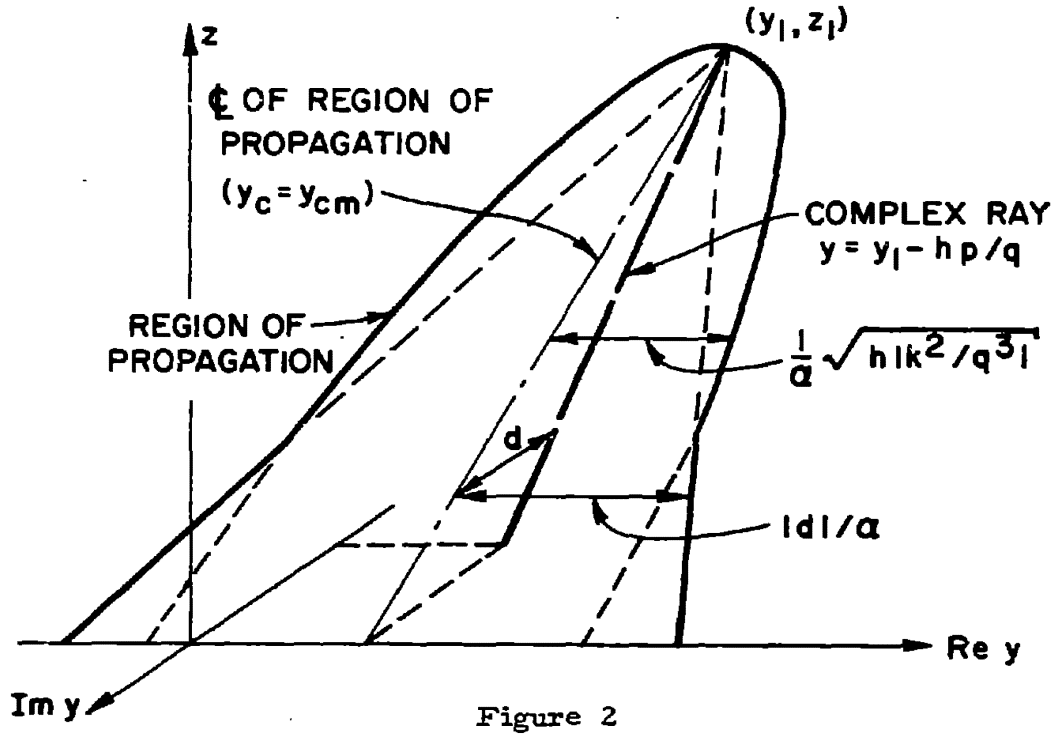

Figure 2

Taking the real part of the ray intercept for h real gives $Re(y)=y_1 - hRe(p/q)$, so that the center y_{cm} of the region whose illumination is principally responsible for the fields at (y_1, z_1) is the normal projection of the complex ray into real space. Taking the imaginary part of the ray intercept gives $Im(y) = -hIm(p/q)$, so that the condition $W > |d|/\alpha$ is seen to require that the half-width of this region be several times the distance that the complex ray lies outside of real space. The local environment, which lies in real space, appropriate to the observation point (y_1, z_1) is outlined by the solid curve in fig. 2 for the case of high loss tangent.

By placing the Gaussian window at values of $z < 0$, it can be shown that the region of propagation in free space is centered about the normal projection, into real space, of the plot (for z real) of that complex ray, which when refracted at the interface, passes through (y_1, z_1). Again, the extent of the region of propagation is the wider of the limits set by the Fresnel criterion and the criterion based on the distance from the ray, when plotted for real z, to real space.

4. References

Budden, K. G. and G. W. Jull (1964), Reciprocity and non-reciprocity with magnetoionic rays, Can. J. of Phys. 42, pp. 113-130.

Furutsu, K. (1952), On the group velocity, wave path and their relation to the Poynting vector of the electromagnetic field in an absorbing medium, J. of Phys. Soc. Japan I, pp. 458-466.

Seckler, B. D. and J. B. Keller (1959), Geometrical theory of diffraction in inhomogeneous media, J. Acoust. Socs. Am. 31, pp. 192-205.

TRANSIENT DIPOLE OVER A DIELECTRIC HALF-SPACE*

by

D. A. Hill

The Ohio State University
ElectroScience Laboratory
Department of Electrical Engineering

Abstract

The transient fields of short electric dipoles located above a dielectric half-space are examined. Closed form solutions are obtained for the cases where the observation point is directly above or below the dipole and where both the dipole and the observation point are located at the dielectric surface.

The problem of radiation from short dipoles with time-harmonic current excitation in the presence of ground results in the well known Sommerfeld-type integral solutions. If the current is a delta function, $\delta(t)$, then the time-dependent solution can be obtained by taking the inverse Fourier transform of the Sommerfeld-type solutions. In this paper, exact closed-form, time-domain solutions are obtained for some special cases.

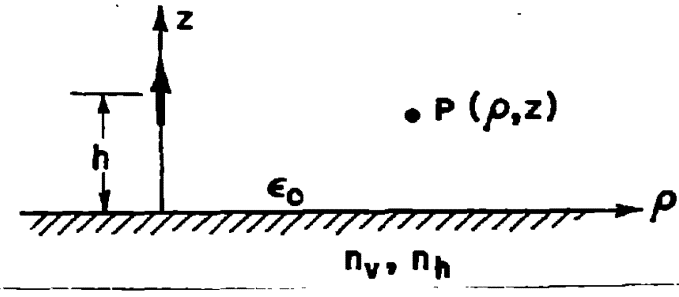

Figure 1. Vertical electric dipole above a uniaxial anisotropic dielectric half-space.

---

*The research reported in this paper was sponsored in part by the Air Force Cambridge Research Laboratories, Office of Aerospace Research, under Contract F 44620-67-C-0095, and by The Ohio State University Research Foundation.

Figure 1 shows a vertical electric dipole located at a height h above a uniaxial nondispersive, anisotropic dielectric half-space with a vertical index of refraction n_v and a horizontal index of refraction n_h. The dipole is of length ds and has a current I $\delta(t)$. Cylindrical coordinates are used since the problem is symmetrical in the ϕ direction. The frequency-domain solution for the z-component of the Hertz vector in the upper medium has been derived by Wait (1966). When the direct term is removed, the frequency-dependent scattered field can be written as

$$\Pi^s_{oz}(\omega) = \frac{I\,ds}{4\pi\varepsilon_o j\omega}\left\{ - \frac{e^{-j\frac{\omega}{c}\sqrt{\rho^2 + (z+h)}}}{\sqrt{\rho^2 + (z+h)}} + 2n_v n_h \int_o^\infty \frac{J_o(\lambda\rho)\, e^{\sqrt{\lambda^2 - (\omega/c)^2}\,(z+h)}\,\lambda d\lambda}{n_v n_h \sqrt{\lambda^2 - (\omega/c)^2} + \sqrt{\lambda^2 - (n_v\omega/c)^2}} \right\}. \quad (1)$$

If the observation point is directly above or below the dipole (ρ=0), the form of (1) is simplified by removal of the Bessel function. The frequency dependence of the integral in (1) can be further simplified by the substitution $\lambda = \omega a$. We are now ready to take the inverse Fourier transform of $\Pi^s_{oz}(\omega)$ to obtain the time-dependent Hertz vector $\tilde{\Pi}^s_{oz}(t)$. Since it is known that $\tilde{\Pi}^s_{oz}(t)$ must be real and causal, $\tilde{\Pi}^s_{oz}(t)$ can be obtained using only the real part of $\Pi^s_{oz}(\omega)$ as shown in Papoulis (1962).

$$\tilde{\Pi}^s_{oz}(t) = \begin{cases} 2F^{-1}\,[\mathrm{Re}\ \Pi^s_{oz}(\omega)] = \frac{2}{\pi}\int_o^\infty [\mathrm{Re}\ \Pi^s_{oz}(\omega)]\cos\omega t\, d\omega, & t > 0 \\ 0, & t < 0 \end{cases} \quad (2)$$

The two integrals on "a" in the expression for $\tilde{\Pi}^s_{oz}(t)$ can be evaluated by use of the delta function properties and by use of standard integral tables. For $t < (z+h)/c$, $\tilde{\Pi}^s_{oz}(t)$ is zero; and for $t>(z+h)/c$, $\tilde{\Pi}^s_{oz}(t)$ is given by

$$\tilde{\Pi}^s_{oz}(t) = \frac{I\,ds}{4\pi\varepsilon_o(z+h)} \frac{n_v n_h\,[ct/(z+h)] - \sqrt{[ct/(z+h)]^2 + n_v^2 - 1}}{n_v n_h\,[ct/(z+h)] + \sqrt{[ct/(z+h)]^2 + n_v^2 - 1}} \quad (3)$$

The magnetic field on the z-axis is zero, and the electric field has only a z-component which is obtained from the time-dependent Hertz vector by the operation, $\tilde{E}^s_{oz}(t) = [\partial^2/\partial z^2 - (1/c)^2\partial^2/\partial t^2]\tilde{\Pi}^s_{oz}(t)$.

The time-dependent Hertz vector can also be obtained when both the dipole and the observation point are located at the interface. In this case the frequency-domain expression for the total Hertz vector is

$$\Pi^t_{oz}(\omega) = \frac{I\,ds\,n_v n_h}{2\pi\varepsilon_o\, j\omega} \int_o^\infty \frac{J_o(\lambda\rho)\,\lambda d\lambda}{n_v n_h \sqrt{\lambda^2 - (\omega/c)^2} + \sqrt{\lambda^2 - (n_v\omega/c)^2}} \quad . \tag{4}$$

The frequency dependence is again simplified by the substitution, $\lambda = \omega a$, and only the inverse transform of the zero-order Bessel function is needed to obtain the following time-dependent Hertz vector. After performing the integration on "a", the following closed form is obtained which agrees with the result of Van der Pol (1956) when the lower medium is isotropic.

$$\hat{\Pi}^t_{oz}(t) = \frac{I\,ds}{2\pi\varepsilon_o\rho}\left\{\left(\frac{n_v^2 n_h^2}{n_v^2 n_h^2 - 1}\right)\left[\frac{1}{\sqrt{n_h^2 - n_v^2 + 1}} - \frac{1}{\sqrt{(n_h^2+1)\frac{ct}{\rho} - n_v^2}}\right]\right.$$

$$\left.\left[U\left(t - \frac{\rho}{c}\right) - U\left(t - \frac{n_v\rho}{c}\right)\right] + \left(\frac{n_v n_h}{n_v^2 n_h^2 - 1}\right)\left[\frac{n_v n_h}{\sqrt{n_h^2 - n_v^2 + 1}}\right] U\left(t - \frac{n_v\rho}{c}\right)\right\}. \tag{5}$$

The electric and magnetic field components can be obtained by operating on $\hat{\Pi}^t_{oz}(t)$: $\hat{E}^t_{\rho z}(t) = -(1/\rho)\,\partial/\partial\rho\,[\partial\,\hat{\Pi}^t_{oz}(t)/\partial\rho]$ and $\hat{H}^t_{o\phi}(t) = -\varepsilon_o\,\partial^2\hat{\Pi}^t_{oz}(t)/\partial\rho\partial t$. There is also a ρ-component of the electric field, but it can not be determined from (7) because the z dependence of $\hat{\Pi}^t_{oz}(t)$ is needed.

The time-dependent Hertz vector in the lower medium can be obtained when the observation point is directly below the dipole (ρ=0). The problem is simplified when the lower medium is isotropic ($n_v = n_h = n$). The frequency-dependent Hertz vector for this special case is

$$\Pi_{1z}(\omega) = \frac{I\,ds}{2\pi\varepsilon_o j\omega} \int_o^\infty \frac{e^{\sqrt{\lambda^2-(n/c)^2}\;z\;-\;\sqrt{\lambda^2-(\omega/c)^2}\;h}}{n^2\sqrt{\lambda^2-(\omega/c)^2} + \sqrt{\lambda^2-(n\omega/c)^2}}\,\lambda d\lambda \quad . \tag{6}$$

If the substitution, $\lambda = \omega a$, is made, the frequency dependence of (8) is simplified. The inverse Fourier transform can then be taken using the same technique which was employed on (1), and the resulting time-dependent Hertz vector is

$$\tilde{\Pi}_{1z}(t) = \frac{I\,ds}{2\pi\varepsilon_o}\left[\frac{z^2+h^2}{h^2-z^2} + zh\,\frac{\frac{2}{h^2-z^2}+\frac{n^2-1}{(ct)^2}}{\sqrt{1+(n^2-1)(h^2-z^2)/(ct)^2}}\right]$$

$$\left[z+n^2h+(h+n^2z)\sqrt{1+(n^2-1)\,\frac{(h^2-z^2)}{(ct)^2}}\right]^{-1} U\left(t-\frac{h-nz}{c}\right) . \qquad (7)$$

The magnetic field is zero for $\rho = 0$ and the electric field has only a z-component given by $\tilde{E}_{1z}(t) = [\partial^2/\partial z^2 - (n/c)^2\,\partial^2/\partial t^2]\,\tilde{\Pi}_{1z}(t)$.

The problem of a horizontal dipole over an isotropic half-space has been treated by Banos (1966). The electric and magnetic fields are given in terms of the usual integrals so that the intermediate calculation of the Hertz vectors is not necessary. If the electric dipole is

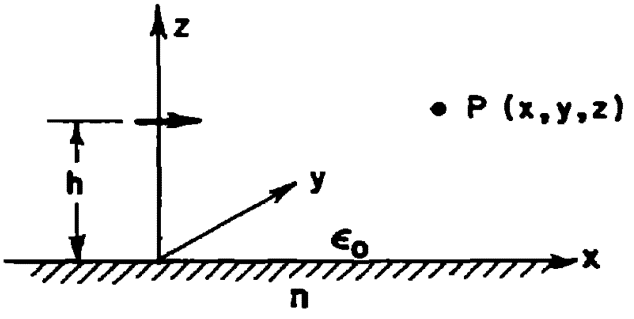

Figure 2. Horizontal electric dipole above an isotropic dielectric half-space.

oriented in the positive x direction at a height h above an isotropic dielectric half-space and the observation point is directly above or below the dipole (x=y=o), then the inverse Fourier transform of the scattered electric field in the upper medium can be taken using the same methods which were used for the vertical on-axis fields. The resulting time-dependent electric field is

$$\tilde{E}^s_{ox}(t) = \frac{I\,ds}{4\pi\varepsilon_o}\left\{\frac{n-1}{n+1}\,\frac{\delta'\left(t-\frac{z+h}{c}\right)}{c^2\,(z+h)} + \frac{n-1}{n+1}\,\frac{\delta\left(t-\frac{z+h}{c}\right)}{c\,(z+h)^2}\right.$$

$$- \frac{U\left(t-\frac{z+h}{c}\right)}{c^2\,(z+h)}\left[\frac{\partial^2}{\partial t^2}\left[\frac{2}{1+\sqrt{1+(n^2-1)(z+h)^2/(ct)^2}}\right.\right.$$

$$\left.\left.\left. + \frac{(ct)^2/(z+h)^2 - 1}{n^2+\sqrt{1+(n^2-1)(z+h)^2/(ct)^2}}\right] - \frac{c^2}{(z+h)^2}\right]\right\} . \qquad (8)$$

Using the same technique, the scattered time-dependent magnetic field on the vertical axis in the upper medium can also be found.

Details of the material in this paper are included in Hill (1969). For an arbitrary location of the source dipole and observation point, application of the techniques used here results in a finite integral which must be evaluated numerically. In this case one must work directly with expressions for the field quantities if the time-dependent field waveforms are desired. The same techniques can be used for the case of magnetic source dipoles since identical integrals are involved. If the half-space is dispersive, a Fourier synthesis technique can be used to secure the waveforms (Hill (1969)) but one is limited to the usual asymptotic estimates of the frequency-dependent fields. However, from quasi-static and high frequency asymptotic approximations and a limited number of synthesis results an estimate of the transient field is feasible. Such an estimate has the advantage of combining several spectral approximations in a single real characteristic waveform which, through convolution, is applicable for arbitrary excitations.

The specific on-axis results detailed in this paper basically yield exact closed form expressions for the interaction between a dipole element and a dielectric half-space. Using these, estimates of the response of linear or Rayleigh objects in the presence of a dielectric half-space for dipole or plane wave illumination can be obtained. Studies of these and related topics are presently in progress.

REFERENCES

Banos, A. (1966), Dipole Radiation in the Presence of a Conducting Half-Space, (Pergamon Press, Oxford).

Hill, D.A. and D.L. Moffatt, The Transient Fields of Dipole Antennas in the Presence of a Dielectric or Conducting Half-Space, Technical Report 2467-2, ElectroScience Laboratory, Department of Electrical Engineering, The Ohio State University; prepared under Contract F44620-67-C-0095, Air Force Cambridge Research Laboratories, Office of Aerospace Research, Bedford, Massachusetts (to be published).

Papoulis, A. (1962), The Fourier Integral and its Applications (McGraw-Hill Book Company, New York).

Van der Pol, B. (1956), On Discontinuous Electromagnetic Waves and the Occurrence of a Surface Wave, Trans. IRE, AP-4, 288.

Wait, J.R. (1966), Electromagnetic Fields of a Dipole over an Anisotropic Half-Space, Can. J. Physics, 44, No. 10, 2387-2401.

The Propagation Constant of a Small-Diameter Insulated Helix

F. P. Ziolkowski
Raytheon Company
Norwood, Massachusetts

Abstract

The influence of an insulating dielectric on the propagation constant and coupling of energy from a tape helix to the ambient media is considered. The solution presented for a pitch angle of 10° demonstrates the proper behavior for thick and thin insulation. The coupling decreases markedly with insulation thickness and slightly with helix size.

The general procedures developed for the solution of the tape helix in air (Klock, 1963 and Sensiper, 1955) is applied to the insulated helix. The notation used in this paper is

r, φ, z	Cylindrical coordinate variables. The axis of the helix is coincident with the z axis and $r = a_1$ is the surface on which the helix lies.
p	Pitch distance between turns of the helix, $\bar{p} = \frac{p}{2\pi}$
a_1	Radius of the helix
ψ	Pitch angle of the helix, $\tan \psi = \bar{p}/a$
δ	Tape width of the helix

The filamentary helix is defined by the relation $\bar{p}\varphi - z = 0$, which for a tape helix of width $-\delta/2 \leq \zeta \leq \delta/2$ is $\bar{p}\varphi - z = \zeta$. By use of group theory the unique perioditicities of the helix have been incorporated into the cylindrical coordinate representation of the solution of Maxwell' s equations. The z components of these fields are of the form

$$\Psi_i = e^{-j\beta z/\bar{p}} \sum_{-\infty}^{\infty} A_n^i L_n(\tau_n^i r/\bar{p})\, e^{-jn(z/\bar{p} - \varphi)} \tag{1}$$

$$\tau_n^i = \sqrt{(\beta + n)^2 - \overline{k^i}^2}$$

$$k^{i^2} = \omega^2 \tilde{\mu}_i \tilde{\epsilon}_i$$

$$\overline{k^i} = k^i \bar{p}$$

$$\tilde{\epsilon}_i = \epsilon_i (1 - jp_i), \quad \tilde{\mu}_i = \mu_i (1 - j\mu_i')$$

where L_n is the modified Bessel function I_n or K_n as is appropriate. The insulated helix consists of a core $0 \leq r \leq a_1$, the insulation $a_1 \leq r \leq a_2$, and the ambient media $a_2 \leq r$, wherein i is 1, 2, or 3 respectively. Once the field expressions for each of these regions is obtained and the current is expanded in a similar manner, the eight boundary conditions

$$E_u^i = E_u^{i+1}$$

$$H_u^i - H_u^{i+1} = j_{u\perp}^i \qquad i = 1, 2 \text{ for } u = \varphi, z \tag{2}$$

together with the requirement that the electric field parallel to the tape be zero yields the determinantal equation. In (2) $j_{u\perp}^1$ is $-j_z, j_\varphi$ for $u = \varphi, z$ and $j_{u\perp}^2 \equiv 0$. The determinantal equation can be simplified to

$$\beta^2 (F_1 + \sin\psi\, S_1) = (\overline{k^2}\ \text{ctn}\ \psi)^2 (F_2/\tau_0^2 + F_1 \tan\psi + S_2) \tan\psi$$

$$\tau_0^2 = \sqrt{\beta^2 + \overline{k^2}^2} \tag{3}$$

where

$$F_1 = I_{21} K_{21} \left(1 + \frac{K'_{22} I_{21} - E\, I_{21} K_{22}}{E\, I_{22} K_{21} - I'_{22} K_{21}} \right)$$

$$E = \frac{\tilde{\epsilon}_3\, \tau_0^2\, K'_{32}}{\tilde{\epsilon}_2\, \tau_0^3\, K_{32}}$$

$$F_2 = \frac{I'_{21}}{I_{21}} \left[1 - \text{ctn}\ \psi\, \tau_0^2\, I'_{21} K_{21} \left(\frac{K'_{22} I_{21} - M\, K_{22} I_{21}}{M\, K_{22} I_{22} - K_{21} I'_{22}} + 1 \right) \right]$$

$$M = \frac{\tilde{\mu}_3}{\tilde{\mu}_2} \frac{\tau_0^2\, K'_{32}}{\tau_0^3\, K_{32}}$$

and

$$S_j = \sum_1^\infty \frac{\sin \alpha n}{\alpha n^2} \left(1 - \xi_j e^{-\lambda n}\right) \qquad j = 1, 2$$

$$\xi_1 = \frac{1 - \frac{\tilde{\epsilon}_3}{\tilde{\epsilon}_2} t}{1 + \frac{\tilde{\epsilon}_3}{\tilde{\epsilon}_2}} \qquad \xi_2 = \frac{1 - \frac{\tilde{\mu}_3}{\tilde{\mu}_2} t}{1 + \frac{\tilde{\mu}_3}{\tilde{\mu}_2}}$$

$$t = \frac{t'}{\sqrt{1 + (t'^2 - 1)\cos^2 \psi}} \qquad t' = \frac{a_2}{a_1}$$

$$\lambda = 2(t' - 1) \operatorname{ctn} \psi$$

$$\alpha = \frac{\delta}{2a_1} \operatorname{ctn} \psi .$$

A shorthand notation has been used so that $I_{ij} = I_\nu (\tau_0^i a_j/\overline{p})$ and similarly for K_{ij}. If $\lambda > 3$ then the last term is negligible for which case $S_1 = S_2 = 1 - \ell n\, \alpha$.

This solution is valid for small-diameter helices such that $|\beta| << 1$ and requires the core and insulating materials to be identical. This core insulation material may have any permeability or permittivity, with or without loss.

The figure is the solution of this equation for a dielectric core-insulation case in rock media. In this case $\mu_2 = \mu_3 = 1$ and $\epsilon_3/\epsilon_2 = 4$, $p_2 = 0$ and p_3 is assumed 0.1 and 1.0. The helix pitch angle is 10° with $t' = 4.0$ and 1.03. The solutions are compared to the asymptotic cases of infinitely thin tapes with infinitely thick or thin insulation. Because of the finite size of the tape of the helix, $\delta/2a_1 = .1$, the expected dispersion from each of the asymptotes is encountered. The ratio β_i/β_r is observed to decrease slightly with increased helix size and markedly with increased insulation. Increasing the loss tangent of the rock median increases this ratio. Computed results indicate

that insulated helices yield values of β_i/β_r that are as much as two orders of magnitude less than comparably dimensioned, insulated solid conductors.

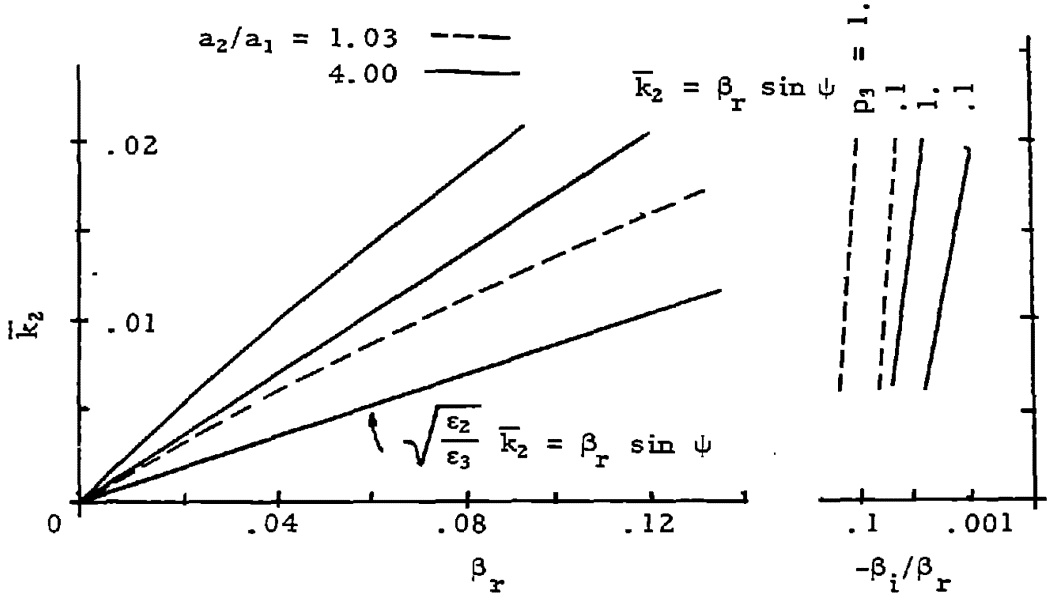

References

Klock, P. W. (March 1963), A Study of Wave Propagation of Helices, PhD Dissertation, Universityof Illinois, also Antenna Laboratory Technical Report 68.

Sensiper, S. (February 1955), Electromagnetic Wave Propagation on Helical Structures: A Review and Survey of Present Progress, Proc. IRE, 43, 149-161.

AN ALTERNATIVE METHOD FOR DERIVING FOCK'S PRINCIPLE OF THE LOCAL FIELD IN THE PENUMBRA

Dr. R. H. Ott, ESSA/ITS

ABSTRACT

An alternative method for deriving Fock's principle of the local field in the penumbra is presented. The method is based on solution of the wave equation in parabolic coordinates, with an impedance boundary condition on the surface and a radiation condition at infinity. It is shown that Fock's principle yields surface currents that are extremely accurate provided the observation point on the cylinder is near the point where the impressed field grazes the cylinder. When the impressed field travels in a direction tangent to the apex of the cylinder, Fock's principle is exact for all observation points on the cylinder. The results presented in this paper are more general than those given by Rice since his results are limited to the perfectly conducting case.

1.0 Introduction

A number of investigators have studied diffraction of radio waves by cylindrical (parabolic and circular) surfaces: Rice (1953), Wait and Conda (1958), Jones (1964), Fock (1965). In this paper we investigate a plane wave striking the parabolic cylinder at an arbitrary angle of incidence (i.e., the incident wave is normal to the axis of the cylinder, but not necessarily tangent to the apex). The field on the surface of the cylinder satisfies an impedance boundary condition. Fock's principle implies that universal formula exist for the field on the surface; i.e., when the incident wave is not tangent to the apex we replace the original wave direction and cylinder geometry by an equivalent geometry with the wave tangent to the apex of a replacement cylinder with a radius of curvature equal to the radius of curvature of the original cylinder at the point of tangency. It is shown that for all angles of incidence, Fock's principle yields extremely accurate results for the penumbral currents, provided the observation point on the cylinder is near the point where the impressed field grazes the cylinder. When the impressed field is tangent to the apex of the cylinder, Fock's principle yields surface currents that are identical to those derived in this paper.

2.0 Analysis

We now consider the field produced by a plane wave, traveling in a direction making an angle φ_o with the positive x-axis, striking the parabolic cylinder in figure 1. It will be assumed that $0 < \varphi_o < \pi$.

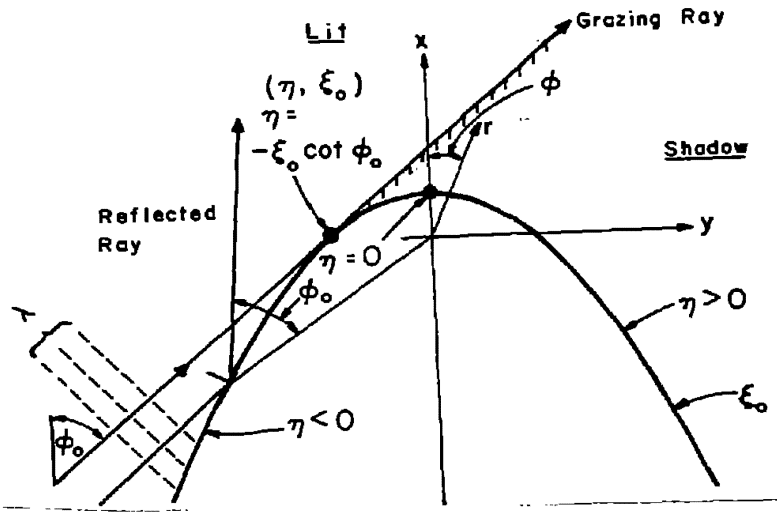

Figure 1. Geometry of incident wave and parabolic cylinder, used in the derivation of the Fock currents. The origin is at the focus of the parabola.

The solution of the wave equation and an impedance boundary condition and the radiation condition at infinity may be shown to be (Ott, 1969)

$$\psi = \frac{-1}{2\sqrt{2\pi}\, i} \int_{-\frac{1}{2}-i\infty}^{-\frac{1}{2}+i\infty} \frac{d\nu}{\sin \nu\pi} \frac{(\tan \frac{1}{2}\varphi_o)^{\nu}}{\cos \frac{1}{2}\varphi_o} \left\{ D_{\nu}(-h\xi) - \frac{z D_{\nu}(-h\xi_o) - h D_{\nu}'(-h\xi_o)}{z D_{\nu}(h\xi_o) + h D_{\nu}'(h\xi_o)} \right.$$

$$\left. D_{\nu}(h\xi) \right\} \; D_{-\nu-1}(h\eta) \quad , \quad \left(h = \sqrt{2k}\; e^{i\pi/4} \right) . \qquad (1)$$

When $h\xi_o$ becomes large, the following asymptotic representation for the parabolic cylinder function is valid (Rice, 1953):

$$D_{i\mu-\frac{1}{2}}(h\xi_o) \sim 2\sqrt{\pi}\,\exp\left\{\tfrac{1}{2}(i\mu-\tfrac{1}{2})\ell n i\mu - i\mu/2 + i\pi/12\right\}\mu^{1/6}\left(\frac{\xi_1}{\frac{2k\xi_o^2}{\mu}-4}\right)^{\frac{1}{4}}$$

$$\times\ Ai\left(e^{i\pi/3}\mu^{2/3}\xi_1\right), \qquad (2)$$

where

$$\frac{2}{3}(\xi_1)^{3/2} = 4\int_1^{\sqrt{k\xi_o^2/2\mu}}\sqrt{s^2-1}\,ds\ , \quad (\nu = i\mu-\tfrac{1}{2})\ .$$

Substituting (2) and an asymptotic expansion for $D'_{i\mu-\frac{1}{2}}$ into (1) yields the following expression for the normal derivative of (1) on the surface:

$$\frac{1}{(\xi_o^2+\eta^2)^{\frac{1}{2}}}\frac{\partial\psi}{\partial\xi_o} = \frac{-zh}{2\pi(\xi_o^2+\eta^2)^{\frac{1}{2}}}\frac{e^{-i\pi/12}}{(\sin\varphi_o)^{\frac{1}{2}}}\int_{-\infty}^{\infty}d\mu\ e^{-i\mu[\xi_2 - \ln\tan(\varphi_o/2)]}$$

$$\times\left(4+\frac{2k\eta^2}{\mu}\right)^{-\frac{1}{4}}\mu^{1/6}\left\{z\left(\frac{\xi_1}{\frac{2k\xi_o^2}{\mu}-4}\right)^{\frac{1}{4}}Ai\left(e^{i\pi/3}\mu^{2/3}\xi_1\right)\right.$$

$$\left.+\frac{he^{i\pi/12}}{2}\mu^{1/6}\left(\frac{\frac{2k\xi_o^2}{\mu}-4}{\xi_1}\right)^{\frac{1}{4}}Ai'\left(e^{i\pi/3}\mu^{2/3}\xi_1\right)\right\}^{-1}\ ,$$

$$\left(\xi_2 = \left(\frac{k\eta^2}{2\mu}\right)^{\frac{1}{2}}\left(1+\frac{k\eta^2}{2\mu}\right)^{\frac{1}{2}} + \ell n\left\{\left(\frac{k\eta^2}{2\mu}\right)^{\frac{1}{2}}+\left(1+\frac{k\eta^2}{2\mu}\right)^{\frac{1}{2}}\right\}\right). \qquad (3)$$

The Laplace approximation (Copson, 1965) states that the major contribution to the integral in (3) will arise from the neighborhoods of the points at which

$$f(\mu,\eta) = \mu[\xi_2 - \ell n\tan(\varphi_o/2)] \qquad (4)$$

attains its supremum. These points will be solutions of $\partial f/\partial\mu = 0$, and it is easy to verify that the point $\eta = -\xi_o\cot\varphi_o$, $\mu = \frac{1}{2}k\xi_o^2$ satisfies the condition. Since we are interested in the integral near the point where it assumes its greatest contribution, it would appear that a Taylor series expansion of $f(\tau,\eta)$ about this point would be useful. That is, consider

$$f(\tau,\eta) = -kr\cos(\varphi-\varphi_o) + f_2(\Omega,\varphi_o) + f_1(\Omega,\varphi_o)\tau\ , \quad (\Omega = \eta/\xi_o), \qquad (5)$$

where

$$\frac{f_1(\Omega,\varphi_o)}{(k\xi_o^2/2)^{1/3}} = (\Omega\sin\varphi_o + \cos\varphi_o)\left[1 + \frac{(\Omega\sin\varphi_o + \cos\varphi_o)\cos\varphi_o}{2}\right], \quad (6)$$

and

$$\frac{f_2(\Omega,\varphi_o)}{(k\xi_o^2)} = \frac{(\Omega\sin\varphi_o + \cos\varphi_o)^3}{6}, \quad (7)$$

and the variable of integration is changed according to

$$\mu = \left(\frac{k\xi_o^2}{2}\right) + \left(\frac{k\xi_o^2}{2}\right)^{1/3}\tau . \quad (8)$$

The corresponding functions given by Fock agree with (6) and (7), provided $\Omega \cong -\cot\varphi_o$.

3.0 Concluding Remarks

The validity of Fock's principle for the local field in the penumbra was investigated for the case of a plane striking a finitely-conducting, parabolic cylinder at an arbitrary angle of incidence. The results show that Fock's principle is extremely accurate provided the observation point on the parabolic cylinder is near the point where the impressed field grazes the cylinder. When the impressed field travels in a direction tangent to the apex of the cylinder, Fock's principle agrees exactly with the results presented in this paper for all observation points.

4.0 References

Copson, E. T. (1965), Asymptotic Expansions (Cambridge University Press, Cambridge, England).

Fock, V. A. (1965), Electromagnetic Diffraction and Propagation Problems, International Series of Monographs on Electromagnetic Waves, Ch. 1, 2, and 5 (Pergamon Press, Oxford, London, Edinburgh, New York, Paris, Frankfurt).

Jones, D. S. (1964), The Theory of Electromagnestism, (The Macmillan Co., New York).

Ott, R. H. (1969), An alternative method for deriving Fock currents, submitted for publication in Jour. of Math. Phys.

Rice, S. O. (1953), Diffraction of plane radio waves by a parabolic cylinder, The Bell System Technical Journal, vol. 33.

Wait, J. R., and Conda, A. M. (1958), Pattern of an antenna on a curved lossy surface, IRE Transactions on Antennas and Propagation, Vol. AP-6, No. 4, pp. 348-359.

BOUNDARY VALUE PROBLEMS IN RADIALLY INHOMOGENEOUS MEDIA *

John G. Fikioris

Department of Electrical Engineering
The University of Toledo, Toledo, Ohio

Abstract

Analytical and numerical solutions of radially inhomogeneous problems are examined. Piecewise constant and analytic approximations to the stratification function are discussed and compared. The advantages of the latter are pointed out. Finally, for a rather general case, the analytic continuation of the associated radial functions is carried out.

1. Introduction

Electromagnetic fields in radially inhomogeneous media, with an obvious extension to ellipsoidal shapes, are of practical interest in antenna, scattering and lens problems (Tai, 1958). If allowed by the shape of boundaries, the method of separation of variables may still be applied to such problems. In a number of situations the precise profile of the stratification function f(r) is not known and, more importantly, not very critical in determining the value of certain quantities. An example is provided by the input impedance of a biconical antenna in such media (Fikioris, 1965a), in particular dissipative near the antenna region. In contrast, the far field of the antenna depends on values of f(r) for all r. For the far field of an inhomogeneous, lossy scatterer of radius d, on the other hand, values of f(r) near r=d are more influential than those near r=0. In lossless media knowledge of f(r) for all r is required; even then, a good approximation to it for all r may suffice for certain problems.

2. Discussion of Various Approaches

The preceding considerations make obvious the importance, from the analytical and computational standpoint, of an optimum choice in approximating f(r). Two practical possibilities exist: a piecewise constant function $f_M(r)$ (M layers in the interval of interest

* Most of the work was done at the Gordon McKay Lab., Harvard University, Cambridge. Mass., and was supported by NSF Grant 20225

$r_o \leq r \leq r_M$) or an analytic function $f_a(r)$ (having continuous derivatives of all orders in $r_o \leq r \leq r_M$). Some immediate advantages are evident in both cases. In the former, the solution $R_\nu(r)$ of the radial differential equation is given in terms of known functions. For instance, in spherical inhomogeneities, $R_\nu = j_\nu$ or $R_n = h_n$, the spherical Bessel or Hankel function, where ν, n denote the separation constant. However, matching of solutions has to be effected at r=d and $r=r_m$ (m=0,1,...M), a tedius task indeed. With $f_a(r)$ matching is required only at $r=d, r_o, r_M$. The cases $r_o=0$, $r_M=\infty$ further reduce the number of matching surfaces. Here d denotes the length of a biconical antenna, or the radius of the lens, scatterer, cylinder, or $\xi=d$ of an ellipsoid, in corresponging cases.

The weight of these considerations becomes clear, when it is noticed that matching at m surfaces involves solution of 2m complex linear equations in 4m real unknown coefficients. Computer limitations in matrix inversion are well known and severely restrict M. For intervals $r_o \leq r \leq r_M$ long compared with λ such limitations on M will produce inaccurate results. For a meaningful approximation to f(r) the width of the layers should be selected as a small fraction of λ rather than by matrix inversion considerations. For instance, $\lambda/4$ coating of a dielectric $\varepsilon_2/\varepsilon_0$ by another $\varepsilon_1/\varepsilon_0 = \sqrt{\varepsilon_2/\varepsilon_0}$ results in 0 reflection (at normal incidence), but for any departure from $d_1 = \lambda/4$, say $d_1 = \lambda/2$, the reflection coefficient is significant. Besides, each layer is a piece of non-uniform transmission line of the same length and corresponding characteristic impedance (Wait, 1962). All this makes evident the advantages, in many cases the necessity, of choosing $f_a(r)$ over $f_M(r)$.

It is often desired to study the effects of changing d in the same medium, particularly in the range $r_o \leq d \leq r_M$. With $f_M(r)$ certain equations must be modified as d moves from $r_m \leq d \leq r_{m+1}$ to $r_{m+1} \leq d \leq r_{m+2}$. In the problem of the biconical antenna R_n (n=integer) changes to R_ν (ν=fractional) and vice versa, in the corresponding intervals. The matching equations are also affected. Such complications are absent, when $f_a(r)$ is chosen.

At first glance, even the advantage of dealing with known functions, like h_n, j_ν, seems minimal. The computer evaluates them, instead of reading their tabulated values. But then, almost as well, it may be programmed to compute $R_\nu(r)$, by means of a variety of infinite series expressions. Programs evaluating recurrence formulas and summing series are simple. However, dealing with solutions of the hypergeometric equation, of which h_n, j_ν are a particular variation, allows use of recursion formulas relating solutions of adjacent order and greatly facilitates the evaluation of such functions. In addition, connection and asymptotic formulas among the various solutions of the equation are known and simple. Unless $f_a(r) = br^c$ (b, c constants), the radial equations possess more than the 3 regular singularities of the hypergeometric equation (or its variations) and, in general, recursion formulas cannot be found. Connection and asymptotic formulas can

be found in certain cases (Fikioris, 1963, 1965b) after involved analytical and computational work. This is the only advantage of $f_M(r)$ over $f_a(r)$, but it is an important one.

3. Analytic Continuation of Radial Functions

In the remaining part of the paper the effect of zeros and singularities of $f_a(r)$ on the analytical complexity of the problem will be discussed in general terms. While details can be found elsewhere (Fikioris, 1963, 1965a, b), certain aspects, available only in thesis and technical report form, will be elaborated upon. As already mentioned, the limits $r_o=0$ and/or $r_M=\infty$, when allowed by the configuration, substantially simplify the solution. The corresponding matching problems disappear; finiteness around $r=0$ and the radiation condition at $r=\infty$ single out proper radial functions, reducing the number of expansion coefficients. However, both $f_a(0)$ and $f_a(\infty)$ must be finite. This rules out simple forms like $f_a(r)=br^c$ and introduces additional singularities in the well known radial equations for TE and TM spherical waves (Tai, 1958)

$$R''+\{f_a(r)-\nu(\nu+1)/r^2\}R=0 \quad (1), \qquad R''-(f_a'/f_a)R'+\{f_a(r)-\nu(\nu+1)/r^2\}R=0 \quad (2),$$

respectively. For certain problems $d=r_o\leq r$ and $f_a(0)$, being of no consequence, may be taken 0 or ∞ resulting in considerable simplification. Similar remarks apply when $d=r_M$, $f_a(r)$=constant for $r\geq r_M$.

In any case, (1) and (2) should be solved over the interval $r_o\leq r\leq r_M$ and the appropriate solutions evaluated at $r=r_o$, d, r_M. The singularities, introduced into the equations by $f_a(r)$, restrict the convergence of the infinite series expressions for $R_\nu(r)$. For intervals long compared with λ, analytic continuation of $R_\nu(r)$ becomes inevitable. As an illustration, (2), whose singularities exceed those of (1) by the number of zeros of f_a, will be solved and analytically continued in case $f_a(r)=(x+a)/(x+b)=1+c/(x+b)$, $c=a-b$, $x=kr=2\pi r/\lambda$, in the interval $0\leq r\leq\infty$ ($r_o=0$, $r_M=\infty$). A biconical antenna in such a medium has been investigated in detail elsewhere (Fikioris, 1965a, b). With $x=kr$ (1) becomes

$$R''(x)+cR'(x)/\{(x+a)(x+b)\}+\{1+c/(x+b)-\nu(\nu+1)/x^2\}R(x) = 0 \quad (\nu\geq 0) \quad (3)$$

and has 3 regular singular points at $x=0$, $x=-a$, $x=-b$ and an irregular singularity of the first rank at $x=\infty$, i.e., two more regular singularities than the Bessel equation. For lossless media x varies along the real axis; for dissipative media along a straight line in the fourth quadrant of the x-plane from 0 to ∞. The method of Frobenius around $x=0$ yields two independent solutions R_1, R_2 in the form $R(x)=x^\sigma \sum_{n=0}^{\infty} a_n x^n$, $|x|<\min(|a|,|b|)$, where $\sigma_1=\nu+1$ for R_1, $\sigma_2=-\nu$ for R_2 (for fractional values of $2\nu+1$). The coefficients a_n for $n=1, 2, \ldots$ can be found by the 5-term recurrence formula

$$\sum_{n=0}^{4} a_{n-m}\, u_m(n+\sigma-m) = 0 \ ; \ a_{-j}=0 \ , \ j=1,2,\ldots \ (a_0=1,\ a_1=-c/2ab) \qquad (4)$$

where $u_0(z)=aby(z)$, $u_1(z)=cz+(a+b)y(z)$, $u_2(z)=a^2+y(z)$, $u_3(z)=2a$, $u_4(z)=1$, $y(z)=z(z-1)-\nu(\nu+1)$.

When $2\nu+1$ equals a positive integer there is no change in R_1, but R_2 becomes logarithmic. It may be defined as follows: $R_2(x)=\ln x\, R_1(x)+\sum_{n=0}^{\infty} b_n x^{n-\nu}$, $|x|<\min(|a|,|b|)$. The b_n's obey an inhomogeneous recurrence formula for $n>2\nu+1$, whose homogeneous part is the same as (4) for $\sigma=-\nu$. For $1\le n\le 2\nu$, $b_n=b_0 d_n$, where with $d_0=1$, $d_{-j}=0$ ($j=1,2,\ldots$) the constants $1, d_1, \ldots d_{2\nu}$ satisfy (4) with $\sigma=-\nu$. Finally, $b_0=-ab(2\nu+1)/\{\sum_{j=0}^{\nu} d_{2\nu-j}u_{j+1}(\nu-j)\}$ and $b_{2\nu+1}=0$.

The analytic continuation of R_1, R_2 beyond the circle $|x|=\min(|a|,|b|)$ can be obtained using a bilinear transformation $t=x/(x+p)$, $x=pt/(1-t)$. The constant p is chosen to optimize the convergence of the resulting series in t. The normal at $x=-p/2$ to the straight segment from $x=0$ to $x=-p/2$, maps onto the unit circle in the t-plane. The half plane containing $x=0$ maps onto $|t|<1$, whereas $x=0$, $-a$, $-b$, ∞ map onto $t=0$, $a/(a-p)$, $b/(b-p)$, 1, respectively. These points are the only singular ones of the differential equation in t,

$$R''(t)+\left[\frac{pc}{\{(p-a)t+a\}\{(p-b)t+b\}}+\frac{2}{t-1}\right]R'(t)+\left[\frac{(p-a)t+a}{(p-b)t+b}\,\frac{p^2}{(t-1)^4}-\right.$$
$$\left.-\nu(\nu+1)/\{t^2(t-1)^2\}\right]R(t)=0 \ . \qquad (5)$$

The first three are regular, the last, $t=1$, is irregular of rank 1. The parameter p can be chosen so that $x=-a$, $x=-b$ are located on the half plane that maps onto $|t|\ge 1$. Then, a power series solution of (5) around $t=0$ will converge for $|t|<1$, providing the analytic continuation of $R(x)$ over the interval of interest $0\le Re(x)\le\infty$. Numerical computations have shown that such series can be used for values of $|x|$ 3 to 4 times larger than those possible in connection with the series in x. It is not necessary, in this respect, to map $x=-a$, $-b$ outside $|t|=1$. Sometimes larger values of $|x|$ can be used with series in t convergent in $|x|<\min(|a/(a-p)|,|b/(b-p)|)<1$. The image of the straight line over which x varies from 0 to ∞, connecting $t=0$ to $t=1$, should be as farther from singularities as possible. This is the optimum criterion for p, for such restricted values of x.

It remains to connect $R(t)$ to $R(x)$. This is done here in the special case $p=2a$, $t=x/(x+2a)$, $x=2at/(1-t)$, mapping $x=-a$ on $t=-1$, a convenient choice in certain applications. The series in t are: $R(t)=At^{\sigma}\sum_{n=0}^{\infty}e_n t^n$, $|t|<\min(1,|h|)$, $h=b/(2a-b)$, where $\sigma_1=\nu+1$ for R_1, $\sigma_2=-\nu$ for R_2 and fractional $2\nu+1$. The e_n's satisfy a 7-term recurrence formula with $e_0=1$, $e_1=\sigma+(1/2)-1/(2h)$. As $x\to 0$, $t=(x/2a)\{1-x/(2a)+\ldots\}$. Substituting: $R(t)=A(x/2a)^{\sigma}(1+x/2a)^{-\sigma}(1+e_1 x/2a+\ldots)=A(2a)^{-\sigma}x^{\sigma}\{1-(e_1-\sigma)x/2a+\ldots\}=A(2a)^{-\sigma}x^{\sigma}\{1-cx/(2ab)+\ldots\}$. With $A=(2a)^{\sigma}$ the solutions in x and t are identical: $R=x^{\sigma}\sum_{n=0}^{\infty}a_n x^n=(2a)^{\sigma}t^{\sigma}\sum_{n=0}^{\infty}e_n t^n$.

For integral values of $2\nu+1$, R_2 becomes logarithmic. In analogy with the series in x: $R_2(t)=\ln\{2at/(1-t)\}R_1(t)+B\sum_{n=o}^{\infty} g_n t^{n-\nu}$, $|t|<\min(1,|h|)$. For $1\leq n\leq 2\nu$ the g_n's are evaluated by a homogeneous recurrence formula, like that for the e_n's of $R_1(t)$, with $\sigma=-\nu$, $g_o=1$, $g_1=-\nu+(1/2)-1/(2h)$. For $n>2\nu+1$ the g_n's obey an inhomogeneous recurrence formula, whereas B and $g_{2\nu+1}$ are chosen so that $R_2(t)\equiv R_2(x)$. This means $Bt^{-\nu}\sum_{n=o}^{\infty} g_n t^n = x^{-\nu}\, b_o \sum_{n=o}^{\infty} d_n x^n$, where $b_n=b_o d_n$ for all n, or $B\sum_{n=o}^{\infty} g_n(x/2a)^n(1+x/2a)^{\nu-n} = (2a)^{-\nu} b_o \sum_{n=o}^{\infty} d_n x^n$. Use of the binomial expansion for small $|x|$, as before, yields: $B=b_o(2a)^{-\nu}$ and (for integral ν) $g_{2\nu+1}=\sum_{m=1}^{\nu}(-1)^{\nu+m}\nu^2 g_{\nu+m}/\{(\nu-m+1)!(m-1)!\}$. For $\nu=n+1/2$, n=integer, slight changes are involved. The result for R_2 is:

$$R_2(x)=R_2(t) = \ln x\, R_1(x) + b_o(2at)^{-\nu}\sum_{n=o}^{\infty} g_n t^n \ , \quad |t|<\min(1,|h|).$$

The formulas are easily checked for functions of low order, $\nu=1,2$; they have been checked numerically for much larger values of ν. It was also found that the coefficients g_n increase faster than the e_n's. More details, as well as methods of obtaining asymptotic expansions of R_1, R_2 as $x\to\infty$, can be found elsewhere (Fikioris, 1963, 1965b).

References

Fikioris, J. G. (1963), Theory of Radially Stratified Media, Part II, Techn. Rept. No. 395, Cruft Lab., Harvard Univ., Cambridge, Mass.

Fikioris, J. G. (1965a), The Biconical Antenna in a Radially Stratified Medium, IEEE Trans. Ant. Prop. AP-13, No. 2, 289-302.

Fikioris, J. G. (1965b), Asymptotic Expansions of Solutions of Differential Equations, J. Math. Phys. 6, No. 7, 1131-1148.

Tai, C. T. (1958), The Electromagnetic Theory of the Spherical Luneberg Lens, Appl. Sci. Res. 7B, 113-130.

Wait, J. R. (1962), Electromagnetic Waves in Stratified Media, (Pergamon Press, Oxford).

RADIATION FROM A PARALLEL-PLATE WAVEGUIDE INTO AN INHOMOGENEOUSLY FILLED SPACE

R.J. Kostelnicek, University of Illinois. Urbana, Ill. 61801, U.S.A.
R. Mittra, University of Illinois. Urbana, Ill. 61801, U.S.A.

A method involving an extension of the function-theoretic technique is presented for solving the problem of a semi-infinite parallel-plate waveguide radiating through a dielectric or plasma slab. Some numerical solutions are presented for both cases.

Introduction

The object of this paper is to present an analysis for the problem shown in Fig. 1.

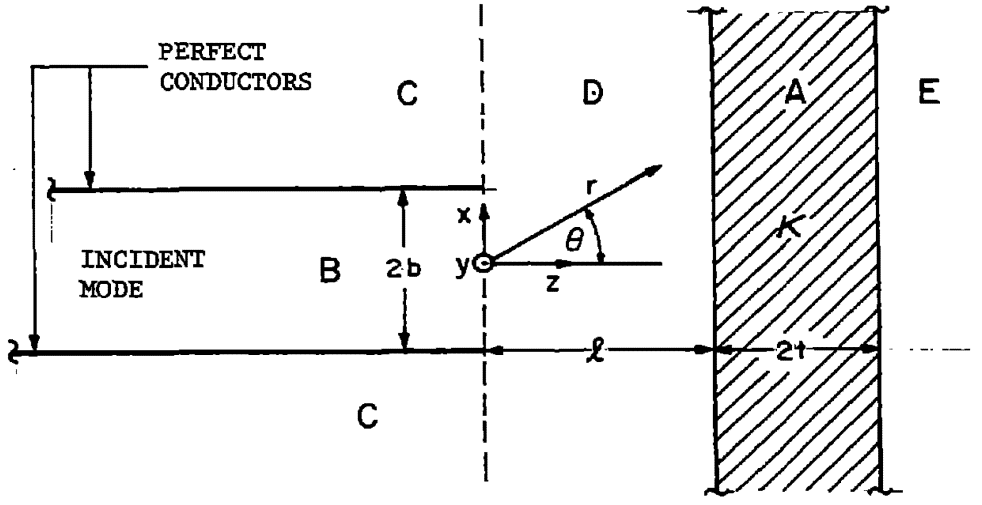

Fig. 1. The radiating waveguide with a slab having a relative dielectric constant κ.

A conventional approach to this problem entails the use of the variational technique. However, this formulation is necessarily approximate, since the Green's function for the region external to the waveguide can not be constructed in a convenient manner. In addition, no direct use is made in the above method of the known exact solution of the canonical problem, i.e., a semi-infinite waveguide radiating into free space.

In contrast, the present formulation for this problem is based on an extension of the method followed by Mittra and Bates (1965)

for the canonical problem. The basic steps involve the writing of the fields in region B in terms of waveguide modes and in region E in terms of a continuous spectrum (Fourier integral) representation. Similar transform representations are also employed in regions A, D, and C. Typical representations for the magnetic intensity in regions B and E for a TM_{po} incident mode of unit amplitude are given by

$$(Hy)_B = \cos\left(\frac{p\pi x}{b}\right)e^{-\beta_o z} + \sum_{s=o}^{\infty} B_s \cos\left(\frac{s\pi x}{b}\right)e^{\beta_s z} \tag{1}$$

and

$$(Hy)_E = \int_o^{\infty} E(\alpha)e^{-\xi(z-\ell-2t)} \cos(\alpha x)\,d\alpha \tag{2}$$

The longitudinal wave numbers are given by $\beta_s = \sqrt{(s\pi/b)^2 - k_o^2}$ in region B, $\xi = \sqrt{\alpha^2 - k_o^2}$ in E, and $\eta = \sqrt{\gamma^2 - k_o^2}$ in C. The mode coefficients and spectral weight functions are B_s, $D(\alpha)$, $E(\alpha)$, $C(\gamma)$, and $A(\alpha)$.

The next step is to solve for the various mode and weight coefficients by matching the transverse field components at $z = \ell$ and $z = \ell + 2t$, thereby obtaining $D(\alpha)$ and $A(\alpha)$ in terms of $E(\alpha)$. Field matching is once more carried out at the $z = 0$ interface for $x \geqslant b$ and subsequently for $x \leqslant -b$. The resulting four equations are Fourier transformed and combined to yield the following relationships:

$$b(1+\delta_p^o)\delta_s^o = \pi E\left(\frac{s\pi}{b}\right) R'\left(\frac{s\pi}{b}\right) \tag{3}$$

$$\pi\eta E(\gamma)R'(\gamma)e^{-j\gamma b} + \int_o^{\infty} E'(\alpha)\left[\frac{R'(\alpha)}{\xi - \eta} - \frac{Q'(\alpha)}{\xi + \eta}\right] d\alpha, \tag{4}$$

together with two companion relationships giving the coefficients B_s and weight function $C(\gamma)$ in terms of an integral relationship involving $E(\alpha)$. In equations (2) and (3) we have written $E'(\alpha) = \alpha \sin(\alpha b)\, E(\alpha)$, $R'(\alpha) = R(\alpha)\exp(\xi\ell)$ and $Q'(\alpha) = Q(\alpha)\exp(-\xi\ell)$. The quotients $1/R(\alpha)$ and $Q(\alpha)/R(\alpha)$ are respectively the transmission and reflection coefficients for a uniform plane wave incident onto the dielectric or plasma slab at an angle given by $\Theta = \sin^{-1}(\alpha/k_o)$. Equations (3) and (4) represent a homogeneous integral equation for $E(\alpha)$ and a requirement that $E(\alpha)$ take on certain specified values at $\alpha = s\pi/b$ ($s = 0, 1, 2, \ldots\ldots$).

The above formulation is exact, and for the limiting case when $\kappa = 1$, an exact solution for $E(\alpha)$ can be constructed using the function-theoretic technique.

Modified Method of Solution

The solution of (3) and (4) for $E(\alpha)$ by the modified function-theoretic technique is accomplished by the construction of a meromorphic function $F(\omega)$ of a complex variable ω, which has a certain pole-zero configuration, and specified branch singularities. Integrations in the complex plane yield results which, when compared with (3) and (4) and the companion relations for B_s and $C(\gamma)$, give the required solutions and the normalization condition. These are:

$$F(-\beta_s) = -b(-1)^s \beta_s (1+\delta_s^o) B_s \tag{5}$$

$$F(\xi) = \pi \xi R'(\alpha) e^{j\alpha b} E(\alpha) \tag{6}$$

$$F(\eta)\frac{Q'(\gamma)}{R'(\gamma)} + F(-\eta) = \pi \eta C(\gamma) \tag{7}$$

and

$$F(\beta_p) = b(-1)^p \beta_p (1+\delta_p^o) \quad . \tag{8}$$

The function $F(\omega)$ may be factored into the form $F(\omega) = F_1(\omega)\, T(\omega)$, where $F_1(\omega)$ represents that function employed in the solution of the canonical problem (Mittra and Bates, 1965), and $T(\omega)$ represents the departure from the canonical function due to the presence of the slab. The preceeding integrations and comparisons together with the factored form of $F(\omega)$ yield an auxiliary integral relationship

$$T(\omega) = \frac{1}{\omega - \beta_p} + \int_\sigma \frac{\lambda(z)\, T(z)}{\omega + z}\, dz \quad . \tag{9}$$

Equation (9) is not very convenient for numerical methods of solution when ω is on the path σ due to the singular nature of the partial kernel $\lambda(z)$, which has poles on σ due to the surface modes excited within the dielectric slab. However, the path σ may be deformed to say σ' on which the integrand of (9) is wholly analytic. Numerical methods are now employed together with a process of analytic continuation, and the required values $T(\omega)$ and $T(-\omega)$ obtained.

The near fields may be obtained from the modal expansion in region B or from the Fourier transforms in the open regions. The radiation fields are obtained directly from the spectral weight coefficients by employing the method of saddle point integration (Collin, 1960). The surface modes may be obtained from the residues of the integrand in the transform representation in region A.

Finally, the function $T(\omega)$ may be solved for exactly as $|\omega| \to \infty$ and shown to satisfy the edge condition (Meixner, 1954). Such consistency is usually difficult if not impossible to demonstrate when other methods are employed.

References

Collin, R. E. (1960), Field Theory of Guided Waves. McGraw-Hill.

Meixner, J. (1954), "The Behavior of Electromagnetic Fields at Edges," N.Y. Univ. Inst. Math. Sci. Res. Report-EM-72, Dec.

Mittra, R. and Bates, C. P. (1965), "An alternative Approach to the Solution of a Class of Weiner-Hopf and Related Problems," Proceedings of the Electromagnetic Wave Theory Symposium, Delf, The Netherlands, Sept.

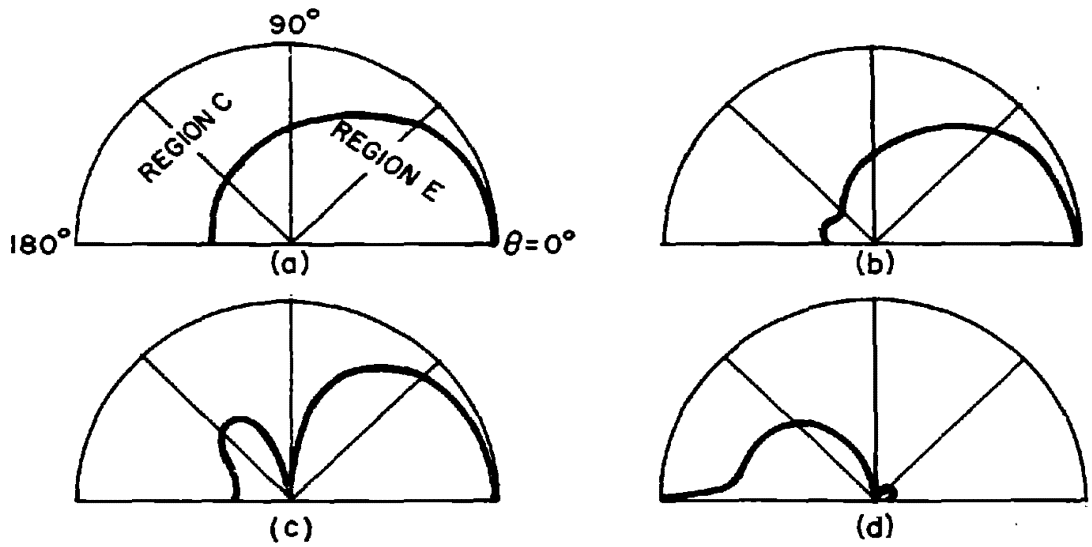

Figure 2. Radiation patterns for (a) canonical problem with $b = .16\Lambda_o$; (b) $b = .16\Lambda_o$, $\kappa = 2$, $2t = \Lambda_o/2$, $\ell = 0$; (c) $b = .16\Lambda_o$, $\kappa = 2$, $2t = \Lambda_o/4$, $\ell = \Lambda_o/4$; (d) $b = .16\Lambda_o$, $\kappa = -2$, $2t = \Lambda_o/2$, $\ell = 0$. The free space wavelength is Λ_o.

Table 1. The distribution of scattered power into the various regions, normalized to one watt incident in TEM mode.

FIGURE 2	TEM MODE P_B WATTS	P_E WATTS	P_C WATTS	SURFACE MODES P_A WATTS TM_o / TM_1
(a)	.135	.691	.182	
(b)	.154	.678	.092	$.72\times10^{-8}$ / .077
(c)	.157	.606	.111	.195 / 0
(d)	.975	$.17\times10^{-3}$	.025	

Metallic and Dielectric Antennas in Conducting Media(†)

Giorgio Franceschetti (††)
O. Bucci, E. Corti, G. Latmiral (††)

Abstract

The input resistance and the effective height of several antennas are computed in the limiting static case, for a gap-type excitation, and for an unbounded surrounding medium; and then for a semi-infinite, two-layer medium. The system equation is also computed. Experiments on models completely confirmed theoretical deductions.

1. Statement of the problem.

For the reception of electromagnetic waves by means of buried or submerged antennas it is rather obvious that metallic antennas (e.g. two closely spaced metallic plates) can collect the current induced in the conductive medium by the propagating field; and that dielectric antennas (e.g., an ellipsoidal cavity) can be used to detect the internal enhanced electric field. Dual reasonings apply for the case of transmitting antennas.

The antenna's characteristics, i.e. the input impedance and the effective heigth, will be obviously dependent on the antenna itself and on the used frequency, as well as on the external conductivity, medium inhomogeneneities and stratification, etc.

In order to get general results, some kind of schematization is therefore necessary. Since the used frequencies are generally very low, it seems to be convenient to develop the simple static case.

Theoretical results of our computations were confirmed by means of experiments on models into a tank. The disturbancies, introduced by the boundaries of the tank, were minimized by using metallic and dielectric walls alternatively, and then properly processing the measured data. Lack of space does not allow us to give further details.

As long as the dynamical case is concerned, it is intuitive that in the low frequency case, the input impedance will remain practically resistive, and equal, as well as the effective heigth,

(†) This work is sponsored by the Italian Consiglio Nazionale delle Ricerche.

(††) Dept. of Electrical Engineering, University of Naples, and Istituto Universitario Navale, Naples, Italy.

to those computed in the static approach.

This part of the problem will be investigated in the near future.

2. Computations in the static case.

Let ξ , η be parameters describing radial and elevation coordinates respectively, $\Phi(\xi,\eta)$ the potential, σ the conductivity of the external medium.

For the considered metallic antennas, whose surface is described by $\xi=\xi_o$ (see the table in the next page), we have:

$$\Phi = \frac{1}{2}\sum_{1}^{n}(4n-1)\,\bar{\Phi}_{2n-1}P_{2n-1}(\eta)\,\frac{U_{2n-1}(\xi)}{U_{2n-1}(\xi_o)};\quad \bar{\Phi}_{2n-1}=\int_{-1}^{1}\Phi^a\,P_{2n-1}(\eta)d\eta, \tag{1}$$

being $P(\eta)$ the Legendre function of first kind, and Φ^a the applied voltage. The U's are suitable functions, describing the radial dependence of the field.

The current injected into the medium is given by:

$$I= -\pi\sigma\sum_{1}^{n}(4n-1)\,\bar{\Phi}_{2n-1}\,\frac{U'_{2n-1}(\xi_o)}{U_{2n-1}(\xi_o)}\int_{o}^{1}\frac{h_\eta\,h_\phi}{h_\xi}P_{2n-1}(\eta)d\eta\ , \tag{2}$$

being the h's scale factors and being the dash derivation in ξ_o.

We have, for the input resistance:

$$R=\frac{\Phi_o}{I}\ , \tag{3}$$

being Φ_o the applied voltage to the exciting gap. The effective height h can be computed from the relation:

$$\lim_{\xi\to\infty}\Phi=\frac{3}{2}\bar{\Phi}_1\,\eta\,\frac{U_1(\xi\to\infty)}{U_1(\xi_o)}=\frac{I\,h}{4\pi\sigma r^2}\cos\theta\ , \tag{4}$$

being $\bar{\Phi}_1$ related to I via (-3).

Similar results hold for the case of the dielectric antennas.

By referring to suitable coordinate systems, we get (for the meaning of the numbers see the table), irrespective to the exciting gap dimension:

$$2:\quad R=\frac{1}{2\sigma\ell}\ ;\quad h=\frac{4}{\pi}L\ ;\quad \ell<<L\ ; \tag{5}$$

$$5:\quad R=\frac{1}{2\pi\sigma\ell}\ ;\quad h=2L\ ;\quad \ell<<L\ . \tag{6}$$

For the other cases, when the exciting gap is assumed to be infinitesimal, we get from (2), being K a known constant:

$$I= -\pi\sigma\,\Phi_o\,K\sum_{1}^{n}\frac{4n-1}{(2n-1)^2}\left[P_{2n}(o)\right]^2\frac{U'_{2n-1}(\xi_o)}{U_{2n-1}(\xi_o)}\ . \tag{7}$$

Since, asymptotically for $n>>1$, $[P_{2n}(o)]^2$ behaves as $1/n$, and U'_{2n-1}/U_{2n-1} as $-n$, the series (7) diverges.

CONSIDERED ANTENNAS

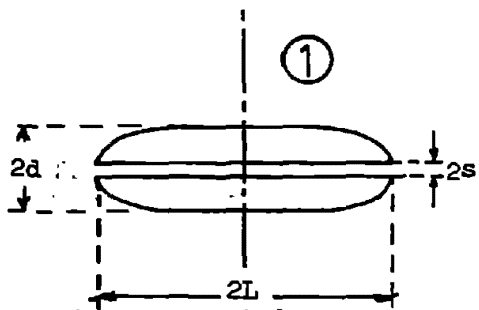

Oblate metallic antenna

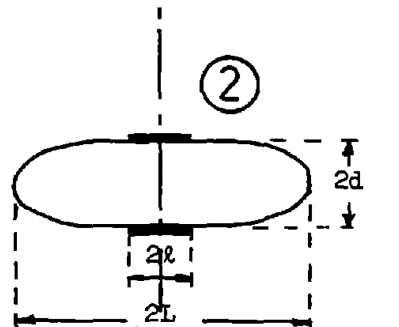

Oblate dielectric antenna

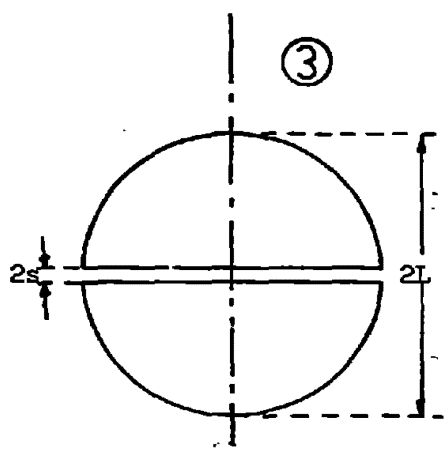

Spherical metallic antenna

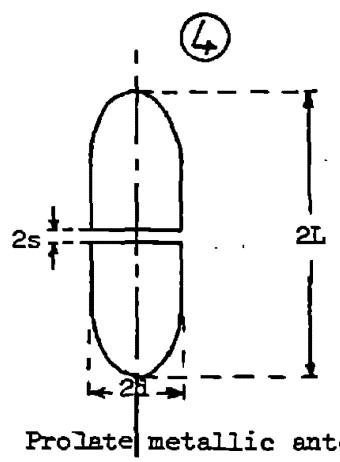

Prolate metallic antenna

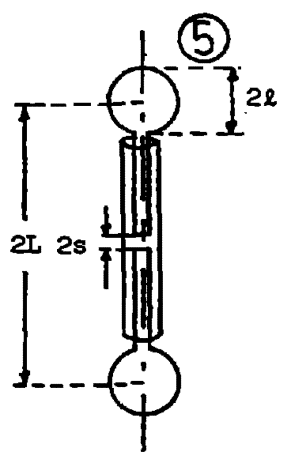

Moore's antenna

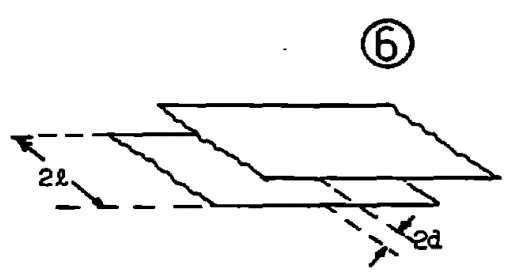

Strip metallic antenna

On the contrary, assuming the gap finite, even if small, and letting $\bar{n}$ the value of n corresponding to s, by means of elaborate computations it is possible to transform (7) as follows:

$$I = -\pi\sigma\,\Phi_o\,K\left[\sum_1^n \frac{3n-1}{n(2n-1)^2}\left[P_{2n}(o)\right]^2 \frac{U'_{2n-1}}{U_{2n-1}} + \frac{1}{\pi}\sum_1^n \frac{1}{n^2}\,\frac{\sin 4n\bar{n}}{4n\bar{n}}\,\frac{U'_{2n-1}}{U_{2n-1}}\right] \tag{8}$$

By using the asymptotic expressions for U_{2n-1} and U'_{2n-1}, (6) can be summed (the first one in terms of the hypergeometric function) and we get (for the meaning of the numbers, see the table):

$$1:\quad \begin{cases} R = \dfrac{2}{3\pi\sigma L}\,\dfrac{1}{\left[1+\frac{4}{3\pi}\,\ell n\,\frac{d}{4s}+\frac{d}{3L}\right]}\ ; \\ h = \dfrac{2L}{3}\,\dfrac{1}{1-\frac{5}{4}\frac{d}{L}+\frac{2}{3}\left(\frac{2}{\pi}-\frac{d}{L}\right)\ell n\,\frac{d}{4s}}\ ; \end{cases} \tag{9}$$

$$3:\quad \begin{cases} R = \dfrac{1}{2\pi\sigma L}\,\dfrac{1}{1+\frac{1}{\pi}\,\ell n\,\frac{L}{4s}}\ ; \\ h = \dfrac{3L}{2}\,\dfrac{1}{1+\frac{1}{\pi}\,\ell n\,\frac{L}{4s}} \end{cases} \tag{10}$$

$$4:\quad \begin{cases} R = \dfrac{2}{\pi\sigma L}\,\dfrac{1}{1+\frac{3d}{L}\left(1+\frac{4}{3\pi}\ell n\,\frac{L}{4s}\right)}\ ; \\ h = \dfrac{2L}{\ell n\,\frac{2L}{a}}\,\dfrac{1}{1+\frac{3d}{L}\left(1+\frac{4}{3\pi}\,\ell n\,\frac{L}{4s}\right)}\ . \end{cases} \tag{11}$$

Eqs. (9 through 11) show the proper logarithmic singularity, as it should be expected.

In the case of strip-type antennas, L>>d, by applying the Schwartz-Christoffel transformation for L→∞, we get:

$$6:\quad \begin{cases} R = \dfrac{4}{\pi\sigma L\left[1+\frac{4}{\pi^2}\left(1+\frac{1}{\pi}\frac{d}{\ell}\right)\ell n\,\frac{\ell}{d}\right]}\ ; \\ h = \dfrac{4\ell}{\pi}\,\dfrac{1}{1+\frac{4}{\pi^2}\left(1+\frac{1}{\pi}\frac{d}{\ell}\right)\ell n\,\frac{\ell}{d}} + d\ . \end{cases}$$

From a practical point of view, it should be remarked that the weight of the logarithmic term can be lowered, by inserting, between the exciting gap, a thin insulating layer, slightly protruding towards the conducting medium.

The system equation between two identical matched antennas can be cast under the following form:

$$\frac{P_r}{P_t} = \left[\frac{h^2}{4\pi\sigma R r^3}\right]^2 = \alpha\left(\frac{L}{r}\right)^6 \quad ; \qquad (12)$$

where, neglecting the logarithmic term, we have:

1	2	3	4	5	6
0.028	$0.067\left(\frac{\ell}{L}\right)^2$	1.26	$\frac{0.25}{\ell n^2 \frac{2L}{d}}$	$4\left(\frac{\ell}{L}\right)^2$	$0.01\left(\frac{\ell}{L}\right)^4$

Although the comparison between so different antennas is difficult, the spherical antenna seems to be very promising.

In the more realistic case of a semi-infinite two-layer medium, (the external of conductivity $\sigma' < \sigma$) it can be shows that, in pratical cases, the expressions for the resistance are still valid, those for the effective height must be multiplied for σ/σ' and the system equations for $(\sigma/\sigma')^4$ (therefore obtaining a consistent increase of the field).

The above results are deduced by the analysis of the antenna immersed into a shell of conductivity σ, while the outer medium is of conductivity σ': even for small dimensions of the shell, the input resistance of the antenna remains equal to that of the same antenna immersed into a homogeneous medium of conductivity σ; while the effective height equals that of the same antenna immersed into the homogeneous medium of conductivity σ'. The increase of the effective height can be computed by applying the image theory.

RADIATION FROM A SEMI-INFINITE DIELECTRIC-COATED SPHERICALLY TIPPED PERFECTLY CONDUCTING CONE

(Mrs.) Rajeswari Chatterjee
Department of Electrical Communication Engineering
Indian Institute of Science, Bangalore 12, India

Abstract

The solution to the problem of electromagnetic radiation from a semi-infinite dielectric-coated spherically tipped perfectly conducting cone excited by delta-function sources has been obtained by using the orthogonal properties of Sommerfeld's spherical Hankel wave functions of complex order. The possibility of radiation of the symmetric as well as unsymmetric TM, TE and hybrid waves from such a structure is discussed.

1. Introduction

Radiation and scattering of electromagnetic waves by a perfectly conducting cone have been studied by many authors (Bailin and Silver, 1956; Felsen, 1957; Adachi, et al. 1959; Wait, 1969). The exact solution for the problem of electromagnetic radiation from a circularly symmetric slot on the conducting surface of a semi-infinite dielectric-coated spherically tipped conducting cone has been obtained by Yeh (1964) for the symmetric TM wave. Closely related problems have also been discussed by Wait (1969). The possibility of radiation of the symmetric as well as unsymmetric TM, TE and hybrid waves from such a structure is discussed here.

2. Formulation

The geometry of the structure is given in Fig. 1. Spherical coordinates (r, θ, ϕ) are used, with the vertex of the cone taken at the origin. To eliminate the singularity at the vertex, a small perfectly conducting spherical boss of radius 'a', with its center at the origin is situated at the tip of the cone.

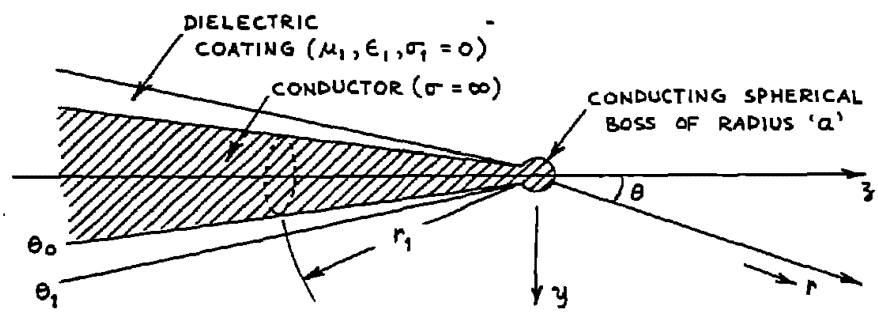

Fig. 1 - The geometry of the structure.

The excitation of the structure is by means of a radial electric field delta-function source at $r = r_1$ for TM waves, a radial magnetic field delta-function source at $r = r_1$ for TE waves, and a combination of these two sources for hybrid waves.

3. Hybrid Waves

The components E_r, E_θ, E_ϕ and H_r, H_θ, H_ϕ of the electric and magnetic fields inside and outside the dielectric coating are assumed to be a superposition of the field components of the TM and TE waves. The field components of TM and those of TE waves consist of an infinite number of terms which are solutions of the wave equation in spherical polar coordinates.

Applying the boundary conditions that E_ϕ and E_θ must vanish at $r = a$ it is found that the order n of the spherical Hankel functions $h_n^{(1)}(k_1 r)$ and $h_n^{(1)}(k_2 r)$ can assume an infinite number of discrete complex values n_ν and n_μ respectively for TM waves and n'_ν and n'_μ respectively for TE waves, where

$$k_1 = \omega\sqrt{\mu_1 \epsilon_1} \quad , \quad k_2 = \omega\sqrt{\mu_2 \epsilon_2} \quad ,$$

ω being the angular frequency. The numbers n_ν and n_μ are respectively the roots of the equations

$$\frac{d}{dr}\left[r\, h_n^{(1)}(k_1 r)\right]_{r=a} = 0 \qquad (1)$$

$$\frac{d}{dr}\left[r\, h_n^{(1)}(k_2\, r)\right]_{r=a} = 0 \qquad (2)$$

and n'_ν and n'_μ are respectively the roots of the equations

$$h_n^{(1)}(k_1\, a) = 0 \qquad (3)$$

$$h_n^{(1)}(k_2\, a) = 0 \qquad (4)$$

The radial electric field delta-function source and the radial magnetic field delta-function source at $\theta = \theta_o$ used for the excitation are given by

$$E_r^{app} = E_o\, d(r_1)\, e^{j\omega t} \cos(m\phi)$$

$$= \frac{1}{r} \sum_{n_\nu} L_{n_\nu}^m\, n_\nu (n_\nu + 1)\, h_{n_\nu}^{(1)}(k_1 r)\, P_{n_\nu}^m(\cos\theta_o) \cos(m\phi)\, e^{j\omega t} \qquad (5)$$

(expanding in terms of Sommerfeld's (1964) complex-order wave functions) where,

$$L_{n_\nu}^m = -\frac{E_o\, r_1\, k_1\, h_{n_\nu}^{(1)}(k_1\, r_1)}{n_\nu (n_\nu + 1)\, P_{n_\nu}^m(\cos\theta_o)\, N_{n_\nu}(k_1\, a)} \qquad (6)$$

$$N_{n_\nu}(k_1\, a) = \int_{k_1 a}^{\infty} \left[h_{n_\nu}^{(1)}(k_1\, r)\right]^2 d(k_1\, r) \qquad (7)$$

$d(r_1)$ = delta-function source (8)

and $H_r^{app} = H_o\, d(r_1) \exp(j\omega t) \sin m\phi$ (9)

which can also be expanded in terms of the complex-order wave functions.

Applying the boundary conditions that the tangential components E_r, $E\phi$, H_r, and $H\phi$ are continuous at $\theta = \theta_1$, by equating the applied electric and magnetic fields E_r^{app} and H_r^{app} to E_r and H_r respectively at $\theta = \theta_o$, and by making use of the orthogonal properties of the spherical Hankel functions, result in an infinite number of equations for the solution of the amplitude coefficients occurring in the expressions for the field components.

For the symmetric as well as the unsymmetric waves, there result six sets of independent equations for six sets of unknown coefficients, and hence it is possible to have a unique solution.

4. TE and TM Waves

Proceeding in a similar manner to that of hybrid waves, it can be shown for both unsymmetric TM and TE waves, there result four sets of independent equations for three sets of unknown coefficients, while for both symmetric TM and TE waves, there are three sets of independent equations for three sets of unknown coefficients. This shows that there is a unique solution for the field components only for the symmetric TE and TM modes and none for the unsymmetric modes.

5. Conclusion

It has been shown that a semi-infinite dielectric-coated spherically tipped perfectly conducting cone can radiate only the symmetric TE and TM modes, but can radiate both the symmetric and unsymmetric hybrid modes.

6. References

Adachi, S., R. G. Kouyoumjian, and R. G. Van Sickle (Dec. 1959), The finite conical antenna, IRE Trans. AP-7, S406-S411.

Bailin, L L., and S. Silver (1956), Exterior electromagnetic boundary value problems for spheres and cones, IRE Trans. AP-4, No. 1, 5-16.

Felsen, L. B. (1957), Plane wave scattering by small angle cones, IRE Trans. AP-5, No. 1, 121-129.

Sommerfeld, A. (1964), Partial Differential Equations (Academic Press, New York, N. Y.).

Wait, J. R. (1969), Electromagnetic radiation from conical structures, Chapter No. 12, in Antenna Theory, ed. by R. E. Collin and F. J. Zucker (McGraw-Hill Book Co., Inc., New York, N. Y.).

Yeh, C. (1964), An application of Sommerfeld's complex-order wave functions to antenna problem, J. Math. Phys. 5, No. 3 344-350.

ELECTROMAGNETIC COUPLING OF HORIZONTAL LOOPS OVER A STRATIFIED GROUND

Herbert Kurss

Institute for Telecommunication Sciences, ESSA
Boulder, Colorado 80302

and

Department of Mathematics, Adelphi University,
Garden City, N. Y. 11530, USA

Abstract. The primary and secondary fields due to a thin horizontal circular loop of uniform current over a stratified ground are found as the superposition of cylindrical modes. The voltage induced in a second horizontal circular loop is then expressed as a single definite integral. These results are shown to generalize and unify related results of Slichter, Havelock, Foster, and Wait.

This paper was motivated by a need to measure the electrical properties of the ground at frequencies in the range of 1 MHz. With this in mind, it was deemed desirable to develop formulae for the self and mutual impedance of loops close to the ground. This goal is achieved here for horizontal circular loops over a vertically stratified ground. The primary loop current is assumed to have no angular variation (the angle being measured from the center of the loop). This is quite reasonable at 1 MHz, since the free space wavelength of 300 m is then large compared with the size of any physical loop.

In free space the electromagnetic field of a circular loop of radius a centered at the origin and with a uniform current I can be expressed in terms of a vector potential which has only a ϕ-component. If A denotes this component then

$$A = \frac{\mu a I}{2} \int_0^\infty J_1(ta)\, J_1(t\rho)\, \frac{\exp(-u_1 |z|)}{u_1} t\,dt \qquad (1)$$

where

$$u_1 = (t^2 - k^2)^{\frac{1}{2}},$$

and

$$k^2 = \omega^2 \mu \epsilon .$$

Variants of (1) have been given by Slichter (1933), Wait (1954), and others.

In the absence of a ground the mutual impedance, Z_1, between the above loop and a second horizontal loop of radius b and centered at $z = -d$, $\rho = c$, $\varphi = \pi$ is then shown to be

$$Z_1 = j\omega\mu\pi ab \int_0^\infty J_1(ta)\, J_1(tb)\, J_0(tc)\, \exp(-u_1 d)\, \frac{tdt}{u_1} . \qquad (2)$$

The static limit of (2) for co-axial loops, i.e., $u_1 = t$ and $c = o$, was derived by Havelock (1908). The resistive component of (2) for coincident loops, i.e., $c = d = o$ and $a = b$, was derived by Foster (1944).

The effect of the ground at $z = -h$, with $h > d$, is to add to Z_1 an additional impedance

$$Z_2 = j\omega\mu\pi ab \int_0^\infty R(t)\, J_1(ta)\, J_1(tb)\, J_0(tc) \exp(-u_1(2h-d)) \frac{tdt}{u_1} \qquad (3)$$

where R(t) is the reflection coefficient of the ground. In particular, if the ground is homogeneous

$$R = \frac{u_1 - u_2}{u_1 - u_2} \qquad (4)$$

where

$$u_2 = \sqrt{t^2 - k_2^2}$$

and k_2 is the propagation constant of the ground.

A particularly important special case of (3) and (4) is when the loops coincide (so that $a = b$ and $c = d = o$) and when k is small compared with $|k_2|$ (so that it is a good approximation to set $u_1 = t$). Separating (3) into its resistive and reactive components one then obtains

$$Z_2 = R_2 + jX_2$$

with

$$R_2 \simeq -\omega\mu\pi a^2 \int_0^\infty I_m\left(\frac{t-u_2}{t+u_2}\right) J_1^2(ta)\exp(-2ht)\,dt$$

$$X_2 \simeq \omega\mu\pi a^2 \int_0^\infty R_e\left(\frac{t-u_2}{t+u_2}\right) J_1^2(ta)\exp(-2ht)\,dt.$$

In all of the above formulae the replacement of $J_1(ta)$ by the first term of its small argument expansion, i. e.,

$$J_1(ta) \simeq ta/2,$$

simply corresponds to the customary dipole approximation of a loop.

ACKNOWLEDGMENT

The author expresses his deep appreciation to D. D. Crombie for suggesting the problem and for his encouragement, interest, and many helpful discussions.

REFERENCES

Foster, D. (1944), Loop antennas with uniform current, Proc. IRE 32, No. 10, 603-607.

Havelock, T. H. (1908), On certain Bessel integrals and the coefficients of mutual induction of coaxial coils, Phil. Mag. 15, 332-345.

Slichter, L. B. (1933), An inverse boundary value problem in electrodynamics, Physics 4, 411-418.

Wait, J. R. (1954), Mutual coupling of loops lying on the ground, Geophysics 19, 290-296.

QUASI-STATIC FIELDS OF SUBSURFACE HORIZONTAL ELECTRIC ANTENNAS

Peter R. Bannister

U. S. Navy Underwater Sound Laboratory, New London, Conn. 06320

Abstract: The horizontal electric field components produced by a horizontal electric dipole (HED) antenna, located at or below the surface of a plane, conducting, homogeneous earth are presented for the quasi-static range. Expressions for the field components produced by a finite length horizontal electric antenna, which have been derived by employing image theory, are also presented.

1. Introduction

Interest in the determination of the quasi-static fields of antennas located within or above a plane, conducting, homogeneous earth has increased in recent years. (In the quasi-static range, the measurement distance is much less than a free-space wavelength but comparable to an earth skin depth $\delta \approx (2/\omega \mu_0 \sigma)^{1/2}$.) Quasi-static fields are utilized in the induction methods of geophysical prospecting, which are discussed in considerable detail by Keller and Frischknecht (1966) and Vanyan (1967). They are also employed in determining the coupling between power lines and other nearby circuits, and for low-frequency, short-range, radio propagation purposes.

In section 2, the field-component expressions are presented for the situation in which both the HED and the receiving antenna are located below the earth's surface (h and $z < 0$). When the HED is buried and the receiving antenna is elevated, the resulting integrals cannot be expressed conveniently in closed form (Bannister, 1967). However, if the depth of burial is small compared to δ, image theory may be employed. The image theory results for a finite length, horizontal electric antenna are presented in section 3.

2. HED Field-Component Expressions for the Subsurface to Subsurface Propagation Case

The HED, of infinitesimal length dl, is oriented in the x direction and is situated at depth h ($h < 0$) with respect to a cylindrical coordinate system (ρ, ϕ, z). The earth occupies the lower half-space ($z < 0$) and the air occupies the upper

half-space ($z > 0$). MKS units are employed and a suppressed time factor of $e^{i\omega t}$ is assumed.

The complicated field-component expressions for the HED subsurface to subsurface propagation case may be derived by following the procedure outlined by Wait (1961). For example, the horizontal electric field-component expressions are given by

$$E_\rho \approx \frac{I\,d\,l\cos\phi}{2\pi\sigma R_1^3}\left\{\frac{R_1^3\,e^{-\gamma R_0}}{2R_0^3}\left[\left(\frac{3\rho^2}{R_0^2}-1\right)(1+\gamma R_0)-\gamma^2(z-h)^2\right]\right.$$

$$-\frac{(z+h)^2\,e^{-\gamma R_1}}{2R_1^2}\left[3+3\gamma R_1+\gamma^2 R_1^2\right] \qquad (1)$$

$$\left.+\frac{\gamma R_1}{2}\left[S^+-\frac{(z+h)\,S^-}{R_1}+\gamma(z+h)\,T^-\right]\right\},$$

$$E_\phi \approx \frac{I\,d\,l\sin\phi}{2\pi\sigma R_1^3}\left[\frac{R_1^3\,e^{-\gamma R_0}}{2R_0^3}(1+\gamma R_0+\gamma^2 R_0^2)-\frac{e^{-\gamma R_1}}{2}\left\{\left[1-\frac{2(z+h)^2}{R_1^2}\right]\right.\right.$$

$$(3+3\gamma R_1+\gamma^2 R_1^2)\Big\}+\frac{\gamma R_1}{2}\left\{\left[2-\frac{3(z+h)^2}{R_1^2}\right]S^+-\frac{(z+h)}{R_1}\left[2-\frac{3(z+h)^2}{R_1^2}\right.\right. \qquad (2)$$

$$\left.\left.\left.+\gamma^2\rho^2\right]S^-+\gamma(z+h)\left(T^+-\frac{3\rho^2\,T^-}{R_1^2}\right)\right\}\right],$$

where $S^+ = I_0K_1 + I_1K_0$, $S^- = I_0K_1 - I_1K_0$, $T^+ = I_1K_1 + I_0K_0$, $T^- = I_1K_1 - I_0K_0$,

$R_0 = [\rho^2 + (z-h)^2]^{1/2}$, $R_1 = [\rho^2 + (z+h)^2]^{1/2}$, and $\gamma \approx (i\sigma\mu_0\omega)^{1/2}$.

Computing numerical results for the subsurface to subsurface field-component expressions is a lengthy and complicated process, but some results have been obtained. One method of obtaining numerical results has recently been discussed by Atzinger, Pensa, and Pigott (1966).

When $R_1 << \delta$, the field-component expressions reduce to results consistent with potential theory. Furthermore when $\rho >> \delta$ and $\rho >> |z+h|$, they reduce to previously derived results.

3. Image Theory Field Component Expressions for a Finite Length Horizontal Electric Antenna

It is well known that the fields produced by a current carrying wire, when placed at height h over a perfectly conducting earth, may be represented by the combined fields of the wire and its image. If the finitely conducting earth is replaced with a perfectly conducting earth, standard image theory may be used to locate the antenna image depth. Ball, Maxwell, and Watt (1966) have shown that when $h << \delta$, the (complex) image depth d for the low frequency case is equal to $-(2/\gamma) = \delta(1 - i)$, where $|d| = \sqrt{2}\,\delta$. Haberland (1926) arrived at an approximate expression for d when he was determining the mutual inductance between two single-wire lines with earth return. Haberland's result ($|d| \approx 1.18\sqrt{2}\,\delta$), is very similar to Ball, Maxwell, and Watt's result.

By employing Ampere's law, the approximate expressions for the field components produced by a finite length horizontal electric antenna for the surface to air propagation case ($h = 0, z \geq 0$) may be expressed as

$$E_x \approx -\frac{i\omega\mu_0 I}{4\pi}\left\{ln\left[\frac{R_{11} - (x + L/2)}{R_{21} - (x + L/2)}\right] - ln\left[\frac{R_{12} - (x - L/2)}{R_{22} - (x - L/2)}\right] + \frac{d^2}{2}\left[\frac{(x + L/2)}{R_{21}^3} - \frac{(x - L/2)}{R_{22}^3}\right]\right\} \quad (3)$$

$$E_y \approx -\frac{Iy}{2\pi\sigma}\left[\frac{1}{R_{21}^3} - \frac{1}{R_{22}^3}\right] \quad (4)$$

$$E_z \approx \frac{i\omega\mu_0 I}{4\pi}\left\{ln\left[\frac{R_{11} - (z + d)}{R_{21} - z}\right] - ln\left[\frac{R_{12} - (z + d)}{R_{22} - z}\right] - \frac{d^2 z}{2}\left[\frac{1}{R_{21}^3} - \frac{1}{R_{22}^3}\right]\right\} \quad (5)$$

$$H_x \approx \frac{Iy}{4\pi}\left\{\frac{1}{[(x - L/2)^2 + y^2]}\left[\frac{z + d}{R_{12}} - \frac{z}{R_{22}}\right] - \frac{1}{[(x + L/2)^2 + y^2]}\left[\frac{z + d}{R_{11}} - \frac{z}{R_{21}}\right]\right\} \quad (6)$$

$$H_y \approx \frac{I}{4\pi}\left\{\frac{(z + d)}{[y^2 + (z + d)^2]}\left[\frac{(x + L/2)}{R_{11}} - \frac{(x - L/2)}{R_{12}}\right] - \frac{z}{(y^2 + z^2)}\left[\frac{(x + L/2)}{R_{21}} - \frac{(x - L/2)}{R_{22}}\right]\right.$$
$$\left. - \frac{(x - L/2)}{[y^2 + (x - L/2)^2]}\left[\frac{z + d}{R_{12}} - \frac{z}{R_{22}}\right] + \frac{(x + L/2)}{[y^2 + (x + L/2)^2]}\left[\frac{z + d}{R_{11}} - \frac{z}{R_{21}}\right]\right\} \quad (7)$$

and

$$H_z \approx -\frac{Iy}{4\pi}\left\{\frac{1}{[y^2+(z+d)^2]}\left[\frac{(x+L/2)}{R_{11}}-\frac{(x-L/2)}{R_{12}}\right]-\frac{1}{(y^2+z^2)}\left[\frac{(x+L/2)}{R_{21}}-\frac{(x-L/2)}{R_{22}}\right]\right\} \quad (8)$$

where $R_{11}=[(x+L/2)^2+y^2+(z+d)^2]^{1/2}$ $\quad R_{21}=[(x+L/2)^2+y^2+z^2]^{1/2}$

$R_{12}=[(x-L/2)^2+y^2+(z+d)^2]^{1/2}$ $\quad R_{22}=[(x-L/2)^2+y^2+z^2]^{1/2}$

$d = (2/\gamma) = \delta(1-i)$

These expressions are also valid for the subsurface to air propagation case when the source is buried at shallow depths (i.e., $|h| \ll \delta$). In these expressions when z appears along (i.e., not as z+d), z must be replaced by $z+|h|$.

When z = 0 and either x or y = 0, the magnetic field-component expressions (6) - (8) reduce to Ball, Maxwell, and Watt's results (1966). When the measurement distance is much greater than the source length L, the above equations (3) - (8) reduce to the image theory HED expressions. Furthermore, when L is much greater than the measurement distance, they reduce to the image theory horizontal line source equations. Moreover, when the measurement distance or L is much greater or much less than δ , the image theory results are consistent with the analytical results.

As a further example of the simplicity of the image theory results, consider the expressions for the electric field component produced by a long horizontal line source for the surface to air propagation case. The analytical expression is

$$E_x \approx -\frac{i\omega\mu_0 I}{2\pi}\left\{\frac{\pi}{2\beta_+}[H_1(\beta_+)-Y_1(\beta_+)]-\frac{2(z^2-y^2)}{y^2r^4}+\frac{\pi}{2\beta_-}[H_1(\beta_-)-Y_1(\beta_-)]\right\} \quad (9)$$

where $H_1(\beta)$ is the struve function of order one, $Y_1(\beta)$ is the Bessel function of the second kind of order one, and $\beta_\pm = \gamma(z \pm iy)$.

The image theory result for this case is

$$E_x \approx -\frac{i\omega\mu_0 I}{2\pi} ln \sqrt{\frac{y^2+(d+z)^2}{y^2+z^2}} \quad (10)$$

A comparison of (9) and (10) reveals that the image theory result is in very good agreement with the analytical result throughout the quasi-static range.

Image theory may also be employed when the height h of the source above the earth is not much less than δ . For this case, the image depth is not d but d+h.

It is the author's opinion that image theory can be extended to include many other cases of quasi-static range propagation and thus provide results (of simple form) even for cases in which the field components cannot be expressed in closed form analytically.

4. References

Atzinger, E. E., A. F. Pensa, and M. T. Pigott (1966), On the application of a calculation by Wait and Campbell: The fields of an oscillating magnetic dipole immersed in a semi-infinite conducting medium, J. Geophys. Res. 71, No. 23, 5765-5769.

Bell, L., E. L. Maxwell, and A. D. Watt (1966), The approximate magnetic fields near a horizontal electric dipole over a conducting earth, Westinghouse Electric Corp., Boulder, Colorado (private communication).

Bannister, P. R. (1967), Quasi-static fields of dipole antennas located above the earth's surface, Radio Sci. 2 (New Series), No. 9, 1093-1103.

Haberland, G. (1926), Theorie der Leiting von Wechselstrom durch die Erde, Zeitschr. f. agnew. Math. u. Mech. 6, 336-379. See also E.T.Z. 48, 456-460, 127.

Keller, G. V. and F. C. Frischknecht (1966), Electrical Methods in Geophysical Prospecting, (Pergamon Press, Oxford).

Vanyan, L. L. (1967), Electromagnetic Depth Soundings, (Consultants Bureau, N. Y.), (translated from the Russian by G. V. Keller).

Wait, J. R. (1961), The electromagnetic fields of a horizontal dipole in the presence of a conducting half-space, Can. J. Phys. 39, 1017-1028.

MAGNETIC FIELD EXCITED BY A LONG HORIZONTAL WIRE ANTENNA NEAR THE EARTH'S SURFACE

David B. Large and Lawrence Ball

Georesearch Laboratory
Westinghouse Electric Corporation
Boulder, Colorado

ABSTRACT

The problem considered is the calculation of the magnetic field excited by a horizontal line source of electric current placed upon or near the earth's surface. The length of the line is arbitrary, but emphasis is placed upon observer ranges at which ionospheric effects may be neglected, and which are of the order of, or less than, a free-space wavelength. The approach to the problem is partially analytical and partially numerical, and represents an assimilation of recent results obtained by Wait and Bannister for infinitesimal dipoles and infinite lines. Some numerical results for long lines operating at 10, 300, and 1,000 Hz are presented, and some of the differences between these solutions and the corresponding dipole and infinite-line solutions are illustrated.

The electromagnetic field excited by a long, horizontal wire antenna (HWA) placed upon or near the earth's surface has application in several problems of geophysics. The frequencies normally range between ten and a few thousand Hertz. The research discussed in this paper was instigated to develop the capability of predicting the total magnetic field excited by a HWA of arbitrary length placed upon or near a homogeneous earth of arbitrary conductivity, with the observer being unrestricted in range and azimuth. The frequencies considered fall between 10 and 2,000 Hz, and an extensive set of calculations for a 30 km HWA operating at 10, 300, and 1,000 Hz have been carried out. The analysis is computer oriented, with the field components often being obtained by numerical integration of the dipole expressions developed over the past ten years by Wait (1961) and Bannister (1966, 1967).

An example calculation of the radial magnetic field component excited by a 30 km HWA is shown in Figure 1, in which ρ is the range to the center of the line, and ϕ is the observer's azimuth measured from the antenna axis, and the amplitude scale is in decibels relative to 1 amp/m. In addition to the results for long antennas with the observer being on the ground, calculations have been carried out for observation points above the ground, and for elevated antennas. These results have been used to develop simple criteria for determining when the height of the antenna above ground may be neglected, as well as for determining at what ranges a line source will appear effectively infinite in length. One interesting conclusion relative to the latter criteria is that, under certain circumstances, a long HWA may never appear effectively infinite, no matter how close the observer moves to the line.

Figure 2 is an example of a second set of calculations which compare the magnetic field components excited by finite length antennas, infinitely long antennas, and infinitesimal dipoles. In this figure. the observer is broadside to the source ($\phi = 90°$), and the range ρ is measured relative to an origin at the center of the 2,000 m antenna. Results of this type have been used to develop simple criteria for determining at what minimum range a given HWA may be adequately represented as a point (dipole) source.

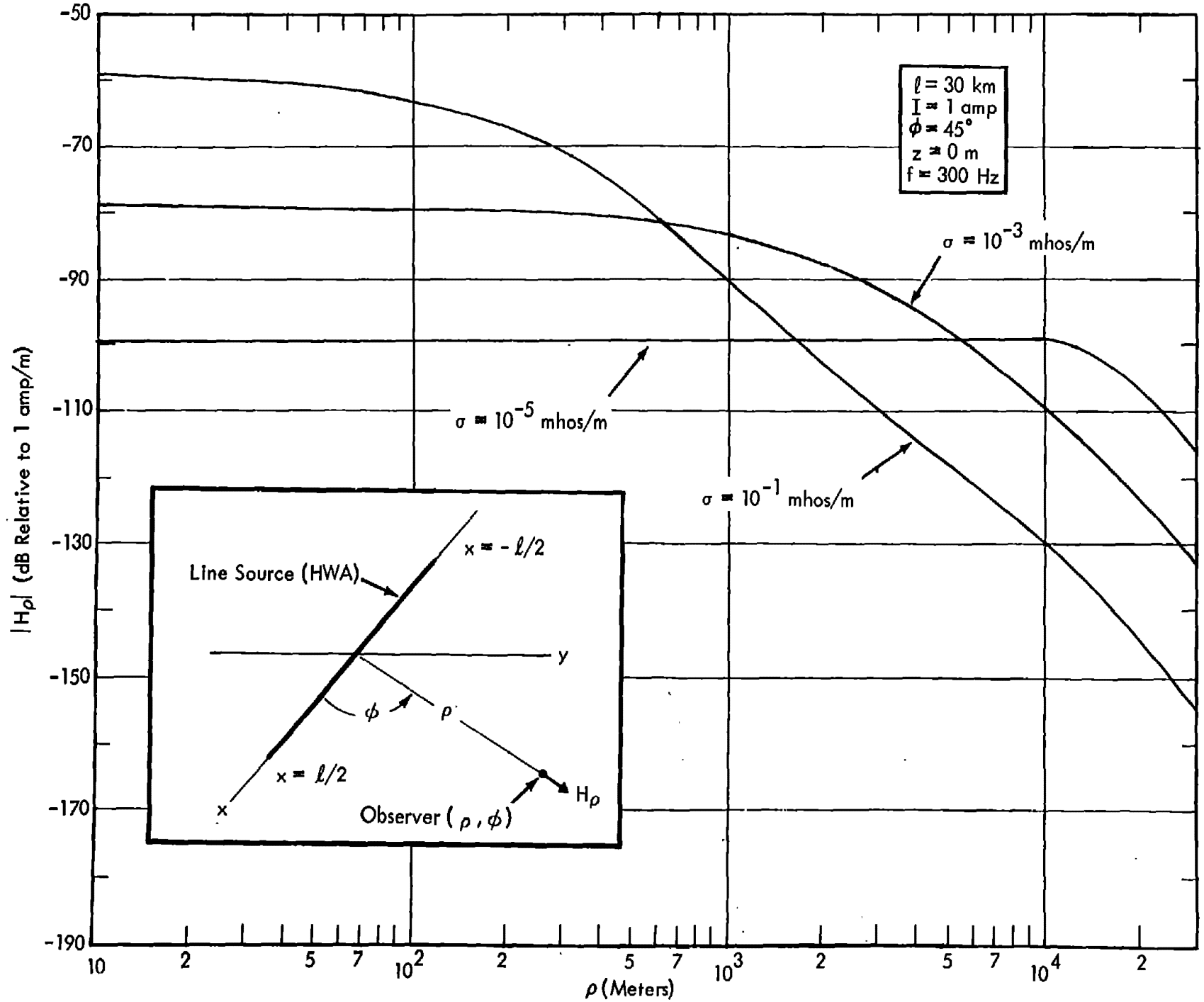
-50
-70
-90
-110
-130
-150
-170
-190
$|H_\rho|$ (dB Relative to 1 amp/m)
10
2
5
7
10^2
2
5
7
10^3
2
5
7
10^4
2
ρ (Meters)
ℓ = 30 km
I = 1 amp
ϕ = 45°
z = 0 m
f = 300 Hz
$\sigma = 10^{-3}$ mhos/m
$\sigma = 10^{-5}$ mhos/m
$\sigma = 10^{-1}$ mhos/m
Line Source (HWA)
$x = -\ell/2$
$x = \ell/2$
x
y
ϕ
ρ
H_ρ
Observer (ρ , ϕ)

Figure 1

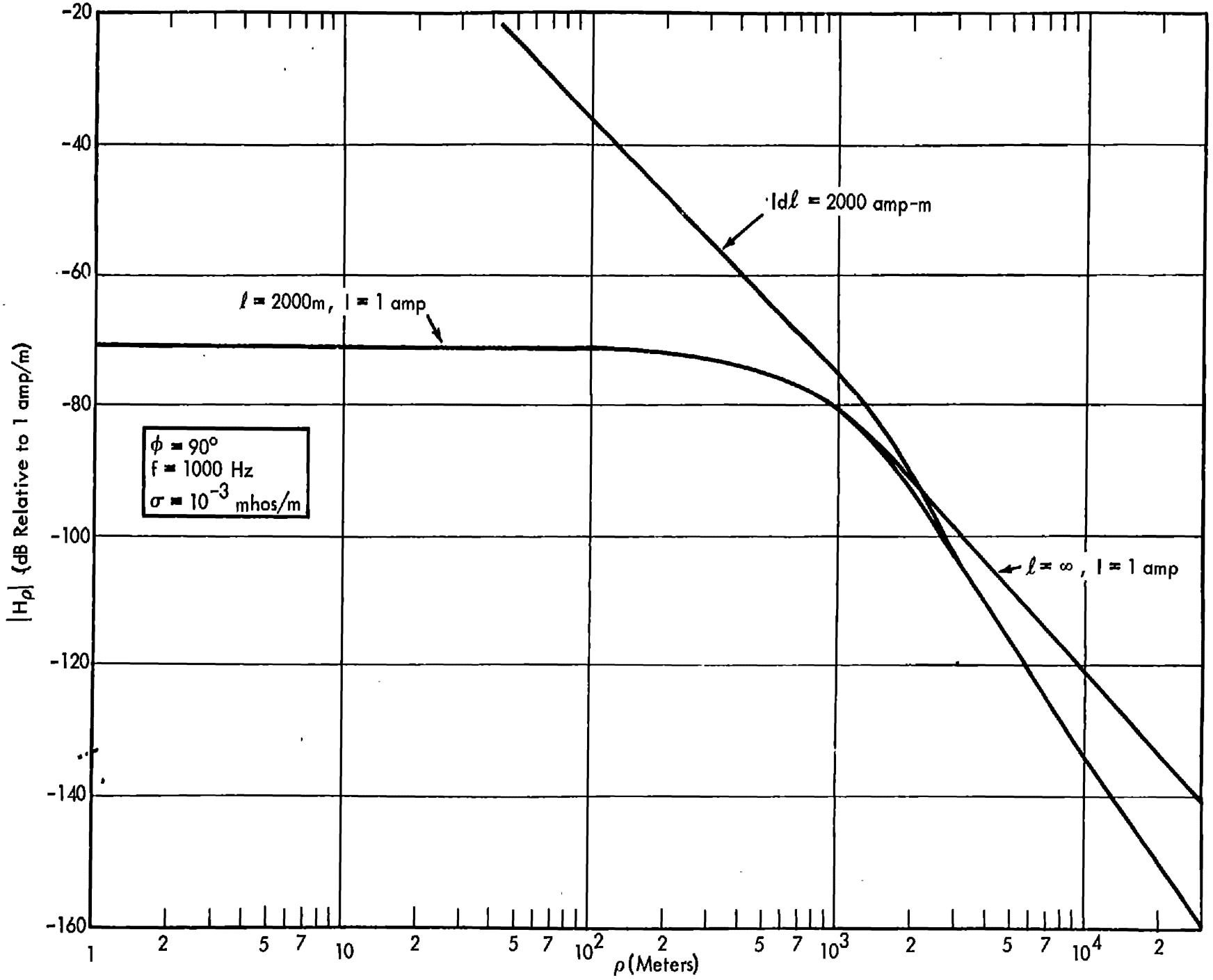
-20
-40
-60
-80
-100
-120
-140
-160
$|H_\rho|$ (dB Relative to 1 amp/m)
$Id\ell$ = 2000 amp-m
ℓ = 2000m, I = 1 amp
$\ell = \infty$, I = 1 amp
ϕ = 90°
f = 1000 Hz
$\sigma = 10^{-3}$ mhos/m
1
2
5
7
10
2
5
7
10^2
2
5
7
10^3
2
5
7
10^4
2
ρ (Meters)

Figure 2

REFERENCES

Wait, J. R. (1961), The electromagnetic fields of a horizontal dipole in the presence of a conducting half-space, Can. J. Phys. 39, 1017-1028.

Bannister, P. R. (1966, Quasi-static fields of dipole antennas on the earth's surface, Radio Sci. 1 (New Series), No. 11, 1321-1330.

Bannister, P. R. (1967), The quasi-near fields of dipole antennas, IEEE Trans. AP, 15, No. 5, 618-626.

NUMERICAL ANALYSIS OF AIRCRAFT ANTENNAS by E. K. Miller, J. B. Morton, G. M. Pjerrou, & B. J. Maxum, MBAssociates, San Ramon, California

ABSTRACT. A numerical method for predicting the performance of an antenna on an aircraft is discussed. The basic features of the approach, which is based on a collocation solution to the thin-wire integral equation, are described. Several numerical examples, including the radiation pattern for the OH-6A helicopter, are presented.

I. INTRODUCTION. Evaluating the performance of antennas on an irregularly shaped conducting body such as an airdraft is now done almost exclusively by experimentation. Models are used for experimental antenna measurements, but because discrepancies may arise, final evaluation often requires use of the actual aircraft.

A reliable analytic method for the parametric study of antenna performance would be an important aid to experimentation, allowing concentration of measurements on the most fruitful areas. The numerical approach used here employs the thin-wire approximation to the electric field integral equation, since this equation can be used both for thin wire structures and solid surfaces modeled by thin wire grids (Richmond, 1966). The integral equation is solved by collocation using sinusoidal interpolation to expand the current on each structure segment (Mei, 1965). The interpolation requires two extra constants, which are found by a current-matching technique, while the required numerical integration uses the Romberg variable interval width technique (Miller and Burke, 1969), and the Gauss-Doolittle method is used to solve the linear system. For large systems, the original structure matrix and its inverse are stored on tape for later re-use. The technique is restricted to structures a few square wavelengths in surface area, but continued progress both in numerical methods and computer development will extend its application to larger, more complex structures.

II. NUMERICAL RESULTS. In Figure 1 is shown the backscatter radar cross section (RCS) of two coaxial-coplanar rings for axial incidence as a function of the outer ring circumference-to-wavelength ratio. Experimental data taken on the MBA Rail Line Range is shown, together with computed results found by the thin-wire approach and by modeling the rings with 16-sided regular polygons. The calculated RCS values correctly predict the antiresonance.

In Figure 2 is shown an experimental-numerical comparison of the backscatter RCS of a 14.57λ straight wire as a function of the angle of the wave incidence measured from a normal to the wire. The wire was modeled with 100 segments, or about 7 segments per wavelength. (Extensive experience shows that 6 segments per wavelength provides an accurate numerical result, although the best segmentation for efficiency and accuracy is structure-dependent.) Experiment and theory agree well, even to RCS values 40 dB below the broadside maximum.

Application of the numerical method to radiation problems is shown in Figure 3, where the element power distribution and radiation patterns of a 12-element log-periodic dipole antenna array are shown. The successive array elements increase in size by 1.07 and are separated by 0.7 of the longer element length, with the longest element 0.6456λ long. The MBA numerical results agree well with the results of Cheong and King (1968).

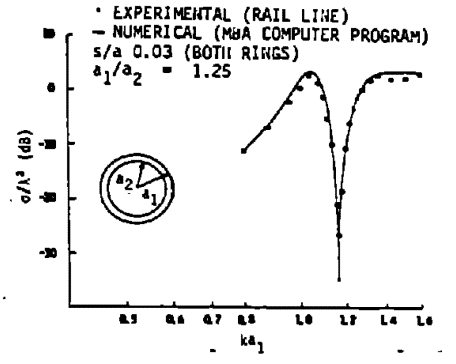

FIGURE 1

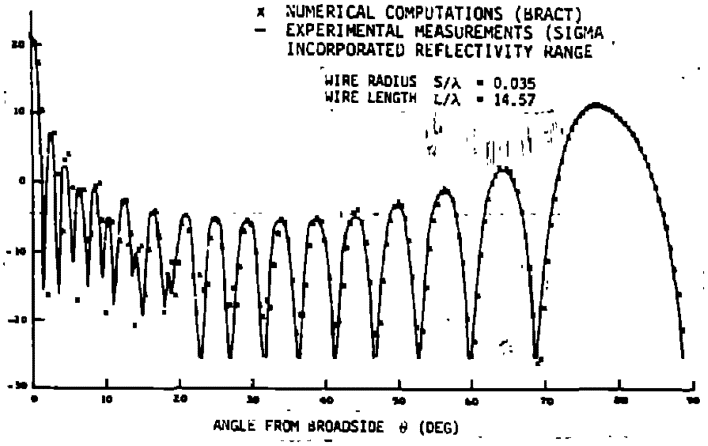

FIGURE 2

Using the thin-wire integral equation to study the aircraft-antenna combination requires modeling a solid, possibly curved, conducting surface by a wire grid. A parallel experimental-numerical study was carried out to determine the modeling criteria. The conclusion of this study was that a flat wire grid with openings less than $1/8\lambda$ per side adequately modeled (within 1 dB) the RCS of a solid conducting surface. A similar study determined that a circular ring 1λ in circumference is modeled to within 1 dB by a regular polygon of equal perimeter with sides of length less than $\lambda/6$.

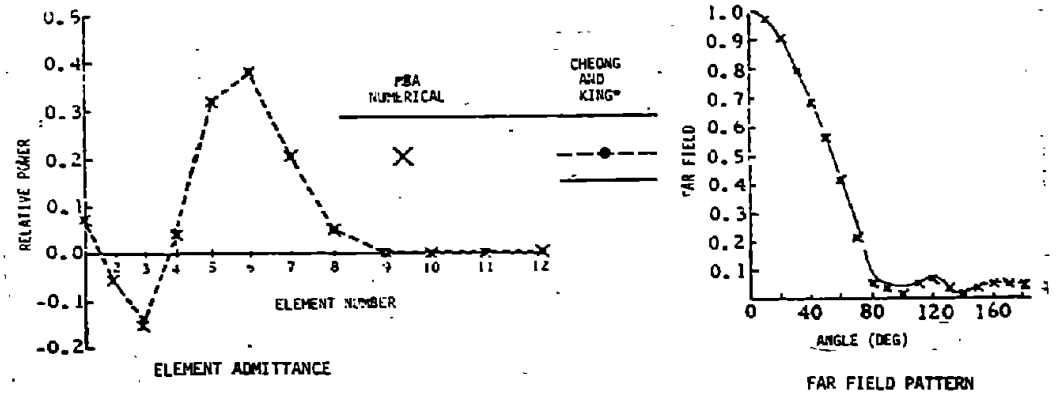

FIGURE 3

A wire-grid model of an OH-6A U.S. Army helicopter was then developed, using 202 wire segments, to provide the structure input for the numerical calculations. A maximum of 205 segments is available on the present computer without overlaying. A computer-drawn side view of the model and a scale drawing of the actual helicopter are shown in Figure 4. The primary interest here is antenna pattern prediction for the frequency range 30 to 70 MHz; the helicopter (actual length 23 ft) is

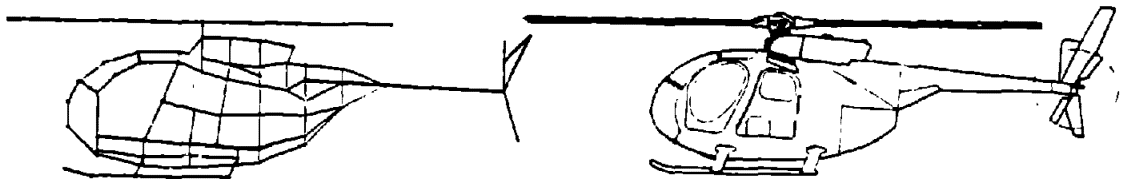

FIGURE 4

about 0.7 to 2 λ long. The average segment length varies from 0.047 to 0.11 λ over this range, while the wire thickness (which conforms to the windshield cross-brace size) varies from 0.0011 to 0.0025 λ.

The towel-bar homing antenna has been considered in the calculations. This antenna is a dielectric-sheathed, U-shaped metal rod driven alternately against the aircraft frame at one end with a matching impedance connected to the frame at the other. This generates two asymmetric patterns about the aircraft axis whose cross-over points are, ideally, axially aligned and serve to orient the aircraft relative to a homing radio transmitter. The horizontal portion of the towel bar, together with its image in the aircraft frame (these are self-cancelling), form a transmission line connecting the two vertical arms which are the effective radiators. The towel bar can be considered as two monopole antennas driven against the aircraft frame by voltages differing in phase by the electrical separation of the vertical arms plus a 180° phase shift (to account for the oppositely-directed arm currents).

The parallel electric field intensity in the plane perpendicular to the midpoint of two half-wave dipoles separated by λ/4 and driven 90° out of phase is shown in Figure 5. Also shown are corresponding results for a two-wire transmission line model of the towel bar. This model consists of a U-shaped two-wire line with a center section 0.25λ long driven by a matched impedance generator at one end and terminated in a matched impedance at the other, with gaps cut in one side of the line of each of the vertical arms. Both of these antennas are reasonable models of the corresponding monopoles and actual towel bar in the presence of the helicopter ground plane. Since their patterns are very similar, the monopole antenna and the towel bar are concluded to be equivalent.

Figure 6 presents a comparison of experimental and numerical results for the vertically polarized receiving pattern of the OH-6A helicopter for a towel bar antenna symmetrically aligned about the aircraft axis and mounted on the top horizontal windshield cross brace. The experimental pattern was taken by Collins Radio (Griffee and Robichaux, 1967) using a 1/5-scale model at an equivalent full-scale frequency of 32 MHz, while the numerical results were obtained with two monopole antennas equal in length to the vertical arms of the towel bar. The numerical pattern is the vector difference between the two monopole base currents, phase shifted by their electrical separation. The agreement between the two patterns is reasonable, although we note that at this frequency the helicopter is less than 1 λ long. These numerical results were obtained by using a total of 205 wire segments, which required omitting the finned tail section (9 segments) to gain the necessary 12 segments for the monopoles.

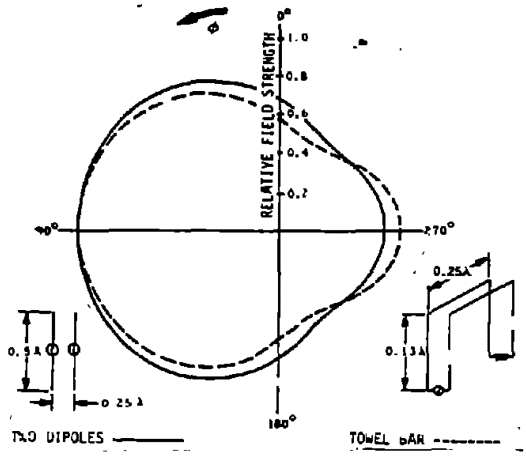

FIGURE 5

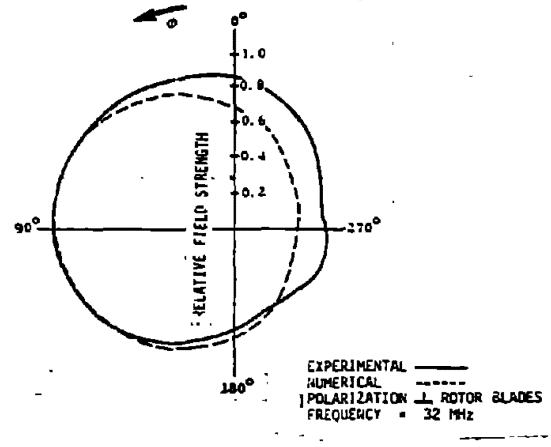

FIGURE 6

REFERENCES

Cheong and King (1968), Radio Science, 2, p. 1315.

Griffee and Robichaux (1967), Collins Radio Co. Tech. Rept. ECOM-02394-T, Dallas, Tex.

Mei (1965), IEEE Trans. Ant. Prop., AP-13, pp. 374-378.

Miller and Burke (1969), to be published in the Sept. 1969 IEEE Proc. Ant. Prop.

Richmond (1966), IEEE Trans. Ant. Prop. AP-14, pp. 782-786.

ACKNOWLEDGMENT

Research in this paper partially supported under USAECOM Contract DAAB07-68-C-0456. Helpful comments and suggestions were made by A. Eckstein of the U.S. Army Electronics Command, Fort Monmouth, and by L. Griffee and W. Robichaux of Collins Radio Co., Dallas, Tex. Appreciation is also expressed to D. Foreman of Sigma, Inc. Melbourne, Florida for supplying the 14.57λ wire RCS data.

FINITE TUBULAR ANTENNA ABOVE A CONDUCTING HALF-SPACE

by

David C. Chang

University of Colorado

ABSTRACT

The characteristics of a finite, tubular, vertical antenna over an infinite, dissipative half-space is studied. The magnitude, but not the distribution, of the antenna current is found to be greatly effected by the presence of the dissipative half-space. At certain distances above the half-space, a resonance is observed as the input conductance of the antenna reaches its maximum.

I. Introduction

The radiation of a dipole antenna in the presence of an infinitely-large, imperfectly-conducting half-space has been widely studied since 1909 (for a complete listing of references, the reader is referred to a book by Baños [1966] and review papers by Wait [1964] and Hansen [1963].) Effects of finite ground conductivity and inhomogeneity are known to have great influence on wave propagation from and the transmitting characteristics of infinitesimal Hertzian dipoles of both electric and magnetic type and were studied extensively. For higher frequency bands, however, the radio source is no longer very short both physically or electrically. Consequently, the treatment of a finite antenna instead of an infinitesimal one is inevitable. Here, we shall present a method to investigate the characteristics of a finite, vertical, tubular dipole antenna over a homogeneous, dissipative half-space.

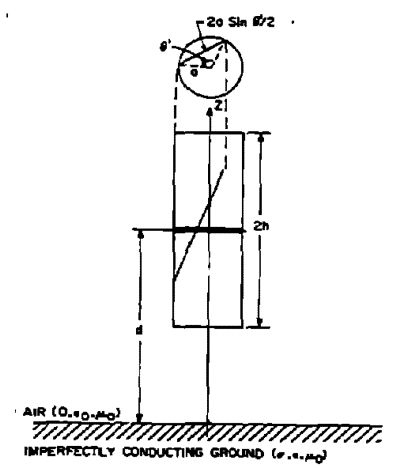

Fig. 1

2. Formulation and Numerical Solution

Consider the geometry of a finite, vertical, tubular, perfectly-conducting antenna of radius a and half-length h, located in the air at a distance d above an infinite, dissipative half-space which has a conductivity σ and a permittivity ε (Fig. 1). At the center of the antenna, a constant voltage source V is maintained across an infinitesimal gap in order to excite a current distribution on the antenna surface. From what appears in the literature, we know that the Hertzian potential in the air region for an infinitesimal, vertical, current element of unit amplitude, located at a distance z' over the half-space, is

$$\bar{p}(\rho;z,z') = p_z(\rho;z,z')\bar{a}_z$$

$$= \frac{\zeta_1}{2\pi k_1} \int_{-\infty}^{+\infty} \{\exp[i\gamma_1(z_<-z_>)] + M(\lambda)\exp[i\gamma_1(z_>+z_<)]\}$$

$$\cdot H_o^{(1)}(\rho\lambda)\ \frac{\lambda d\lambda}{\gamma_1}\ , \qquad (1)$$

where $\bar{M}(\lambda)=(\gamma_1 k_2^2 + \gamma_1 k_1^2)^{-1}(\gamma_1 k_2^2 - \gamma_2 k_1^2)$,

$$\gamma_{1,2} = (k_{1,2}^2 - \lambda^2)^{1/2} \quad ; \quad 0 \le \arg(\gamma_1,\gamma_2) \le \pi,$$

$$k_1 = \omega\sqrt{\mu_o\varepsilon_o} \quad ; \; k_2 = i\omega\mu_o(\sigma - i\omega\varepsilon) \quad ; \; \zeta_1 = 120\pi\,\text{ohm},$$

$z_{\gtrless} = \begin{matrix}\text{larger}\\ \text{smaller}\end{matrix}$ value of (z,z') and $\bar{a}_z$ is a unit vector along $\bar{z}$-direction, for a time factor $\exp(-i\omega t)$. By superposition of all current sources which are uniformly distributed on the antenna surface, we obtain the total Hertzian potential as

$$\pi_z(\rho,z)\bar{a}_z = \frac{1}{2\pi}\int_{-h}^{+h} dz' \int_0^{2\pi} d\theta'\ I_z(z')\bar{p}\left(r(\rho,\theta');z,z'\right), \qquad (2)$$

where $r(\rho,\theta') = (\rho^2 + a^2 - 2\rho a\cos\theta')^{1/2}$ and $I_z(z')$ is the undetermined total current distribution on the antenna surface. Since the boundary condition on the

surface requires the tangential electric field to vanish except at the excitation gap, we have

$$E_z(a,z) = \left(\frac{d^2}{dz^2} + k_1^2\right)\pi_z(a,z) = -V\delta(z-d); \qquad -h+d \le z \le h+d. \tag{3}$$

The solution of (3) is readily known as

$$\pi_z(a,z) = C_1' \cos k_1 z + C_2' \sin k_1 z + V/(2k_o)\sin k_1|z-d|; \qquad -h+d \le z \le h+d. \tag{4}$$

Now, comparing (2) with (4) and after some arrangements, we can obtain a normalized integral for the unknown current distribution $I_z(z)$:

$$\int_0^{2H} I_z(Z)K(Z,Z')dZ' = \frac{i4\pi}{\zeta_1}\left[C_1 \cos Z + C_2 \sin Z + \frac{V}{2}\sin|Z-H|\right]; \qquad 0 \le Z \le 2H, \tag{5}$$

where

$$K(Z,Z') = i\int_0^{\infty} \{\exp[i\gamma_1'(Z_>-Z_<)]+\bar{M}(\lambda) \cdot \exp[i\gamma_1'(2H+2D-Z_>-Z_<)]\}\, J_o^2(\lambda A)\,\frac{\lambda d\lambda}{\gamma_1'}, \tag{6}$$

$$\bar{M}(\lambda) = (n^2\gamma_1'+\gamma_2')^{-1}(n^2\gamma_1'-\gamma_2'); \quad n = k_2/k_1,$$

$$\gamma_1' = (1-\lambda^2)^{1/2}\ ;\ \gamma_2' = (n^2-\lambda^2)^{1/2}\ ;$$

$$0 \le \arg(\gamma_1',\gamma_2') \le \pi,$$

and $Z = k_1(h+d-z)$, $A = k_1 a$, $H = k_1 h$. The two unknown constants C_1 and C_2 are some combination of C_1' and C_2' which can be determined by the end-condition: $I_z(z=0,H) = 0$.

To find the numerical solution of (5), we first approximate $I_z(Z)$ by a parabolic function over each

small segment $U_{2n-1} \le Z \le U_{2n+1}$ where $U_m = (m-1)\Delta$ and $\Delta = H/(2N)$, for $n = 1,2 \ldots 2N$. By matching both sides of (5) at sample points $z = U_K$, $K = 1,2,\ldots 4N+1$, we can obtain 4N+1 algebraic equations. But because the end-condition imposes $I(z=U_1)$ and $I(z=U_{4N+1})$ to vanish, we have 4N+1 unknown, including C_1 and C_2, in these equations:

$$\sum_{m=1}^{4N+1} \beta_{K,m} I_z(U_m) = \frac{i2\pi V}{\zeta_1} \sin|U_K - H|; \quad K = 1,2,\ldots 4N+1 \quad (7)$$

where $I_z(U_1)$ and $I_z(U_{4N+1})$ have been redefined as C_1 and C_2, respectively. Hence, the value of I_z at sample points are obtained by a matrix inversion. Except for m=1 and 4N+1, the matrix elements $\beta_{K,m}$ are found to be some combination of the following moment functions:

$$\mu^{(1)}(m,s) = i \int_0^1 e^{+i(m-1)\Delta\lambda} g_s(-i\lambda\Delta) J_o^2(\gamma_1' A) d\lambda + \int_0^\infty e^{-(m-1)\Delta\lambda} g_s(\lambda\Delta) J_o^2(A\sqrt{1+\lambda^2}) d\lambda; \quad m=0,1,\ldots 4N-1 \quad (8)$$

$$\mu^{(2)}(m,s) = i \int_0^1 e^{+i(2H+2D-m\Delta-\Delta)} g_s(-i\lambda\Delta) \bar{M}(\gamma_1') J_o^2(\gamma_1' A) d\lambda + \int_0^\infty e^{-(2H+2D-m\Delta-\Delta)\lambda} g_s(\lambda\Delta) \bar{M}(\sqrt{1+\lambda^2}) J_o^2(A\sqrt{1+\lambda^2}) d\lambda; \quad m=1,2,\ldots 8N-1 \quad (9)$$

where s = 1,2,3 and $g_s(x)$ is some smooth function which approaches to $1/\lambda$ as $\lambda \to \infty$. Notice that the second integrand in both (8) and (9) decays exponentially as $\lambda \to \infty$ for m>1 and is suitable for numerical evaluation. For m=1, the second integration should be truncated at λ_c, where λ_c is the larger value of 20/A and $5/\lambda\Delta$. Leading term in the integrand from λ_c to ∞ which contribute to the the integral, can be evaluated analytically from its asymptotic expression.

3. Discussions

Fig. 2 shows the total current of a center-fed antenna of $a = 0.1\lambda_o$ and $h = 0.2\lambda_o$, over a wet-earth at 100 MHz. Due to the intrinsic characteristic of the non-physical excitation, the imaginary current becomes increasingly capacitive at the feeding point. Away from z = 0, both the magnitude and the distribution of the

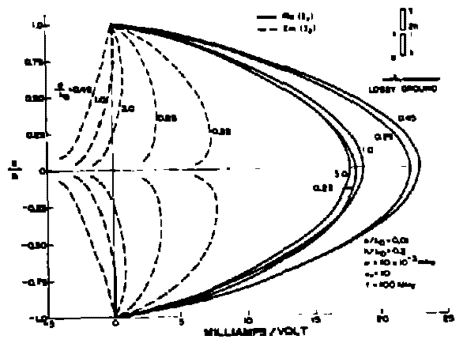

Fig. 2

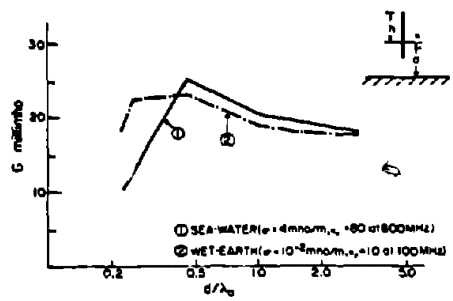

Fig. 3

total current are effected by the presence of the imperfectly-conducting ground; the proximity effect seems to draw the current to the lower half of the antenna. This effect rapidly diminishes as soon as it moves away (compare $d = 0.22\lambda_o$ and $d = 3.0\lambda_o$ in Fig. 2). However, the magnitude of the total current is very sensitive to the change of the ground distance: a strong resonance seems to have occurred near $d \sim 0.5\lambda_o$.

The input conductances, which equal to the values of the real current at the feeding-point for both wet-earth and sea-water are plotted in Fig. 3 as functions of the ground distance. We observe that the coupling with a highly-conducting sea-water is much greater. In both cases, distinct resonances occur - a similar fact was observed earlier by Wait [1953] in his study of an infinitesimal horizontal loop antenna. At a distance of more than three wavelengths away, input conductances in both cases converge to the value corresponding to the one without a ground. For detailed derivation and discussion the reader is referred to a paper by Chang and Wait [1969].

REFERENCES

Baños, A., (1966), Dipole Radiation in the Presence of a Conducting Half-space, Pergamon Press, (Oxford).

Hansen, R. C., (1963), IEEE Trans. PGAP, Vol. AP-11, 207-216.

Wait, J. R. (1964), Advances in Radio Research, edited by J. A. Saxton, Vol. 1, 157-217, Academic Press (London).

Wait, J. R., (1953), J. Appl. Phys. Vol. 24, 646-649.

Chang, D. C. and J. R. Wait, (1969), to be published.

EM PROPAGATION OVER A CONSTANT IMPEDANCE PLANE

R.J. King
University of Wisconsin, Madison, 53706

Abstract: The possibility of exciting a surface wave over a plane surface which has an index of refraction comparable to that of air is discussed. Such a surface wave can exist if the exciting source is sufficiently close to the surface.

A recent paper by the author [King, 1969] reformulated the Sommerfeld problem of EM propagation over a flat earth using the Compensation Theorem. The solution confirmed the results of Norton, Hufford, Bremmer, Baños and others, who assumed the earth-air interface was characterized by a large index of refraction, n. One is (erroneously) led to the conclusion that this large index of refraction is the mechanism by which surface waves are generated and sustained along the surface. Actually, this is a consequence of basic assumptions made at the outset of the formulation and it is now well recognized that surface waves can propagate over media with $n \tilde{>} 1$ if the exciting source launches waves near grazing incidence, e.g., "tree-top" or lateral waves propagating over dense vegetation [Tamir, 1967]. This is in agreement with the conclusions of the author. There are two basic restrictions to the solution:

$$|\sin \psi_r + \Delta_r|^2 \ll 1 \qquad \text{and} \qquad \left|\frac{\partial \Delta_r}{\partial \psi_r}\right| \ll \cos \psi_r . \tag{1}$$

for parallel polarization (TM wave), where ψ_r is the specular angle of reflection from the horizontal and Δ_r ($= Z_s/\eta_o$) is the normalized surface impedance evaluated at ψ_r. For perpendicular polarization (TE wave), Δ_r is replaced by δ_r, the normalized surface admittance. Both restrictions are necessary for the solution to satisfy the wave equation, while only the second is necessary to satisfy the boundary conditions at the interface. Nowhere in the solution was it found necessary to assume $1 \ll n$ ($= \gamma_1/\gamma_o$). Note, however, that a large index of refraction is a sufficient but not a necessary condition to satisfy $|\sin \psi_r + \Delta_r|^2 \ll 1$ (see the previous paper). An inspection of the solution shows that the surface wave simply does not propagate well if the surface impedance is not small, since the leading term of the asymptotic expansion appears in the near zone if $|\Delta_r| \tilde{\ll} 1$. For a homogeneous earth, the second condition in (1) is

$$\left|\frac{\gamma_o}{\gamma_1}\right|^4 \left|\frac{\mu_1}{\mu_o}\right|^2 \sin \psi_r \ll |\Delta_r| \tag{2}$$

which is readily satisfied for large n, and can also be satisfied for small n ($= 1 + \partial n$), for then (2) becomes

$$\sin \psi_r \ll (2\partial n)^{1/2}, \tag{3}$$

for both TM and TE waves. It is apparent from (3) that surface waves can propagate over media with n≤1, provided that the angle ψ_r is sufficiently small. The question remains whether this restriction is a consequence of the formulation used or whether it is nature's way of saying that this condition must exist in order to launch a surface wave.

Since the compensation theorem is essentially a perturbation theorem and a perfectly conducting plane ($n=\infty$) was used as the unperturbed case, there was a possibility that a better solution might be obtained using a free-space plane for the unperturbed situation. An attenuation function, G, was defined which multiplied the free space field to account for the presence of the impedance plane, and the second formulation was carried through in the same way as before to obtain

$$G(d,h,z)=1+\frac{iDe^{ikD}}{\cos\psi_d}\sqrt{\frac{-ik}{2\pi d}}\int_0^d [\sin\psi_2-\Delta(\psi_1)]\frac{G(\rho_1,h,0)}{\sqrt{\rho_1\rho_2}}\, e^{-ik\left(\frac{\rho_1}{\cos\psi_1}+\frac{\rho_2}{\cos\psi_2}\right)}\, d\rho_1 \tag{4}$$

The angles ψ_1 and ψ_2 are angles of incidence for waves from sources 1 and 2 at heights h and z, D is the direct distance between the dipoles, d is the horizontal projection of D, $\cos\psi_d = d/D$, and ρ_1 and ρ_2 are circular cylindrical radii to a general point on the surface. The main difference between (4) and the expression for the attenuation function used in the earlier formulation is the presence of the $\sin\psi_2$ term. This is essentially the same integral formulated by Hufford [1952], but he was unable to reduce the result to correspond to that obtained by Norton [1937]. Although the manipulations are somewhat more tedious than the previous case, they are essentially the same and one can obtain precisely the same result by assuming $\sin\psi_2 \simeq z/\rho_2$ and $\Delta(\psi_1) = \Delta_r(\psi_r)$ in (4). This is reassuring since one obtains the same solution of a perturbation problem by starting from two extremes--a perfect conductor and a free space plane.

King, R.J., (1969), Electromagnetic wave propagation over a constant impedance plane, Radio Science, 4(3),,255-268.

Tamir, T., (1967), On radio-wave propagation in forest environments, IEEE Trans. Antennas,Propagation, 15(6), 806-817.

Hufford, G.A., (1952), An integral equation approach to the problem of wave propagation over an irregular surface, Quart. J. Appl. Math., 9, 391-404; also see NBS Rept. CRPL-6-2, Feb. 1951.

Norton, K.A., (1937), The propagation of radio waves over the surface of the earth and in the upper atmosphere, 2, Proc. IRE, 25(9), 1203-1236.

This research supported by NSF, GK-2311.

ON THE SURFACE IMPEDANCE CONCEPT

R.J. King
University of Wisconsin, Madison, 53706

Abstract: The general application of the surface impedance (admittance) is discussed, and two extreme cases are considered; when the scattering medium is a perfect conductor and free space. The surface impedance can represent nearly exact boundary conditions and need not be reciprocal.

The utility of the surface impedance concept is often questioned because of the doubt as to its exactness and applicability to certain problems. To define surface impedance, Z_s, let there be a uniform plane wave incident upon a homogeneous plane surface such that the propagation vector $\bar{k}$, makes an angle ψ with the surface. Then, $E_{tang}/H_{tang}=-Z_s$ for parallel polarized (TM) waves, while for perpendicular polarized (TE) waves we define a surface admittance Y_s through $H_{tang}/E_{tang}=Y_s$. For a TM wave in free space (with $\gamma_o=ik_o$) obliquely incident upon the plane which is entirely homogeneous inside with complex propagation constant γ_1,

$$Z_s = \eta_o \frac{\gamma_o}{\gamma_1} \frac{\mu_1}{\mu_o} [1 - (\frac{\gamma_o}{\gamma_1})^2 \cos^2\psi]^{1/2}. \quad (1)$$

Since the TE case is the dual, one gets

$$Y_s = \frac{1}{\eta_o} \frac{\gamma_o}{\gamma_1} \frac{\varepsilon_1}{\varepsilon_o} [1 - (\gamma_o/\gamma_1)^2 \cos^2\psi]^{1/2}. \quad (2)$$

The surface impedance (admittance) given by (1) or (2) should not be confused with the "Leontovich boundary condition" which would be obtained if $(\gamma_o/\gamma_1)^2 \cos^2\psi \ll 1$. This has been discussed in detail by Godzinski [1961], who goes on to show that the surface impedance is applicable to much more general problems <u>if the change in the field along the surface over a distance of the order of a wavelength, λ_1, in medium 1 is small</u>. In other words, the field <u>inside</u> medium 1 should be locally plane, but the field outside the medium need not be locally plane with respect to λ_o.

Two extreme cases are when medium 1 is a perfect conductor or free space. The perfectly conducting case is obviously an exact boundary condition regardless of shape of the conductor. If medium 1 is free space, the field along the interface must not change appreciably over a distance λ_o. Other situations lie somewhere between these two extremes.

To illustrate, consider a Hertzian dipole above an impedance plane as shown. Using well known field expressions, it is a simple exercise to show that if the plane is free space, then over the shaded regions, $E_\rho/H_\phi=-\eta_o\sin\psi$ for the VED and $H_\rho/E_\theta=\frac{\sin\psi}{\eta_o}$ for the HED. Now, from (1) and (2) letting $\gamma_1\to\gamma_o$ and $\mu_1=\mu_o$, one gets $Z_s=\eta_o\sin\psi$ and $Y_s=\sin\psi/\eta_o$. Therefore, $Z_s(Y_s)$ given by (1) and (2) would seem to apply at least to distances where $r>\lambda_o$ in the free space (worst)

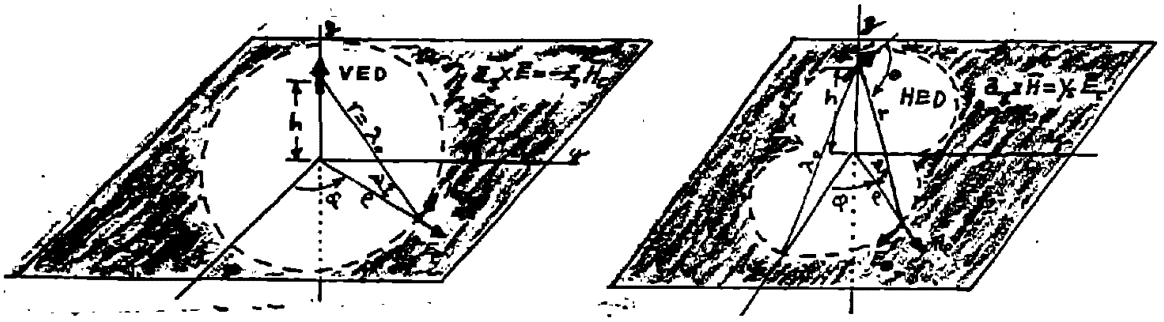

case and there is little reason to believe that it could not also be applied at even closer ranges when the lower medium becomes a dielectric or conducting medium, being exact everywhere for the perfectly conducting case. The same remarks apply to vertical or horizontal magnetic dipoles since they are duals of the electric dipoles. Finally, if $h>\lambda_o$ the concept can be applied everywhere over a free space plane. When seeking solutions to problems outside of the near zone where $r>>\lambda_o$ the questionable region immediately beneath the dipole often becomes an insignificant part of the total surface and the error incurred in using Z_s (Y_s) becomes negligibly small.

The impedance (admittance) may be variable over the surface if it changes slowly in a distance λ_1 along the surface. If the region where this requirement is violated is a negligible portion of the total surface, small error is incurred. When the surface is curved, the local radius of surface curvature must be much less then λ_1. Godzinski [1961] discusses these situations in more detail, and gives an extensive list of references.

One should not leave this topic without some comment as to reciprocity, and the corresponding demands upon the surface impedance (admittance). Since waves originating from two different sources (a and b) arrive at different angles (ψ_a and ψ_b) from different directions and possibly undergo different internal reflections in the case of nonparallel stratified media, the surface impedances (admittances) will differ at every point. If the sources are both outside of the scattering medium defined by surface s, the application of the reciprocity theorem and (1) gives

$$\int_s Z_a(\psi_a)\overline{H}_{Ta}\cdot\overline{H}_{Tb}\,ds = \int_s Z_b(\psi_b)\overline{H}_{Ta}\cdot\overline{H}_{Tb}\,ds \qquad (3)$$

where the $\overline{H}_t$'s are the tangential magnetic fields of the two sources. A similar dual equation results if (2) is used instead of (1). Thus, (3) shows that it is not necessary that $Z_a(\psi_a)=Z_b(\psi_b)$. It is therefore apparent that the two surface impedances need not be equal, and therefore "reciprocal", but rather, we require (3) be satisfied which is a distinctively different situation.

Godzinski, Z., (1961), The Surface Impedance Concept and the Structure of Radio Waves over Real Earth, Proc. IEE, C., 108(14), 362-373.

THE IMPEDANCE OF A FINITE HORIZONTAL ANTENNA ABOVE GROUND

W.J. Surtees, Defence Research Board, Ottawa.

Using equations for the radiated field of a thin linear antenna with sinusoidal current distribution in an expression derived from the compensation theorem, the change in self-impedance of a horizontal antenna of any length placed over a homogeneous ground of finite conductivity is obtained. Calculations for a half wavelength dipole are compared with some experimental values.

1. Introduction

Sometime ago I developed expressions (Surtees, 1952) for the change in self-impedance as a thin, linear antenna is brought into proximity of a homogeneous ground of arbitrary electrical constants. The explicit results were never published nor have I seen similar results available in the literature. Although FitzGerrel (1967) has used these results to check his work on the gain of linear antennas over imperfect ground, the work remained essentially unpublished. The purpose of this digest is to rectify this situation and make the results more generally available.

2. Formulation

Monteath (1951) has shown that the self-impedance Z_A of an antenna placed over a perfectly-conducting ground would change to Z_A' when placed in the same location over a ground of surface impedance η'. By applying the compensation theorem he has shown that the change in self impedance is approximated by:

$$\Delta Z_A = Z_A' - Z_A \simeq \frac{\eta'}{I_0^2} \iint H_{at}^2 \, ds \qquad (1)$$

when I_0, the current applied to the antenna produces a radiated tangential magnetic field, H_{at} along the surface of the perfectly-conducting ground with the integration extended over the whole surface.

When a thin, linear center-fed horizontal antenna of length 2ℓ is placed at a height h above a perfectly-conducting ground the tangential magnetic field is given by:

$$H_t = \frac{-j\, I_0}{2\pi \sin k\ell} \frac{h}{(x^2 + h^2)} \left(e^{-jkr_1} + e^{-jkr_2} - 2 \cos k\ell \; e^{-jkr_0}\right) \qquad (2)$$

where: $r_1^2 = x^2 + h^2 + (Z - \ell)^2$,

$r_2^2 = x^2 + h^2 + (Z + \ell)^2$,

$r_0^2 = x^2 + h^2 + Z^2$.

$k = 2\pi/\lambda$, λ is wavelength of the radiation.

The origin of rectangular coordinates is placed at the terminals of the antenna and the Z-axis directed along the antenna with the y-axis into the ground. After placing (2) in (1) and carrying out the integrations the final result is

$$\Delta Z_A = \frac{-\eta'}{4\pi \sin^2 k\ell} \left(\left\{ e^{-j2kh} \left(1 + \frac{1}{j2kh}\right) + j2kh \text{ Ei } (-j2kh) \right\} (2 + 4 \cos^2 k\ell) \right.$$

$$+ e^{j2k\ell} \left[e^{-j2kh\omega_1} \left(\frac{1}{\omega_1} + \frac{1}{j2kh}\right) + j2kh \text{ Ei } (-j2kh\omega_1) \right] + e^{-j2k\ell} \left[e^{-j2kh/\omega_1} \right.$$

$$\left(\omega_1 + \frac{1}{j2kh}\right) + j2kh \text{ Ei } \left(\frac{-j2kh}{\omega_1}\right) \Big] - 4 \cos k\ell \left\{ e^{jk\ell} \left[e^{-j2kh\omega_2} \left(\frac{1}{\omega_2} + \frac{1}{j2kh}\right) \right.\right.$$

$$+ j2kh \text{ Ei } (-j2kh\omega_2) \Big] + e^{-jk\ell} \left[e^{\frac{-j2kh}{\omega_2}} \left(\omega_2 + \frac{1}{j2kh}\right) \right.$$

$$\left. \left. \left. + j2kh \text{ Ei } (-j2kh\omega_2) \right] \right\} \right) \qquad (3)$$

where: $\omega_1 = \left(\frac{\ell^2}{h^2} + 1\right)^{\frac{1}{2}} + \frac{\ell}{h}$,

and $\omega_2 = \left(\frac{\ell^2}{4h^2} + 1\right)^{\frac{1}{2}} + \frac{\ell}{2h}$;

and $\text{Ei } (-jy) = \text{Ci } (y) - j \text{ Si } (y) + j\pi/2$

$= \int_y^\infty e^{-j\omega} \frac{d\omega}{\omega}$ is the exponential integral of imaginary argument.

The change in self-impedance for the center-fed, half-wave horizontal antenna is obtained from (3), by putting $\ell = \lambda/4$ and is:

$$\Delta Z_A = -\frac{\eta'}{4\pi} \left[2e^{-j2kh} \left(1 + \frac{1}{j2kh}\right) + j4kh \text{ Ei } (-j2kh) \right.$$

$$- e^{-j2kh\omega} \left(\frac{1}{\omega} + \frac{1}{j2kh}\right) - j2kh \text{ Ei } (-j2kh\omega)$$

$$\left. - e^{-j2kh/\omega} \left(\omega + \frac{1}{j2kh}\right) - j2kh \text{ Ei } \left(\frac{-j2kh}{\omega}\right) \right] \qquad (4)$$

$$= \frac{\eta'}{4\pi} He^{j\theta}$$

and $\omega = \left(\frac{\ell^2}{h^2} + 1\right)^{\frac{1}{2}} + \frac{\ell}{h}$, $\ell = \lambda/4$.

The function H and Θ are tabulated in Table 1.

Antenna height	Change in self-impedance x $4\pi/\eta'$	
h/λ	H	θ (degrees)
0	∞	360
0.01	50.2	359.65
0.025	20.3	357.86
0.04	12.9	354.71
0.06	8.86	348.72
0.08	6.82	341.13
0.10	5.58	332.29
1/8	4.57	319.91
1/4	2.43	245.87
3/8	1.67	162.70
1/2	1.26	76.88
5/8	1.01	349.50
3/4	0.84	261.20
7/8	0.72	172.43
1	0.63	83.36

Table 1. Horizontal half-wave antenna at a height h above imperfect ground.

3. Results

Some experimental results relating to the resistance of a horizontal antenna over an imperfect ground of dielectric constant $\varepsilon' = 25$ and conductivity $\sigma = 0.013$ mhos/m have been reported by Friis et al. (1934) and are compared in Table 2 with corresponding values calculated from (4).

Antenna height h/λ	Wavelength λ (metres)	Resistance over Perfect ground (ohms)	Change in Resistance (ohms)	
			Experiment	Theory
0.01	8	1	89.0	295
0.07	8	13.3	31.7	45.2
0.18	8	55.5	6.7	10.4
0.345	27	98.0	-6.0	-8.8
0.36	17	97.7	-6.9	-9.8
0.625	17	57.8	4.0	5.7
0.83	17	83.5	-4.1	-3.4

Table 2. Input resistance of a horizontal half-wave antenna over ground of surface impedance $\eta' = \dfrac{120\pi}{(25 - j\ 0.78\lambda)^{\frac{1}{2}}}$.

It is seen that the input resistance as predicted by (4) is within 5 percent of the experimental results, when the antenna is placed at heights greater than 0.2 wavelengths above the ground. At low heights, where the change in resistance is largest, the theoretical results have the greatest error. This is to be expected as the approximations are not true at low antenna heights. Also at the frequencies employed, $|\frac{\eta'}{4\pi}|$ is approximately 6, which is considerably larger than the value for a highly conducting ground. It is therefore expected that the predicted values from (4) would be more nearly true if the ground had a larger conductivity, or if the frequency were decreased.

4. References

FitzGerrel, R.G. (1967), Gain measurements of vertically polarized antennas over imperfect ground, Trans. IEEE, AP-15, 211-216.

Friis, H.T., C.B. Feldman, and W.M. Sharpless, (1934), The determination of direction of arrival of short radio waves, Proc. IRE, 22, 47-78.

Monteath, G.D. (1951), Application of the compensation theorem to certain radiating and propagation problems, Proc. IEE, Pt. IV, 98, 23-30.

Surtees, W.J. (1952), Antenna performance as affected by an inhomogeneous, imperfectly-conducting ground, Ph.D. Thesis, University of Toronto, Toronto, Ontario.

Impedance of a Finite-Length Insulated Dipole in Dissipative Media

Carson K. H. Tsao and J. T. deBettencourt
Raytheon Company, Norwood, Massachusetts

1. Introduction

Theory of cylindrical insulated wire antenna in a dissipative media has been treated in the past as an infinitely long coaxial transmission line (for example, Iizuka and King 1962). The propagation constant and characteristic impedance are obtained in terms of cylindrical waves. In this paper, the cylindrical wave solution is modified for application to finite length dipoles.

The present consideration relates to the notion that within the antenna region, there must be electric flux lines connecting the opposite halves of the dipole as depicted by the spherical TEM wave.

2. Transmission Line Parameters

An insulated wire has an inner conductor of radius a_1 and is covered by a layer of insulation having outer radius a_2 and dielectric constant ϵ_2. External to the insulation is the propagation medium with dielectric constant ϵ_3. Corresponding to ϵ_2 and ϵ_3 are the plane wave propagation constants k_2 and k_3 respectively.

In the cylindrical wave solution, and axial propagation constant k is determined from the boundary conditions at $\rho = a_2, a_1$. For a finite-length dipole, if relatively thin, the feed-point and the ends can be expected to have little effect on the current distribution so that the same propagation constant k satisfies the local boundary conditions, although the distribution of fields may be different in the case of the dipole than for an infinitely long wire. Thus, the propagation constant k is given by

$$k^2 = k_2^2 \left(\ell n \frac{a_2}{a_1} + \Delta\right) \Big/ \left(\ell n \frac{a_2}{a_1} + \frac{\epsilon_2}{\epsilon_3} \Delta\right) \qquad (1)$$

where

$$\Delta = \frac{1}{\ell_3 a_2} \left[H_0^{(2)} (\ell_3 a_2) \Big/ H_1^{(2)} (\ell_3 a_2)\right]$$

$$k^2 = k_2^2 - \ell_2^2 = k_3^2 - \ell_3^2 .$$

Although the propagation constant k for a dipole is regarded as the same as that for an infinite wire, it is not expected that the impedances will be the same for the two cases because of the need to account for the principal TEM wave. In the cylindrical wave solution, for relatively thin insulation, i.e. $|\ell_2 a_1| < \ell_2 a_2| << 1$ the tangential magnetic and the radial electric fields in the insulation are

$$E_{z_2} = \frac{I\omega\mu k}{2\pi\rho k_2^2} \text{ and } H_{\varphi_2} = \frac{I}{2\pi\rho}. \tag{2}$$

These are equivalent to the $E\theta_2$ and H_{φ_2} components of the spherical TEM wave by substituting $\rho = n \sin\theta$.

Although higher order spherical waves are expected to exist, these waves do not contribute to the evaluation of potential drop V between the opposite halves of the dipole because of the symmetry; V is necessary in determining the characteristic impedance Z_0. The evaluation of V is simplified if the cylindrical dipole is replaced by a biconical antenna. With this substitution, it is readily shown that the average characteristic impedance for the corresponding cylindrical dipole is

$$Z_0 = \frac{k}{\pi\omega\epsilon_2} \left(\ell n \frac{a_2}{a_1} + \frac{\epsilon_2}{\epsilon_3} \frac{\psi}{2}\right) \tag{3}$$

where

$$\psi = 2\left(\ell n \frac{2h}{a_2} - 1\right)$$

is the thickness parameter. The corresponding distributed immittances of an equivalent transmission line are

$$z = \frac{jk^2}{\pi\omega\epsilon_2} \left(\ell n \frac{a_2}{a_1} + \frac{\epsilon_2}{\epsilon_3} \frac{\psi}{2}\right);$$
$$y = j\omega\epsilon_2\pi / \left(\ell n \frac{a_2}{a_1} + \frac{\epsilon_2}{\epsilon_3} \frac{\psi}{2}\right). \tag{4}$$

It is noted that the results in (3 and 4) are valid for bare antennas, i.e. $a_2 = a_1$.

Of the four transmission line parameters, only two are independent. In the case of the dipole, the two forming the independent set are k and y. The behavior of the propagation constant is well understood and has been experimentally observed (Iizuka and King, 1962) and will not be considered further here. The distributed shunt admittance y obtained here differs from the one obtained in the cylindrical wave solution due to the term involving ψ and experiments have been conducted to verify this.

3. Experimental Results

The experiments involved measuring the input resistance of an electrically short, open-circuited, insulated monopole in a water tank (5.5 meters in diameter and 1 m in depth). If the water has large loss tangent, the input resistance of the monopole of length h is

$$R_{in} = \text{Re}\ \frac{jk}{2y \tan h\, jkh} \approx \text{Re}\ \frac{1}{2yh} \approx \frac{\psi}{4\pi\sigma_3 h} \qquad (5)$$

where σ_3 is the conductivity of the water.

In the experimental setup, a ground plane ($1\,m^2$) is placed just below the water surface. The monopole is attached to the underside of the ground plane. From considerations of electrical length of monopole, loss tangent of water, tank dimensions, and input reactance, the set of test parameters are chosen: f = 1 MHz, a_2 = .0814 cm (No. 14 wire), a_2/a_1 = 1.5 (teflon tubing), h = 10 to 40 cm, and σ_3 = .03 to 1 mhos/m.

Input resistance of the insulated monopoles are made in water at two values of salinity (S = 0 and 20 lbs of salt in tank capacity of 3700 gallons). The measured resistances and the deduced water conductivities are shown in Figure 1. The constancy of the deduced conductivity as a function of antenna length is a verification of equation (5).

Input resistances of an 25 cm insulated and a 20 cm bare monopole are measured. Conductivities deduced from the input resistances are shown in Figure 2 as function of water salinity. There is good agreement between the data on the two types of monopoles and the correct functional dependancy between conductivity and salinity of the water.

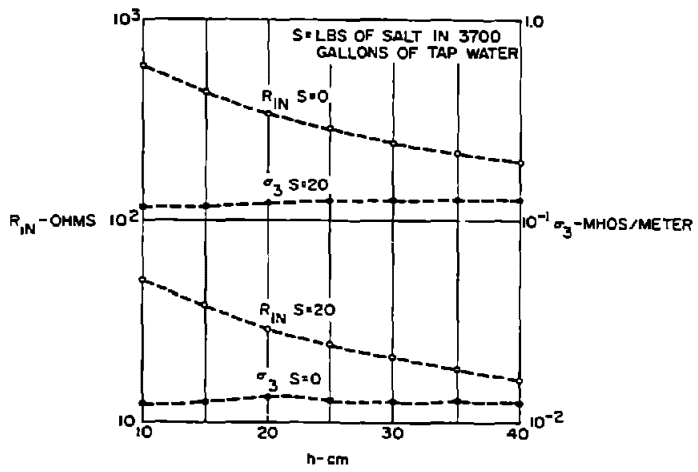

Figure 1. Input Resistive and Solution Conductivity as Function of Monopole Length

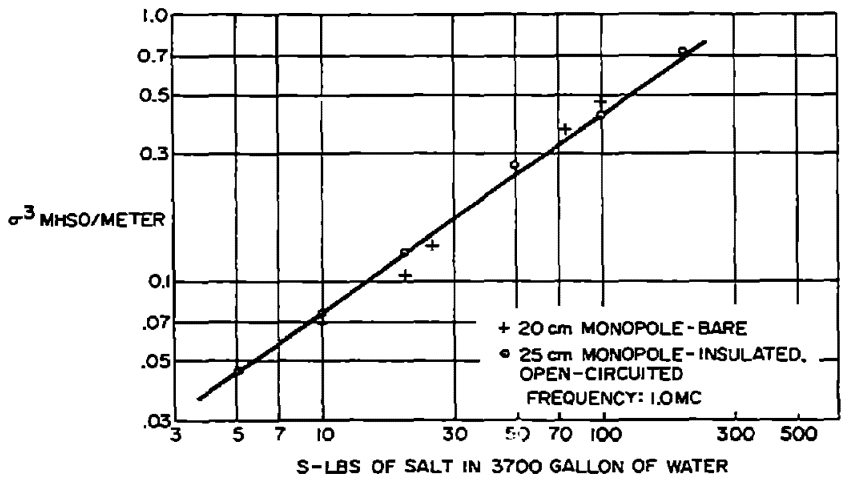

Figure 2. Conductivity versus Salt Content of Solution

In studying subsurface radio transmissions, antennas are immersed in the rock strata through deep drill holes. There are impedance data on a number of insulated antennas in the drill holes (Tsao, 1964). It has been possible to deduce with reasonable success the conductivities of the rock media around the antennas from their resonance frequencies. Difficulties have been

encountered, however, in interpreting the low frequency input resistances, being much higher than predicted by the cylindrical wave solution. With the modified solution obtained from the insulated biconical antenna approach given above, these earlier data have been reinterpreted to deduce the local conductivity values. The results are summarized in Table 1 (Tsao, and deBettencourt 1966).

Table 1. Conductivities in Drill Holes

LOCATION	300 M MONOPOLES	R_{in} OHMS (10 KHZ)	RESONANCE FREQUENCY f_0 IN KHZ	CONDUCTIVITY MILLIMHOS/M	
				DEDUCED FROM R_{in}	DEDUCED FROM f_0
HOLE NO.1	NO. 18 PVC 1 RG-8/U 2	46 46	28 53	.138 122	.26 .36
HOLE NO.6	NO. 18 PVC 1	72.5	33	.089	.15
HOLE NO.9	NO. 18 PVC 1 RG-8/U 2	62 86	32 60 9	.104 .067	.14 .093
SARANAC LAKE	RG-8/U 2	121	63	.048	.11

The previous impedance solution for the insulated antenna is modified by viewing it as an insulated biconical antenna. This results in a unified solution which can readily be shown to be applicable for a number of special cases: (a) the insulation is vanishingly thin, i. e. the insulated antenna degenerates into a bare antenna; (b) the medium has low loss tangent, i. e. for very high frequency applications of antennas in ground; (c) the medium is highly conducting; and (d) the antenna is electrically short.

4. References

[1] Iizuka, K. and R. W. P. King, (1962), "The Dipole Antenna Immersed in a Homogeneous Conducting Medium," IRE Trans., Vol. AP-10, No. 4.

[2] Tsao, C. K. H., (1964), "Investigations of Electrical Characteristics of Rock Medium in Northern New York State," Raytheon Company, Contract AF-19-(628)-2362, Sci. Rept No. 3, CFSTI Doc. No. AD-600-758.

[3] Tsao, C. K. H. and J. T. deBettencourt, (1966) "Subsurface Radio Propagation Experiments," Paper presented at AGARD/NATO 12th Symposium on "Subsurface Communications," held at Ministre Des Postes El Télécommunications, Paris, 25-29 April 1966.

Distributed Shunt Admittance of Horizontal Dipole over Lossy Ground

Carson K. H. Tsao
Raytheon Company
Norwood, Massachusetts

1. Introduction

A cylindrical dipole antenna, located near a lossy ground and parallel to the surface, can be studied as a lossy transmission line. The distributed series impedance of a horizontal long wire over ground has been reported by Wait (1961). In the discussion here, only the distributed shunt admittance is considered.

2. Distributed Shunt Admittance

A horizontal cylindrical dipole is above the surface of the ground. The two sections of the dipole cylinders have radius a and length L. The axis of the dipole is at a height h + a above the ground. The dipole is considered thin, i.e. $a << L$.

The air and the ground are two dielectric media with dielectric constants ϵ_0 and $\epsilon_1 = \epsilon_0 \epsilon_r (1 - jp)$ respectively, where $p = \sigma/\omega \epsilon_0 \epsilon_r$. The distributed shunt admittance y of the dipole can be obtained from the distributed capacitance c between the opposite halves of the dipole; $y = j\omega c$.

In an electrostatic case, it is assumed that dipole cylinders are oppositely charged and can be represented by line charges with densities +q and -q coulombs per meter on the two cylinders. The presence of the ground is accounted for by allowing an image dipole. The charge densities are $-\frac{\epsilon_1 - \epsilon_0}{\epsilon_1 + \epsilon_0} q$ and $+\frac{\epsilon_1 - \epsilon_0}{\epsilon_1 + \epsilon_0} q$ on the two halves of the image dipole. Given these line charges, the potential drop between the dipole cylinders is readily determined. Because of the assumption of uniform charge density on each dipole section, the resultant potential drop between corresponding points on the two dipole cylinders is a function of distance from the center of the dipole. In a dipole with perfectly conducting cylinders, a voltage gradient along the dipole does not exist. For a thin dipole, this gradient will be small and the average value potential drop can be used. This results in a distributed shunt admittance of

$$y = j\omega c = \frac{j2\pi\omega\epsilon_0}{\psi - K\frac{\epsilon_1 - \epsilon_0}{\epsilon_1 + \epsilon_0}}, \quad \psi = 2\left(\ell n \frac{2L}{a} - 1\right).$$

In the above, ψ is the thickness parameter, K is the correction factor accounting for the effect of proximity to ground and y_0 is the free space distributed admittance.

It can be shown that K = 0 if h >> L; that is, for the dipole sufficiently removed from ground y = y_0. The same result is obtained if $\epsilon_1 = \epsilon_0$. It is also interesting to note that K = ψ if h = 0; this results in a

$$y = j \frac{2\pi\omega}{\psi} \left(\frac{\epsilon_1 + \epsilon_0}{2}\right),$$

i. e. the distributed admittance is proportional to average value of dielectric constants for the air and the ground.

Although the admittance derived here is for a dipole in air parallel to a lossy ground, it should be noted that the result is applicable to any semi-infinite media.

3. Input Resistance of Electrically Short Dipole

The result in the preceeding section can be used to determine the input resistance, due to ground loss, of an electrically short dipole parallel to the ground surface. The dipole is regarded as an open-circuited transmission line of length L. Therefore the input impedance is $Z_{in} = R_{in} + jX_{in} = 1/yL$. The corresponding input resistance R_{in} represents ground loss and is, from the electrostatic method;

$$R_{in} = \frac{K}{2\pi\omega\epsilon_0 L} \frac{2\epsilon_r p}{(\epsilon_r + 1)^2 + (\epsilon_r p)^2}, \quad \text{(Electrostatic)}$$

where

$$p = \frac{\sigma}{\omega\epsilon_0\epsilon_r}.$$

This can be compared with the ground loss expression due to Sommerfeld (See Sommerfeld, 1949, or King, 1956):

$$R_{in} = \frac{60\left(\frac{L}{h+a}\right)^2}{\left[\epsilon_r^2 + (\epsilon_r p)^2\right]^{\frac{1}{4}}}, \quad \text{(Sommerfeld)}.$$

These two expressions for input resistance due to ground loss are totally different, although both predict an increase in input resistance when the dipole is lowered toward the ground surface.

The electrostatic solution predicts that the input resistance of the short dipole is maximum when the loss tangent of the ground is unity and decreased to zero when the loss tangent (or conductivity) becomes either very large or very small. On the other hand, the Sommerfeld solution indicates that the resistance rises monotonically to an asymptotic value when the ground conductivity decreases.

4. Experimental Results

A set of measurements were made with dipoles placed on the surface of the ground. The dipole lengths ranged from L = 0.075 to 15 meters. The dipoles were made from the braids of RG-8/U coaxial cable with the resultant radius a = .00375 m; this provided a flexible dipole which could be readily bent to follow the contour of and be in contact with the ground. The measurements were made in the Boston area in a late winter month when the ground was still frozen excetp the surface was wet due to thawing. The ground conductivity was estimated to be of the order of 10^{-3} mhos per meter due to the gravel subsoil base and low temperature.

The measured data, taken at .1, 1 and 10 kHz, are summarized in Figure 1 as function of dipole half length L. Theoretical curves from the electrostatic and the Sommerfeld solutions are also shown for comparison.

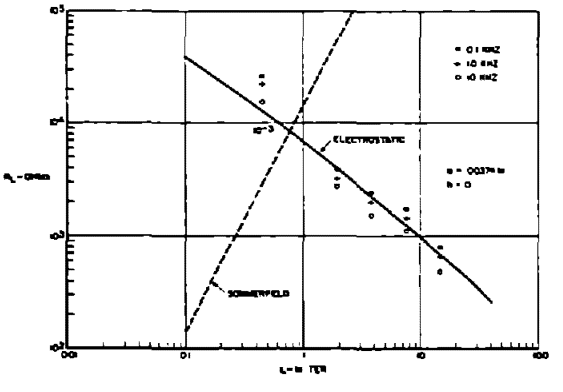

Figure 1

In Figure 2, the measured input resistance of the dipole with L = 1.9 meter is shown as function of frequency and is also compared with the theoretically predicted values.

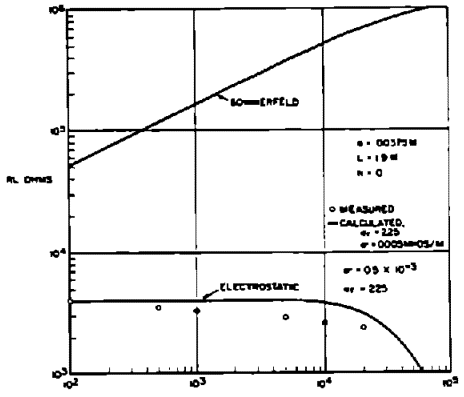

Figure 2.

In both Figures 1 and 2, ground constants assumed are $\sigma = .5 \times 10^{-3}$ mhos/meter and $\epsilon_r = 225$.

5. Discussion

The solution formulated by Sommerfeld starts by considering a primary field excited dipole current and a secondary field reflected from the ground due to the incident primary field. The dipole resistance is obtained by considering net power flow across two planes above and below the horizontal dipole. This method neglects the interaction between the dipole and the secondary field incident on it. That is, there should be a third field or the scattered field from the dipole due to the secondary field.

The effect of neglecting the interaction between the dipole and the secondary field is believed to result in the discrepancy between loss resistances predicted by the Sommerfeld solution and the electrostatic solution.

6. References

J. R. Wait, 1961, "On the Impedance of Long Wire Suspended Over the Ground," Proc. of IRE, Vol. 49, No. 10, p. 1576.

A. Sommerfeld, 1949, "Partial Differential Equations," Academic Press, Sec. 36.

King, 1956, "The Theory of Linear Antenna," Harvard University Press, Chapter 7.

THE LINEAR ANTENNA IN A PIECEWISE HOMOGENEOUS ENVIRONMENT

D.V. Otto[1]

ElectroScience Laboratory
Department of Electrical Engineering
The Ohio State University
Columbus, Ohio 43212
23 April 1969

Abstract

Numerically efficient and accurate techniques for solving three canonical problems of the antenna in a piecewise homogeneous medium are developed, these problems being (a) the current induced on a thin lossy wire by an arbitrary incident field, and the treatment of inhomogeneities in the (b), Fresnel or far zone, and the (c), near zone. Examples dealt with are a simple array, an antenna on a finite size ground plane and a dipole on a sphere.

Introduction. A typical problem of current interest is that of the array of linear wires mounted on an aircraft, rocket or satellite. In this situation one readily distinguishes three canonical problems. First, there is the general problem of the linear lossy wire immersed in an arbitrary field. Second, techniques are required to deal with the effects of inhomogeneities in the far and Fresnel zones, and third, inhomogeneities in the near field have to be accounted for. This paper deals with efficient numerical methods of solving these problems.

The Exact Current on a Thin Lossy Wire. Assume first that the fields some distance from the wire can be calculated approximately from the equivalent line current. Then we can let the line current be represented by a piecewise sinusoidal function (Otto and Richmond, 1969) so that the E_z (for example), is given by

$$E_z(r,z) = \frac{iZ_o}{4\pi} \sum_{j=1}^{N} \Delta I'_j \frac{e^{-ikR_j}}{kR_j} \qquad (1)$$

Now suppose an arbitrary incident field impinges upon the wire. Then $\Delta I'_1$ and $\Delta I'_N$ become dominant in (1) and the field near

[1]Presently with the Department of Electrical Engineering, University of Auckland, Auckland, New Zealand.

the ends of the wire is given by the 1st and Nth terms of (1). Consequently a zero order solution for the current on the wire may be written using the Fourier Transform (F.T.) theory of antennas (Otto, 1968):

$$I_o(z) = I^i(z) + A_o I_R(h-z) + B_o I_R(h+z), \quad |z| < h, \tag{2}$$

where

$$I^i(z) = -\int_{-(h+\Delta)}^{h+\Delta} E_z^i(z') I_e(z-z')dz', \quad |z| < h, \tag{3}$$

and (for a solid wire),

$$I_R(z) = k\int_o^\infty \{1+(z/a)^2\}^{1/6}\ (z/a)^{-1/3}\ \frac{e^{-ik\sqrt{z^2+a^2}}}{k\sqrt{z^2+a^2}}\ I_e(z+z')dz'. \tag{4}$$

Once $I_o(z)$ has been calculated, an iterative scheme is easily set up to determine the current more accurately, for now the I_j, (j=2,N-1) may be evaluated. In general, therefore we have

$$I_M(z) = I^i(z) + A_M I_R(h-z) + B_M I_R(h+z) + \Delta I_{M-1}(z). \tag{5}$$

Convergence is extremely fast, a factor of 20 per iteration being typical. This implies that an accuracy of about five percent is obtained with the zero order solution.

The effect of finite conductivity of the wire can be taken into account since the effect is a contribution to $E^i(z)$ through the surface impedance. For normal conductors the rate of convergence given previously is not affected significantly.

Fresnel and Far Zone Inhomogeneities. If the inhomogeneities are sufficiently remote, iterative methods provide efficient solutions. Two typical cases in which this situation is found is the large array and the antenna (or array) mounted on a finite size ground plane.

For the arbitrary array the zero order solution (which has about five percent accuracy), is

$$I_n(z) = I_{S_n}(z) - \int_{L_n} E_{nm}(z') I_e(z-z')dz' + A_n I_R(h_n-z) + B_n I_R(h_n+z), \tag{6}$$

where E_{nm} is the axial field incident on the nth. element due to

the mth. and is determined by use of the piecewise sinusoidal approximation. $I_{S_n}(z)$ is the primary current whose form depends on the nature of the excitation.

Since $I_n(z)$ appears only on the left of (6) an iterative scheme for the solution of (6) becomes obvious. Figure 1 shows the results for a pair of monopoles. Also shown are the experimental results due to Mack (1963) and the number of iterations required for one percent convergence. Clearly iteration is very efficient only in the Fresnel or far zone. In the near zone other methods are better.

In the case of the antenna (array) mounted on a finite size ground plane, it is convenient to utilize the geometrical theory of diffraction to account for the ground plane edges. The results for a coaxially driven, finitely conducting monopole, at the centre of a small ground plane ($D_{gp}=1.25\lambda, D_g=6.25\lambda$) are displayed in figure 2. Two iterations and a first order geometrical theory of diffraction were used to obtain an extremely accurate solution.

Near Zone Inhomogeneities. One case where the inhomogeneity is in the near zone, is that of the dipole symmetrically mounted on a sphere (or other rotationally symmetrical body). The approach here is to use a combination of point matching and "imaging" in order to satisfy the boundary conditions on the surface of the body. Figure 3 shows the problem considered and the equivalent (image) source system. For the sphere, static image concepts lead to the system shown. The four interior "frill" sources are located where the maxima in the static image E_z lie. The amplitudes of these sources are obtained from two equations: (i), an aperture condition $I'(a_s-\varepsilon)=-I'(a_s+\varepsilon)$, and (ii) a point matching condition that $E_\phi=0$, at some point on the sphere. This point was determined by variational considerations. The zero order results are shown in figure 4 along with some experimental values. Bearing in mind the relationship between the zero order and experimental results of figure 2, these results are seen to be excellent.

High Speed Techniques. A basic improvement in computer execution time is possible if functions like I_e, I_R are evaluated prior to execution, stored in tabulated form and interpolative techniques used during execution. (Typical access time with the 7094 computer is about 800 μsecs using quadratic interpolation).

A second technique, is to utilize similarly accessed current distributions for a few commonly encountered excitation fields. Such currents are the currents on infinite antennas with frill source, or plane wave excitation.

Finally, in an array it is possible to evaluate $I^1(z)$ prior to execution due to a single term of (1) for the various values of z that are encountered. Then the execution time evaluation of the integral in (3) is eliminated.

Acknowledgment. The author is indebted to L.L. Tsai for carrying out the numerical work for near zone inhomogeneities, and to D. Lekhyananda who performed the experimental work.

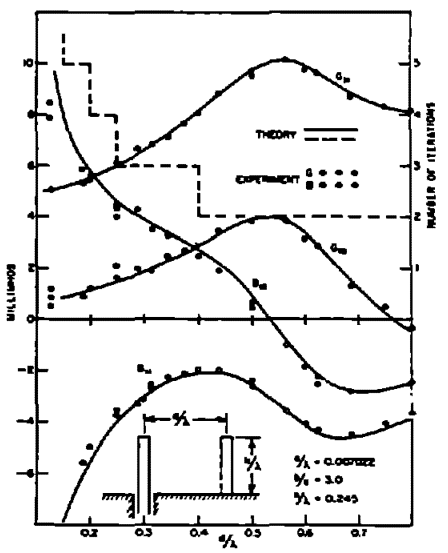

Fig. 1. Admittance of an array of two antennas.

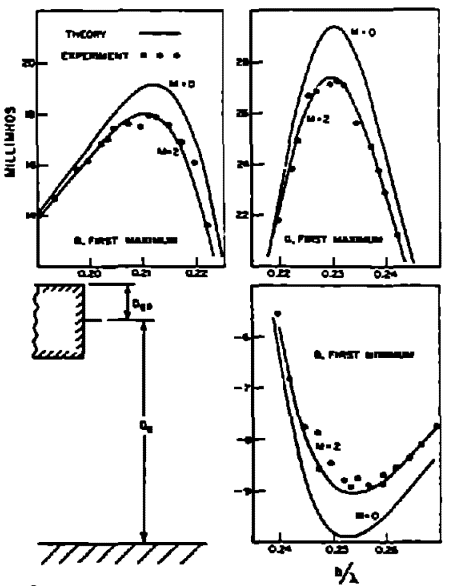

Fig. 2. Admittance of an antenna on a small square ground plane. (a/λ=.002, b/a=2.23, σ=10.4 Mmhos/m)

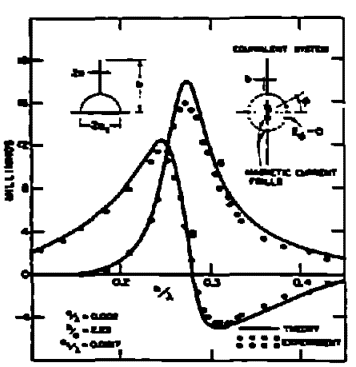

Fig. 3. Admittance of a dipole on a sphere.

CHARACTERISTICS OF THE GROUND WAVE ATTENUATION FUNCTION FOR HIGHLY INDUCTIVE SURFACES

D.B. Ross
National Radio Propagation Laboratory
Communications Research Centre, Ottawa, Canada

Abstract The numerical distance p between two dipoles over a plane surface depends on wave frequency, path geometry and surface impedance. The parallel polarized surface fields of the ground wave are proportional to the attenuation function F(p), which exhibits oscillations and rapid phase changes with range over a highly inductive surface, due to the existence of a trapped surface wave. Twenty-four values of p (of an infinite number) which make F equal to zero are given.

1. Introduction and Field Equations For the air-earth interface, a surface impedance to electromagnetic waves is defined, having generally two components, represented by the impedance Δ and admittance Γ (normalized to ζ_o, the free space impedance), which may be calculated for a given surface. This paper is concerned with the propagation of ground wave fields over plane earth surfaces, particularly ones with highly inductive impedances.

Let $\bar{z}$, $\bar{\rho}$ and $\bar{\phi}$ be the cylindrical co-ordinates of the receiver with respect to an origin on the surface below the dipole source. Further ψ is the angle of incidence at the surface; θ the zenith angle of the receiver with respect to the dipole; and r, r' the direct and reflected dipole-receiver distances. Use the abbreviations $S = \sin\psi$, $C = \cos\psi$, $S' = \sin\theta$, $C' = \cos\theta$, $S'' = \sin\phi$, $C'' = \cos\phi$. By geometry, $\bar{\psi} = -\bar{z}S+\bar{\rho}C$, $\bar{\theta} = -\bar{z}S'+\bar{\rho}C'$, and let $\bar{\alpha}_{\parallel} = -(\bar{z}S+\bar{\rho}\Delta)$, $\bar{\alpha}_{\perp} = -(\bar{z}S+\bar{\rho}\Gamma)$, $e = \exp j(\omega t-kr)/r$, $e' = \exp j(\omega t-kr')/r'$. The plane wave earth reflection coefficients are $R_{\parallel} = (C-\Delta)/(C+\Delta)$, $R_{\perp} = (C-\Gamma)/(C+\Gamma)$. Define reference fields at unit distance from the electric (e) and magnetic (m) dipoles in the equatorial plane: $E_e = \zeta_o H_e$, $E_m = \zeta_o H_m$.

Norton's (1942) equations (as numbered) for the ground wave fields of the elementary dipoles parallel ($_{\parallel}$) and transverse ($_{\perp}$) to the plane of incidence, for $r > 2\pi/k$, become:

Vertical Electric
(150) $\bar{E}_{\parallel} = jE_e \{ \bar{\theta}S'e+\bar{\psi}SR_{\parallel}e'+\bar{\alpha}_{\parallel}S(1-R_{\parallel})F_e e' \}$
(151) $\bar{H}_{\perp} = \bar{\phi}jH_e \{ S'e+ SR_{\parallel}e'+ S(1-R_{\parallel})F_e e' \}$

Vertical Magnetic
(153) $\bar{H}_{\parallel} = - H_m \{ \bar{\theta}S'e+\bar{\psi}SR_{\perp}e'+\bar{\alpha}_{\perp}S(1-R_{\perp})F_m e' \}$
(152) $\bar{E}_{\perp} = \bar{\phi} E_m \{ S'e+ SR_{\perp}e'+ S(1-R_{\perp})F_m e' \}$

Horizontal Magnetic
(200) $\bar{E}_{\parallel} = - E_m S'' \{ \bar{\theta} e+\bar{\psi} R_{\parallel}e'+\bar{\alpha}_{\parallel} (1-R_{\parallel})F_e e' \}$
(202) $\bar{H}_{\perp} = -\bar{\phi} H_m S'' \{ e+ R_{\parallel}e'+ (1-R_{\parallel})F_e e' \}$
(203) $\bar{H}_{\parallel} = - H_m C'' \{ -\bar{\theta}C'e+\bar{\psi}CR_{\perp}e'+\bar{\alpha}_{\perp}\Gamma(1-R_{\perp})F_m e' \}$
(201) $\bar{E}_{\perp} = \bar{\phi} E_m C'' \{ - C'e+ CR_{\perp}e'+ \Gamma(1-R_{\perp})F_m e' \}$

Fig. 1.
Relief of F on p plane.

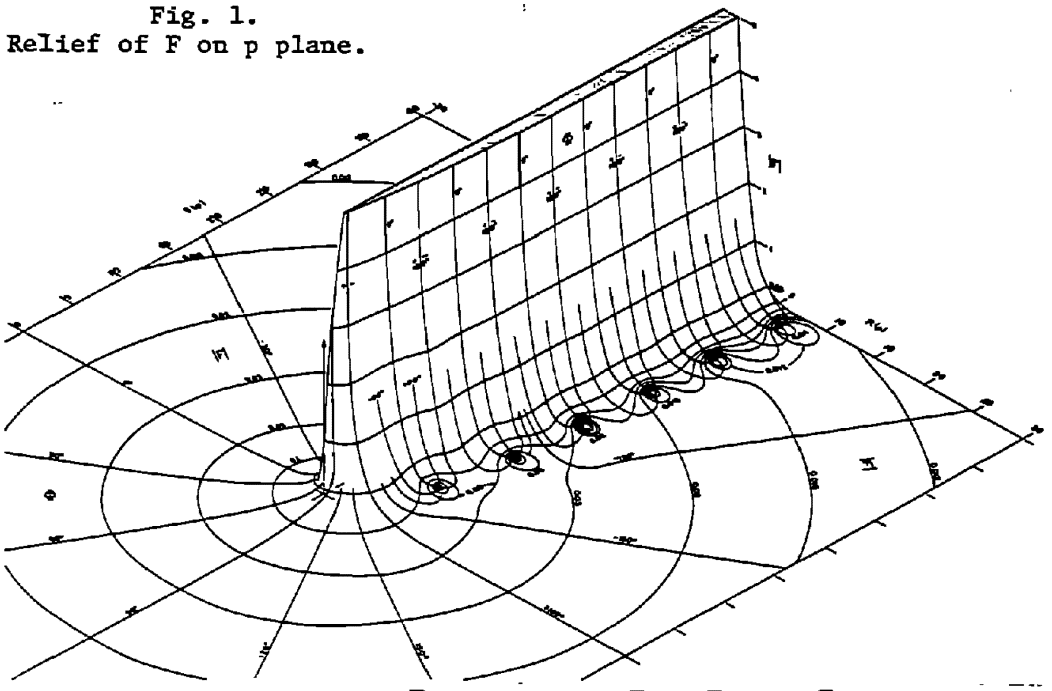

Horizontal Electric (198) $\bar{H}_{\shortparallel} = -\, jH_e S''\{\ \bar{\theta}\ \ e+\bar{\psi}\ R_{\perp}e'+\bar{\alpha}_{\perp}\ (1-R_{\perp})F_m e'\}$

(196) $\bar{E}_{\perp} = \bar{\phi} jE_e S''\{\ \ \ e+\ R_{\perp}e'+\ \ (1-R_{\perp})F_m e'\}$

(197) $\bar{E}_{\shortparallel} = \ jE_e C''\{-\bar{\theta}C'e+\bar{\psi}CR_{\shortparallel}e'+\bar{\alpha}_{\shortparallel}\Delta(1-R_{\shortparallel})F_e e'\}$

(199) $\bar{H}_{\perp} = \bar{\phi} jH_e C''\{-\ C'e+\ CR_{\shortparallel}e'+\ \ \Delta(1-R_{\shortparallel})F_e e'\}$

Each field has three components: (i) one direct from the dipole source, (ii) one reflected from the surface, and (iii) a surface wave field, proportional to the attenuation function F. When both source and receiver are on the surface, the space wave (sum of (i) and (ii)) disappears, leaving the surface wave, and so the ground wave field near the surface is determined by the behaviour of F.

2. The Numerical Distance and Attenuation Function F is expressed in terms of the numerical distance $p = |p|\exp(jb) = -jkr'(C+\gamma)^2/2S^2$, where $R = R_{\shortparallel}$, $\gamma = \Delta$ for evaluating F_e, and $R = R_{\perp}$, $\gamma = \Gamma$ for F_m. Thus $|p|$ is proportional to r', and $b = 2\beta - 90°$, where β is the phase of $(C+\gamma)$. For the homogeneous earth, the restriction $(n^2 >> 1)$ assumed in the derivation of F gives $\Delta^2 = 1/\Gamma^2 << 1$. Sommerfeld (1909) defined F for propagation over a homogeneous earth, which has a slightly inductive surface. However, the use of the function may be extended to propagation over a stratified or rough surface (*e.g.* Wait, 1957), which may be highly inductive. Such a surface is characterized by $0° < b_{\Delta} < 90°$, $-180° > b_{\Gamma} > -270°$. Norton's (1941) series expansion for F(p) is poorly convergent for large $|p|$, and the corresponding asymptotic

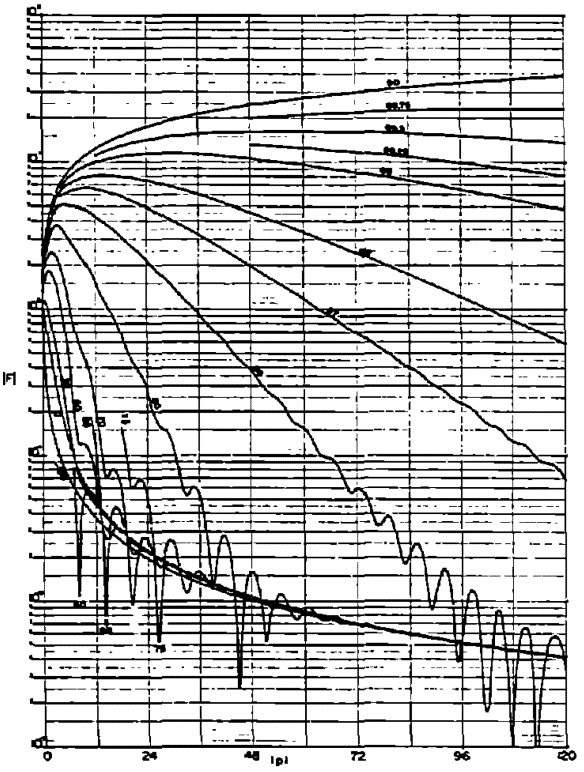

Fig. 2.
$|F|$ *v.* $|p|$ for various b values.

expansion is the 'Norton surface wave' $F_{Norton} = -1/(2p) - 1\cdot3/(2p)^2 - 1\cdot3\cdot5/(2p)^3 \ldots$ with the addition of the 'trapped surface wave' term $(-2j\sqrt{\pi p}\exp(-p))$ if $0° < b < 90°$ (Wait, 1957). $F(p)$ has an infinite number of zeroes in this region of b, which can be considered to be the result of destructive interference between F_{Norton} and the trapped wave. Vogler (1964) and King and Schlak (1967) discuss the locations of the minima and maxima in $|F|$. Table 1 gives the $|p|$, b values corresponding to the first 24 zeroes.

3. Discussion The trapped wave appears in F_e for a highly inductive surface and in F_m for a highly capacitive surface. Since a plane earth surface will not be capacitive, the field equations show that the trapped surface wave will be present in the $\bar{E}_{\parallel}$ and $\bar{H}_{\perp}$ fields of the parallel polarized waves over a highly inductive surface. The fields of the transverse polarized waves, which involve F_m, will not have a trapped component.

The relief of $F \equiv |F|\exp(-j\Phi)$ on the complex $p \equiv R(p) + jI(p)$ plane is shown in Fig. 1. Each curve of $|F|$ *v.* $|p|$ in Fig. 2 may be viewed as a section of the relief along the radial of Fig. 1 corresponding to the value of b used. Similarly, Fig. 3 shows curves of Φ *v.* $|p|$ for certain values of b. Near a value of p giving a function zero, Φ changes very rapidly, and is indeterminate at a zero. Curves may also be drawn of Φ *v.* b, and will in general give values differing from those in Fig. 3 for the same $|p|$, b values. The differences are multiples of one cycle or 360° and depend on the way in which the function zeroes are bypassed when p is changed. Fig. 1 shows that the accumulated phase observed in changing p depends on the path chosen and contains an arbitrary number of cycles.

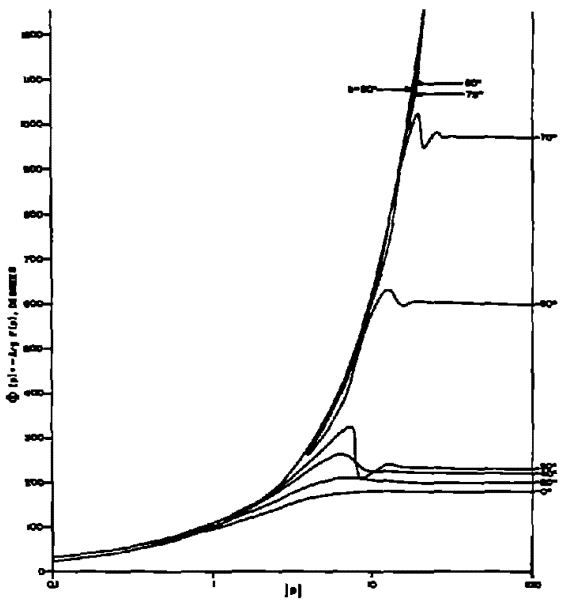

Fig. 3.
Φ *v.* |p| for various b values.

Table 1 - Zeroes of F(p)

n	|p|	b
1	7.988872	51.374694
2	14.100918	65.288811
3	20.277101	71.436984
4	26.485654	74.983401
5	32.713100	77.316614
6	38.952686	78.979073
7	45.200610	80.229111
8	51.454549	81.206308
9	57.712991	81.993043
10	63.974907	82.641237
11	70.239568	83.185317
12	76.506441	83.649054
13	82.775128	84.049418
14	89.045323	84.398862
15	95.316787	84.706740
16	101.589331	84.980222
17	107.862803	85.224899
18	114.137080	85.445200
19	120.412058	85.644679
20	126.687653	85.826223
21	132.963793	85.992204
22	139.240418	86.144586
23	145.517477	86.285014
24	151.794925	86.414875

4. References

King, R.J. and G.A. Schlak (1967), Groundwave attenuation function for propagation over a highly inductive earth, *Radio Sci.*, *2*(7), 687 - 693.

Norton, K.A. (1941), The calculation of ground-wave field intensity over a finitely conducting spherical earth, *Proc. IRE*, *29*(12), 623 - 639.

Norton, K.A. (1942), The polarization of down-coming ionospheric radio waves, *FCC Report 60047*.

Sommerfeld, A. (1909), Uber die Ausbreitung der Wellen in der drahtlosen Telegraphie, *Ann. Phys. IV*, *28*(4), 665 - 736.

Vogler, L.E. (1964), A note on the attenuation function for propagation over a flat layered ground, *IEEE Trans. Ant. Prop.*, *AP-12*(2), 240 - 242.

Wait, J.R. (1957) Excitation of surface waves on conducting, stratified, dielectric-clad and corrugated surfaces, *J. Res. NBS*, *59*(6), 365 - 377.

IMPEDANCE OF A HERTZIAN DIPOLE OVER A CONDUCTING HALF-SPACE

James R. Wait
ESSA Research Laboratories, Boulder, Colorado

Abstract

Various formulations are presented and their consistency is checked by a direct numerical evaluation of the basic integral representation. The usefulness of the compensation theorem approach is demonstrated.

Probably the most basic environmental antenna problem is the vertical electric dipole of fixed current moment $I_o\,ds$ located in free space at a height z_o over an homogeneous half space of conductivity σ and dielectric constant ϵ. The magnetic permeability of the whole space is μ_o and is assumed to be constant. With respect to a cylindrical coordinate system (ρ, ϕ, z), the interface is the plane $z = 0$ and the dipole source is located at $z = z_o$ on the z axis. The situation is illustrated in Fig. 1 where N designates the complex refractive index of the half-space.

When the current in the dipole varies as $\exp(i\omega t)$, the fields can be found from the solution of a well-known boundary value problem [Sommerfeld, 1949]. The Hertz vector $\vec{\Pi}$ has only a z component and, for $z > 0$, is given by $\Pi_z = \Pi_z^{(p)} + \Pi_z^{(s)}$, (1), where the primary influence is

$$\Pi_z^{(p)} = \frac{I_o\,ds}{4\pi i \epsilon_o \omega} \frac{\exp\left[-ik\left[\rho^2 + (z-z_o)^2\right]^{\frac{1}{2}}\right]}{\left[\rho^2 + (z-z_o)^2\right]^{\frac{1}{2}}} \qquad (2)$$

and the secondary influence is

$$\Pi_z^{(s)} = \frac{I_o\,ds}{4\pi i \epsilon_o \omega} \int_o^\infty R(\lambda)\, J_o(\lambda\rho)\, \frac{e^{-u(z+z_o)}}{u}\, \lambda\, d\lambda \qquad (3)$$

$$u_1 = (\lambda^2 - N_1^2 k^2)^{\frac{1}{2}} ,$$

where $R(\lambda) = (u N^2 - u_1)(u N^2 + u_1)^{-1}$, (4), $u = (\lambda^2 - k^2)^{\frac{1}{2}}$, $N = [(\sigma + i\epsilon\omega)/(i\epsilon_o\omega)]^{\frac{1}{2}}$ and $k = (\epsilon_o \mu_o)^{\frac{1}{2}}\omega = 2\pi/(\text{wavelength})$. To satisfy the radiation conditions at infinity, the real parts of u and u_1 are defined to be positive for λ ranging from 0 to ∞ on the real axis.

To carry out a complete calculation of the self impedance of the source dipole requires that the current distribution on the dipole be determined. This aspect of the problem, however, may be deferred if we confine our attention to the change of the impedance resulting from the presence of the lower half-space. Thus, for electrically short antennas, it is permissible to retain the dipole approximation.

By definition, the impedance change δZ is given by $\delta Z = Z - Z_o$, where Z is the self impedance of the dipole in the presence of the half-space while Z_o is the impedance of the same dipole located in free space. Thus, $Z_o = \text{Lim}\,(z_o \to \infty)\, Z$.

According to the "e. m. f. method," if follows that $\delta Z = \mathrm{Lim}(z \to z_o\,,\ \rho \to 0)[\delta E_z\, ds/I_o]$, (5), where the limits are taken after performing ths operation $\delta E_z = (k^2 + \partial^2/\partial z^2)\,\Pi_z^{(s)}$, (6). This leads to the result

$$\delta Z = -\frac{(ds)^2}{4\pi i\, \varepsilon_o\, \omega} \int_o^\infty R(\lambda)\, \frac{\lambda^3}{u}\, e^{-\alpha u}\, d\lambda \qquad (7)$$

where $\alpha \doteq 2\, z_o$. It is convenient to normalize this by writing $\delta Z = R_o\, T$ where $R_o = 20\, k^2 (ds)^2$ is the real part of Z_o and is the radiation resistance of the dipole in free space.

To gain insight into the problem we now develop an asymptotic expansion by expanding $R(\lambda)$ in a series about $\lambda = 0$. As it happens, in this particular case, $R'(0)$, $R'''(0)$ and all odd-numbered derivatives vanish. Therefore. we have $R(\lambda) = R(0) + \lambda^2 R''(0)/2! + \lambda^4 R^{iv}(0)/4! + \ldots$ (8). This leads to an expansion of the type

$$\Lambda \sim -R(0)\left(k^2 + \frac{\partial^2}{\partial \alpha^2}\right)\frac{e^{-ik\alpha}}{\alpha} - \frac{R''(0)}{2!}\left(k^2 + \frac{\partial^2}{\partial \alpha^2}\right)^2 \frac{e^{-ik\alpha}}{\alpha} - \frac{R^{iv}(0)}{4!}\left(k^2 + \frac{\partial^2}{\partial \alpha^2}\right)^4 \frac{e^{-ik\alpha}}{\alpha} \qquad (9)$$

and so on. [A constant factor has been omitted on the right-hand side.] Retaining just the first two terms (and including the correct multiplying factor), we obtain

$$T \simeq -3|R(0)|\, A \exp\{i[\arg R(0) - \phi_a - k\alpha]\} - 6\,|k^2 R''(0)|\, B \exp\{i[\arg R''(0) - \phi_a - k\alpha]\} \qquad (10)$$

where $A\, e^{-i\phi_a} = [1 - i/(k\alpha)](k\alpha)^{-2}$ (11)

and $B\, e^{-i\phi_b} = \left[\frac{3}{(k\alpha)^2} - i\left(\frac{3}{(k\alpha^3)} - \frac{1}{k\alpha}\right)\right]\frac{1}{(k\alpha)^2}$ (12)

$$R(0) = (N-1)/(N+1)\ , \quad k R''(0) = -(2/N)(N-1)/(N+1) = -(2/N) R(0)\ .$$

The question of the convergence of expansions of this type is discussed elsewhere [Wait, 1962]. Suffice it to say here that the results are asymptotic, being strictly valid only if $k \to \infty$.

If we now regard $|N|$ as a large parameter, (10) can be written in the form

$$T \simeq \frac{3i e^{-ik\alpha}}{(k\alpha)^3}(1 + ik\alpha) + 6\, e^{-ik\alpha} N^{-1}[(k\alpha)^{-2} + i(k\alpha)^{-3} + \text{terms in } (k\alpha)^{-4}, \text{ etc.}]\ , \qquad (13)$$

where we also neglect terms contained in $1/N^2$, $1/N^3$, etc.

In a closely related study, Vogler and Noble [1964], in close collaboration with the present writer, investigated this same problem. Under the condition $|k\alpha\, N| \gg 1$, they obtained the following result for the vertical electric dipole

$$T \simeq \frac{3i e^{-ik\alpha}}{(k\alpha)^3}\left[\frac{N-1}{N+1}\right]\left\{1 + \frac{4}{N} + i\left[k\alpha + \frac{6}{k\alpha\, N}\left(1 - \frac{2N-3}{N^2}\right)\right]\right\}\ . \qquad (14)$$

This asymptotic formula was obtained by a repeated integration by parts of the basic integral (7). It is interesting to note that (14) also reduces to (13) under the additional restriction that $|N| >> 1$.

We come now to another approach to the impedance problem. Lavrov and Knyazev [1965] make approximations directly to the integrand of (3) which is the Hertz potential of the secondary field. Tney argue that if $|N| >> 1$, we can make the substitutions $u_1 = (\lambda^2 - N^2 k^2)^{\frac{1}{2}} \simeq i N k$ and

$$u N^2 + u_1 = (\lambda^2 - k^2)^{\frac{1}{2}} N^2 + (\lambda^2 - N^2 k^2)^{\frac{1}{2}} \simeq N^2 (\lambda^2 - k^2)^{\frac{1}{2}} , \qquad (15)$$

Assuming that these are good approximations over the whole significant range of the integration variable λ, we see that

$$\Pi_z^{(s)} = \frac{I_o \, ds}{4\pi i \, \epsilon_o \, \omega} \left[\frac{e^{-ikR}}{R} - 2ik \frac{1}{N} P \right] \qquad (16)$$

where $$P = \int_o^\infty J_o [\lambda (R^2 - \hat{z}^2)^{\frac{1}{2}}] \exp[- \hat{z} (\lambda^2 - k^2)^{\frac{1}{2}}] \frac{\lambda \, d\lambda}{\lambda^2 - k^2} \qquad (17)$$

where $R^2 = \rho^2 + \hat{z}^2$ and $\hat{z} = z_o + z$. We immediately see that P satisfies the differential equation

$$\frac{\partial P}{\partial \hat{z}} = - \frac{e^{-ikR}}{R}$$

To evaluate P we first of all recognize that values of $\hat{z}$ near R are significant when dealing with self impedance estimates (i.e., $\rho << \hat{z}$). In this case,

$$P \simeq \int_R^\infty \frac{e^{-ikx}}{x} dx = - Ei(-ikR) \qquad (18)$$

which satisfies $$\frac{\partial P}{\partial \hat{z}} = - \frac{e^{-ikR}}{R} \frac{\hat{z}}{(\rho^2 + \hat{z}^2)^{\frac{1}{2}}} \simeq - \frac{e^{-ikR}}{R} . \qquad (19)$$

Using this result with (5) and (6), we readily deduce that

$$T \simeq \frac{3}{N} \left[\frac{i}{k\alpha} \left(1 - \frac{i}{k\alpha} \right) e^{-ik\alpha} - Ei(-ik\alpha) \right] \quad \text{where} \quad \alpha = 2 z_o . \qquad (20)$$

Noting that $$Ei(-ix) \sim \frac{e^{-ix}}{-ix} \left[1 + \frac{1}{(-ix)} + \frac{2!}{(-ix)^2} + \frac{3!}{(ix)^3} + \quad \right] \qquad (21)$$

it is evident that (20) reduces, for $k\alpha >> 1$, to (13) at least to the order shown.

Another approach to the self-impedance problem, which has been favored in recent years, is based on the compensation theorem [Monteath, 1951; Wait, 1969]. Using this method, we have $\delta Z = \delta Z^{(\infty)} + \Delta Z$, (21) where $\delta Z^{(\infty)} = \text{Lim} \, (\sigma \to \infty) \, \delta Z$. The impedance increment which accounts for the finite conductivity of the half-space is given exactly by

$$\Delta Z = - \frac{1}{I_o^2} \int_o^\infty H_\phi^{(\infty)}(\rho, o) \, E_\rho (\rho, o) \, 2\pi \rho \, d\rho \qquad (22)$$

where $H_\phi^{(\infty)}(\rho, o)$ is the magnetic field of the dipole on a perfectly conducting ground plane at $z = 0$ and $E_\rho (\rho, o)$ is the <u>actual</u> tangential electric field at

$z = 0$. The joker is that $E_\rho(\rho, 0)$ is not known; otherwise, the problem would be trivial. However, the argument usually goes that the tangential electric field is proportional to the tangential magnetic field which, in turn, is replaced by its value for a perfectly conducting half-space. Thus, if $|N| \gg 1$, we may say that $E_\rho(\rho, o) \simeq -(120\pi/N)\, H_\phi^{(\infty)}(\rho, 0)$, (23) , where $120\pi/N$ is the effective surface impedance of the half-space. Inserting this into (22) and using the appropriate value for $\delta Z^{(\infty)}$ in (21), leads back without further approximations to (20). Thus, we come to the remarkable conclusion that the compensation theorem approach leads to identical results for the simplified integral formulation described above.

In many cases of practical interest, the approximate formulas for the impedance increment are not valid. Such is the case, for example, when $|N|$ is not reasonably large compared with unity. Then we must resort to numerical integration. For this purpose, a new variable $\lambda = kg$ is employed. Then T can be expressed in the form

$$T = \int_o^\infty \frac{F(g)}{(g-1)^{\frac{1}{2}}}\, dg \tag{24}$$

where $F(g) = i\frac{3}{2} R(kg)\, g^3 (1+g)^{-\frac{1}{2}} \exp\left[-k\alpha (g^2-1)^{\frac{1}{2}}\right]$ (25)

and $R(kg) = \left[N^2(g^2-1)^{\frac{1}{2}} - (g^2-N^2)^{\frac{1}{2}}\right]\left[N^2(g^2-1)^{\frac{1}{2}} + (g^2-N^2)^{\frac{1}{2}}\right]^{-1}$ (26)

To comply with appropriate radiation conditions, we require that $\mathrm{Lim}(g\to\infty)(g^2-1)^{\frac{1}{2}} = g$, $\mathrm{Lim}(g\to\infty)(g^2-N^2)^{\frac{1}{2}} = g$, $\mathrm{Lim}(g\to 0)(g^2-1)^{\frac{1}{2}} = i$, and $\mathrm{Lim}(g\to 0)(g^2-N^2)^{\frac{1}{2}} = iN$. To simplify the integration we rewrite (24) as a sum of two parts. Thus,

$$T = -i\int_o^1 F(g)(1-g)^{-\frac{1}{2}}\, dg + \int_1^\infty P(g)(g-1)^{-\frac{1}{2}}\, dg \quad . \tag{27}$$

Further simplification is achieved by setting $x = \sqrt{g-1}$ in the first integral and $y = \sqrt{1-g}$ in the second integral. Then, finally,

$$T = \frac{\delta Z}{R_o} = 2\int_o^\infty F(1+x^2)\, dx - 2i\int_o^1 F(1-y^2)\, dy \quad , \tag{28}$$

where the function F with the arguments indicated is defined by (25).

Some numerical results based on the above formulas are now considered. For $|N| = \infty$, corresponding to a perfectly conducting plane at $z = 0$, the impedance increment is given exactly by (10). The results for this case are shown in Figure 2 in the form of an Argand plot with the values of $k\alpha$ indicated on the curves. It is immediately apparent that the impedance increment becomes indefinitely large as $k\alpha$ becomes small. However, the real part of T approaches unity as $k\alpha$ tends to zero.† This is physically acceptable and

†This follows from the relation $\mathrm{Lim}(x\to 0)\left\{\mathrm{Re}\left[-\frac{3}{x^2}\left(1-\frac{i}{x}\right)e^{-ix}\right]\right\} = 1$.

represents the doubling of the free-space radiation resistance as the dipole approaches the conducting plane.

Some results for finite values of N are shown in Figures 3a and 3b for $N = 30\, e^{-i\pi/4}$ and $10\, e^{-i\pi/4}$, respectively. These would correspond to a highly conducting half-space where displacement currents are negligible. The solid curves are based on using two terms in the asymptotic formula for T given by (15). The dashed curves correspond to just using the first term in the same formula (i.e., set B = 0). The distance between these curves (measured on a radius from the origin) gives some idea as to the accuracy of the two-term asymptotic formula for T. In the case of $|N| = 30$, it appears that the results should be quite accurate even for relatively small values of $k\alpha$. A further check for these two cases is afforded by a numerical integrataion for $k\alpha = 3$ for each case. This is shown by a small circle in both Figure 3a and Figure 3b.

The formula for δZ or T based on the compensation theorem is also shown in Figures 3a and 3b and indicated by broken curves. In both cases, it falls in between the curves for the one- and two-term asymptotic formulas. Also, it appears to agree quite closely with the points obtained from a direct numerical integration.

References

Lavrov, G. A., and A. S. Knyazev (1965), Prizemnye i Podzemmyye Antenny (Sovetskoye Radio, Moscow).

Monteath, G. D. (1951), Proc. IEE(London), 98, Pt. IV, 23-31.

Sommerfeld, A. N. (1949), Partial Differential Equations (Academic Press, N. Y.)

Vogler, L. E., and J. L. Noble (Jan. 31, 1964), Nat. Bur. Stds. Monograph 72.

Wait, J. R. (1962), J. Research NBS 66D, No. 5, 563-569.

Wait, J. R. (1969), Chapter 23, in Antenna Theory, vol. 2 (ed. by R. E. Collin and F. J. Zucker) McGraw-Hill Book Co., Inc., N. Y.

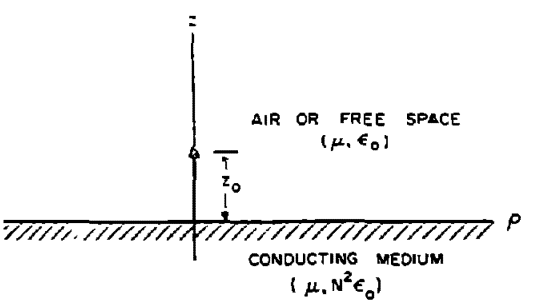

Fig. 1 - Dipole over conducting half-space.

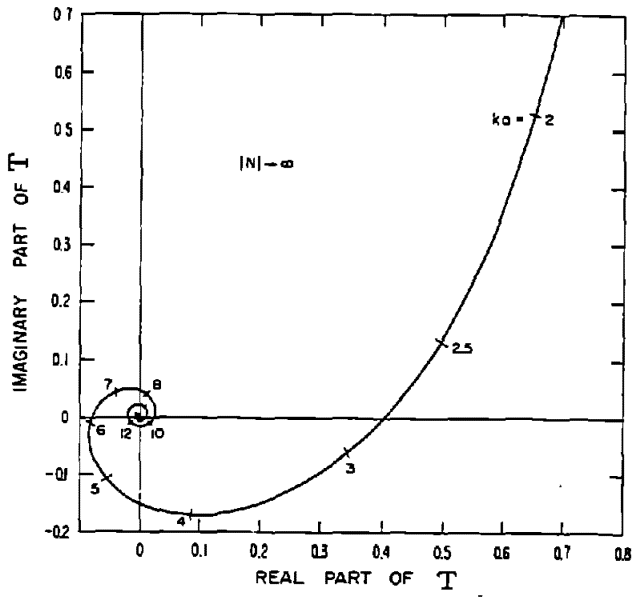

Fig. 2 - The change of impedance of a vertical dipole over a horizontal perfectly conducting plane.
(The results are expressed as a ratio to the free-space radiation resistance.)

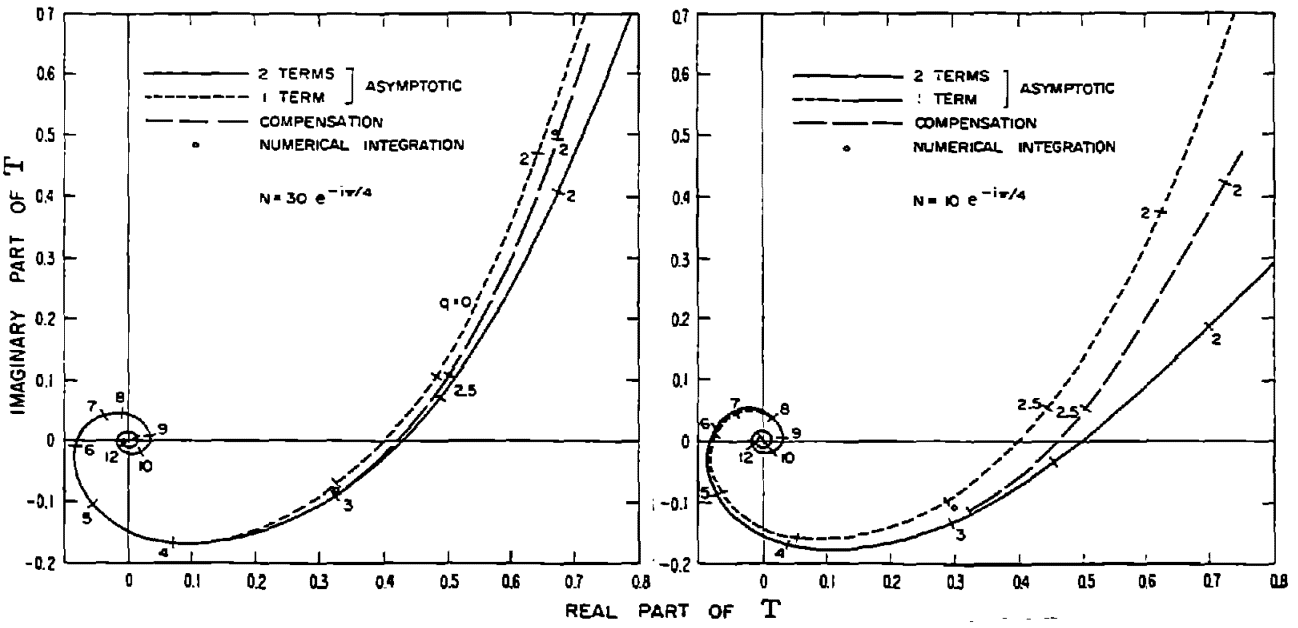

Fig. 3a Fig. 3b

The change of impedance of a vertical dipole over a horizontal imperfectly conducting plane.
(The results are expressed as a ratio to the free-space radiation resistance.)

Effect of the Ground Screen on the Field Radiated from a Monopole

W. J. Surtees, ESSA / ITS

The ground wave field intensity is calculated from a simple application of the compensation theorem for a thin, vertical antenna with sinusoidal current distribution when placed over a circular ground screen laid upon homogeneous flat earth. Results are in agreement with those obtained by Wait (1956). Some additional numerical results are presented showing the effect of antennas of different lengths and height.

1. Introduction

The improvement to low-angle radiation from vertical antennas by the use of ground screens has been investigated theoretically over a number of years since the compensation theorem approach of Monteath (1951) was first published.

The purpose of this paper is to apply the compensation theorem to develop expressions for the field radiated by thin linear vertical antennas of finite length when placed on or raised over a circular ground screen which is laid upon a ground of arbitrary electrical constants.

2. Formulation

The problem of determining the effect of a finite surface impedance η', varying from point to point, on the performance of an antenna has been formulated by Monteath (1951, 1958) using the compensation theorem of network analysis. He obtains the following expression for the change in mutual impedance between two antennas A and B.

$$Z_{AB}' - Z_{AB} = \frac{1}{I_0^2} \int\int (\eta' - \eta)\, (\overline{H}_{At}' \cdot \overline{H}_{Bt}) \, ds. \qquad (1)$$

where ds is a surface element (Monteath, 1951).

If η represented the surface impedance of a uniform ground, and η' represents the surface impedance of the ground plus a ground system then the change in mutual impedance can be calculated from (1) if $\overline{H}_{At}'$ and $\overline{H}_{Bt}$ were known. The fields in fact are not known and therefore must be replaced by an approximation. The approximation used is to replace $\overline{H}_{At}'$ and $\overline{H}_{Bt}$ by $\overline{H}_{A1}^{\infty}$ and $\overline{H}_{B1}^{\infty}$ the magnetic fields that would exist if the ground were everywhere a perfect conductor, and Z_{AB} would become Z_{AB}^{∞}. One would thus expect the results to be best for a highly conducting ground.

Applying the above to find the field from a vertical center-fed antenna of length 2ℓ whose terminals are at a height $h + \ell$ above the center of a circular perfectly conducting ground screen of radius a and using the field from the thin, linear, center-fed antenna as given (Jordan, 1950) by

$$H_{At}^{\infty} = \frac{jI_o}{2\pi\rho \sin k\ell}\left(e^{-jkr_1} + e^{-jkr_2} - 2e^{-jkr_o}\cos k\ell\right), \qquad (2)$$

we obtain

$$G_c - 1 = -\frac{\eta k \cos\psi}{\eta_o E}\int_o^a \left(e^{-jkr_1} + e^{-jkr_2} - 2e^{-jkr_o}\cos k\ell\right) \cdot J_1(k\rho\cos\psi)\, d\rho , \qquad (3)$$

where G_c is the complex ratio of the radiated field at B in the presence of the earth system to the field at B over a perfect conductor, and

$$E = \cos[k(h + 2\ell)\sin\psi] + \cos[kh\sin\psi] - 2\cos[k(h+\ell)\sin\psi]\cos k\ell . \qquad (4)$$

The distances can be determined from the geometry shown in Fig. 1, and

$k = \frac{2\pi}{\lambda}$, λ is the operating wavelength.

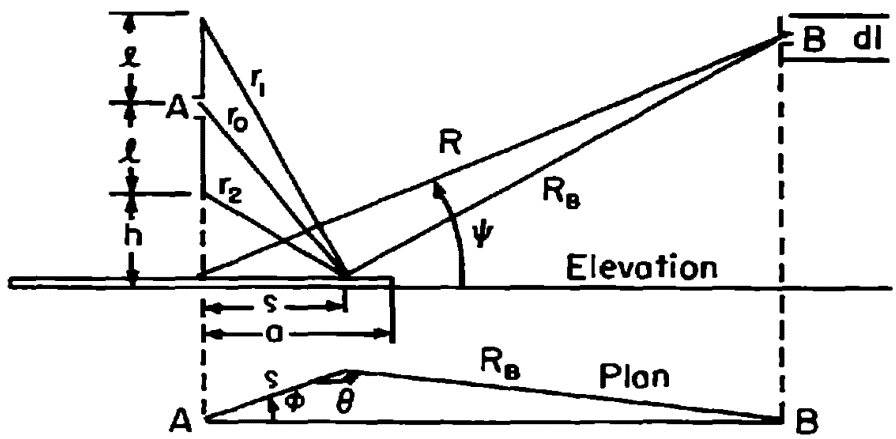

Fig. 1.

Along the ground, $\psi = 0$, and (3) may be written as

$$G_{oc} - 1 = -\frac{\eta}{\eta_o}\frac{1}{E_o}\left[V(ka,\ h + 2\ell) + V(ka,h) - 2\cos k\ell\ V(ka, h+\ell)\right] \qquad (5)$$

where we define $V(x,\ell) = \int_o^x e^{-j\sqrt{y^2 + (k\ell)^2}}\, J_1(y)\, dy$, (6)

and E_o is the value of E when $\psi = 0$.

In (3), if $k\rho = y$ we may approximate

$$J_1(y\cos\psi) \text{ by } \cos\psi\, J_1(y) \text{ if } \frac{y}{2}\sin^2\psi << 1 \text{ , and } y < 3.3,$$

and,

$$G_c - 1 = \left(G_{oc} - 1\right)\frac{E_o}{E}\cos^2\psi \qquad (7)$$

Similar considerations will yield expressions for the field radiated by a thin, base-or loop-fed antenna of any length ℓ when it is placed on the center of the ground screen by letting $h = -\ell$ in the above.

3. Results

The integrals represented by the function $V(x,\ell)$ defined by (6) must be evaluated numerically. A few cases have been computed by Mrs. Lillie C. Walters by the method of Gaussian quadrature, and the results are presented in Figs. 2 and 3 for vertical antennas.

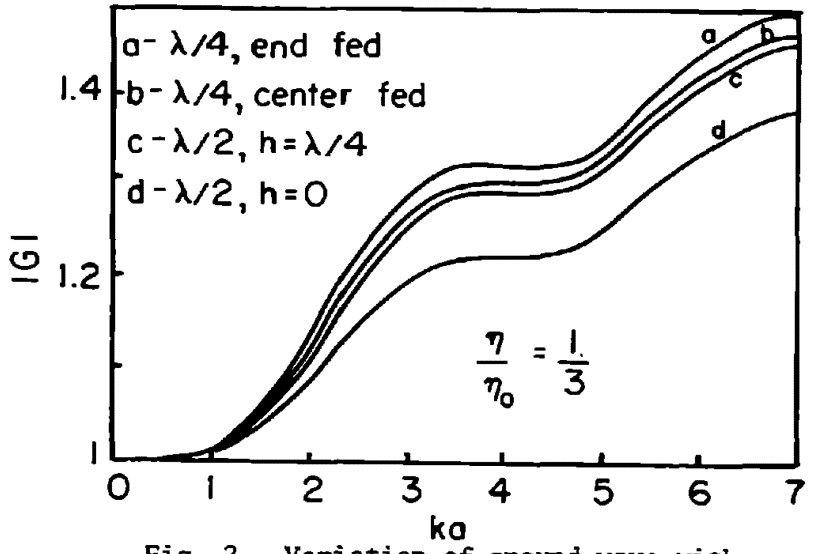

Fig. 2. Variation of ground wave with radius of ground screen.

Fig. 2 shows $|G|$ as a function of screen radius a, for the four antennas considered when a perfectly conducting circular ground screen is laid upon a poorly conducting ground. Comparing curves a and b indicates that the performance of the short quarter wave monopole over the ground screen is better when base fed than when center fed and that the ground screen has the most effect if the antenna is short. Curve a is in agreement with the results of Wait (1956).

The curves for cases c and d show that raising the center fed half-wave antenna a distance of one quarter wavelength improves the ground wave field by a factor of about 1.05.

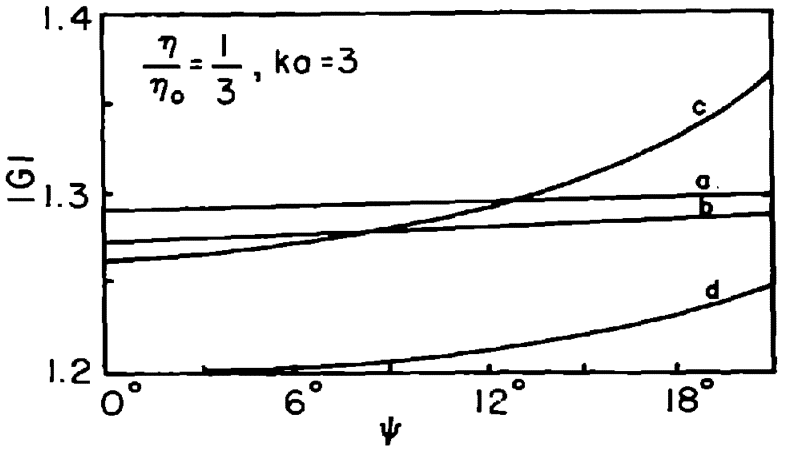

Fig. 3. Variation of radiation with low elevation angle.

Fig. 3 was produced from (5) and (7) and shows the variation of the low angle radiation for the four cases considered when the radius of the ground screen was close to a half wavelength (ka = 3). The ground screen becomes even more effective as the elevation angle ψ is increased. Cases c and d show that the field of the elevated half-wave antenna would equal the field of the ground based one at an elevation angle near 20°, and there would be an advantage in raising the antenna to improve the low angle radiation.

4. References

Jordan, E. C. (1950), Electromagnetic waves and radiating systems, p. 323, (Prentice-Hall Inc., New York, N. Y.)

Monteath, G. D. (1951), Application of the compensation theorem to certain radiation and propagation problems, Proc. IEE, 98 Pt IV, 23-30.

Monteath, G. D. (1958), The effect of the ground constants, and of the earth system, on the performance of a vertical medium wave aerial, Monograph 279R Proc. IEE, Pt C, 1-15.

Wait, J. R. (1956), Effect of the ground screen on the field radiated from a monopole, Trans. IRE, AP-4, 179-181.

RADIATION OF A MONOPOLE ANTENNA ON THE BASE OF A CONICAL STRUCTURE*

by
G.A. Thiele and M. Travieso-Diaz
The Ohio State University ElectroScience Laboratory
H.S. Jones
Harry Diamond Laboratories, Washington, D.C.

ABSTRACT

The point-matching technique is used to calculate the far-field patterns of a monopole located axially at the base of a perfectly conducting cone. Agreement among experimental patterns and theoretical calculations was very good.

TECHNICAL DISCUSSION AND RESULTS

In this paper, the point-matching technique (Richmond, 1965; Harrington, 1968) is used to enforce the tangential electric field boundary condition at discrete points on the surface of a cone. The cone is excited by a monopole at the center of its base, as shown in Fig. 1. The current distribution on the monopole is assumed. That is, the interaction between the cone and the monopole is ignored. To facilitate the application of the point-matching technique, the cone is represented by a grid of wire segments as shown in Fig. 1. Due to the symmetry of the problem, no wire segments are required around the cone.

In matching boundary conditions on the cone, we require that the tangential component of the field from the monopole cancel the tangential component of the field scattered by all the segments at the center of each segment. To obtain an expression for the near fields of a monopole placed on the positive z-axis with source at the origin, one can start with expressions in Jordan (1950) using a current distribution of the form

$$(1) \qquad I(z) = \begin{cases} |I| \sin(H-z) & z > 0 \\ 0 & z < 0 \end{cases}.$$

For the field scattered by a wire segment of length s and having a constant current on it, one can use expressions given by Richmond (1966).

*The work reported in this paper was supported in part by Contract DAAG-39-68-C-0061 between Harry Diamond Laboratories, and The Ohio State University Research Foundation.

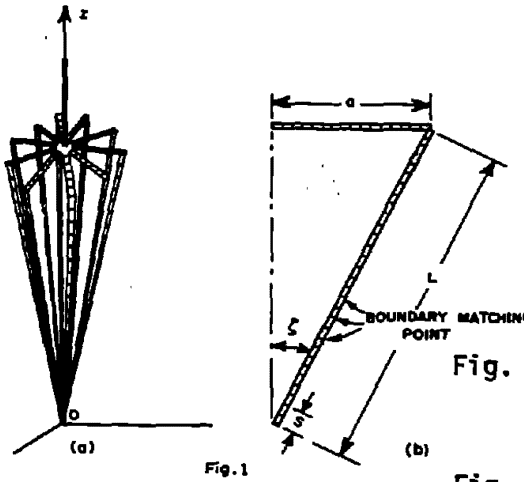

Fig. 1. (a) Wire-grid model of the monopole and cone; (b) cone generating line showing position of segments.

Fig. 2. Experimental wire-grid cone.

Thus, when the tangential electric field boundary condition is enforced at segment K,

$$(2) \qquad \sum_{j=1}^{N} S_{Kj} I_j = - E_K^{inc.} \qquad K = 1,2,\cdots N$$

where N is the total number of segments used to simulate the cone, E_K^{inc} is the tangential component of the field from the monopole, I_j is the undetermined value of the current on segment j and S_{Kj} is proportional to the field from segment j evaluated at segment K.

Enforcement of the boundary condition at each of the N segments results in a system of N simultaneous linear equations which may readily be solved for the N unknowns, I_j. Once the currents are known on the cone, the associated far-fields radiated by these currents may be superimposed with the far-field of the monopole to obtain the patterns of the monopole-cone structure.

Due to the symmetry of the problem, it is not necessary to solve for the currents on all the segments shown in Fig. 1. If the same number and size segments are used in each of the ten "generating lines" of Fig. 1, then the currents on each line will be the same. Hence, if there are M segments on each line and L lines, then

$$(3) \qquad I_j = I_{j+M} = I_{j+2M} = \cdots = I_{j+(L-1)M}$$

Thus, Eq. (2) reduces to

$$(4) \qquad \sum_{j=1}^{M} I_j \left(\sum_{n=0}^{L-1} S_{K(j+nM)} \right) = - E_K^{inc} \quad , K = 1,2,\cdots M$$

This permits us to reduce the number of unknown currents to M, while the actual number of unknowns is L·M. Furthermore, computer storage limits M, not L·M. For the following power patterns, L was chosen to be ten. The cone of interest is actually the frustrum of a cone having a slant height of 30.5", a base radius of 7.2", a half angle of 9.7°, a spherical cap radius of 2.5" and a monopole whose length is between 0.203 and 0.312λ. Patterns are taken at frequencies between 300 and 500 MHz.

Figure 2 shows the wire-grid experimental model. Not shown is the solid cone of the same size as the wire-grid model. Figure 3 shows a typical comparison of the experimental patterns taken for the two models. Since agreement between them is good, one can deduce that the wire-grid model closely approximates the solid cone.

Figures 4 and 5 show two patterns where the monopole is a quarter wavelength. Both the experimental patterns for the wire grid cone and the theoretical patterns are shown. Agreement is seen to be good, particularly the locations of the pattern maxima and minima.

Figure 6 shows patterns taken at 500 MHz for a monopole whose length is λ/4 at 400 MHz. Agreement is good except in the tip region where the effects of the cable leaving the spherical cap are thought to influence the pattern in this region. Further experimental work is needed to verify the extent of the influence of the cable.

In conclusion, the point-matching technique has been applied to the problem of a cone excited by a monopole located on its base. A wire grid-model has been used for the theoretical calculations. Experimental patterns were taken for a wire-grid experimental model and also for the solid cone which it approximates. Agreement among the two types of experimental patterns and the theoretical patterns was good.

REFERENCES

Richmond, J.H. (1965), Digital computer solutions of the rigorous equations for scattering problems, Proc. of the IEEE, 53, No. 8, 796-804.

Harrington, R.F. (1968), Field Computation by Moment Methods, (The Macmillan Company, New York, N.Y.)

Jordan, E.C. (1950), Electromagnetic Waves and Radiating Systems, pp. 320-324, (Prentice-Hall, Inc., Englewood Cliffs, N.J.)

Richmond, J.H. (1966), A wire-grid model for scattering by conducting bodies, IEEE Trans., Ant. Prop. AP-14, No. 6, 782-786.

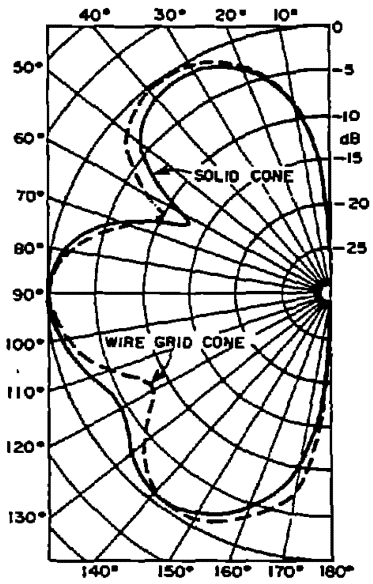

Fig. 3. Experimental comparison at 400 MHz with a λ/4 monopole.

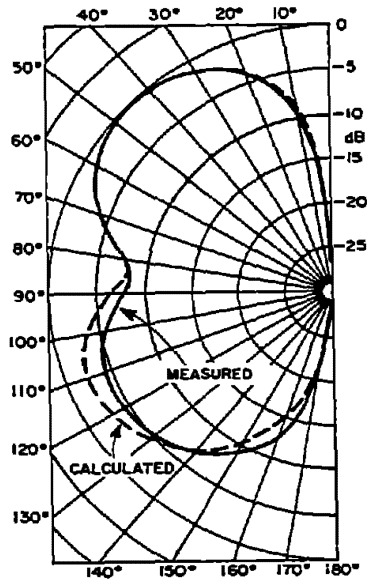

Fig. 4. Patterns at 300 MHz using a λ/4 monopole.

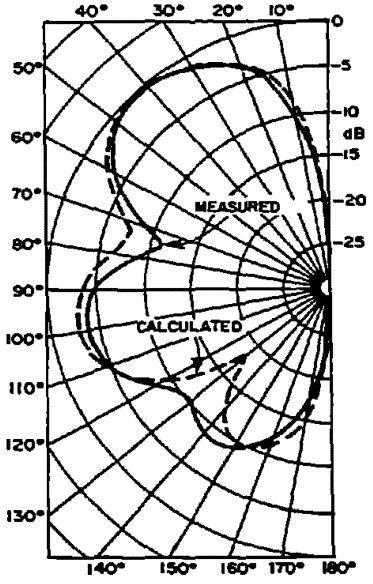

Fig. 5. Patterns at 350 MHz using a λ/4 monopole.

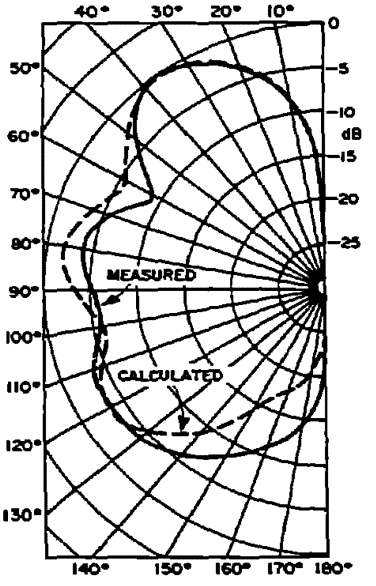

Fig. 6. Patterns at 500 MHz using a .312λ monopole.

REFLECTION OF WAVES OF ARBITRARY POLARIZATION FROM A RECTANGULAR MESH GROUND SCREEN

G.A. Otteni

HMES – General Electric Company, Syracuse, New York

The reflection of plane electromagnetic waves of arbitrary polarization and incidence from an infinite rectangular mesh of small circular wires is treated. The screen is parallel to a plane earth so that the effects of ground reflection are included. Some representative results are shown.

1. Introduction

The theory of scattering of an electromagnetic wave from a grating of parallel wires has received considerable attention because of the possible applications of the diffraction and reflecting properties of such grids. A survey of the theory of wire grid effects has been published by Larsen (1962) and some additional papers have been listed here as references.

There appears to be little work published for scattering of waves of arbitrary polarization and incidence by parallel wire screens or scattering from crossed wire screens. This paper considers, in particular, the reflection properties of a rectangular mesh of circular wires for arbitrary polarization and incidence. It should be noted that the theory also describes parallel wire grids when the limit of large spacing is taken for one dimension of the rectangular mesh.

2. Mathematical Description

The method of solution chosen for the problem is similar to the approach used by Wait (1962) in describing a parallel wire grid except that the potential functions chosen here are directed normal to the screen so that the field expansions are in terms of TE and TM modes with respect to the screen normal.

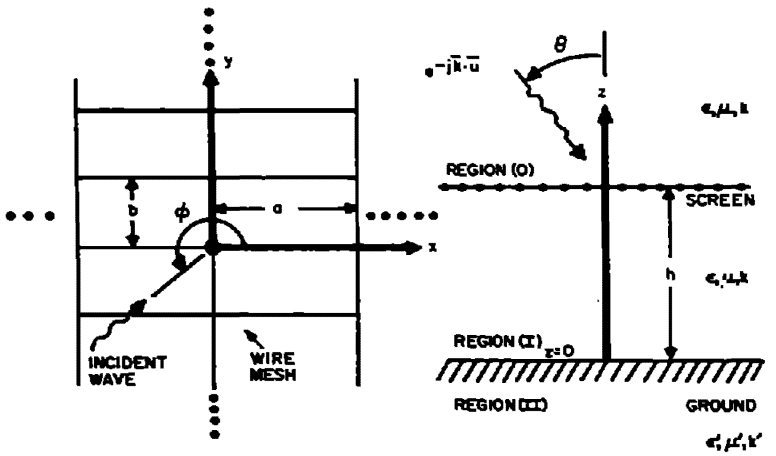

FIGURE 1. Ground-screen geometry.

The rectangular mesh has a cell dimension a by b and is located parallel to and a distance h above a homogeneous ground region bounded by z=O. The wires are of circular cross section of radius r and are assumed to be much smaller than any cell dimension of the screen. The time and phase factors are of the form:

$$e^{j(\omega t - \bar{k}\cdot\bar{u})}$$

where $\bar{u}$ is the position vector from the origin of the rectangular coordinate system.

The description of each mode for expansion of the scattered field in Region (O), (see Fig. 1) in terms of TE and TM modes, is given by the following relations where the summation indices n,m are not shown explicitly:

$$H_z = k_\perp^2 \psi_h \left\{ e^{-\Gamma(z-h)} + R_h e^{-\Gamma(z+h)} \right\}, \tag{1}$$

$$E_z = -k_\perp^2 \psi_e \left\{ e^{-\Gamma(z-h)} - R_e e^{-\Gamma(z+h)} \right\}, \tag{2}$$

$$\bar{H}_t = j\bar{k}_\perp \Gamma \psi_h \left\{ e^{-\Gamma(z-h)} + R_h e^{-\Gamma(z+h)} \right\} - jY_e \Gamma (\bar{a}_z \times \bar{k}_\perp) \psi_e \left\{ e^{-\Gamma(z-h)} - R_e e^{-\Gamma(z+h)} \right\}, \tag{3}$$

$$\bar{E}_t = -j\bar{k}_\perp \Gamma \psi_e \left\{ e^{-\Gamma(z-h)} - R_e e^{-\Gamma(z+h)} \right\} - jZ_h \Gamma (\bar{a}_z \times \bar{k}_\perp) \psi_h \left\{ e^{-\Gamma(z-h)} + R_h e^{-\Gamma(z+h)} \right\}, \tag{4}$$

where

$$\bar{k} = k_x \bar{a}_x + k_y \bar{a}_y - k_z \bar{a}_z ,$$

$$\bar{k}_\perp = \left(k_x + \frac{2n\pi}{a}\right) \bar{a}_x + \left(k_y + \frac{2m\pi}{b}\right) \bar{a}_y ,$$

$$k_\perp^2 = |\bar{k}_\perp|^2 , \; k^2 = |\bar{k}|^2 = \omega^2 \mu\epsilon ,$$

$$\Gamma = (k_\perp^2 - k^2)^{1/2} ,$$

$Y_e = \frac{j\omega\epsilon}{\Gamma}$, $Z_h = \frac{j\omega\mu}{\Gamma}$ are the TM wave admittances and TE wave impedances, respectively, and

ψ_e, ψ_h are the TM and TE wave functions.

The subscript t refers to the transverse field components which are the fields parallel to the screen. Similar expressions are valid for Regions (I) and (II) except that for Region (II) the reflection coefficients, R, are replaced by transmission coefficients, T, and the electromagnetic parameters, ϵ, μ, k are replaced by the corresponding primed (′) quantities.

The boundary conditions at z=O ($\bar{H}_t$ and $\bar{E}_t$-continuous) and at z=h ($\bar{E}_t$-continuous) give expressions for the reflection coefficients.

$$R_e = \frac{Y_e' - Y_e}{Y_e' + Y_e} , \tag{5}$$

$$R_h = \frac{Z_h' - Z_h}{Z_h' + Z_h} , \tag{6}$$

where the primes (′) refer to the corresponding quantities for the ground region (Region II).

It is assumed that the field around each wire is uniform and the impedance boundary condition gives the total axial electric field along a wire as

$$E = \frac{Z_i I}{2\pi r} ,$$

for an axial current I flowing on each wire of radius r with surface impedance Z_i. In addition, it is assumed that the scattered field is not appreciably different from that of infinitesimal wires carrying a current I. The possible currents in the azimuthal direction around each wire are neglected.

Calculations of the scattered field is made by a Green's function approach (see for example Collin) assuming that the amplitudes of the current modes are unknown. The expressions for the x-directed vector potential is given by (7) in terms of the unknown current mode amplitudes in the x direction with the time factor $e^{j\omega t}$ suppressed

$$A_x = \mu \sum_{n=-\infty}^{\infty} \sum_{m=-\infty}^{\infty} \frac{I_{xn}}{2\Gamma b} e^{-j(2n\pi)\, x/a} e^{-j(2m\pi)\, y/b} e^{-\Gamma |z-h|} \cdot e^{-jk_x x} e^{-jk_y y} . \tag{7}$$

A similar expression holds for the y-directed vector potential and in fact, all expressions obtained for x can be used for y if the substitutions

$$\begin{aligned} &x \longleftrightarrow y \\ &n \longleftrightarrow m \\ &a \longleftrightarrow b , \end{aligned} \tag{8}$$

are made.

The scattered electric field is found from

$$\bar{E}_s = -j\omega\bar{A} + \frac{\nabla\nabla\cdot\bar{A}}{j\omega\mu\varepsilon} , \tag{9}$$

where $\bar{A}$ is the total vector potential for the screen and the wave functions ψ_e, ψ_h are obtained by equating the expressions for scattered field at the screen. The incident plane wave is decomposed into a TM and TE representation. The incident and ground-reflected plane wave components are added to the scattered and ground-reflected scattered field to obtain an expression for the total axial electric field at the surface of each wire (z=h+r). The impedance condition is then used to solve for the current mode amplitudes and the effective reflection for the TM and TE wave components are then calculated from the currents.

The current mode amplitudes are given by

$$I_{xo} = \frac{E_{xo}\left\{e^{jk_z(h+r)} - \frac{k_x^2}{k_t^2} R_{oe} e^{-jk_z(h+r)} + \frac{k_y^2}{k_t^2} R_{oh} e^{-jk_z(h+r)}\right\}}{Z_{wxo}} \tag{10}$$

$$\frac{-E_{yo}\left\{\frac{k_x k_y}{k_t^2}(R_{oe} + R_{oh}) e^{-jk_z(h+r)}\right\}}{Z_{wxo}} + \frac{B_{x0}}{Z_{wxo}}$$

$$\text{where } Z_{wx} = Z_i - \frac{1}{j\omega\varepsilon} \sum_{m=-\infty}^{\infty} \left[\left\{\frac{k^2 - k_{\perp x}^2}{2\Gamma b}\right\} + R_e\left\{\frac{k_{\perp x}^2 \Gamma^2}{2\Gamma b k_\perp^2} e^{-2\Gamma h}\right\}\right. \tag{11}$$

$$\left. + R_h\left\{\frac{k^2 k_{\perp y}^2}{2\Gamma b\, k_\perp^2} e^{-2\Gamma h}\right\}\right] e^{-\Gamma r} ,$$

$$\text{and } Z_{wxo} = Z_{wx}\,|_{n=0} ; \tag{12}$$

$$B_x = -\frac{1}{j\omega\varepsilon} \sum_{m=-\infty}^{\infty} \left\{\frac{k_{\perp x} k_{\perp y} I_{ym}}{2\Gamma a}\right\} \cdot \left\{1 - \frac{\Gamma^2}{k_\perp^2} R_e e^{-2\Gamma h}\right. \tag{13}$$

$$\left. + \frac{k^2}{k_\perp^2} R_h e^{-2\Gamma h}\right\} e^{-\Gamma r} ,$$

and

$$B_{xo} = B_x\,|_{n=0} . \tag{14}$$

where

$$R_{oe} = R_{e|m=n=o}$$

$$R_{oh} = R_{h|m=n=o} , \tag{15}$$

$$k_t^2 = k_x^2 + k_y^2 ,$$

$$k_{\perp x} = k_x + \frac{2n\pi}{a} , \tag{16}$$

and $$k_{\perp y} = k_y + \frac{2m\pi}{b} . \tag{17}$$

Similarly, the higher order currents for the x directed wires are given by

$$I_{xn} = \frac{B_{xn}}{Z_{wxn}} . \tag{18}$$

Again, the expressions for the y directed currents may be obtained by using the relations of (8).

If the cell dimensions are both somewhat less than a wavelength, there will only be one dominant plane wave mode scattered from the screen and the reflected plane wave will have the same values of k_x and k_y with k_z replaced by $-k_z$. The higher order modes are highly damped in the z direction if the cell dimensions are much smaller than a wavelength and the field above the screen is essentially a plane wave at a distance corresponding to the largest cell dimension. The actual restrictions placed on the spacing can be obtained from the conditions that Γ be real when n and m are not both equal to zero. It will be assumed in the following that the cell dimensions are such that only the dominant plane wave is scattered.

The reflection of the incident TM and TE plane wave modes may be obtained simply from a knowledge of the zeroth order currents on the mesh. The reflected components E_z and H_z for the combined ground-screen system are given by the following expressions multiplied by the factor

$$e^{-jk_x x} e^{-jk_y y} :$$

$$\underline{TM} \quad E_{zr} = E_{zo} R_{oc} e^{-jk_z z}$$

$$+ \left\{ \frac{k_x I_{xo}}{2\omega\epsilon b} + \frac{k_y I_{yo}}{2\omega\epsilon a} \right\} \cdot \left\{ e^{jk_z h} - R_{oe} e^{-jk_z h} \right\} e^{-jk_z z} ,$$

$$\underline{TE} \quad H_{zr} = H_{zo} R_{oh} e^{-jk_z z} \tag{19}$$

$$- \frac{1}{2k_z} \left\{ \frac{k_x I_{yo}}{a} - \frac{k_y I_{xo}}{b} \right\} \left\{ e^{jk_z h} + R_{oh} e^{-jk_z h} \right\} e^{-jk_z z} , \tag{20}$$

where E_{zo} and H_{zo} are the incident z components of the plane wave field.

Solutions of the equations describing I_{xo} and I_{yo} involve the infinite sets of currents I_{ym} and I_{xn}. The zeroth order terms can be solved by a perturbation technique using only a few terms if the currents fall off rapidly in magnitude with increasing order.

3. Example Calculations

The expressions obtained in (10)-(18) reduce to an equivalent form obtained by Wait (1962) for parallel wires when the currents in the cross wires are set equal to zero or the spacing of these wires approaches a very large value. In order to compare the effects of parallel wire and cross wire screens, the reflection coefficients for the z component of electric field (TM reflection coefficient) was calculated for the same parameters and conditions used by Wait except that the direction of incidence was varied in azimuth from 0 to 90 degrees (parallel to perpendicular for the parallel wires). Two values of elevation angle were used, 85 and 89 degrees with respect to the normal. The following ground and screen conditions were used corresponding to those of Wait:

Frequency = 100 kHz.
Ground conductivity = 5×10^{-3} mho/m.
Relative dielectric constant of ground = 15
Grid wire spacing (a=O, b=2m.– parallel wire)
(a=2m., b=2m. – square mesh)
Wire radius r=2mm
Wire conductivity = 10^{7} mho/m.
Height of screen h=.2, .4, .6 m.

The results of the computations are shown in Fig. 2 where the reflection from the ground-screen system had no appreciable variation with the height h for the values of h chosen.

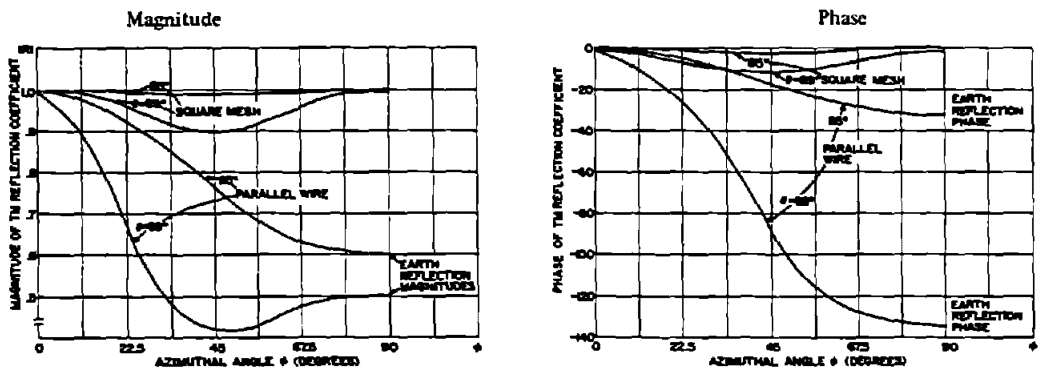

FIGURE 2. Ground-screen reflection coefficient.

4. Discussion and Conclusions

It is apparent from the results of Fig. 2 that a parallel wire ground screen system can become quite transparent at very low elevation angles if the angle of incidence differs greatly from the axis of the wires even though, in this case, the spacing of the wires is 1/1500 wavelength. It is seen that the ground-screen system could produce less reflection than the ground without the screen with conditions of low elevation angle.

The square mesh screen placed above the earth a fraction of a wavelength here also becomes less desirable as a reflecting combination for incidence at 45 degrees with respect to a wire axis.

The calculations of the higher order currents indicated that for rectangular mesh spacings much less than a wavelength these currents were small and did not contribute greatly to the calculations of the zeroth order currents so that only the additional term I_{yo} was needed to correct the original estimate for I_{xo}.

The author is grateful to Professor R.E Collin for his suggestions and discussions of this work.

5. References

Larsen, Tove (1962), A survey of the theory of wire grids, IEEE Trans. Microwave Th. Tech. MTT-10, No. 3, 191-201.

Wait, J.R. (1962), Effective impedance of a wire grid parallel to the earth's surface, IEEE Trans. Ant. Prop. AP-10, No. 5, 538-542.

Collin, R.E. (1960), Field Theory of Guided Waves, sec. 5.6, (McGraw Hill, New York).

Twersky, Victor (1962), On scattering of waves by the infinite grating of circular cylinders, IEEE Trans. Ant. Prop., AP-10, No. 6, 737-766.

CURRENT DISTRIBUTION AND INPUT ADMITTANCE OF A CYLINDRICAL ANTENNA IN A GYROTROPIC MEDIUM

H. S. Lu and K. K. Mei*

ABSTRACT

A finite cylindrical antenna of arbitrary orientation in a gyrotropic medium is solved as a boundary value problem using a numerical technique. The kernel of the integral equation is obtained from an approximate dyadic Green's function of Maxwell's equations for the medium. The results indicate that the quasi-static theory gives correct results for $kh<0.20$ radian. In the hyperbolic region the input resistance also shows the trend of approaching infinity for an infinitesimal dipole.

Introduction

When a cylindrical antenna is immersed in a gyrotropic medium, a major difficulty in predicting the behavior of a source is the determination of the correct current distribution on the source. Hurd (1965), by a Wiener-Hopf technique, and Lu and Mei (1968), by a numerical technique, studied the current distribution on a cylindrical antenna in a uniaxial medium. Lee and Lo (1966) and Graff (1967) investigated that of an infinitely long antenna in a plasma with applied d.c. magnetic field along the axis of the antenna. Aoki (1966) also investigated that of a finite cylindrical antenna.

An integral-differential equation associated with the antenna of arbitrary orientation in a gyrotropic medium is formulated and solved numerically. The kernel of the equation relates to the second order Green's dyadic of Mei's (1966). The input impedance of a short antenna in a hyperbolic region has also been studied. The result indicates that the input resistance increases and independs on the off diagonal term of the permittivity tensor, which confirms the formula given by Balmain (1964).

Integro-differential Equation

Mei (1966), by a perturbational method, showed the solution of the Green's function of the vector wave equation,

$$-\nabla\times\nabla\times G(r/r_0) + \omega^2\mu_0\underline{\underline{\varepsilon}}\cdot G(r/r_0) = I\delta(r/r_0),$$

is

$$G(r/r_0) = \sum_{n=0}^{\infty}\left(I + \frac{\nabla\nabla}{k^2}\right)\cdot\left[\underline{\underline{\delta}}\cdot\left(I + \frac{\nabla\nabla}{k^2}\right)\right]^n \phi_n, \qquad (1)$$

where

*Electrical Engineering and Computer Sciences and the Electronics Research Laboratory, University of California, Berkeley, California.

Research sponsored by the National Science Foundation under Grant GK-2553.

$$\phi_n = (-1)^n \frac{1}{n!} \frac{\partial^n}{\partial p^n} \left[\frac{e^{-j\sqrt{p}(\bar{r}-\bar{r}_0)}}{-4\pi(\bar{r}-\bar{r}_0)} \right]_{p=k^2},$$

$$\underline{\underline{\varepsilon}} = \begin{bmatrix} \varepsilon_1 & +j\varepsilon_{12} & 0 \\ -j\varepsilon_{12} & \varepsilon_1 & 0 \\ 0 & 0 & \varepsilon_3 \end{bmatrix}, \quad \underline{\underline{\delta}} = \frac{(\underline{\underline{\varepsilon}}-\varepsilon_1 I)}{\varepsilon_1} \triangleq \begin{bmatrix} 0 & +j\gamma & 0 \\ -j\gamma & 0 & 0 \\ 0 & 0 & \delta_3 \end{bmatrix}$$

and $k^2 = \omega^2\mu_0\varepsilon_1$. To simplify numerical computation, Mei also gave a second order solution, which contains at least the first three terms of Equation (1).

The antenna, in this paper, is assumed to have length 2h, radius a and to be center-fed by a voltage V across a gap. Its axis is taken to lie in X_2X_3 plane and is inclined at an angle ψ with respect to the X_3 axis as shown in Fig. 1. The antenna is also assumed to be thin, so that the current density can be considered uniform around the circumference and that the end effect can be neglected. For convenience, we shall use the cylindrical coordinate (ρ,θ,Z) of which Z-axis coincides the axis of the antenna, and the positive X_1 axis lies on the plane $\theta = 0$. Through matching boundary condition and transforming the coordinate one obtains an antenna integro-differential equation as

$$j\omega\mu_0 \int_L \oint_C \left[\frac{1}{k^2} \frac{\partial^2}{\partial z^2} \phi^{(1)} + \frac{\partial}{\partial z} \phi^{(2)} + \phi^{(3)} \right] J(z')dc'dz' = - E^{inc} \qquad (2)$$

where

$$\phi^{(1)} = - \frac{e^{-jkR(\delta_3)}}{4\pi\sqrt{1+\delta_3}R(\delta_3)} + \frac{e^{-jk\sqrt{1-\gamma^2/4}R(0)}}{-4\pi(R(0))} \left\{ \cosh \frac{k\gamma(X_1-X_1')}{2} + \cosh \frac{k\gamma(X_2-X_2')}{2} + \cosh \frac{k\delta_3(X_3-X_3')}{2} \right\} + \frac{3e^{-jkR(0)}}{4\pi R(0)}$$

$$\phi^{(2)} = \int_0^{\delta_3} \left\{ 2 \sin\psi \frac{\gamma(X_2-X_2')\mathrm{Exp}(-jk\sqrt{1+\gamma(\delta_3-\eta)/\delta_3}R(\eta))}{16\pi\delta_3\sqrt{1+\eta}\, R(\eta)} \right.$$

$$\left. + (-2) \sin\psi \frac{\gamma(X_2-X_2')\mathrm{Exp}(-jk\sqrt{1-\gamma(\delta_3-\eta)/\delta_3}R(\eta))}{16\pi\delta_3\sqrt{1+\eta}\, R(\eta)} \right.$$

$$+ 2\cos\psi \left.\frac{(X_3-X_3')\,\mathrm{Exp}(-jk\sqrt{1+\delta_3-\eta}\,R(\eta))}{8\pi(1+\eta)^{3/2}\,R(\eta)}\right\} d\eta$$

$$\phi^{(3)} = \frac{1}{2}\sin^2\psi\left[\frac{e^{-jk\sqrt{1+\gamma}\,R(0)}}{-4\pi R(0)} + \frac{e^{-jk\sqrt{1-\gamma}\,R(0)}}{-4\pi R(0)}\right] + \cos^2\psi\,\frac{e^{-jk\sqrt{1+\delta_3}R(0)}}{-4\pi R(0)}$$

$$+\left(-\frac{jk}{32\pi}\right)\left[\delta_3\cos^2\psi\left(1-\frac{jk(X_3-X_3')^2}{R(0)}\right)+\gamma^2\sin^2\psi\left(1-\frac{jk(X_1-X_1')^2}{R(0)}\right)\right]e^{-jkR(0)}$$

and

$$R(\alpha) = \sqrt{(X_1-X_1')^2 + (X_2-X_2')^2 + \frac{(X_3-X_3')^2}{1+\alpha}}\,.$$

It should be noticed that the Eq. (2) is not directly derived from Mei's second order Green's dyadic but rather from a modified second order Green's dyadic. We shall assume E_z^{inc} to be zero except at the gap, and the integration $\oint dc'$ in Eq. (2) represents the integration around the periphery of the cylinder. Equation (2) can be solved using the well-known numerical technique.

Some Results

The range of δ_3 in which Eq. (2) is applicable may be estimated by comparing the solution of Eq. (2) with that obtained from the exact equation in the case of a uniaxial medium. It is found that, when $kh<3.14$ rad., the error in $|Y \text{ input}|$ is less than 10% as $-0.6<\delta_3<1.2$. We will estimate the range of γ to be $|\gamma| < 0.6$. Some representative results are shown in Figs. (2) and (3).

When $\delta_3 < -1.0$, most investigators (e.g. Balmain, Staras) found that the radiation resistance of a point dipole is infinite, while Lee and Papas (1966) claimed otherwise. This paper tries to resolve this problem by calculating the input resistance of the dipole. Although Eq. (2) is unable to deal with this problem, one can obtain an equation by considering the solution to Eq. (1) to be perturbation of the solution to a uniaxial medium. Some results are shown in Fig. (4). The values of the input impedance obtained from Balmain's formula are also given on the same graph. It is found that input resistance as well as the reactance increase and almost independs on γ for short antennas. This confirms the Balmain's formulation, which is obtained by using quasi-static electromagnetic theory. Fig. (4) also indicates that Balmain's formulation gives rather accurate results, when $kh < 0.20$ radians.

References

Aoki, K. (1966), On a cylindrical antenna in a homogeneous anisotropic medium, Can. J. Phys. 44, 1239-1266.

Balmain, K.G. (1964), The impedance of a short dipole antenna in a magnetoplasma, IEEE Trans. Ant. Prop. AP-12, 605-617.

Hurd, R.A. (1965), The admittance of a linear antenna in a uniaxial medium, Can. J. Phys. 44, 2276-2309.

Lu, H.S. and K.K. Mei, Current distribution and input admittance of a cylindrical antenna in a uniaxial medium, Stresa URSI Symp. June 1968.

Mei, K.K. (1966), Perturbational solutions to the dyadic Green's functions of Maxwell's equations in anisotropic media, ERL-M189, Electronics Research Lab., University of California, Berkeley.

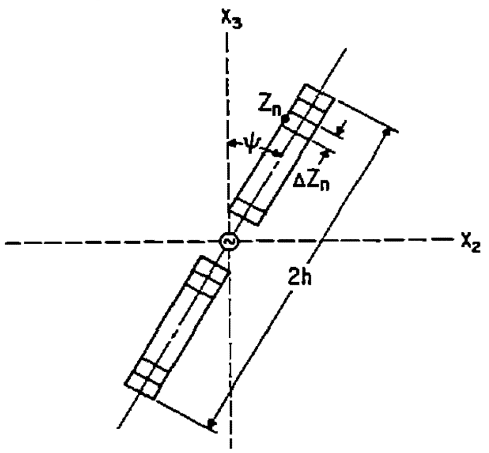

Fig. 1. Dipole Antenna

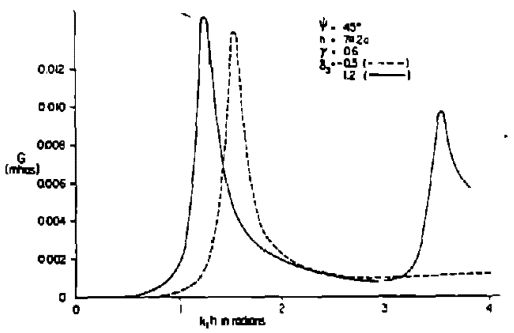

Fig. 2. Conductance

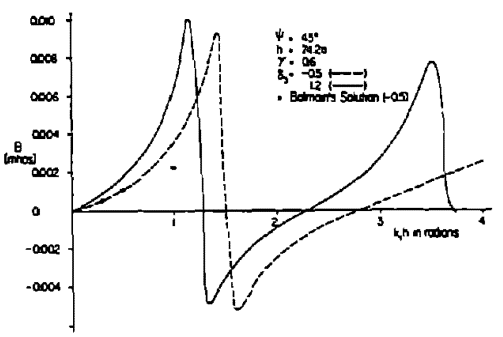

Fig. 3. Susceptance

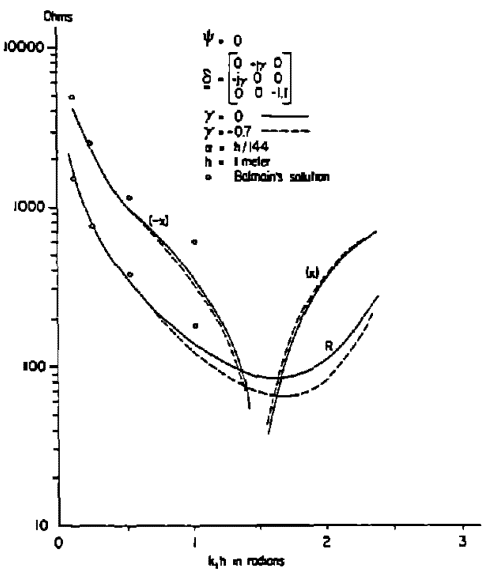

Fig. 4. Impedance

NUMERICAL SOLUTION OF DIPOLE RADIATION IN A COMPRESSIBLE PLASMA WITH A VACUUM SHEATH SURROUNDING THE ANTENNA

S. H. Lin† and K. K. Mei*

ABSTRACT

The results of an investigation of a dipole antenna with a vacuum sheath in a compressible plasma are presented. The problem is formulated in a set of four coupled integral equations and solved numerically by the method of collocation. The results include the effects of the vacuum sheath and the collision loss on the input impedance and the maximum driving voltage of the antenna.

Introduction

In a previous paper (Lin and Mei, 1968), we have presented the results of the numerical solution of a sheathless dipole antenna immersed in a homogeneous, compressible, lossless plasma. It is the objective of this paper to present the results of an investigation of the effects of the ion sheath surrounding the antenna and the collision loss on the antenna performance in a compressible plasma. The model is a finite length cylindrical antenna in an isotropic homogeneous compressible lossy plasma with a finite length cylindrical vacuum sheath surrounding the antenna.

Antenna Configuration

The geometry of the cylindrical antenna with the vacuum sheath in the plasma is shown in Fig. 1. We shall consider the antenna as a scatterer which is illuminated by a finite source $\overline{M}_g$. If $\overline{M}_g = -\frac{V}{\delta}\hat{\phi}\, e^{j\omega t}$ is a band of magnetic current of width δ and is wrapped around the cylindrical scatterer, it is equivalent to an antenna excited by a uniform axial electric field V/δ in a gap of width δ, where V is the applied voltage. The region V_1 is the antenna body made of perfect conductor, V_2 is the vacuum sheath and V_3 is the homogeneous isotropic compressible lossy plasma.

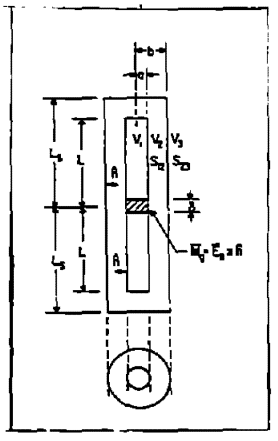

Fig. 1. Configuration of the dipole antenna with a vacuum sheath in the plasma with the associated parameters.

Research sponsored by the Joint Service Electronics Program under Grant AFOSR-68-1488.

†IBM Fellow

*Department of Electrical Engineering and Computer Sciences, Electronics Research Laboratory, University of California, Berkeley 94720

Integral Equation Formulation of the Multi-region Boundary value Problem

The set of basic equations to describe the fields and the sources in the plasma consists of the linearized hydrodynamic equations and Maxwell's equations. These equations are the same as the set of equations (2) in (Lin and Mei, 1968), except that we have introduced a damping term, $n_0 m\nu\overline{V}$ in the last equations of the set (2) to account for the collision effect, where ν is the effective collision frequency.

The equivalent source principle (Harrington, 1961; Schelkunoff, 1939) is useful when dealing with boundary value problems in electromagnetic theory. The application of the equivalent source principle to the integral equation formulation of multi-region boundary value problems is resulted from Mei's lectures on "Boundary Value Problems in Electromagnetic Theory" at Berkeley. The advantage of this approach lies in the simplicity of the kernels in the integral equations. Even though the multi-region boundary value problem involves several types of media, the kernels are the well-known Green's functions, or their derivatives, of the Helmholtz equation in an infinite homogeneous medium.

Cohen (1962), Carlin and Mittra (1967) have generalized the equivalent source principle to include the problems involving compressible plasmas. Based on the inhomogeneous Helmholtz equations for $\overline{H}$(EM wave) and n_1 (electro-acoustic wave) (Lin and Mei, 1968; Carlin and Mittra, 1967), and the equivalent source principle, the total fields in the plasma region V_3 and the sheath region V_2 can be represented as the integrals of four unknown functions (i.e. the equivalent sources) and the primary driving source $\overline{M}_g$ with the appropriate kernels. The four unknown functions are: (1) $J_z(z)$ the current distribution on the antenna surface S_{12}, (2) $E_z(z)$ the tangential electric field on the surface S_{23}, (3) $H_\phi(z)$ the tangential magnetic field on the surface S_{23}, (4) $n_1(z)$ the systematic variation of the plasma electron density distribution on the surface S_{23}.

The boundary value problem posed is then formulated in a set of four coupled integral equations by enforcing the following boundary conditions on the integral representation of the fields on the surfaces S_{12} and S_{23}: (I) the continuity of the tangential electric field at the surface S_{23}, (II) the continuity of the tangential magnetic field at the surface S_{23}, (III) the vanishing of $\hat{n}\cdot\overline{V}$ on the surface S_{23} (assuming rigid boundary), (IV) $\hat{n} \times \overline{H} = \overline{J}$ on the antenna surface S_{12}. The set of the four coupled integral equations written in a symbolic form is:

$$(\tfrac{1}{2} + T_{11})H_\phi(z) + T_{12}E_z(z) + T_{13}n_1(z) = 0$$

$$(\tfrac{1}{2} + T_{21})H_\phi(z) + T_{22}E_z(z) + T_{24}J_z(z) = H_{\phi 2}^{inc}(z)$$

$$T_{31}H_\phi(z) + (\tfrac{1}{2} + T_{33})n_1(z) = 0$$

$$T_{41}H_\phi(z) + T_{42}E_z(z) + (\tfrac{1}{2} + T_{44})J_z(z) = H_{\phi 1}^{inc}(z)$$

where the T_{mn}'s are the integral operators. The integrations are taken over the surface S_{23} or S_{12} depending on the functions on which they operate. $H_{\phi 1}^{inc}(z)$ and $H_{\phi 2}^{inc}(z)$ are the primary fields on the surfaces S_{12} and S_{23} produced by the antenna driving source $\bar{M}_g$. The explicit expressions of these integral equations are rather lengthy and will be reported in a later paper.

This set of integral equations is solved numerically by the method of collocation using finite zoning functions and quadratic interpolations. This numericla procedure is described in (Lin and Mei, 1968). Readers interested in the details of this method are referred to the references (Harrington, 1968; Hildebrand, 1965; Lin and Mei, 1968; Mei, 1968).

The Input Impedance and the Upper Bound of Driving Voltage

For the range of the antenna parameters considered in this paper, the general shapes of the electric current distribution and the electron density distribution on S_{23} are very similar to those of sheathless model (Lin and Mei, 1968), except that some perturbation is introduced by the presence of the sheath.

The definition of the maximum driving voltage is explained in (Lin and Mei, 1968). Fig. 2 shows the maximum driving voltage and the input impedance as a function of sheath thickness t_s = b-a/a for a dipole antenna of total length $2L = \lambda_p/2$. The comparison of the results for the sheath and the sheathless models, Fig. 2 shows that the vacuum sheath has a screening effect which reduces the input resistance, makes the short antenna more capacitive, and raises the upper bound of the antenna driving voltage. A similar screening effect has also been found in the analysis of spherical antennas by (Wait and Spies, 1966) and of prolate spheroid antennas by Lytle (1968). Fig. 2 also indicates that the rate of increase of V_{max} is greater than the rate of decrease of input resistance R. This fact suggests that a dielectric coated dipole antenna in a warm plasma can be operated at a higher power level than an uncoated antenna in the plasma and still satisfy the linearization assumption.

Collision Effect

Fig. 3 shows the collision effect on the input impedance as a function of ω_p^2/ω^2. The Debye length λ_D rather than λ_p is used as the reference of antenna dimensions in Fig. 3 because λ_p looses its meaning when $\omega_p^2/\omega^2 > 1$. It is seen that the resonance effect of a lossless plasma on the antenna impedance at ω_p is damped out when the normalized collision frequency is significant ($\nu/\omega_p = 0.2$).

We also observe that for short antennas ($L = 3.84\lambda_D$) the input reactance which is capacitive, does not change sign at $\omega = \omega_p$. This behavior of input reactance near ω_p is in agreement with that for short dipoles and small spherical electrodes found by Balmain (1965,1966), but is in contrast with that for infinitely long cylindrical antenna found by Miller (1968). This seeming conflict can be resolved by the variational analysis of antenna impedance by Carlin and Mittra (1967). Balmain (1965), Carlin and Mittra (1967) have shown that the total

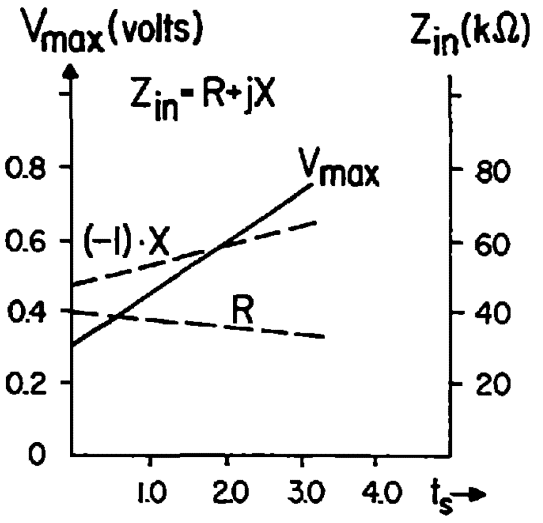

Fig. 2. Input impedance and V_{max} of an antenna of $L = \lambda_p/4$, $a = \lambda_p/75$, $\delta = 4a$, $C/V_o = 1000$, $\omega_p^2/\omega^2 = 0.8$, $\nu/\omega_p = 0$.

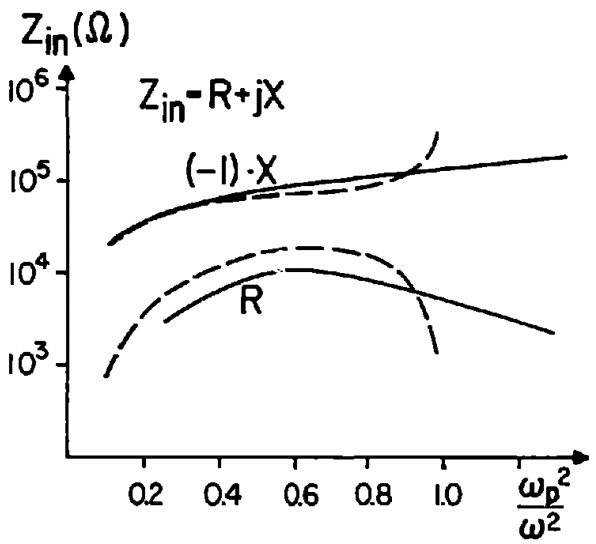

Fig. 3. Input impedance of an antenna of $L = 3.84\lambda_D$, $a = 0.204\lambda_D$, $\delta = 4a$, $C/V_o = 1000$, solid lines: $\nu/\omega_p = 0.2$, $t_s = 3$, dashed lines: $\nu/\omega_p = 0$, $t_s = 0$.

impedance Z_{in} contains a component ZJEM due to EM wave and a component ZJP due to the electro-acoustic wave. Their results indicate that the reactive part of ZJEM changes sign at $\omega = \omega_p$, but the reactive part of ZJP does not. It is also well-known that EM wave dominates when the antenna is long whereas the electro-acoustic wave dominates when the antenna is short. Therefore, the input reactance of short antenna may not change sign at ω_p.

Concluding Remarks

For the probing of the tenuous plasmas in the upper ionosphere, the solar wind and the interplanetary media by the spacecraft borne antennas, the electron kinetic temperature is high and the plasma frequency is so low that the electro-acoustic wavelength is comparable to or greater than the antenna length (2 ~ 3 meters). The interpretation of the experimental data in these situations must take into account the screening effect of the sheath and the fact that the input reactance may not change sing at $\omega = \omega_p$, the collision effect may significantly damp out the anti-resonance behavior of Z_{in} at $\omega = \omega_p$ even though the collision frequency is low.

References

Balmain, K.G. (1965), Impedance of a Short Dipole in a Compressible Plasma, Radio Sci., Vol. 69D, 559.

Balmain, K.G. (1966), Impedance of a Radio-Frequency Plasma Probe with an absorptive Surface, Radio Sci., Vol. 1, 1.

Carlin, J. and Mittra, R. (1967), Effects of Induced Acoustic Sources on the Impedance of a Cylindrical Dipole in a Warm Plasma, Radio Sci., Vol. 2, 1327.

Cohen, M.H. (1962), Radiation in a Plasma, II Equivalent Sources, III Metal Boundaries, Phys. Rev. 126, 389.

Harrington, R.F. (1961), Time Harmonic Electromagnetic Fields, McGraw Hill Book Company, Inc., New York.

Harrington, R.F. (1968), Field Computation by Moment Methods, Macmillan Company, New York.

Hildebrand, F. B. (1965), Method of Applied Mathematics, Prentice Hall, New York, 2nd. Ed., 284.

Lin, S.H. and Mei, K.K. (1968), Numerical solution of Dipole Radiation in a Compressible Plasma, IEEE Trans. Ant. and Prop. Vol. AP-16, 235-241.

Lytle, R.J. (1968), Linear Antennas in Plasma Media, Ph.D. Thesis, Purdue University.

Mei, K.K. (1968), Numerical methods in Electromagnetic Wave Problems, A Short Course Presented at Harry Diamond Lab, Washington, D. C., May 27 - June 19, 1968.

Miller, E.K. (1968), Admittance of an Infinite Cylindrical Antenna Immersed in a Lossy Compressible Plasma, IEEE Trans. Ant. Prop., Vol. AP-16, 111.

Schelkunoff, S.A. (1939), On Diffraction and Radiation of Electromagnetic Waves, Phys. Rev., 56, 308.

Wait, J. and Spies, K.P. (1966), Theory of a Slotted-Sphere Antenna immersed in a Compressible Plasma, Part III, Radio Sci., Vol. 1, 21.

PLANE WAVE SYNTHESIS OF PLASMA COATED APERTURE ADMITTANCE AND RADIATION PATTERN

by

H. Hodara
Tetra Tech, Inc., Pasadena, California

and

D. Damlamayan
California Institute of Technology, Pasadena, California

ABSTRACT

In this paper we present a method for calculating the aperture admittance and radiation pattern of radiating apertures in flat planes coated with plasma slabs, by-passing the boundary value approach. We show that the aperture admittance and radiation pattern can be described by expressions involving the spatial two dimensional Fourier spectrum of the aperture electric field and the two plane wave reflection and transmission coefficients of the slab for each of the two independent incidence directions of polarization. The method has obvious advantages. It is valid for inhomogeneous as well as turbulent plasmas in the direction perpendicular to the aperture; it is a perfect match for modern computing routines since plane wave reflection and transmission coefficient programs in stratified plasmas are already available; it yields the radiation directly through a trivial integration.

DIGEST

Geometry of the System

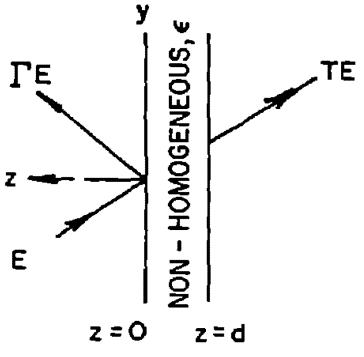

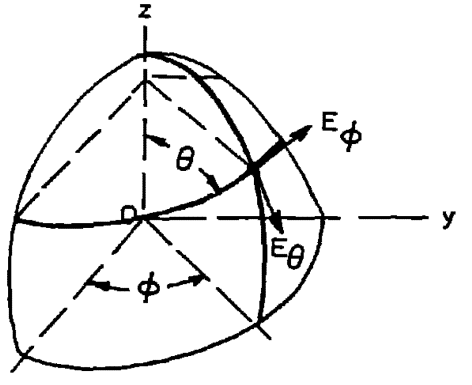

where $u = c\phi s\theta$, $v = s\phi s\theta$, $w = c\theta$, $\rho = s\theta = \sqrt{u^2 + v^2}$

Superposition of Plane Waves

With $e^{i\omega t}$ dependencies, a bunch of plane waves arriving at 0 at $z = o$ are of the form

$$e^{ik_o r}\Big|_{z=o} = e^{ik_o(ux + vy)}.$$

Assume a prescribed field in the $z = o$ plane. It can be synthetized as a superposition of two sets of plane waves with polarization perpendicular to the plane of incidence (E_ϕ) and parallel to it (E_θ). The total field in the plane is:

$$\underline{E}(x, y, o) = k_o^2 \iint \left\{ \underline{\hat{E}}_\phi (1 + \Gamma_\phi) e^{ik_o(ux + vy)} + \underline{\hat{E}}_\theta (1 + \Gamma_\theta) e^{ik_o(ux + vy)} \right\} du\,dv \qquad (1a)$$

Similarly,

$$\underline{H}(x, y, o) = k_o^2 \iint \left\{ \underline{\hat{H}}_\phi (1 - \Gamma_\phi) e^{ik_o(ux + vy)} + \underline{\hat{H}}_\theta (1 - \Gamma_\theta) e^{ik_o(ux + vy)} \right\} du\,dv \qquad (1b)$$

The reflection coefficient Γ is a function of θ and ϕ or u and v. It is the reflection coefficient for a plane wave with direction cosines, u and v incident on a plasma slab. The slab does not have to be homogeneous in the z direction.

Defining a Fourier transform:

$$\underline{\hat{E}}(u,v) = 1/(2\pi)^2 \iint \underline{E}\, e^{ik_o(ux+vy)} dxdy \tag{2}$$

We now adjust each plane wave field amplitude so that the total field is identical with the prescribed field in the z = o plane.

$$\underline{\hat{E}}(u,v) = \underline{\hat{E}}_\phi(1+\Gamma_\phi) + \underline{\hat{E}}_\theta(1+\Gamma_\theta) \tag{3a}$$

$$\underline{\hat{H}}(u,v) = \underline{\hat{H}}_\phi(1-\Gamma_\phi) + \underline{\hat{H}}_\theta(1-\Gamma_\theta) \tag{3b}$$

In terms of cartesian coordinates we have:

$$\hat{E}_y = \hat{E}_\theta(1+\Gamma_\theta)s\phi c\theta + \hat{E}_\phi(1+\Gamma_\phi)c\phi \tag{4a}$$

$$\hat{E}_x = \hat{E}_\theta(1+\Gamma_\theta)c\phi c\theta - \hat{E}_\phi(1+\Gamma_\phi)s\phi \tag{4b}$$

Since for plane waves, $Y_o = \sqrt{\epsilon_o/\mu_o}$

$$\hat{H}_\theta = Y_o\hat{E}_\phi\,, \qquad \hat{H}_\phi = -Y_o\hat{E}_\theta \tag{5}$$

We have

$$\hat{H}_y = Y_o E_\phi(1-\Gamma_\phi)s\phi c\theta - Y_o E_\theta(1-\Gamma_\theta)c\phi \tag{6a}$$

$$\hat{H}_x = Y_o E_\phi(1-\Gamma_\phi)c\phi c\theta + Y_o E_\theta(1-\Gamma_\theta)s\phi \tag{6b}$$

Aperture Admittance

Without loss of generality, assume an aperture field distribution in the plane such that $\hat{E}_x = 0$. Such a case is illustrated below:

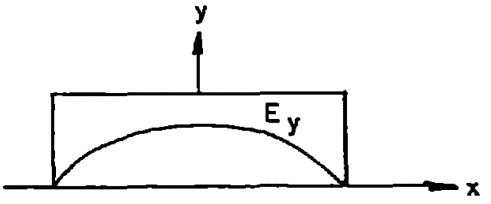

Then from Eq. 4

$$\hat{E}_\theta = \hat{E}_y \frac{s\phi}{c\theta} \frac{1}{1+\Gamma_\theta}, \qquad \hat{E}_\phi = \hat{E}_y c\phi \frac{1}{1+\Gamma_\phi} \tag{7}$$

The aperture admittance expressed in stationary form is

$$Y_{ext} = (2\pi k_o)^2 \frac{\iint \hat{E}_y \hat{H}_x \rho d\rho d\phi}{V_o^2} \tag{8}$$

where

$$\hat{E}_y \hat{H}_x = |\hat{E}_y|^2 \left(\frac{Y_o}{c\theta} \frac{1-\Gamma_\theta}{1+\Gamma_\theta}\right) s^2\phi + |\hat{E}_y|^2 \left(Y_o c\theta \frac{1-\Gamma_\phi}{1+\Gamma_\phi}\right) c^2\phi \tag{9}$$

The terms in parenthesis are recognized as plane wave admittances respectively for TM mode (E parallel to plane of incidence) and TE mode (E perpendicular to plane of incidence),

$$y_M = \frac{Y_{TM}}{Y_o} = \frac{H_\phi}{E_\theta c\theta} = \frac{1}{c\theta} \frac{1-\Gamma_\theta}{1+\Gamma_\phi} \tag{10a}$$

$$y_E = \frac{Y_{TE}}{Y_o} = \frac{H_\theta c\theta}{E_\phi} = c\theta \frac{1-\Gamma_\phi}{1+\Gamma_\phi} \tag{10b}$$

Finally,

$$Y_{ext} = (2\pi k_o)^2 Y_o \int_o^{2\pi} \int_o^{\infty} |\hat{E}_y / V_o^2|^2 (y_M s^2\phi + y_E c^2\phi) \rho d\rho d\phi \tag{11}$$

or

$$Y_{ext} = (2\pi k_o)^2 Y_o \int_{-\infty}^{\infty} \int |\hat{E}_y / V_o^2|^2 \left[y_M(u,v) \frac{v^2}{u^2+v^2} + y_E(u,v) \frac{u^2}{u^2+v^2} \right] du dv \tag{12}$$

Radiation Field

The transmitted wave in the region $z \geq d$ is according to Fourier's superposition

$$\underline{E}(\underline{r}) = k_o^2 \iint (\underline{\hat{E}}_\phi T_\phi + \underline{\hat{E}}_\theta T_\theta) e^{ik_o z\sqrt{1-(u^2+v^2)}} e^{ik_o(ux+vy)} du dv \tag{13}$$

where T_ϕ and T_θ are the slab transmission coefficients as a function of angle for polarizations perpendicular and parallel to the plane of incidence. The far field is given by:

$$\underline{E}(x,y,z) = k_o^2 \iint \left\{ \frac{-\hat{E}_x v + \hat{E}_y u}{\sqrt{u^2+v^2}} \frac{T_\phi}{1+\Gamma_\phi} \underline{e}_\phi + \frac{\hat{E}_x u + \hat{E}_y v}{\sqrt{1-u^2-v^2}\sqrt{u^2+v^2}} \frac{T_\theta}{1+\Gamma_\theta} \underline{e}_\theta \right\} e^{ik_o z\sqrt{1-u^2-v^2}} e^{ik_o(ux+vy)} du\,dv \qquad (14)$$

The stationary values for large r in the evaluation of these integrals are

$$u_o = s\theta_o c\phi_o, \qquad v_o = s\theta_o s\phi_o \qquad (15)$$

Thus, only one plane wave out of the continuum, with directions given by Eq. 15, contributes to the far field, yielding

$$E_\phi = \frac{i(2\pi)^2}{\lambda r} e^{ik_o r} (-\hat{E}_x s\phi_o + \hat{E}_y c\phi_o) \frac{T_\phi}{1+\Gamma_\phi} c\theta_o$$

$$E_\theta = \frac{i(2\pi)^2}{\lambda r} e^{ik_o r} (+\hat{E}_x c\phi_o + \hat{E}_y s\phi_o) \frac{T_\theta}{1+\Gamma_\theta}$$

Conclusions

We have synthetized the near field in terms of a sum of plane waves over an angular spectrum. The extent of the spectrum depends on the aperture distribution. In the full paper we show how the spectrum can be approximated by a few discrete plane waves. Of course, only one of these waves whose ray is in the direction of the observation point in the far field contributes to that field.

RADIATION CHARACTERISTICS OF A SLOTTED GROUND PLANE INTO A TWO-FLUID COMPRESSIBLE PLASMA

K. R. Cook
Colorado State University
Fort Collins, Colorado

R. B. Buchanan
Sylvania Electronics Sys.
Mountain View, Calif.

Abstract

A theoretical investigation of the radiation from a slotted ground plane covered with an infinite two-fluid compressible plasma has been conducted. Emphasis has been placed on the frequency spectrum near and below the ion plasma frequency. Preliminary results indicate a significant amount of power may be radiated in the ion-acoustic mode.

Introduction

In a two-fluid compressible plasma two longitudinal waves and one transverse wave may exist. The longitudinal waves represent collective motions of the electrons and ions, denoted hereafter as the electron-acoustic and ion-acoustic modes. The transverse wave is denoted as the optical mode. The optical and electron-acoustic modes experience cutoff at the hybrid plasma frequency, defined as $\omega_c = (\omega_e^2 + \omega_i^2)^{1/2}$ where ω_e and ω_i are the electron and ion plasma frequencies. However, the ion-acoustic wave propagates with a zero cutoff frequency. The zero cutoff frequency and the relatively short wavelength of the ion-acoustic mode indicates possible diagnostic or communication applications for these waves below the plasma frequency. However, kinetic theory must be utilized to account for losses due to Landau damping of such waves.

Related Previous Work

Seshadri (1965) considered the radiation of an infinitesimal electric dipole in an unbounded two-fluid compressible plasma. His results indicate that a large amount of power is launched into the ion-acoustic mode. However, his results were based on a collisionless hydrodynamic model. He also assumes that Landau damping will be nominal below the ion plasma frequency for the ion-acoustic mode.

Sessler (1966) conducted experiments in an rf gas discharge plasma having an ion plasma frequency of about 1 MHz. The transducers used for launching ion-acoustic waves consisted of wire grids excited by an 0.1-10 MHz generator. Detection was achieved by a similar transducer. His results indicate that well below the ion plasma frequency the loss mechanism is dominated by collisions. Landau damping becomes the dominant loss factor near

the ion plasma frequency as predicted. However, his experimental results showed that the attenuation decreased with increasing frequency, contrary to theoretical predictions. Measured phase velocities compared well with theoretical predictions.

Alexeff et. al. (1968) have investigated the effects of electron temperature on ion-acoustic wave propagation in a discharge plasma and were able to accurately measure the phase velocity and attenuations for frequencies well below the ion plasma frequency. In plasmas having electron densities of 10^8 - 10^{10} cm^{-3}, pulses of rf energy were transmitted over a distance of 20 cm. The measured phase velocity and attenuation compared favorably with kinetic theory predictions. The transducers in their experiments were negatively biased probes extending into the plasma and excited by a pulse generator.

In many diagnostic or communication applications it is not practical to extend probes into the plasma. The following discussion considers the use of a slotted ground plane contiguous to an infinite plasma as a transducer for launching ion-acoustic waves for purposes of diagnostics or communications.

FORMULATION OF THE PROBLEM

Consider a ground plane coincident with the x-z plane with an infinitesimal slot lying along the z-axis. The region $y \geq 0$ contains a two-fluid compressible plasma described by the linearized hydrodynamic equations. The slot has an uniform electric field oriented in the x-direction, normal to the slot axis.

It is assumed the ground plane is negatively biased and that no sheath exists at the surface $y = 0$. Furthermore, rigid boundary conditions are imposed on the ground plane.

The fields in the plasma are represented in terms of three potential integrals describing the two longitudinal acoustic modes and the transverse optical mode. The radiation structure for the three modes has been evaluated by the method of steepest descent. However, since only the ion mode is of interest, the following discussion will concentrate on the results describing the ion-acoustic mode. A real pole of the integrand was found near the ion mode wave number signifying a surface wave with a phase velocity near the ion-acoustic velocity. At the present time a rigorous investigation of the surface wave structure has not been completed. However, since the main concern of this preliminary investigation is the radiation mode, the surface wave structure will not be discussed.

NUMERICAL RESULTS FOR THE RADIATION MODES

Numerical evaluation of the radiation integrals was conducted for a dense plasma having an electron density of 1.5×10^{14} cm^{-3}; ion thermal speed of 4.2×10^3 m/s; electron thermal speed of 6.74×10^5 m/s and an ion mass of 2.34×10^{-26} kg. These data produce an electron plasma frequency of 110 GHz and an ion plasma frequency of 690 MHz.

Two radiation patterns for the ion-acoustic mode are presented in Figures 1 and 2; representative of a frequency spectrum from approximately 8 MHz to 1.6 GHz. It is anticipated that collisional losses would become severe for frequencies below this spectrum and Landau damping becomes severe above this spectrum. The patterns become increasingly sharper for higher frequencies and there is a very narrow null broadside to the slot. However, these patterns should only be interpreted as indicating the general pattern structure in view of the fact that no loss mechanisms have been accounted for in the calculations. The power densities are relative to one watt/m^2.

In Figure 3, peak power densities are plotted for the ion-acoustic, electron-acoustic and optical modes. Again, it is anticipated that the acoustic modes will suffer heavy attenuation due to Landau damping over certain frequency spectra. In particular, the electron-acoustic mode may suffer heavy attenuation except for a very narrow frequency band just above the electron plasma frequency. Note that the optical mode power is proportional to ω for $\omega/\omega_{pe} >> 1$ while the electron-acoustic and ion-acoustic modes are proportional to $1/\omega$ for high frequencies. Also, the acoustic-type modes have a maximum slightly above the plasma frequency. Although not shown in the plot, the ion-acoustic mode approaches zero as ω tends to zero. However, below the frequency spectrum shown, collision losses will be severe and this region was of no interest in the present calculations.

CONCLUSIONS

Within the limitations of the hydrodynamic model, it has been shown that a significant amount of power may be radiated into the ion-acoustic mode by a slotted ground plane contiguous with a two-fluid compressible plasma. Based on experimental results of other researchers, it is anticipated that below the ion plasma frequency the radiated energy will not suffer from heavy attenuation due to collisions and Landau damping. If so, the ion-acoustic system may provide possible diagnostic or communication methods two or three orders of magnitude below the electron plasma frequency. However, kinetic theory must be used to investigate the propagation characteristics in this frequency spectrum.

REFERENCES

Alexeff, I., W. D. Jones and D. Montgomery (1968), Effects of Electron-Temperature Variation on Ion-Acoustic Waves, Phys. of Fluids, 11, No. 1, 167.

Seshadri, S. R. (1965), Radiation from Electromagnetic Sources in a Plasma, IEEE Trans. Ant. Prop. AP-13, No. 1, 79.

Sessler, G. M. (1966), Excitation and Measurement of Acoustic-Ion Waves, J. Acoustical Soc. of America, 42, No. 2, 360.

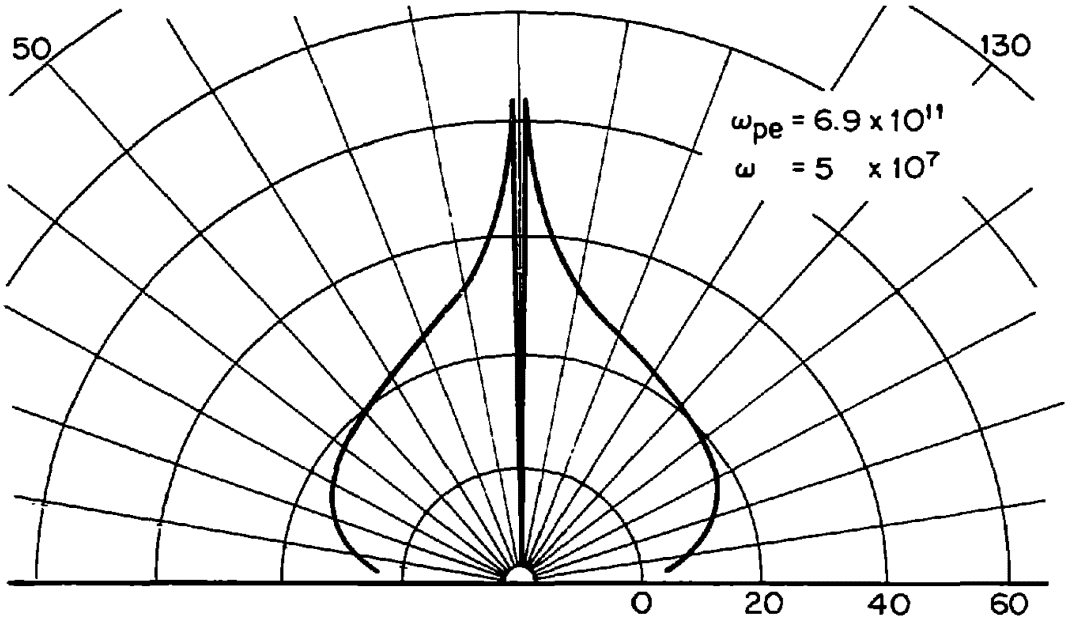

Figure 1 ION MODE POWER DENSITY (dB)

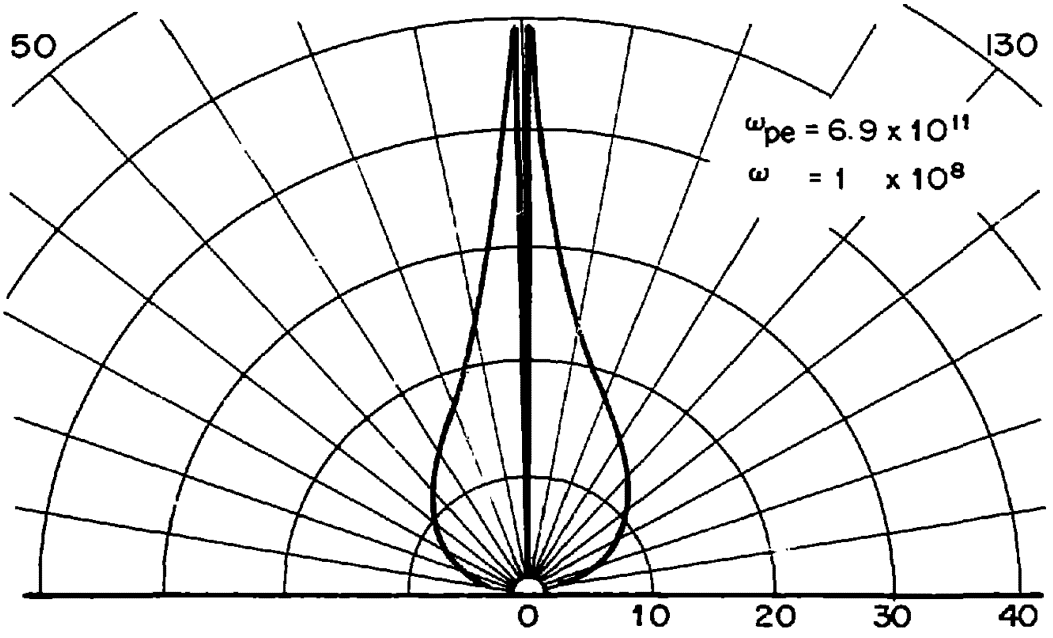

Figure 2 ION MODE POWER DENSITY (dB)

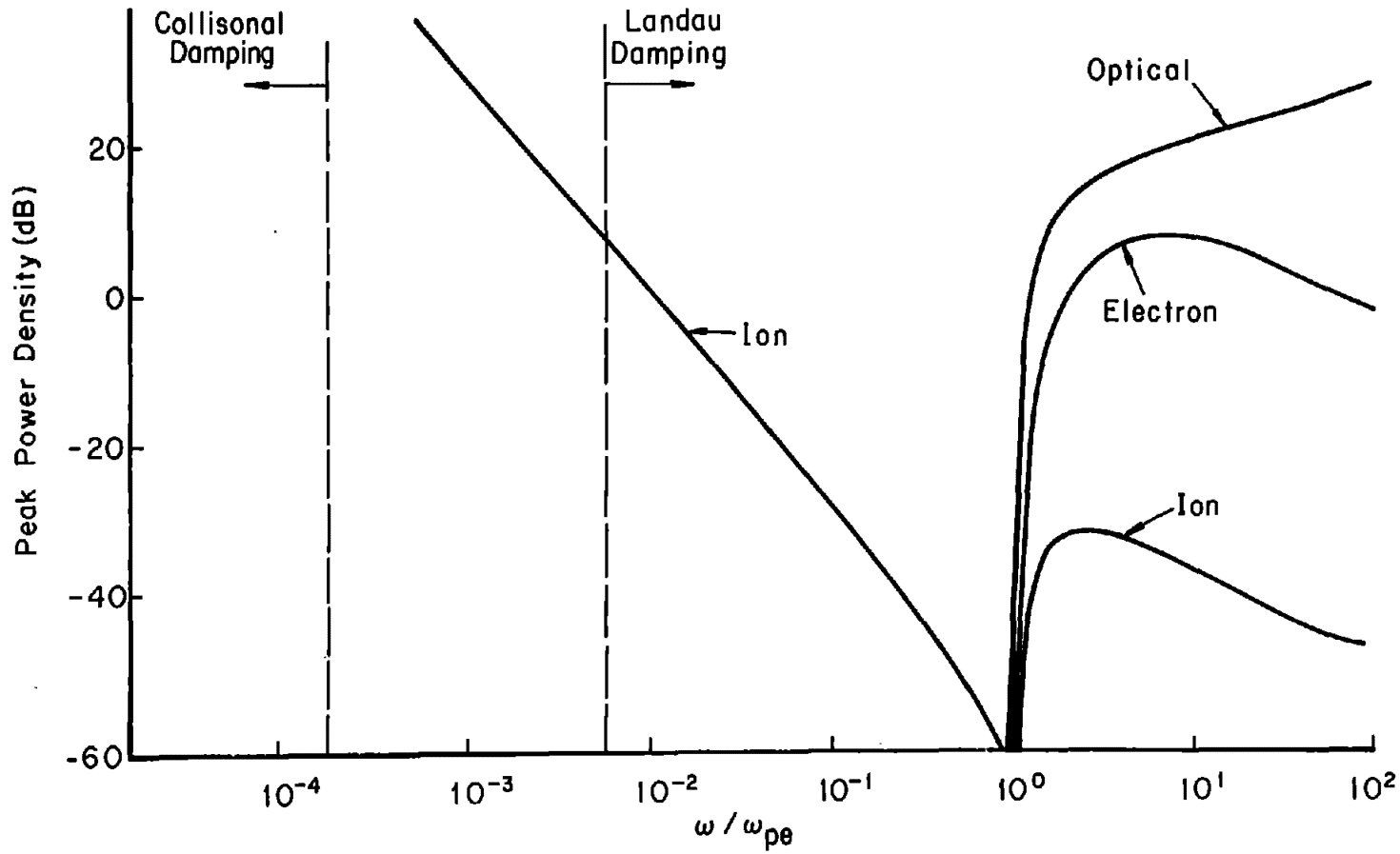

Figure 3 Peak Power Density Versus Frequency

STUDIES OF VLF RADIATION PATTERNS OF A DIPOLE IMMERSED IN A LOSSY MAGNETOPLASMA

D. P. GiaRusso
J. E. Bergeson
Boeing Scientific Research Laboratories, Seattle, Wash.

Abstract

Power patterns are presented for VLF radiation (500 Hz to 30 kHz) from magnetic and electric dipole sources in a two-component lossy magnetoplasma. The patterns show that energy tends to be transported primarily along the magnetic axis of a confinement cone for higher VLF frequencies, but that the inclusion of ion motion destroys the confinement cone for extremely low frequencies.

The subject of electromagnetic radiation from sources embedded in anisotropic media has been extensively discussed in the literature. Of particular interest today are the radiation patterns of localized sources immersed in plasmas which become anisotropic by virtue of an impressed magnetostatic field. This interest is practical, as well as academic, since satellite-to-satellite and satellite-to-ground or undersea communication problems require a thorough understanding of radiation patterns in ionospheric or magnetospheric plasmas.

The purpose of this study is to construct some representative far-zone radiation patterns (radial Poynting vector component) for monochromatic VLF radiation from dipole sources in a lossy magnetoplasma. The effects of ion motion and a finite collision frequency are included in the calculations. Driving frequencies between 500 Hz and 30 kHz have been chosen for investigation. Two sets of plasma parameters (plasma frequency, gyro frequency, and collision frequency) were used in the study; one set is descriptive of a magnetospheric plasma at a height of 6500 km and the other of an ionospheric plasma at a height of 1500 km. In constructing the radiation patterns, it was assumed that the plasma responds linearly to the (weak) electromagnetic disturbances excited by the dipole source, i.e., that the plasma's properties are adequately characterized by a relative permittivity tensor $\overleftrightarrow{\varepsilon}$. It was also assumed that the plasma is homogeneous and of infinite extent, and that its temperature is low enough that electron thermal velocities may be neglected.

From Maxwell's equations it follows that the wave equation for the electric field in an anisotropic homogeneous medium with relative permittivity tensor $\overleftrightarrow{\varepsilon}$, free space permeability μ_o and

free space permittivity ε_o is

$$\nabla x(\nabla x \vec{E}) - \omega^2 \mu_o \varepsilon_o \overleftrightarrow{\mathcal{E}} \cdot \vec{E} = - i\omega\mu_o \vec{J}$$

The general solution for $\vec{E}$ (since Maxwell's equations are linear and the medium is unbounded) can be written as,

$$\vec{E}(\vec{r}) = \int_{\vec{r}'} d\vec{r}' \overleftrightarrow{\Gamma}(\vec{r},\vec{r}') \cdot \vec{J}(\vec{r}')$$

where $\overleftrightarrow{\Gamma}$ is a dyadic Green's function, $\vec{J}$ is the source current density, $\vec{r}$ specifies the observer's position, and $\vec{r}'$ refers to the coordinates of an element of source current. There are several ways of determining the Green's function $\overleftrightarrow{\Gamma}(\vec{r},\vec{r}')$ in the expression above. The basic method used for this study, an asymptotic evaluation of the exact plane wave integral representation of $\Gamma(\vec{r},\vec{r}')$, was first suggested by Bunkin (1957), was later modified by Kuehl (1960), and has been used successfully by Mittra and Duff (1965).

The results of this study are summarized in figures 1 through 5.

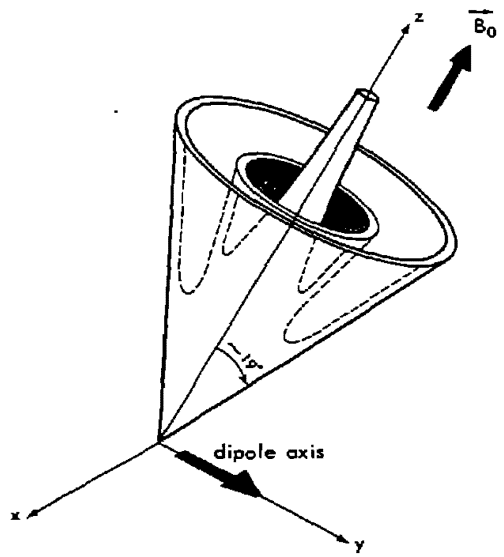

Fig. 1 – Typical three-dimensional power pattern for driving frequencies in the 5–30 kHz range.

Figure 1, which is representative of the power patterns for higher frequencies within the VLF range, shows that power tends to flow primarily along the magnetic axis of a confinement cone with apex at the dipole. The half-angle of this cone varies with the plasma parameters but is usually taken to be about 19°.

The existence of such a confinement cone is, of course, well known and has been discussed extensively in the literature. The axial power beam is intense for dipole orientation perpendicular to the magnetic field; it vanishes when a magnetic dipole is parallel to the field, but is still present when an electric dipole is parallel to the field. The figure also shows that there is an apparent enhancement of radiation intensity in the region near the confinement cone, and that a conical "spike" or "ring" of enhanced radiation intensity may exist within the confinement cone. The propagation angle of the radiation "spike" with respect to the d-c magnetic field is a function of the plasma parameters. Such spikes are associated with the fact that the refractive index surface may become very large (open branch regions) at certain propagation angles.

Figure 2 displays a typical refractive index surface for the plasma parameters and driving frequencies applicable to fig. 1.

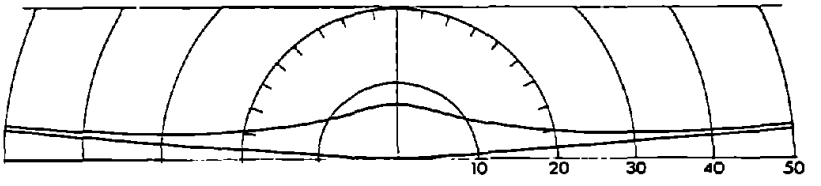

Fig. 2 - Representative refractive index surface (real part) associated with the power pattern of fig. 1.

Figures 3 and 4 reveal that the inclusion of ion motion destroys the confinement cone at extremely low frequencies (500 Hz is used for these figures).

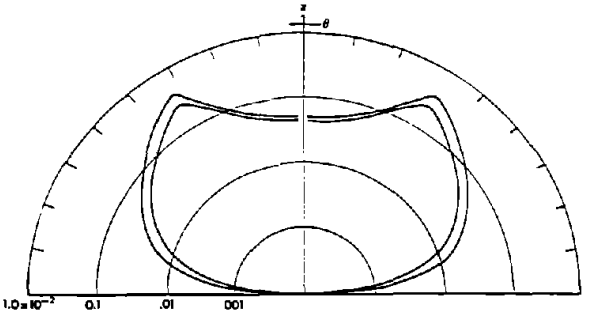

Fig. 3 - Power pattern for a magnetic dipole (dipole axis perpendicular to the d-c magnetic field) in a two-component magnetospheric plasma. The outer curve corresponds to the lossless case, the inner curve to a slightly lossy case. Dipole driving frequency is 500 Hz.

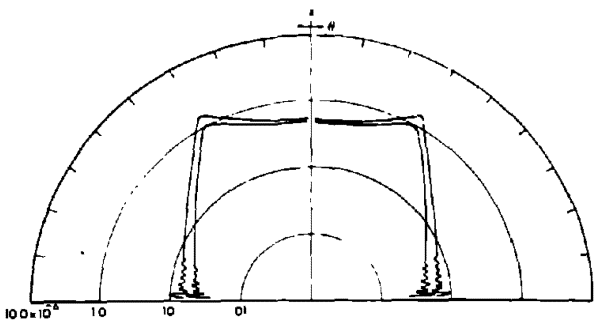

Fig. 4 - Electric dipole power pattern analogous to fig. 3.

Figure 3 gives power plots for a magnetic dipole immersed in both lossless and lossy two-component plasmas while fig. 4 gives power plots for an electric dipole in the same two plasmas.

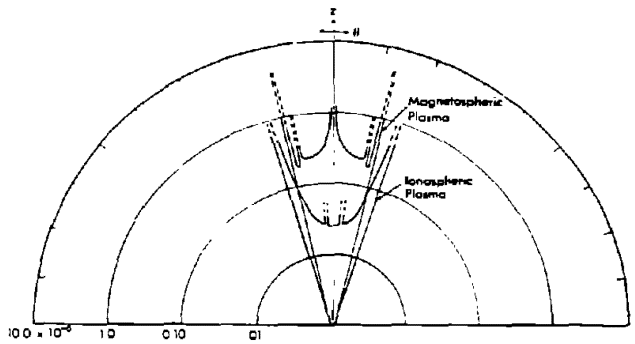

Fig. 5 - Power patterns for a magnetic dipole (dipole axis perpendicular to the d-c magnetic field) corresponding to heights of 6500 km and 1500 km. Dipole driving frequency is 30 kHz. Losses are included.

Figure 5, which superimposes power patterns for a magnetic dipole in both magnetospheric and ionospheric plasmas, shows that power absorption is much greater in the latter medium due to the higher collision frequency. It also appears as though the axial beam intensity is greatly reduced in plasmas typical of the upper ionosphere (at 30 kHz).

Some notes of caution should be mentioned regarding the validity of the power patterns in certain regions. Strictly speaking, the plots become inaccurate for three different limiting situations:

(a) as the polar angle, θ, approaches zero
(b) as θ approaches the confinement cone
and (c) for θ associated with an open branch region of the refractive index surface.

These situations correspond, of course, to just those regions in fig. 1 where the power intensity is greatest. However, the work of others (particularly Arbel and Felsen) has shown that power enhancement in these regions actually exists-- at least within the restrictions of small signal analysis.

Finally, it should be emphasized that spatial interference effects, which arise from the superposition of several contributing far-zone waves, have not been considered in constructing the power patterns. The patterns represent, when applicable, the sum of the individual time average radial Poynting vectors of the far-zone waves.

An extensive discussion of this study has been given by the authors in a report which is listed in the references.

References

Arbel, E. (1960), Radiation from a point source in an anisotropic medium, Report PIB-MRI-861-60, Microwave Research Institute, Polytechnic Institute of Brooklyn.

Arbel, E. and L. B. Felsen (1963), Theory of radiation from sources in anisotropic media, Part II. Proc. Symposium on Electromagnetic Theory and Antennas (URSI) Copenhagen, 1962, ed. E. C. Jordan, 421-459, (Pergamon Press, Oxford, England).

Bunkin, F. V. (1957), J. Exp. Theor. Phys. (USSR) 32, 338-346.

GiaRusso, D. P. and J. E. Bergeson (1969) Studies of VLF radiation patterns of a dipole immersed in a lossy magnetoplasma, Boeing document D1-82-0797.

Kuehl, H. H. (1960), Radiation from an electric dipole in an anisotropic cold plasma, Antenna Lab. Report 24, Calif. Inst. of Tech.; see also J. Phys. Fluids 5, No. 9, 1095, 1962.

Mittra, R. and G. L. Duff (1965), A systematic study of the radiation patterns of a dipole in a magnetoplasma based on a classification of the associated dispersion surfaces, Radio Sci. J. Res. NBS/USNC-URSI 69D, No. 5, 681-692.

SOME FEATURES OF ELECTROACOUSTIC WAVES EXCITED BY LINEAR ANTENNAS IN HOT PLASMA

by

V.L.Talekar
Plasma Physics Division
Malaviya Regional Engineering College
Jaipur, India

ABSTRACT: When a radiating source is immersed in an isotropic compressive plasma, a longitudinal electroacoustic wave may be excited in addition to the usual electromagnetic wave. The present communication deals with some features of the electric field associated with electroacoustic waves excited by linear antennas. It is shown that the distribution of the field is oscillatory with discrete ray like structure, and that the maximum occurs almost in the broad side direction.

INTRODUCTION

The excitation of electroacoustic wave in a hot plasma by an electric source has been the topic for early studies by several workers (Wait, 1965; Cook and Edgar, 1966; Talekar and Gupta, 1966). Numerous papers on the subject have been published to this date reporting theoretical as well as experimental results. However, the experimental studies are comparatively few in number evidently since the direct detection of an electroacoustic wave in a hot plasma is rather difficult if not impossible. In the recent experimental study of electroacoustic waves excited by a monopole in a mercury vapour plasma Chen and his coworkers (1967) have measured composite radiation field patterns outside the plasma and have concluded the existence of a strong electroacoustic wave in the direction along the antenna axis.

For the comprehensive assessment and understanding of the experimental results further theoretical investigation of the plasma mode radiation field patterns due to various electric sources, is called for. In the present work, it is intended to restrict attention to resonant and non-resonant linear antennas.

GENERAL EXPRESSIONS

The plasma is assumed to be hot, homogeneous and neutral in the unperturbed state. Perturbation of the plasma due to the radiating source is taken to be small with an $\exp(j\omega t)$ time dependence. Electron gas forms the only effective component of the plasma and presence of ions is disregarded. Also the collisions of the electrons with neutral particles are neglected. The source frequencies are confined to the first Fraunhofer zone (Talekar and Gupta, 1966).

For the above plasma model with the specified frequencies and the linear antenna having simusoidal current distribution placed along z-axis with feed point at the origin of the spherical co-ordinate system, the electric field of the electroacoustic wave (Plasma Mode) is found to have only the radial component in the far region. The spatial distribution of this field is given by the pattern factor which can be written as product of two functions, first independent of the antenna length and second dependent on it. Thus

$$P_f(\theta, A, \beta) = F \times F(k) \tag{1}$$

The functions can be shown to be

(i) for the resonant centre-fed linear antenna (RCFLA), in the range $0 < \theta < \pi/2$,

$$F = (1-A^2)(c/v_o)^2 \frac{(\beta o/\beta)\cos\theta}{1-(\beta o/\beta)^2 (c/v_o)^2 A^2 \cos^2\theta} \tag{2}$$

$$F(k) = \cos(\pi k.c/v_o.A\cos\theta) - \cos(\pi k\,\beta/\beta o) \tag{3}$$

(ii) for the non-resonant end-fed linear antenna (NREFLA), in the range $0 \leq \theta < \pi$,

$$F = \frac{((1-A^2)/A).(c/v_o)}{1-(\beta o/\beta)(c/v_o) A\cos\theta} \tag{4}$$

$$F(k) = \sin\pi k(\beta/\beta_o - c/v_o.A\cos\theta) \tag{5}$$

where the frequency parameter $A = (1 - W_p^2/W^2)^{1/2}$ (6)

and the length parameter $k = \beta_o l/2\pi$ (7)

The symbols have the following meanings: c velocity of light in free space, v_o r.m.s. thermal velocity of electrons, β phase propagation constant of current on antenna, β_o phase propagation constant of EM wave in free space, W angular source frequency, W_p angular plasma frequency, l antenna length.

COMPUTED FIELD PATTERNS

In a compressible plasma there are, in general, three types of waves on antenna: electromagnetic, electroacoustic and surface waves. In the range of source frequencies under consideration, with sufficient accuracy, their wave numbers respectively are

$$\beta_e = \beta_o A,\ \beta_p = (c/v_o)\beta_o A \text{ and } \beta_s = (c/v_o)\beta_o/(2-A^2)^{1/2} \tag{8}$$

It is rather difficult to decide summarily which one of the different wave numbers is effective. However, for the numerical computation of the F and F(k) functions β_e has been chosen to be the appropriate wave number and c/v_o is taken as 10^3 a minimum value usually obtained in most applications. Some salient features of these computed functions may now be mentioned.

The F function, almost identical for the two types of linear antenna starts with the finite value $(1-A^2)/A$ at 0^0 and increases slowly upto 85^0. Thereafter it rises rapidly attaining maximum value within few minutes short of 90^0. Actually at 90^0 the function suddenly drops to zero for the RCFLA and equals $(c/v_o).(1-A^2)/A$ for the NREFLA. As for the oscillatory function, its periodicity is governed by the product of k and A parameters, increasing the oscillations with higher values of the same. Thus the overall field pattern becomes oscillatory and attains the maximum almost in the broad side direction. As the kA product is increased, the pattern develops more and more oscillations, finally so numerous amounting to discrete ray like structure.

CONCLUSION

At the outset, inviting attention to the controversy as regards the form and propagation constant of the current distribution on cylindrical dipoles immersed in hot plasma, it may be remarked that the situation is far from being conclusive. On one hand, Lin and Mei (1968) find from numerical computations that the sinusoidal current distribution is not a good description of the solution of equations which describe the plasma. On the other hand Ting and his coworkers (1968) conclude that when A^2 lies between zero and one, the current distribution is still somewhat sinusoidal but with larger wavelength. For the work presented in this paper we have assumed sinusoidal current distribution with βe as the propagation constant following the experimental work of Judson and his coworkers (1968). The resulting field pattern for RCFLA is found to be in conformity with the electroacoustic power radiation pattern computed by Wunsch (1968) for the cylindrical dipole using delta function driving voltage and representing total current by a Fourier series. However, no results are available for comparison in case of NREFLA.

In the end it may be concluded that for frequencies confined to first Fraunhofer zone, the assumed current distribution forms a workable and reasonably simple model to describe main salient features of antenna performance in hot plasma.

REFERENCES

1. K.M. Chen, H.Judson and C.C. Lin, " Experimental study of an electroacoustic wave excited by an antenna in a hot plasma ", Proc. IEEE, Vol.55, pp.1656-1657, 1967.

2. K.R. Cook and B.C.Edgar, " Current distribution and impedance of a cylindrical antenna in an isotropic compressible plasma", Radio Science, Vol.1 (new series), pp. 13-19, 1966.

3. H.Judson, K.M.Chen, and R.Lundquist, " Measurement of the current distribution on monopoles in a large volume of hot plasma", Electronics Letters, Vol.4, pp.289-291, 1968.

4. S.H. Lin and K.K.Mei, " Numerical solution of dipole radiation in a compressible plasma", IEEE Trans. Antennas and Propagation, Vol. AP-16, pp.235-241, 1968.

5. V.L.Talekar and R.K.Gupta, " Radiation from linear antenna in weakly ionized plasma", Int.J.Electron, Vol.21, pp. 443-455,1966.

6. C.Y.Ting, B.R.Rao and W.A. Saxton, " Theoretical and experimental study of a finite cylindrical antenna in plasma column ", IEEE Trans. Antennas and Propagation, Vol.AP-16, pp.246-255, 1968.

7. J.R.Wait, " On radiation of electromagnetic and electroacoustic waves in plasma", Appl.Sci. Res., Vol.B-12, pp. 130-138, 1965.

8. A.D. Wunsch, " The finite tubular antenna in a warm plasma", Radio Science, Vol. 3, pp. 901-920, 1968.

. . . . . .

LINEAR ANTENNA IN ANISOTROPIC MEDIUM

Pascal Meyer
C. N. E. T. - R. S. R.
92, Issy-les-Moulineaux, France

Abstract

The general solution of the current distribution along a cylindrical antenna in cold magnetoactive plasma is given. A converging sequence of approximation is found by reduction to a Hilbert problem. The method involves the solution of Fredholm integral equations and numerical integrations.

The study of antenna in ionospheric plasma encounters two difficulties: 1) the plasma is hot and inhomogeneous, 2) it is anisotropic. Our purpose here is to extend the theory of linear antennas to take account of the anisotropy. Taking a reference system with Oz along the antenna axis, we have the time harmonic Maxwell equations:

$$\begin{cases} \nabla \times H = 0 \\ \nabla \times E = k_o^2 \, \varepsilon \cdot E + J \end{cases} \tag{1}$$

Here, ε is the dielectric tensor in this system and J is the unknown current distribution. For a cylinder of length $2h$ and radius a, we have

$$\vec{J}(z, \varphi, r) = \begin{cases} \vec{J}(z, \varphi) \dfrac{\delta(r-a)}{2\pi a}, & |z| < h \\ 0, & |z| > h \end{cases} \tag{2}$$

This can be expressed as a Fourier series in φ and a transform in z

$$\vec{J}(z, \varphi) = \int_{-\infty}^{\infty} d\lambda \sum_{n=-\infty}^{+\infty} e^{i\lambda z} e^{in\varphi} \vec{J}(r, \lambda) \tag{3}$$

Thus, we can solve (1) by a spatial Fourier transform; after some calculations, this gives the electric field as

$$\vec{E}(r, z, \varphi) = \int_{-\infty}^{\infty} d\lambda \sum_{\beta=-\infty}^{+\infty} e^{i\lambda z} e^{i\beta\varphi} \vec{E}(r, \beta, \lambda) \tag{4}$$

with

$$\vec{E}(r,\beta,\lambda) = \sum_{n=-\infty}^{\infty} \vec{\vec{F}}(r,\beta,n,\lambda) \cdot \vec{J}(n,\lambda)$$

and $\vec{\vec{F}}$ is a matrix function of λ defined by a sum of terms like

$$F(\lambda) = \int_0^{2\pi} d\theta\, e^{i(\beta+n)\theta} \int_0^{\infty} dk\, J_n(ka)\, J_\beta(kr)\, k\, \frac{P_{ij}(k,\theta,\lambda)}{\Delta(k,\theta,\lambda)} \qquad (5)$$

Here, P_{ij}/Δ is obtained by inversion of the Maxwell relations so that $\Delta = 0$ is the wave equation in the medium. In some particular case, $a = 0$ (i.e., isotropic case), F reduces to Hankel functions but, generally, it is a complicated new transcendental. Also, one finds that it is 4-valued and to build E, its causal branch must be used. This branch has singular points λ_s which can be found using the pinch method (Hwa and Teplitz, 1966). They are the real roots of

$$\begin{cases} \Delta(k,\theta=0,\lambda) = 0 \\ \Delta'_k(k,\theta=0,\lambda) = 0 \end{cases}$$

We note that the λ_s are logarithmic branch points.

To obtain the current distribution, we take account of the boundary conditions on the cylinder at $r = a$. We have three parts:

1) $|z| < \delta$ [where δ is very small; the field in this feed region is $E_z = V\delta(z)$; $E_\varphi = E_r = 0$],

2) $\delta < |z| < h$ [where $E_z = E_\varphi = 0$],

3) $h < |z|$ [where E_z and E_φ are unknown].

For an infinite antenna, this last condition does not exist and $J(n,\lambda)$ is found by inversion of (4); this is done by truncation at $\beta, n \leq N$ because $F(\beta,n)$ is the representation of a completely continuous operator and one obtains a converging sequence of current $J^N(z,\varphi)$. This case is of more than academic interest because it contains the so-called gap problem and also because, near the plasma resonances, the end of the antenna is unimportant.

When the antenna is finite, we must first find $E(z,\varphi)$, for $|z| > h$, and thus we again truncate (4) at β, $n \leq N$. Furthermore, we now write (4), at $r = a$, as a $2N \times 2N$ matrix relation between $2N$ vectors:

$$E(\lambda) = F(\lambda) \cdot J(\lambda) \quad .$$

Then, introducing the unknown field for $|z| > h$,

$$E(\lambda) = \int_{+h}^{+\infty} E(z)\, e^{i\lambda z} \quad ,$$

the boundary condition is written

$$E(\lambda) + E(-\lambda) + V = F(\lambda) \cdot J(\lambda)$$

[When $|z| < h$, we obtain $E(-\lambda)$]. Here, $J(\lambda)$, being a finite $(-h, +h)$ Fourier transform is entire and E is holomorphic in $\mathrm{Im}\,\lambda > 0$. We then see that the L.H.S. has the same singular points λ_s as $F(\lambda)$. This relation can be analytically continued from the real axis to the whole λ plan. Here, we must draw cuts from the λ_s, and the L.H.S. has discontinuities along these cuts. On the other hand, $\big(E(\lambda) + E(-\lambda) + V\big) F^{-1}$ is entire and has no discontinuities in $\mathrm{Im}\,\lambda < 0$. We use + and - to designate the two limiting values along the cuts. Thus, we obtain the relation

$$\frac{E^+}{F^+} - \frac{E^-}{F^-} + \frac{E(-\lambda) + V}{F^+ - F^-} = J^+ - J^- = 0 \quad .$$

This is nothing else than an inhomogeneous Hilbert problem (Muskevishvili, 1958). It has a standard solution which expresses E in terms of the inhomogeneous term. This term includes E so that it is a Fredholm integral equation for E. Using the solution of the homogeneous problem, this can be solved here with complications. This solution is complicated but several practical approximations can be used and numerical analysis is under progress.

References

Hwa, R.C., and V. L. Teplitz (1966), Homology and Feynman Integrals (Benjamin, Inc., New York, N.Y.).

Muskevishvili, N.I. (1958), Singular Integral Equations (P. Noordhoff).

STUDIES OF ANTENNA-INDUCED IONIZATION PROBLEMS

W. C. Taylor, J. B. Chown, and T. Morita
Stanford Research Institute

ABSTRACT

This paper discusses voltage breakdown problems encountered with antennas in hypersonic flight in space and reentry. The discussion concerns: (1) predictions of ionization rates based on the Boltzmann equation; (2) injection of attaching gases to raise breakdown thresholds; (3) convective effects of flow of gas and of dc electric fields; and (4) multipactor-triggered gas discharges at low pressures.

1. INTRODUCTION

It is the purpose of this paper to interpret from an engineering perspective recent findings in the laboratory of the authors and elsewhere.

2. BOLTZMANN-DERIVED IONIZATION RATES

Recently, Epstein and Lenander (1968) formulated a basic model for ionization rates in air using the kinetic theory approach of the Boltzmann equation. Their results for a frequency of 10 GHz are shown in Fig. 1 and compared with data of several experimenters, as a function of $\overline{E}_e/p$, where $\overline{E}_e$ is $E_{rms}(1+\omega^2/\nu_c^2)^{-\frac{1}{2}}$, E_{rms} is the electric field strength, ω the radian frequency, and $\nu_c = 5.3\times10^9 p$, where p is the pressure in torr.

The data were taken at various values of pressures and frequencies. The theory of Epstein and Lenander takes into account the variation of collision frequency with energy. The results show that there is no more than 1.5 dB difference between the new theoretical calculations and those of the phenomenological theory, based on the effective-field concept with $\nu_c = 5.3\times10^9 p$. Considerable experimental data of the authors shows that scaling laws based on this simple theory are applicable within the 1.5 dB error. Thus it is seen that as a practical matter, the continued use of the phenomenological theory in engineering calculations appears warranted.

3. ALLEVIANT INJECTION

Recently, attention has been given to the possibility of alleviating the breakdown problem in reentry through local injection of a chemical into the layer of hot gas, thereby decreasing the electron density and net electron production rate by attaching electrons and by cooling. This technique is being evaluated in a shock-tube measurements program, using sulfur hexafluoride initially as the injectant. Room-temperature data, shown in Fig. 2, shows that a 10 dB

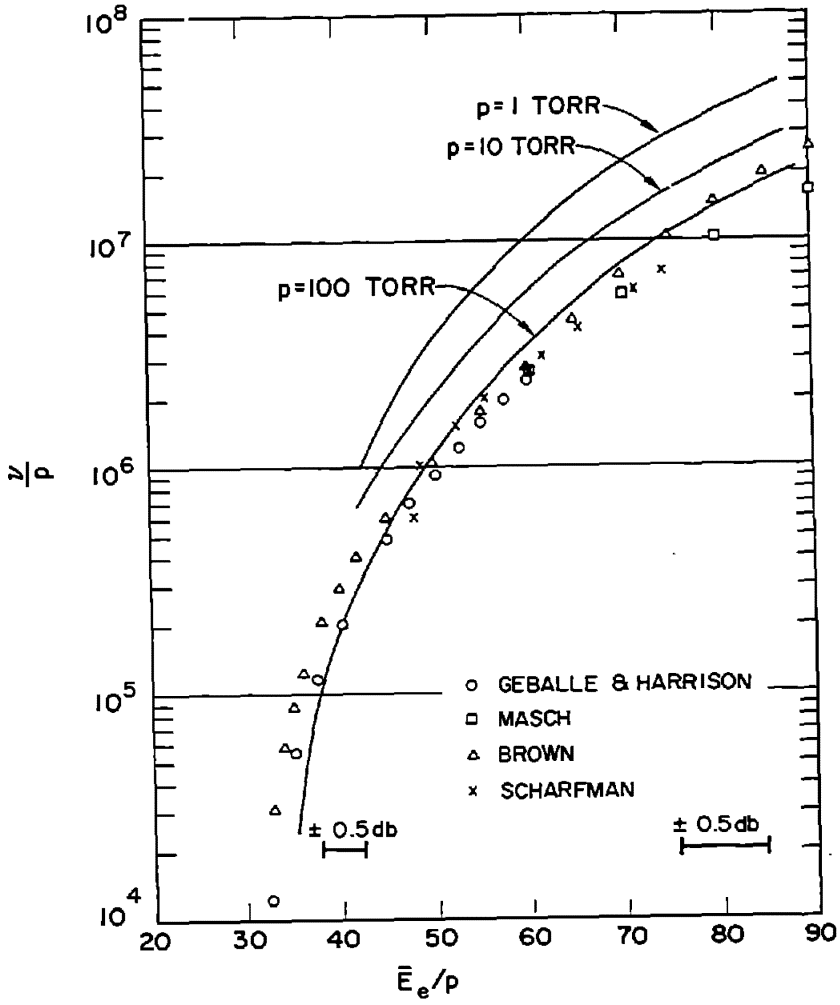

Figure 1. Ionization Rates vs. Field, Theory, and Experiment

improvement is possible in the critical pressure regime around the minimum in the limit of no thermal deterioration of the SF_6 molecules. The effect of high temperature will be to decrease the effectiveness of the SF_6 because of its dissociation. Hence the problem is finding a chemical that will attach sufficiently and will continue to do so in the thermal environment for the transit time over the antenna. Although considerable data is now available for the effects of injectants, including water, on the thermal electron generation problem, little data is available on the field-induced ionization problem.

4. CONVECTIVE EFFECTS

The convective effects of flow of a gas and of DC electric fields are quite similar in principle in that they transport the

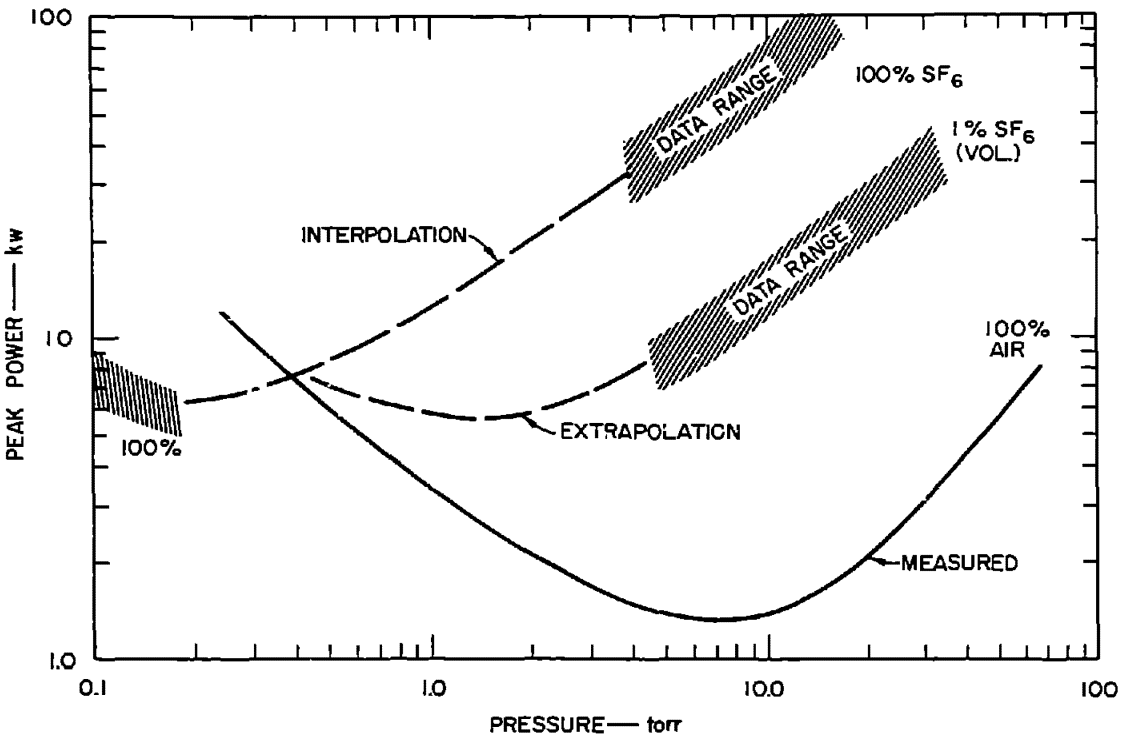

Figure 2. Breakdown Thresholds of X-band Slot

RF-induced ionization out of the high-field regions. However they are different in their configurations and in their limitations.

Figure 3 shows the effect of the flow convection upon power breakdown thresholds of an X-band antenna as predicted by three different theoretical methods. The gas flow is directed across the narrow (1cm) dimension of the slot antenna at 20,000 fps. The high-pressure approximation of Kelly and Margenau (1960) at the calculation for the limiting case of the final "breakdown" density, n_f, going to infinity, as treated by Romig (1960) and Fante (1965), are seen to predict too large an effect of the convection in pressure regions. The "exact" calculation of the authors (1968) allows both arbitrary pressure and n_f. It is seen that the effect is not large in any case, and it is difficult to conceive of a configuration showing more effects than the one treated here.

On the other hand, DC electric fields may be intentionally configured in many different ways, and the applied voltage is limited by the voltage that will cause DC breakdown. However, in an existing plasma, the ability of a field to penetrate is limited by the space-charge sheath around one electrode. Measurements of the effect

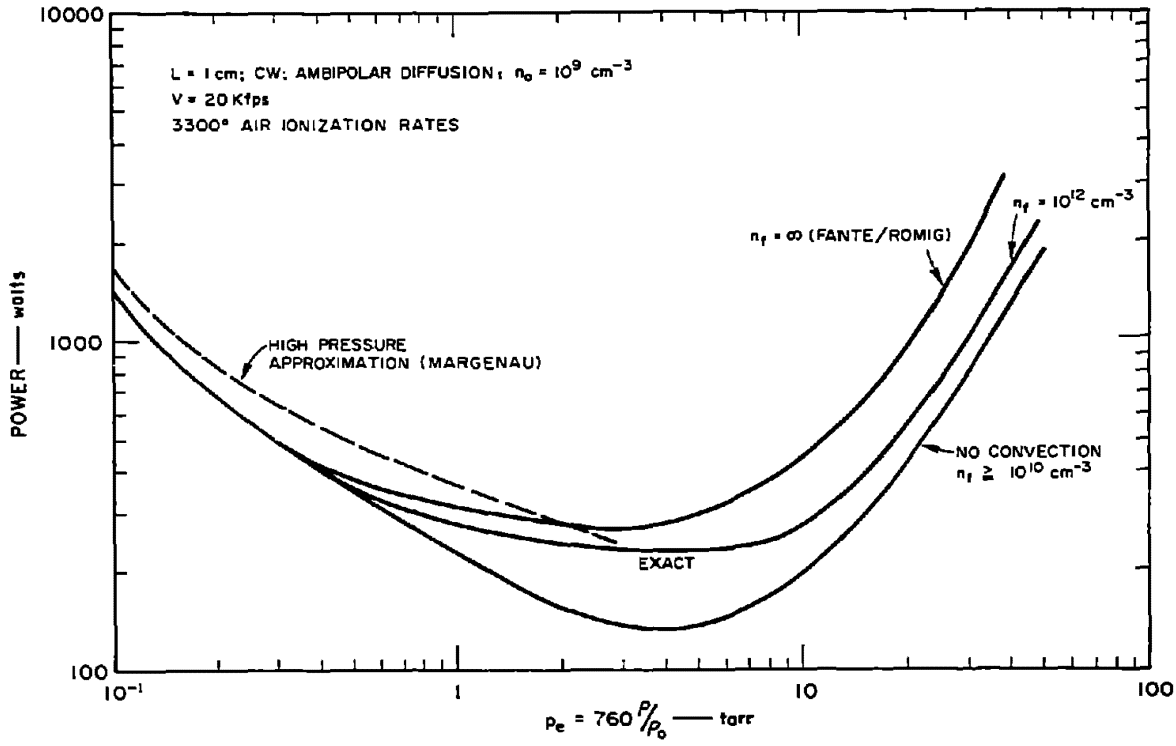

Figure 3. Effects of Gas Flow Predicted by Various Methods

of DC bias on monopole breakdown were made under varying plasma conditions, and are shown in Fig. 4. The monopole was biased negative compared with the ground plane. The theoretical calculations were made on the assumption that the electric field is sufficiently effective where it penetrates the plasma (in the ion sheath around the monopole) to prevent breakdown in this region, such that breakdown must occur at the edge of the sheath, where the fields do not sweep away the RF-generated electrons. The sheath thickness increases with voltage, but decreased with initial electron density, n_0. It is seen that this relatively simple theory is a qualified success in predicting the measured data throughout the high n_0 regime.

5. MULTIPACTOR-INDUCED BREAKDOWN

Multipactor discharge (secondary-electron resonance discharge) does not directly limit the power-handling capability of RF structures, but by its consequences. Although the multipacting must start under conditions when the electron mean free path is large compared with electrode spacing, surface-absorbed gases released by the bombardment of multipacting electrons can increase the local gas density. The

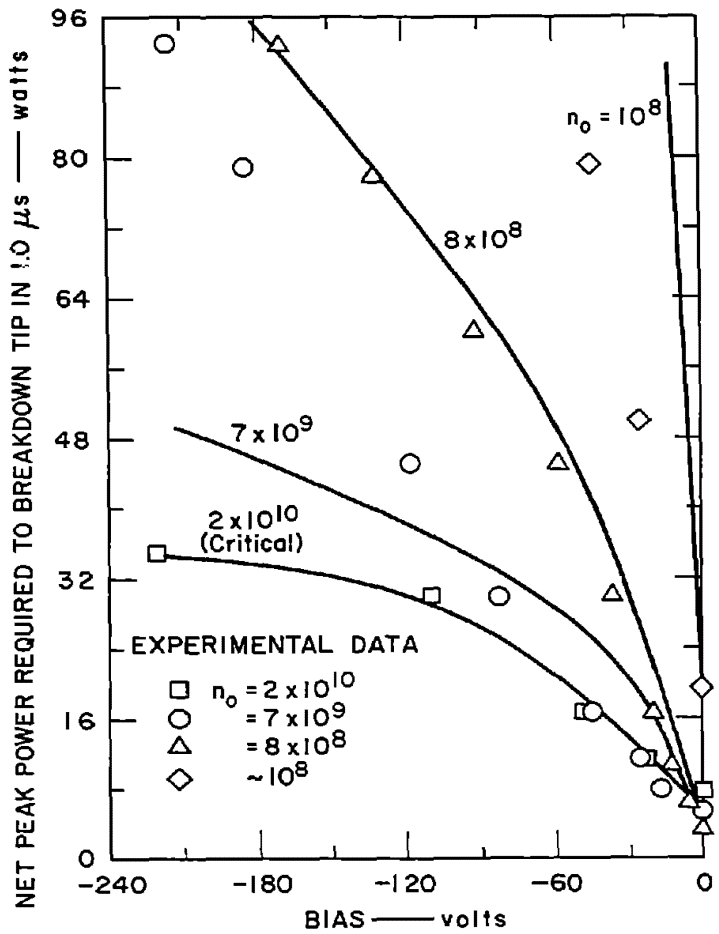

Figure 4. Effect of DC bias on Monopole Tip Breakdown in Plasma

combined effect of the high RF field, high enough electron density for ambipolar diffusion, and enhanced local density can result in transition to a gas discharge, which, in turn, does limit the radiated power. Figure 5 shows data taken for such a transition. It shows the power thresholds for initiating (free diffusion) and extinguishing ordinary gas discharge in the fields of a log-periodic antenna, as a function of pressure/altitude, and the (constant) threshold for ordinary multipactor discharge on the same configuration. The data points at pressure $< 10^{-3}$ are for the multipactor-induced gas discharge. Thus power levels of only a few hundred watts are sufficient to produce a gas discharge which would require several thousand watts without the multipacting trigger. Data points numbered 1, 2, and 3, indicating thresholds measured with

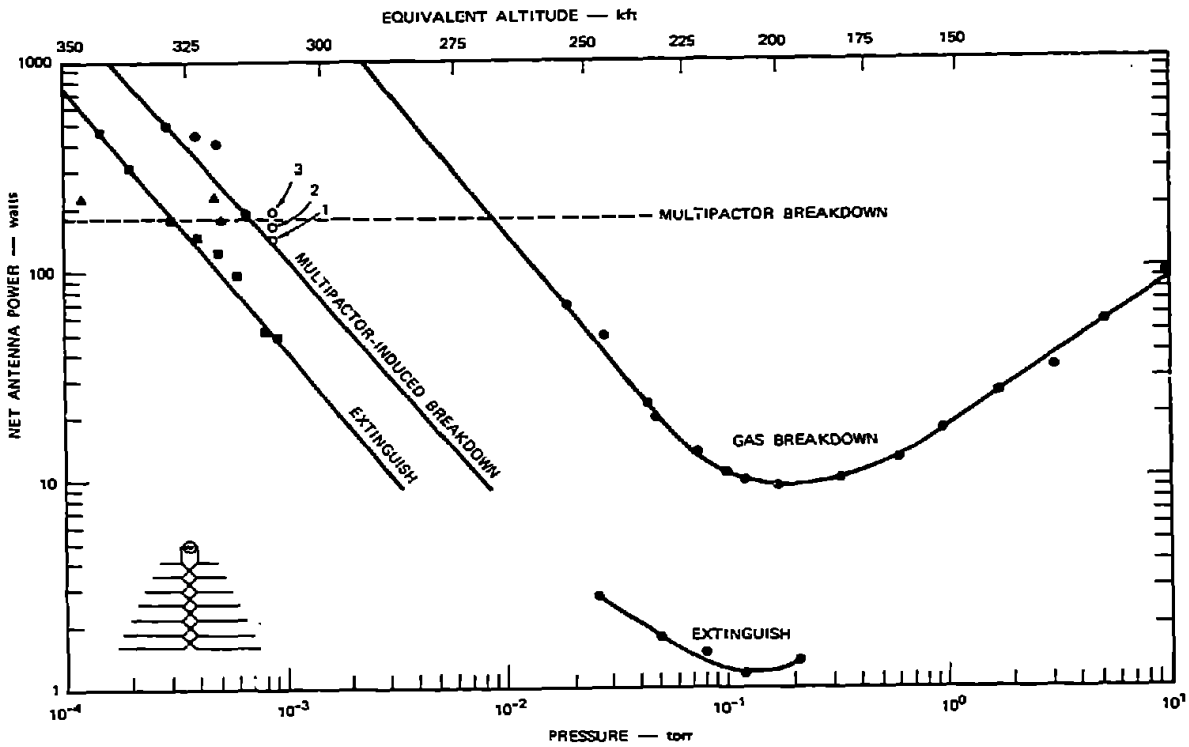

Figure 5. Multipactor-Induced Breakdown Data

lapses of several minutes in between, show the effect of surface clean-up as the multipactor proceeds.

6. REFERENCES

Epstein, M., and C. J. Lenander (1968), Fundamental Approach to High Frequency Breakdown of Gases, Phys. Fluids 11, No. 12, 2753-2758.

Kelly, D., and H. Margenau (1960), High-Frequency Breakdown of Air, J. Appl. Phys. 31, No. 9, 1617-1620.

Romig, M. F. (1960), Steady State Solutions of the Radiofrequency Discharge with Flow, Phys. Fluids, 3, No. 1, 129-133.

Fante, R. L. (1965), Mathematical Analysis of Microwave Breakdown in Flowing Gases, IEEE Trans. Ant. Prop. AP-13, No. 5, 781-788.

Taylor, W. C., J. A. Martin, and T. Morita (1968), Effects of Convection and DC electric Fields on Breakdown in Plasma, Digest of 1968 G-AP Symposium, Boston, Mass., Sept. 9-11.

BEHAVIOR OF STRONG FIELD ELECTROMAGNETIC WAVES IN ANISOTROPIC PLASMAS

M. P. Bachynski, B. W. Gibbs
Research Laboratories, RCA Limited
Montreal, Canada

- Abstract -

The effect of the electric field strength of the wave on the propagation of e-m waves in an anisotropic plasma has been investigated both experimentally and theoretically. It is found that near the electron cyclotron frequency, decreased attenuation occurs for strong field strengths. This phenomenon cannot be fully accounted for theoretically. At frequencies removed from electron cyclotron resonance, the strong field waves suffer increased attenuation. This is consistent with the heating of the electrons in the plasma by the wave.

1. INTRODUCTION

Most investigations of electromagnetic wave interaction with plasmas are based on a "small signal" approach where it is assumed that the electric field strength is too weak to appreciably affect the properties of the plasma. Little effort appears to have been devoted to the situation where the field strengths of the electromagnetic wave are not negligible and the properties of the plasma are dependent on the field strength of the wave.

In the practical situations in which radio transmitters are located in satellites or rockets in the ionosphere or on space vehicles re-entering the earth's atmosphere, since the antennas are in direct contact with the plasma, the field strengths of the wave can no longer be considered as negligible. Nevertheless, most analysis of such measurements are based on the simple small signal linear theory. Thus, an investigation of strong field electromagnetic wave interaction with plasmas is of practical as well as academic concern.

2. EXPERIMENTAL ARRANGEMENT

A laboratory experiment has been conducted to investigate the effect of the electric field strength of the wave on the transmission of an e-m wave through a plasma. In the experiment, a right-hand circularly polarized plane wave at a frequency of 9.2 GHz is normally incident on a 5 cm layer of plasma generated in helium at a pressure of 0.6 Torr. (Right-hand polarization denotes rotation in the same direction as electrons gyrate in a magnetic field.) The plasma is located between the coils of an electro-magnet and the arrangement is such that the wave propagates along the direction of the magnetic field. At a preset magnetic field strength, the plasma is pulsed and allowed to decay. Measurements of the wave transmitted through the plasma are then made in the afterglow using continuous wave electromagnetic waves of a given power density. The measurements are then repeated for various power densities and various magnetic field strengths. The plasma properties are monitored by simultaneous transmission of a left-hand circularly polarized wave through the plasma.

Such an arrangement has previously[1] shown very good agreement between theory and experiment using low field strength incident waves. Details of the experimental arrangement and measurement techniques can also be found in that paper[1].

3. MEASUREMENTS AND COMPARISON WITH THEORY

Typical experimental results of the propagation through plasmas of strong field electromagnetic waves are shown in Fig. 1 for the maximum (2.5×10^{-3} watts/cm^2) and minimum (0.1×10^{-3} watts/cm^2) power levels available in the experiment. These power levels correspond to 27.4 and 137 volts/meter respectively. The measurements are for a normally incident ($\theta = 0^\circ$) plane wave transmitted through the plasma and are normalized to the field strength of the incident wave. The results for various normalized magnetic field values can be summarized as follows:

(i) At $Y = \omega_b/\omega = 0$ (isotropic plasma) no dependence of the intensity of the transmitted wave on the field strength (power density) of the incident wave was observed for the range of power densities available in the experiment.

(ii) At $0 < Y < \sim 0.9$, the higher incident power signals showed greater attenuation than the lower power incident wave.

(iii) At $\sim 0.95 < Y < \sim 1.05$, the higher the incident power, the less was the attenuation of the transmitted signal - i.e. the attenuation coefficient of the plasma is seen to decrease with increasing electric field strength. This is exactly opposite to the "plasma shield" effect[2]. For the higher power incident wave, the transmitted signal is very nearly the same for all values of magnetic field in the region of electron cyclotron resonance [Y=0.98, 1.0, 1.02]

(IV) At $Y > 1.10$, the stronger incident signal is attenuated more than the low power incident signal as was the case for low magnetic field strengths.

For the regime removed from electron cyclotron resonance, the increased attenuation with increased strength of the incident wave is consistent with heating of the electrons by the wave resulting in a higher value for the collision frequency and hence greater attenuation of the wave.

In the region about electron cyclotron resonance, the cold plasma approximation based on a Maxwellian velocity distribution for the electrons does not predict quantitative results anywhere near the measurements. In fact, the wrong trends are predicted for increasing power densities of the incident wave. The assumption of a Maxwellian electron velocity distribution is not well justified for this regime, particularly at strong fields and lower electron densities. Calculations based on a Druyvesteyn velocity distribution for the electrons (more appropriate for the strong fields) shows a decrease of the attenuation coefficient of the plasma with increasing electric field strength of the wave as observed experimentally. The calculations also show only small differences in the attenuation as the magnetic field is changed by $\pm$ 1% off cyclotron resonance (in agreement with experiment). The experimental results at low powers agree well quantitatively with theory. The observed attenuation for high field incident waves is, however, considerably less than predicted by theory based on a Druyvesteyn velocity distribution for the electrons although the predicted trends are correct.

4. CONCLUSIONS

Marked non-linear interaction of electromagnetic waves propagating in an anisotropic plasma occurs even at very modest field strengths (27-137 volts/meter) of the incident wave. In the regime off

electron cyclotron resonance, collisional heating can account for the observations. In the region of electron cyclotron resonance, considerably less attenuation is observed at the higher field strengths. Theory based on a non-Maxwellian velocity distribution explains the observed trends but not the quantitative results at high incident field strengths. Better agreement between experiment and theory may be possible by a proper inclusion of electron-electron effects[3] in the theory or by considering the progressive interaction of the wave as it penetrates into the plasma as has been done by Papa and Haskell[4].

5. REFERENCES

1. Bachynski, M.P. and B. W. Gibbs (1966), Propagation in Plasmas Along the Magnetic Field - I Circular Polarization, Phys. of Fluids, 9, 520-531.

2. Papa, R. J. and C. T. Case (1965), The Nonlinear Interaction of a Radio-Frequency Wave with an Inhomogeneous Plasma Slab, Can. J. Phys. 43, 2036-2044.

3. Shkarofsky, I. P., T. W. Johnston, M. P. Bachynski (1966), The Particle Kinetics of Plasmas, Addison-Wesley Publishing Co. Inc., Reading, Mass.

4. Papa, R. J. and R. E. Haskell (1966), Wave Propagation in a Non-Maxwellian Magnetoactive, Nonlinear Plasma, Air Force Cambridge Research Laboratories Report 66-372.

ACKNOWLEDGEMENTS

This work was supported by the U.S. Air Force Cambridge Research Laboratories on contract F19 628-67-C-0206.

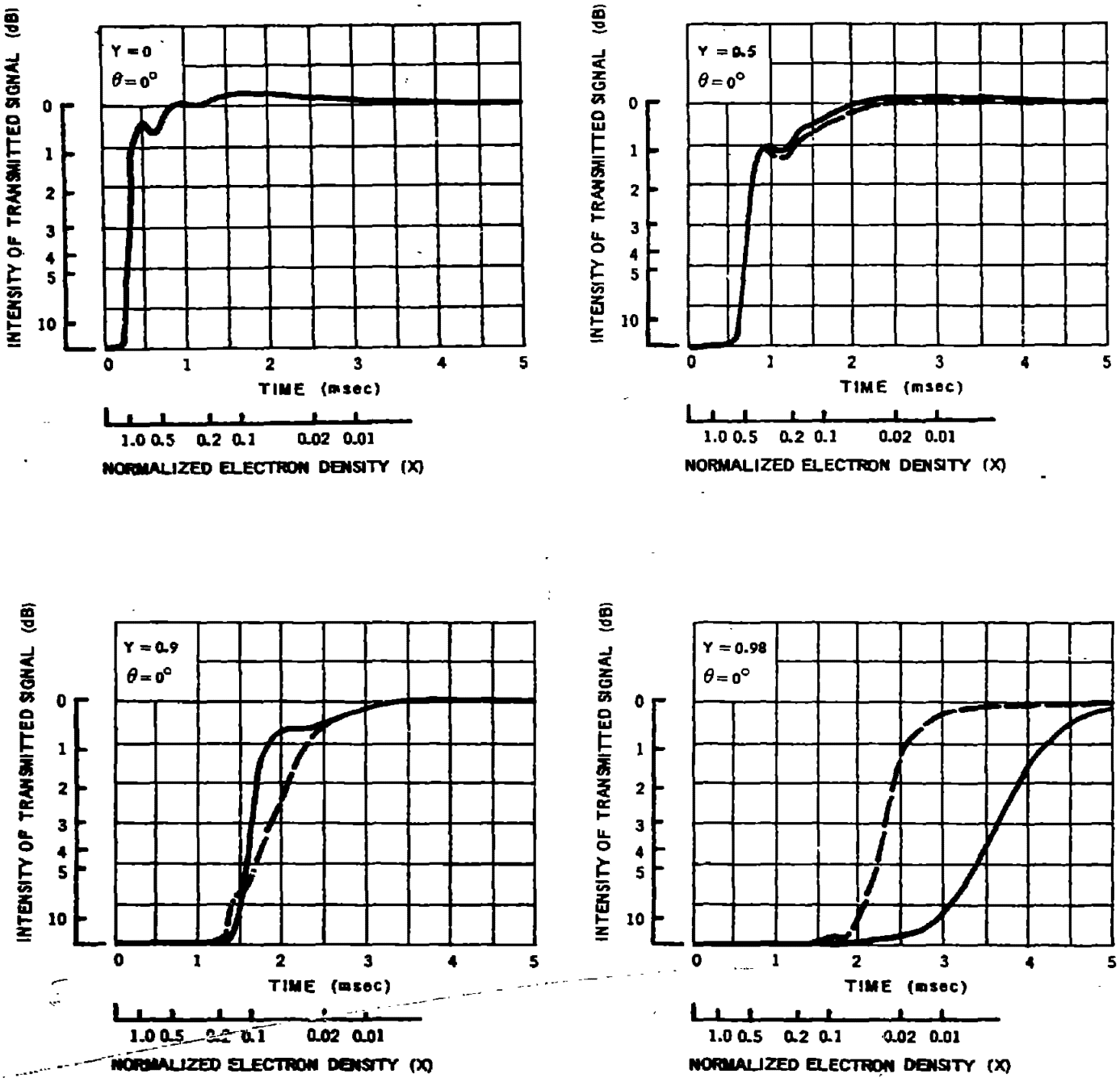

Fig. 1(a): Intensity variations of e-m wave transmission through a plasma for incident power levels of 2.5×10^{-3} watts/cm^2 (BROKEN LINE) and 0.1×10^{-3} watts/cm^2 (SOLID LINE) at normal incidence ($\theta = 0°$).

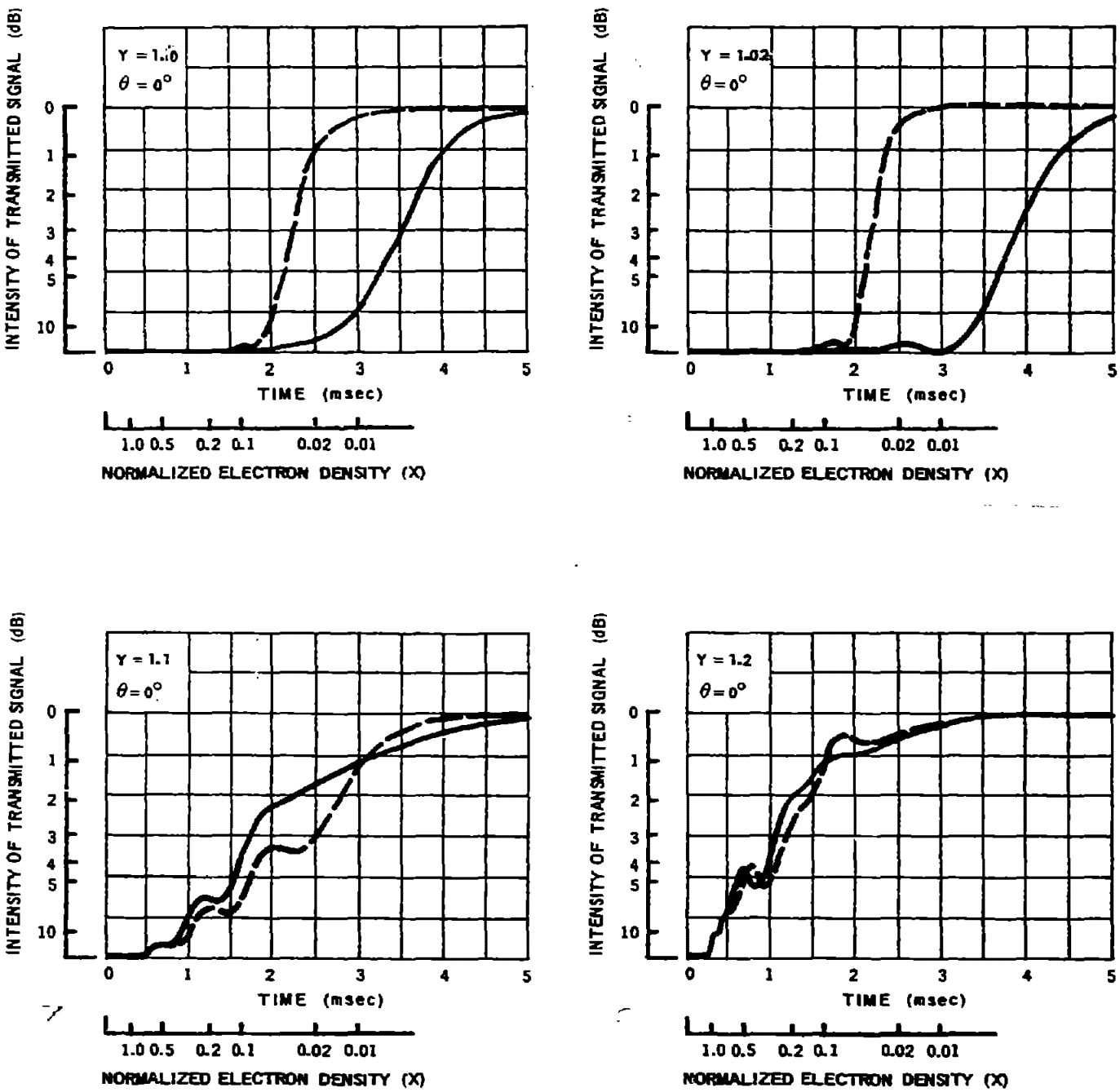

Fig. 1(b): Intensity variations of e-m wave transmission through a plasma for incident power levels of 2.5×10^{-3} watts/cm^2 (BROKEN LINE) and 0.1×10^{-3} watts/cm^2 (SOLID LINE) at normal incidence ($\theta = 0^\circ$).

THE TRAILBLAZER II REENTRY ANTENNA TEST PROGRAM

J. Leon Poirier, Walter Rotman,
Dallas Hayes, and John Lennon

Air Force Cambridge Research Laboratories (OAR)
L. G. Hanscom Field, Bedford, Massachusetts 01730

Abstract

A number of results are presented which were obtained in the first flight test of a reentry vehicle designed to determine the properties of the plasma sheath and its effect upon microwave antenna performance.

This paper presents a synopsis of the results obtained from analysis of data from the first flight test of a Trailblazer II reentry vehicle designed to study the properties of the plasma sheath and its effect upon radiating systems at velocities in the ballistic range. The reentry payload (Figure 1) consisted of three major subsystems: a plasma diagnostic probe system; an

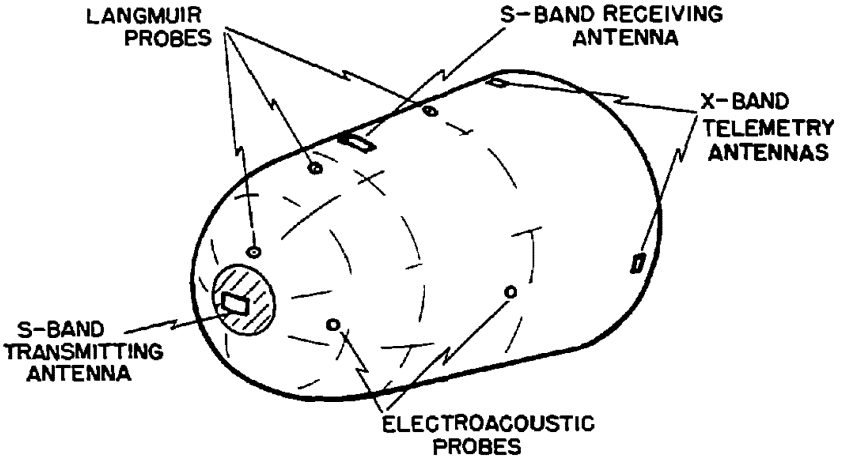

Figure 1. Reentry Vehicle

S-band transponder system, and an X-band telemetry system. The flight data allowed: (1) measurement of the influence of the plasma sheath upon the radiation pattern distortion,

signal attenuation, and impedance mismatch for an S-band slot antenna located at the stagnation point of the nose cone; (2) measurement of the plasma sheath effects upon the interantenna coupling between two S-band antennas on the nose cone, and (3) determination of the electron density profile and gradients about the nose cone.

The S-band transmitting antenna consisted of a dielectric-filled, waveguide-fed slot with coaxial input located at the stagnation point of the reentry nose cone. A similar receiving antenna with identical internal dimensions, but with a T-bar feed was located at the shoulder of the nose cone for measurement of the interantenna coupling. Both antennas were adjusted to provide an impedance match to the input coaxial cable under free-space conditions.

Two computer programs were used to predict the operational characteristics of the antenna system. Both programs assume a multilayered plasma. The first is based upon the theoretical analysis of Galejs [1] and was developed by the Cornell Aeronautical Laboratory. The output consists of the terminal admittance of a slot antenna located on a flat ground plane and the mutual admittance and coupling of this antenna with a like antenna located upon the same ground plane. The second computer program, developed by Avco [2] gives the far-field radiation pattern, as well as the terminal admittance, for the open-ended waveguide. The flow-field properties were obtained by using nonequilibrium binary scaling for the stagnation-streamline applied to results given by Cornell Aeronautical Laboratory.[3] The boundary layer properties were taken from stagnation boundary layer calculations given in a report by Nerem.[4]

The measured reflection coefficient of the S-band antenna is shown in Figure 2. Also shown is the theoretical prediction of the reflection coefficient based upon Galejs' analysis. The effect of losses in the antenna structure were not included in the calculation. A good engineering estimate of this loss would be ~ 1 dB. If a correction of 1.5 dB is made, it is seen that the predicted maximum reflection coefficient is in good agreement with the measured one. The theoretical calculation does not predict very well the altitude at which the maximum reflection coefficient is reached. This discrepancy is, in all probability, due to the inadequacy of the flow-field calculations to make predictions for altitudes above 240,000 ft.

In so far as the plasma sheath can be considered lossless and is overdense, it can be shown that the power reflection coefficient is a unique function of the distance from the antenna surface out to the beginning of the overdense region. This distance (termed the electromagnetic boundary layer thickness δ) is shown in Figure 3. The results of both the flight and the theoretical determination of δ are shown. The discrepancy between theory and flight data at altitudes below 220,000 ft is not significant. This is due to the difficulty in measuring small changes in the reflection coefficient occurring after it had leveled off near its maximum value.

The measured and theoretical values of the mutual coupling loss versus altitude are shown

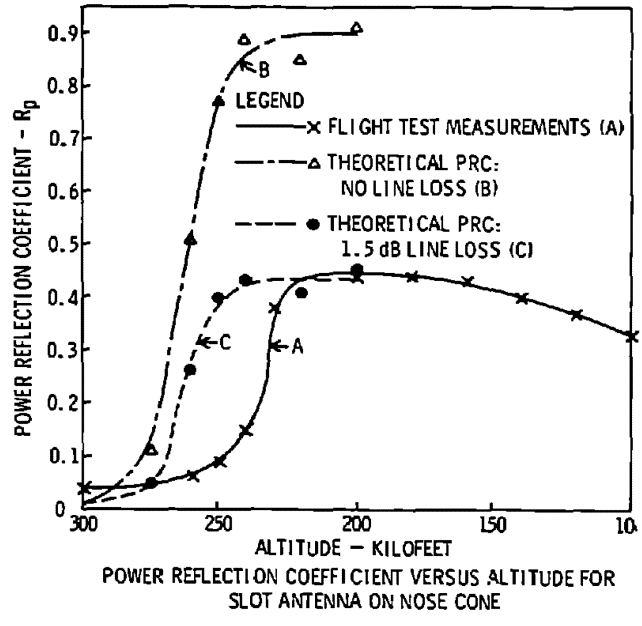

POWER REFLECTION COEFFICIENT VERSUS ALTITUDE FOR SLOT ANTENNA ON NOSE CONE

Figure 2

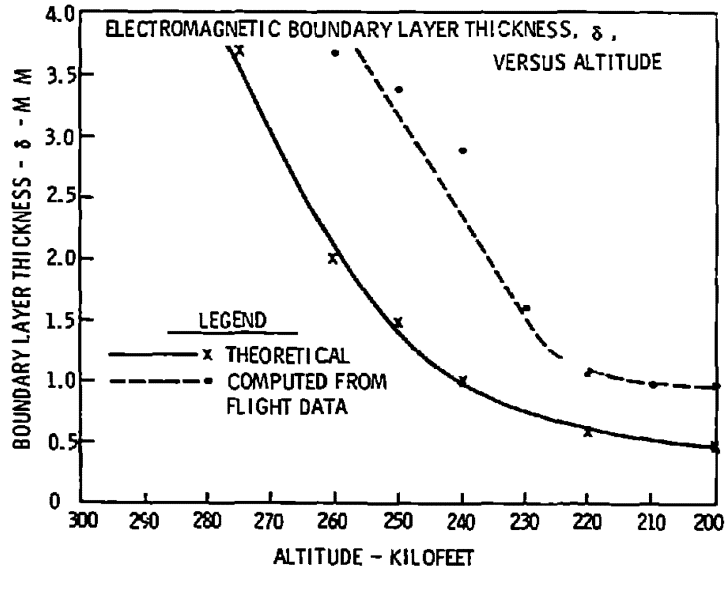

Figure 3

in Figure 4 normalized to the free-space value. Two things are to be noticed. Coupling increases at first from its value at 300,000 ft where negligible plasma is present. This is probably due to ducting along the surface caused by the presence of the plasma. This is followed by an abrupt decrease of greater than 10 dB at about 250,000 ft. Theory predicts a sharp decrease at about this altitude. Also shown in the figure is an estimate of the amount of decoupling due to power reflection loss at the transmitting antenna. As this curve also shows a sharp decrease in this altitude range, it is to be concluded that the antenna decoupling is due primarily to reflection from the plasma in front of the antenna and not to attenuation caused by transmission through the plasma.

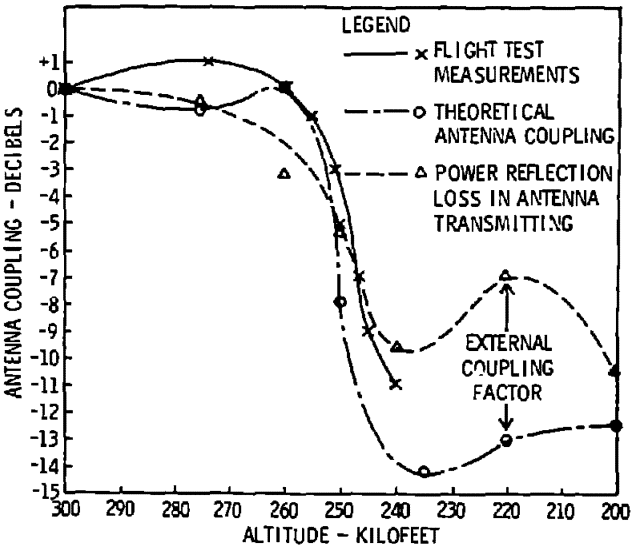

MUTUAL COUPLING LOSS VERSUS ALTITUDE FOR TWO SLOT ANTENNAS ON NOSE CONE

Figure 4

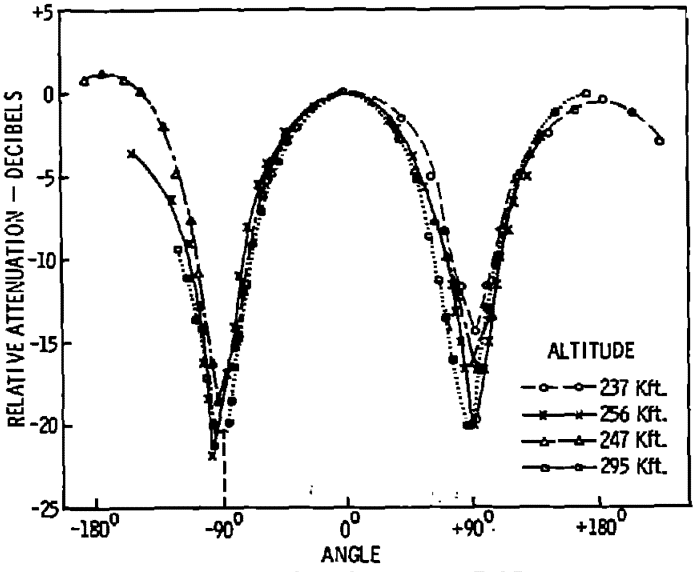

RADIATION PATTERNS VS ALTITUDE: TRAILBLAZER II FLIGHT DATA

Figure 5

Several in-flight radiation patterns are shown in Figure 5 for altitudes at which signal attenuation is changing substantially. The curves, normalized so that the peak values correspond to zero dB, show that the shape of the radiation pattern does not change substantially even under conditions for which the plasma sheath is attenuating the signal by over 20 dB. This has been predicted for overdense plasma sheaths which are physically thin compared to the wavelength of the transmitted signal.[5] Under these conditions the plasma sheath is equivalent to an impedance sheet which attenuates the signal level without changing the pattern shape. This conclusion has also been confirmed by the computer calculations using the Avco program which shows that the radiation patterns are attenuated, but otherwise unchanged, as a function of altitude.

The plasma diagnostic system contained four electro-acoustic probes designed to measure the electron density gradient in the boundary layer, and three flush mounted Langmuir probes. This was the first flight test of the electroacoustic probe. Valid data was obtained from each type of probe throughout the reentry trajectory. Substantial agreement was obtained between the data of both types of probe.

References

1. Galejs, J. (1965), Self and mutual admittance of waveguides radiating into plasma layers, Radio Sci. J. Res. NBS 69D, 179-189.

2. Fante, R.L., J.R. Mclaughlin, and J.E. Trousdale (1966), A study of ablation material effects on antenna performance, Avco Corp., Wilmington, Mass., Report No. AVSSD-0277-66-RR; prepared under NASA Contract 9-4916.

3. Curtis, J., A. Burke, and R. Hayman (1963), An analytical and experimental study of the ionized flow-field about a hemisphere cylinder and its effect on the radiation pattern of a slot antenna, Cornell Aeronautical Laboratory, Final Report AFCRL-63-339.

4. Nerem, R. M. (1962), Stagnation region plasma properties including some nonuniform effects, Ohio State University Report 1021-25.

5. Fante, R.L. (1967), Effect of thin plasmas on an aperture antenna in an infinite ground plane, Radio Sci. 2 (new series), 87-100.

Single and Multislot Antennas in an Inhomogeneous Reentry Plasma Environment*

K. E. Golden and G. E. Stewart
Laboratory Operations
Aerospace Corporation, Los Angeles, Calif.

ABSTRACT

A short linear slot array radiating through an inhomogeneous reentry boundary-layer plasma is analyzed for free, standing-wave-feed, and traveling-wave-feed aperture excitations. Calculations are presented for self- and mutual-admittance, aperture voltages, element pattern, and the resulting antenna gain for free space and typical low-altitude reentry plasma conditions for a sharp, slender, conical vehicle.

1. Introduction

Performance of a short linear E-plane array of slot antennas in the presence of a reentry plasma sheath is analyzed (figure 1). The short-circuit admittance matrix representing the N-element array in a reentry plasma environment is obtained by an extension of the slot self- and mutual admittance analyses given in Golden and Stewart (1968). From the definition of the short-circuit admittance parameters, elements of the aperture admittance matrix are for $i = j$

$$Y_{ij}^{ap} = Y(0) = y_{11},$$

and for $i \neq j$

$$Y_{ij}^{ap} = Y(|i-j|) = y_{12}(|i-j|k_0\delta),$$

where y_{11} and $y_{12}(|i-j|k_0\delta)$ are the normalized self- and mutual admittances of a pair of E-plane slots separated by $|i-j|k_0\delta$. Short-circuit admittances normalized to the dominant-mode guide admittance Y_g are on figure 2 for standard X-band waveguide apertures radiating into free space and on figure 3 for the typical reentry plasma shown in figure 1.

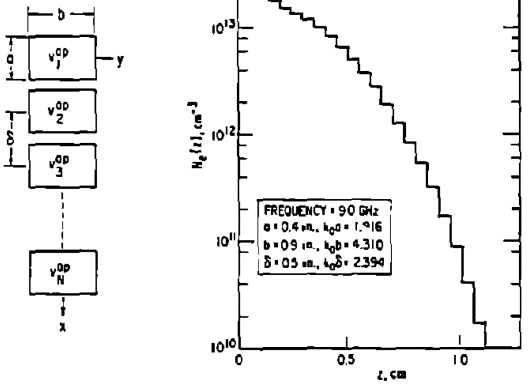

Figure 1. Linear array geometry and reentry plasma sheath

*The research reported in this paper was sponsored by the U.S. Air Force under Contract AF04701-68-C-0200.

NORMALIZED APERTURE VOLTAGES			
	FREE	TRAVELING	STANDING
1	0.350 /-7 deg	0.318 /-175 deg	0.318 /-1 deg
2	0.327 /-14 deg	0.321 /+160 deg	0.302 /+25 deg
3	0.355 /-37 deg	0.310 /+133 deg	0.347 /-25 deg
4	0.342 /-59 deg	0.298 /+109 deg	0.358 /-61 deg
5	0.336 /-76 deg	0.289 /+90 deg	0.369 /-68 deg
6	0.352 /-98 deg	0.285 /+73 deg	0.390 /-100 deg
7	0.339 /-117 deg	0.283 /+58 deg	0.365 /-119 deg
8	0.341 /-139 deg	0.282 /+41 deg	0.353 /-145 deg
9	0.353 /-154 deg	0.282 /+23 deg	0.347 /-162 deg
10	0.326 /+174 deg	0.282 /+2 deg	0.318 /+179 deg

APERTURE ADMITTANCES
Y(0) = 0.7772 + j0.4181
Y(1) = 0.1416 - j0.3394
Y(2) = -0.2069 + j0.0683
Y(3) = 0.1538 + j0.0715
Y(4) = -0.0341 - j0.1105
Y(5) = -0.0418 + j0.0833
Y(6) = 0.0734 - j0.0265
Y(7) = -0.0615 + j0.0265
Y(8) = 0.0237 + j0.0538
Y(9) = 0.0172 - j0.0494

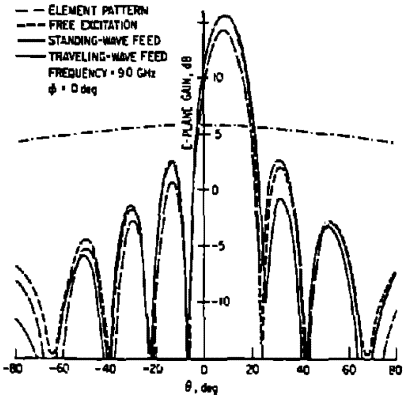

Figure 2. Ten-element linear array gain in free space

NORMALIZED APERTURE VOLTAGES			
	FREE	TRAVELING	STANDING
1	0.0956 /+43 deg	0.0923 /-19 deg	0.287 /+16 deg
2	0.0957 /+23 deg	0.0812 /-89 deg	0.102 /-11 deg
3	0.0956 /+3 deg	0.122 /-146 deg	0.0649 /-17 deg
4	0.0957 /-17 deg	0.141 /+178 deg	0.0521 /-21 deg
5	0.0957 /-39 deg	0.143 /+147 deg	0.0482 /-23 deg
6	0.0956 /-57 deg	0.145 /+117 deg	0.0505 /-25 deg
7	0.0956 /-77 deg	0.155 /+87 deg	0.0604 /-28 deg
8	0.0956 /-98 deg	0.178 /+58 deg	0.0889 /-33 deg
9	0.0956 /-117 deg	0.200 /+29 deg	0.198 /-50 deg
10	0.0953 /-137 deg	0.230 /0 deg	0.287 /-164 deg

APERTURE ADMITTANCES
Y(0) = 3.8755 - j4.5108
Y(1) = -0.0298 - j0.0069
Y(2) = -0.0186 - j0.0030
Y(3) = -0.0006 - j0.0016
Y(4)
Y(5)
Y(6)
Y(7)
Y(8)
Y(9)

NEGLIGIBLE

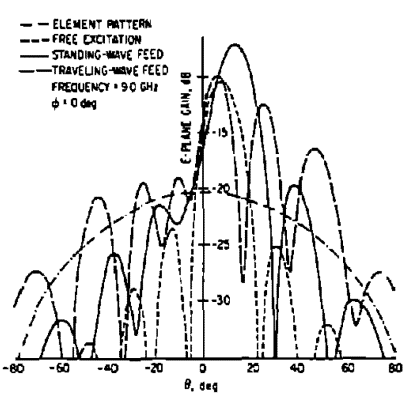

Figure 3. Ten-element linear array gain in reentry environment

2. Aperture Voltage Determination

To determine the antenna gain for a linear array, it is necessary to calculate the dominant-mode aperture voltages. The feed scattering matrix for an N-element linear array has (N + 1) x (N + 1) elements when the termination G_L is assumed to be internal to the feed and can be partitioned in the following manner:

$$\left[S^F\right] = \left[\begin{array}{c|c} S^{FNN} & \vec{c} \\ \hline \overleftarrow{c} & \Gamma_F \end{array}\right] . \qquad (1)$$

The i^{th} component of the column vector $\vec{c}$ is the voltage appearing at the i^{th} aperture with all the apertures terminated in matched loads assuming unit incident voltage at the N + 1 input port. The i^{th} component of the row vector $\overleftarrow{c}$ is the voltage transmitted back to the input port for unit incident excitation at the i^{th} aperture with all other ports matched. The input reflection coefficient for matched aperture conditions is Γ_F.

If $[S^{FNN}]$ is nonzero, the reflections from, and coupling between, the apertures modify the incident voltage. The aperture scattering matrix can be written in terms of the admittance matrix $[Y^{ap}]$

$$[S^{ap}] = \left([U] + [Y^{ap}]\right) \cdot \left([U] - [Y^{ap}]\right)^{-1} \quad . \tag{2}$$

The resulting incident $\vec{c}'$ and scattered $\vec{d}'$ voltages are related by

$$\vec{d}' = [S^{ap}]\,\vec{c}' \quad , \tag{3}$$

with linear superposition and unit incident voltage at the N + 1 terminal

$$\vec{c}' = [S^{FNN}]\,\vec{d}' + \vec{c} \quad . \tag{4}$$

Aperture voltage is determined from (3) and (4), and then

$$\vec{v}^{ap} = (\vec{c}' + \vec{d}') = \left([S^{ap}] + [U]\right) \cdot \left([U] - [S^{FNN}][S^{ap}]\right)^{-1} \vec{c} \quad . \tag{5}$$

For a freely excited array [Oliner and Malich (1966)], $[S^{FNN}]$ is zero, which simplifies $\vec{v}^{ap}$ to

$$\vec{v}^{ap} = \left([S^{ap}] + [U]\right) \cdot \vec{c} \quad .$$

To obtain numerical results, the standing- and traveling-wave feeds are approximated by the equivalent circuit in figure 4.

	STANDING-WAVE FEED $G_L = 0$, $\psi_1^B = 360$ deg		TRAVELING-WAVE FEED $G_L = 1.00$, $\psi_1^B = 0$ deg	
i	η_i	ψ_i^B, deg	η_i	ψ_i^M, deg
1	0.316	0	0.632	340
2	0.316	20	0.600	340
3	0.316	40	0.511	340
4	0.316	60	0.415	340
5	0.316	80	0.347	340
6	0.316	100	0.307	340
7	0.316	120	0.288	340
8	0.316	140	0.285	340
9	0.316	160	0.295	340
10	0.316	180	0.307	360

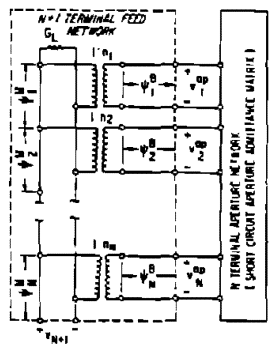

Figure 4. Feed Network

The free, standing-wave-feed, and traveling-wave-feed aperture excitations are designed to provide uniform illumination with a 20-deg phase shift between elements when the aperture is matched and the external mutual coupling is neglected. The traveling-wave-feed was designed to absorb 20% of the available power in the termination G_L. The actual circuit elements are tabulated in figure 4. The elements of the scattering matrix of the feed can be calculated using standard transmission line theory with the slots alternately excited in the manner used in measuring scattering matrices.

3. Radiation Pattern Calculations

The antenna gain for unity input voltage is defined as

$$g(\theta, \phi) = 4\pi r^2 (Y_0/Y_g) \left\{ |E_\theta(r, \theta, \phi)|^2 + |E_\phi(r, \theta, \phi)|^2 \right\} \quad , \tag{6}$$

where Y_0 is the characteristic admittance of free space, and E_θ and E_ϕ are the far-field components of the electric field for the prescribed excitation.

The far field can be written in terms of the Fourier transform of the electric field at $z = z_0$ when the sources are bounded in extent and z_0 is sufficiently large that only free space exists for $z>z_0$. Evaluating the inverse Fourier transform asymptotically results in

$$\lim_{k_0 r\to\infty} \vec{E}(r,\theta,\phi) = j\frac{2\pi}{r\lambda_0}\cos\theta\,\vec{\xi}(k_{x_s}, k_{y_s}, z_0)\exp[jk_0(z_0\cos\theta - r)] \quad , \quad (7)$$

where $\vec{\xi}(k_{x_s}, k_{y_s}, z=z_0)$ is the transform of the electric field evaluated at the stationary point in transverse wavenumber space defined by $k_{x_s} = k_0\sin\theta\cos\phi$ and $k_{y_s}\sin\theta\sin\phi$. The Fourier transform of the field at $z=z_0$ can be determined by expressing the electric field at the aperture in terms of TE_z and TM_z components and then transforming these components through the dielectric and plasma regions using standard transmission line theory [Golden and Stewart (1969)]. The gain for an N-element array of rectangular slots from (6) and (7) is then

$$g(\theta,\phi) = \frac{32ab}{\pi\lambda_0^2}\frac{Y_0}{Y_g}P_e(\theta,\phi)\left|\sum_1^N v_n^{ap}\exp[+j(n-1)\,k_{x_s}\delta]\right|^2 \quad . \quad (8)$$

The element factor P_e in (8) is

$$P_e(\theta,\phi) = \frac{\pi^2}{16}\left[\frac{\sin u_1}{u_1}\left(\frac{\sin u_2}{u_2} + \frac{\sin u_3}{u_3}\right)\right]^2\left[\frac{\cos^2\phi}{|G_{TM}|^2} + \frac{\sin^2\phi\cos^2\theta}{|G_{TE}|^2}\right], \quad (9)$$

and u_1 is $0.5\,k_{x_s}a$, u_2 is $0.5\,(k_{y_s}b + \pi)$, and u_3 is $0.5\,(k_{y_s}b - \pi)$. The voltage transfer functions G_{TE} and G_{TM} are equal to unity when the array is radiating into free space.

4. Numerical Results

The aperture voltage for a freely excited single-slot antenna is equal to

$$v_1^{ap} = 2/(1 + y_{11}) \quad . \quad (10)$$

The single-slot results for both bare and plasma-clad ground planes are in figures 2 and 3 respectively. The inhomogeneous plasma layer was approximated by 22 equivalent slabs (figure 1).

The results of the feed aperture voltage and antenna gain calculations for free-space conditions are shown in figure 2. The maximum array gain for the traveling-wave feed is 1.3 dB less than the standing-wave feed because of the power absorbed in the load. The systematic errors caused by aperture reflections are reduced by the mutual coupling for this example.

The results of the antenna gain and aperture voltage computations for a plasma environment are displayed in figure 3. Since the mutual coupling is greatly reduced by the plasma, the aperture reflection effects produce the majority of the pattern degradation. The array side-lobe level of the standing-wave feed was degraded to -2.7 dB because of the multiple reflections in the branch lines. The plasma sheath increased the progressive element phase shift by 10 deg causing the main beam of the traveling-wave feed to be scanned from 8.4 to 13.5 deg. The patterns of the freely excited array are less sensitive to plasma effects (figures 2 and 3).

5. Conclusions

The performance of a small array antenna in a reentry environment was analyzed including internal feed effects as well as reflection loss, absorption and antenna element pattern distortion. The problem was formulated using scattering matrices so that either readily measured scattering matrix elements or analytically determined values could be used for the feed. The effects of the plasma layers on the effective scattering matrix of the N-element aperture can be calculated if the electron density and collision frequency profiles of the plasma layer are known. The resulting effect on aperture voltages is easily determined. Because of the high cost of flight experiments, performance problems, and availability of preflight predictions of electron density, a detailed analysis appears warranted. Furthermore, for arrays of small beamwidth, flight-test measurements of radiation patterns become increasingly difficult, considering usual ground station limitations. A more reasonable approach would be to measure single-element radiation patterns and to infer array factors from the measurements of the individual aperture voltage during reentry.

6. References

1. K. E. Golden and G. E. Stewart, "Admittance and Isolation of Slot Antennas in the Presence of an Inhomogeneous Plasma Layer," IEEE Summary Digest, 1968 International Antennas and Propagation Symposium, p. 52.

2. A. A. Oliner and R. G. Malich, "Mutual Coupling in Infinite Microwave Scanning Antennas," Vol. II: Array Theory and Practices, ed. R. C. Hansen (Academic Press, Inc., New York, 1966), chapt. 3, p. 211.

3. K. E. Golden and G. E. Stewart, "Self and Mutual Admittances of Rectangular Slot Antennas in the Presence of an Inhomogeneous Plasma Layer," TR-0200(4220-10)-1, Aerospace Corp. Report (February 1969).

IONOSPHERIC ANTENNA IMPEDANCE PROBE

by E. K. Miller[1], H. F. Schulte[2], J. W. Kuiper[2] ([1]MBAssociates, San Ramon, California, [2]High Altitude Engineering Laboratory, University of Michigan)

ABSTRACT. The results of a parallel theoretical-experimental investigation into the use of an antenna as a diagnostic probe in the ionosphere are described. The salient features of the antenna impedance are found to be in agreement with the theoretical predictions, and provide several methods for determining the ionospheric electron density.

I. INTRODUCTION. A parallel theoretical-experimental program was undertaken to resolve some of the questions which arise in using an antenna as a diagnostic device in the ionosphere. To clarify the relative importance of the physical processes which may influence the impedance, an infinite gap-excited cylindrical antenna immersed in a plasma was investigated theoretically. The results of this study have been reported elsewhere (Miller, 1967, 1968); only a summary will be given here.

The experimental part of the program used ionospheric sounding rockets carrying several complementary electron density determination experiments. These included a Langmuir probe, a relaxation resonance detector, a transmission experiment, and an antenna impedance experiment. The latter three experiments used a 30 ft tip-to-tip balanced electric dipole whose frequency was swept continuously from 0.8 to 10 MHz. Results presented here will be confined principally to the antenna impedance measurement.

II. RESULTS OF THE INVESTIGATION. The aspects of the theoretical infinite antenna study which apply to the ionosphere are: (1) for an incompressible, anisotropic plasma (magnetic field parallel to the antenna axis), the impedance has a minimum at the cyclotron frequency f_h, a slight maximum at the electron plasma frequency f_p, and a sharp maximum at the upper hybrid frequency $f_t = \sqrt{f_p^2 + f_h^2}$; (2) the addition of a concentric vacuum sheath a few Debye lengths thick shifts the f_h impedance minimum upward in frequency and increases the minimum impedance value, but does not significantly alter the impedance above $2f_h$; (3) the plasma compressibility and vacuum sheath separately produce similar effects on the antenna impedance for both the isotropic and anisotropic plasma. Comparing the infinite antenna results with Balmain's (1964) finite antenna quasistatic analysis shows that the qualitative predictions of the two theories are equivalent. Thus the infinite antenna results may be applied when the quasistatic theory cannot be used conveniently. This equivalence also suggests that Balmain's theory is reliable for quantitative interpretation of experimental impedance data.

94 complete impedance frequency sweeps were obtained during a rocket flight (NASA 4.207) to a 292 Km altitude. A computer-plotted curve for the impedance of half the balanced dipole (the equivalent monopole) is shown in Figure 1. The impedance is a linear function of time (there are 833 data points per second) for the two overlapping bands, 0.8 to 3.5 MHz and 2.6 to 10 MHz, used to cover the 0.8 to 10 MHz range. Sweep frequency with respect to time is not quite linear in either band; a slight transformation is required to obtain an impedance-frequency plot.

These impedance curves (moving upward in frequency) exhibit a broad minimum, a slight oscillation, a sharp peak and a discontinuity. These features were regularly observed throughout the flight. The peak shape differs on the two sweeps due to the variation in sweep rate in the overlapping frequency range. At the right side of the high frequency sweep is seen the typical behavior resulting from the telemetry signal dropout which occurred infrequently during the flight.

A smoothed version of Figure 1 versus frequency is shown in Figure 2. Also shown (the x'd curve) is the impedance calculated from Balmain's formula, and (the circles) two calculated free-space impedance curves for the antenna which has a half-length h of 4.58 m and a radius

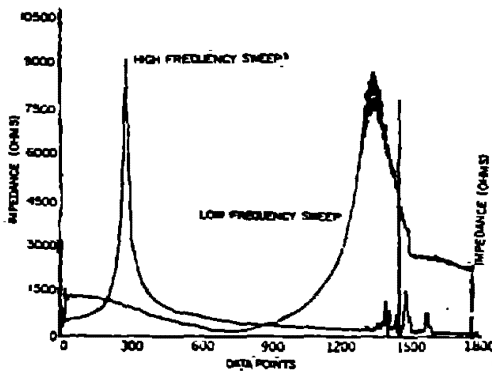

FIGURE 1

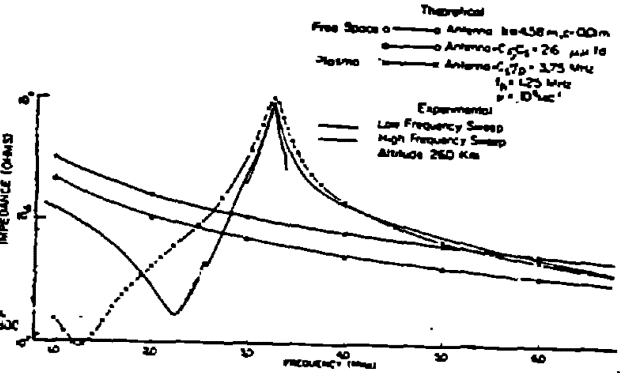

FIGURE 2

c of 1 cm. The free-space curves show the isolated antenna impedance and that which results from including the effect of the shunt capacitance C_s of the antenna deployment mechanism. This capacitance shifts the f_t peak downward in frequency. It is included in the plasma-immersed theoretical curve (the antenna is assumed parallel to the magnetic field). Quite good agreement is obtained between theory and experiment using the indicated plasma parameters (ν is the electron collision frequency) down to a frequency of about 2.5 f_h. The upward-shifted impedance minimum agrees with the infinite antenna theory as well as with the spherical quasistatic analysis of Balmain et al (1967). The plasma parameters were chosen to produce an apparent best-fit curve to the experimental data, and the unrealistically high value required for ν may be due to neglecting the sheath (Balmain et al, 1967).

Similar agreement between theory and experiment was obtained throughout the flight. The experimental data provided three independent ways to obtain f_p; using (1) the frequency (f_M) of the impedance peak associated with f_t, (2) the absolute impedance above f_t, and (3) the impedance discontinuity at f_p. The first two methods are generally independent of ν, while the latter requires no theoretical interposition, although the downward-shifted impedance peak often obscures the f_p discontinuity.

An interesting use for the upward-shifted impedance minimum associated with f_h is to determine the sheath thickness and electron temperature. If, for example, the equivalence between the actual inhomo-

geneous sheath and the vacuum sheath model is known in terms of the minimum impedance frequency f_m, then the equivalent vacuum sheath thickness can be obtained from f_m and f_p. Since the sheath thickness is a function of f_p (which is already known) and the temperature, the temperature can then be solved for. There has been some success in obtaining electron temperature values this way, but not enough data has been analyzed to validate the technique.

Since the rocket rotation period was about 21 sec, and nearly 4 complete frequency sweeps over the 0.8 to 10 MHz range were obtained during a complete rotation, it is possible to resolve the influence of the magnetic field and rocket wake on the impedance. Figure 3 is a plot of the impedance at 5.25 MHz as a function of time (or altitude). The individual impedance points are joined by straight lines to clarify the variation. Also shown are the ionospheric magnetic field and plasma stream velocity components tangential to the monopole whose impedance was monitored. A positive velocity indicates the monopole is facing in the direction of rocket travel. The impedance maxima correlate well with positive tangential velocities, demonstrating the decreased electron density in the rocket wake. Using Balmain's theory, the impedance swings may be translated to electron density variations of as much as two to one.

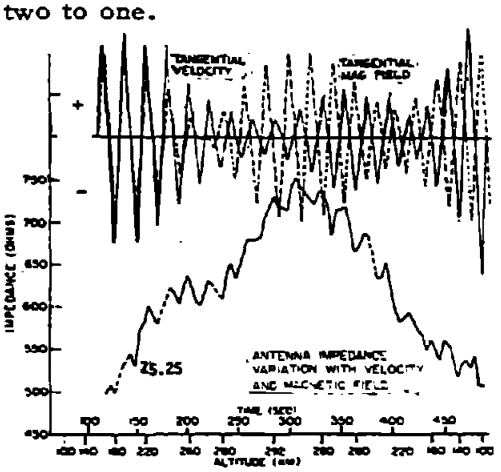

FIGURE 3

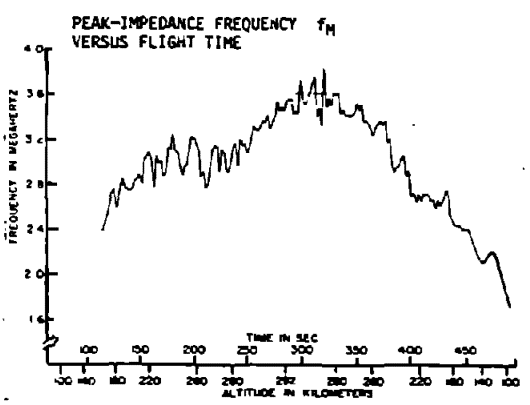

FIGURE 4

Figure 4 shows the peak-impedance frequency f_M as a function of time. There is a correlation between f_M and both tangential magnetic field magnitude and velocity, as f_M oscillates twice per period. The amplitude of the f_M swings is also correlated with the amplitudes of the velocity and magnetic field changes. Generally, f_M has maxima at positive velocity maxima and seems more sensitive to the velocity than to the magnetic field. Agreement of these results for f_M with Balmain's theory may be verified.

Figure 5 shows the minimum-impedance frequency f_m. The f_m maxima are correlated principally with maxima in the tangential velocity. This agrees with the infinite-antenna vacuum-sheath theory, which shows that f_m increases with increasing f_p. Further, the insen-

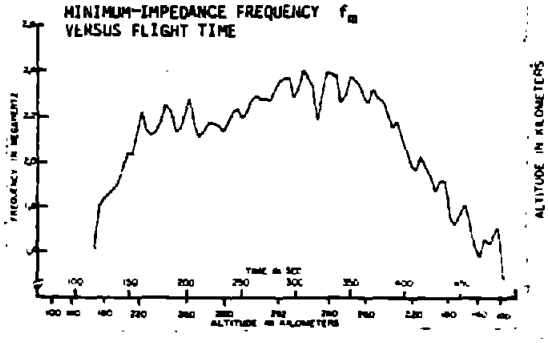

FIGURE 5

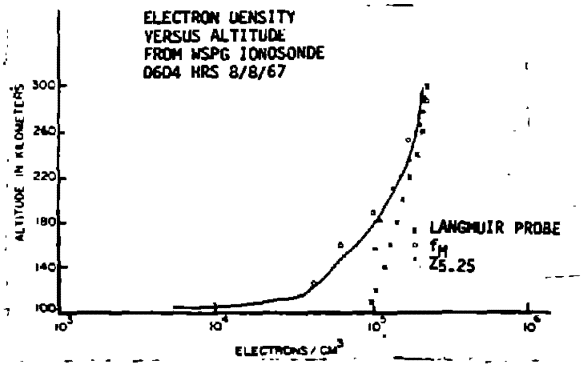

FIGURE 6

sitivity of f_m to the tangential magnetic field agrees with Balmain's theory for the sheathless case.

The experimental magnetic field and wake orientation dependence of the antenna impedance and the infinite antenna-quasistatic finite antenna predictions also agree for several other distinctive impedance features. Among these are the impedance values associated with f_M and f_m, and the impedance discontinuity associated with f_p. However, the impedance oscillation between f_M and f_m on Figure 2 is not predicted by the present theory. This particular impedance characteristic, which consistently occurred at about $2f_h$ during the flight, may be due to plasma compressibility effects (Johnston, 1968).

In Figure 6, we show the electron density-height profile as obtained from the impedance data compared with Langmuir probe and ground-based ionosonde results. The electron density results using the impedance data are obtained from the f_M values and the impedance value at 5.25 MHz ($Z_{5.25}$). There is good agreement between these independent methods for obtaining the electron density. The comparison reveals the usefulness of the swept frequency impedance probe to obtain ionospheric electron density and further shows the general validity of Balmain's theory which has been used to translate the impedance data to electron density values.

REFERENCES

Balmain (1964), IEEE Trans. Ant. Prop. AP-12, p. 605.

Balmain, Oksiutik and Feyer (1967), Spring URSE Meeting, Ottawa, Ontario, Canada.

Johnston (1968), private communication.

Miller (1967), Can. J. Phys. 45, p. 4019; (1968) Can. J. Phys. 46, p. 1109; (1968) IEEE Trans. Ant. Prop. AP-16, p. 111.

ACKNOWLEDGMENT

Research supported by NASA under Headquarters Contract NASr-r-54(05).

ON THE TRANSIENT RESPONSE OF AN ANTENNA AND THE TIME DECREASE OF ALOUETTE SPIKES

Philippe Graff
C. N. E. T. - R. S. R.
92 - Issy-les-Moulineaux, France

Abstract

After a justification of the necessity of introducing collisions, it is shown how this introduction modifies the calculation of the time decrease of Alouette spikes and that the result obtained though deeply modified, still disagrees with experience.

1. INTRODUCTION

Spikes appear on the top-side ionograms when the transient response of the antenna has a long duration. This occurs when it emits a pulse whose frequency spectrum contains one of the ω_k solution of

$$D(\vec{k}, \omega) = 0 \; ; \quad \vec{V}_g(\vec{k}, \omega) = \vec{0}$$

which express the group velocity of the characteristic waves to be zero and that the antenna impedance has a branch point singularity. The envelope of this transient decreases in time; its asymptotic form, evaluated among others by Deering and Fejer (1965), Nuttall (1965), Watson (1968), is found proportional to $(t - t_o)^{-\alpha}$ (t_o, time of end of emission; $1/2 \leq \alpha \leq 7/2$ according to the ω_k under consideration).

Petit (1968) showed the incompatibility of such a time dependence with the satellite data. Moreover this time dependance is based on Vlasov equation; it has been pointed out (Graff, 1968) that this equation is invalid to describe a perturbation during an interval of time Δt not such that $\Delta t \ll \tau$ where

$$\tau = n L_D^3 \omega_p^{-1} = 5810\, n^{-1} T^{3/2}$$

(n, L_D, ω_p, T are the standard electron density, Debye length, plasma frequency, temperature in MKSA units). Figure 1 shows that over a few milliseconds (typical spike duration), the preceding inequality does not hold. Therefore, the introduction of collisions is both an experimental and a theoretical necessity.

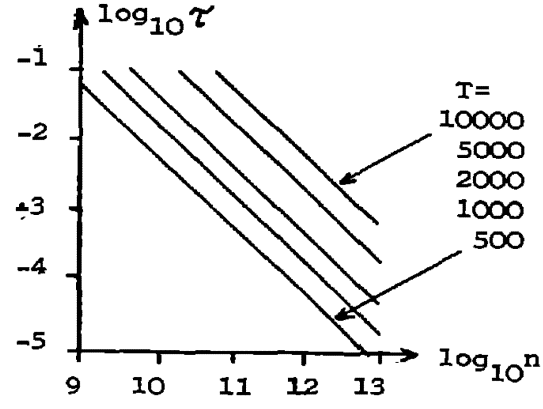

FIGURE 1

2. TRANSIENT RESPONSE OF AN ANTENNA IN A COLLISIONAL ISOTROPIC PLASMA

An antenna of current distribution $\vec{J}(\vec{r}, t)$ emits an electric field of Fourier-Laplace transform

$$\vec{E}(\vec{k}, \omega) = \vec{\vec{G}}(\vec{k}, \omega) \cdot \vec{J}(\vec{k}, \omega) \qquad (1)$$

where the components of the Green's tensor $\vec{\vec{G}}$ are

$$G_{\lambda\mu} = i\omega\mu_o \frac{(\omega/c)^2 \varepsilon_{\parallel} \delta_{ij} - k_i k_j [1 + (\omega/kc)^2 (\varepsilon_{\parallel} - \varepsilon_{\perp})]}{(\omega/c)^2 \varepsilon_{\parallel} [k^2 - (\omega/c)^2 \varepsilon_{\perp}]}$$

The transient response is concerned with frequencies close to $\pm \omega_p$, therefore,

$$\varepsilon_{\perp} = 1 - \omega_p^2/(\omega - i\nu)^2 \; ; \; \varepsilon_{\parallel} = 1 - \omega_p^2/(\omega - i\nu)^2 - (k V_T/\omega)^2 - i\lambda \qquad (2)$$

($V_T = \sqrt{3KT/m}$ = Boltzmann's K, m : electron mass). Replacing the collision frequency ν and the Landau damping term λ by their limits as $\omega \to \omega_p$, $\nu(\omega_p) = \nu_o$ and $\lambda(\omega_p) = 0$, it is possible to evaluate the transient response of the antenna by inverting (1). One thus obtains the voltage at the terminals of a dipole of length 2L fed by a current $I(t) = \delta(t)$

$$V(t) = \frac{(2)^{\frac{1}{2}}}{12} \frac{L^2}{\varepsilon_o \pi^{3/2}} \frac{\omega_p^{3/2}}{V_T^3} \frac{\sin(\omega_p t - \pi/4)}{t^{3/\omega}} e^{-\nu_o t} \qquad (3)$$

Let us now justify the expressions (2) by deducing ν from the kinetic equation of the plasma.

3. PLASMA DESCRIBED BY THE FOKKER-PLANCK EQUATION

Solving the Fokker-Planck equation shows that the collisions to take account of in Alouette conditions are between electrons and ions. Shkarofsky, et al. (1966), define a sequence of approximations which allows to establish (2) with $\nu_1 = <\nu_{ei}> = (2/\pi)^{\frac{1}{2}} L_n \Lambda/\Lambda$ where $\Lambda = 12\pi n L_D^3 = 1.24 \times 10^7 T^{3/2} N^{-\frac{1}{2}}$. A basic assumption of the Fokker-Planck equation is that during a collision the distribution function of the electrons does not vary, that is $L_o/V_T \ll 1/\omega$ or $\omega \ll \omega_p$. At $\omega = \omega_p$ or greater, this assumption does not hold.

4. PLASMA DESCRIBED BY THE BBGKY HIERARCHY

By expanding the hierarchy at the first order in powers of the small parameter $\delta = 1/n L_D^3$, one obtains a kinetic equation which correctly describes the collective effects occurring when $\omega \ll \omega_p$ is false. Thus, Oberman, et al. (1962) have calculated the plasma conductivity and one is led to (2) with

$$\nu = \frac{2\omega_p}{\pi^{\frac{1}{2}} \Lambda} [Ln \Lambda + Q(\omega/\omega_p)] \quad .$$

The function Q(u) varies according to Figure 2.

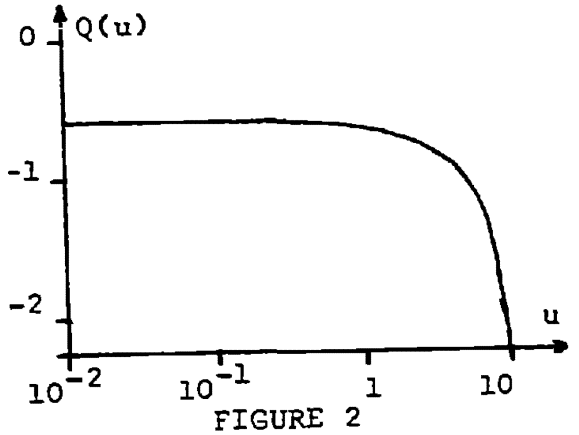

FIGURE 2

Figure 3 shows the improvement due to the introduction of collisions. A gap remains between experience and theory and, surely, other effects like inhomogeneity or non-linearity should be taken into account to provide an actually satisfactory result.

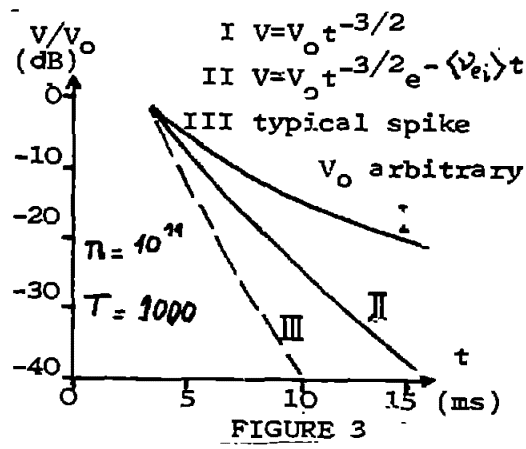

FIGURE 3

5. CONCLUSION

It is at the present time unrealistic to compare the theoretical predictions with the absolute value of the experimental data. Yet we tried a comparison between the shape of the experimental and the theoretical decrease laws.

6. REFERENCES

Deering, W.D., and J.A. Fejer (Nov. 1965), Phys. Fluids 8, No. 11, 2066-2079.

Graff, P. (Apr. 1968), Communication at the NATO Advanced Study Institute on plasma waves in space and in the laboratory (Røros, Norway).

Nuttall, J. (Feb. 1965), Phys. Fluids 8, No. 2, 286-296.

Oberman, C., A. Ron and J. Dawson (Dec. 1962), Phys. Fluids 5, No. 12, 1514-1522.

Petit, M. (Apr. 1968), Communication at the NATO Advanced Study Institute on plasma waves in space and in the laboratory (Røros, Norway).

Shkarofsky, I.P., T.W. Johnson, and M.P. Bachynski (1966). The Particle Kinetics of Plasmas (Addison-Wesley Publishing Co., Reading, Mass.).

Watson, S.R. (1968), J. Plasma Physics 2, No. 3, 437-438.

and the dipoles are oriented along the static magnetic field, $\bar{B}_o$, to preserve θ symmetry. The coupled wave equation is written as:

$$\left[\nabla_T^2 + \bar{\bar{S}}(k_z,\omega)\right] \bar{F}(r,k_z,\omega) = \bar{J}_{ez}(r,k_z,\omega) \text{ or } \bar{J}_{mz}(r,k_z,\omega) \qquad (1)$$

where ∇_T^2 is the transverse Laplacian operator, $\bar{\bar{S}}(k_z,\omega)$ is a 3 x 3 matrix propagation constant, and $\bar{J}_{ez}$ and $\bar{J}_{mz}$ are source vectors for electric and magnetic dipoles, respectively. $\bar{F}$ is a vector of the primary field quantities:

$$\bar{F}'(r,k_z,\omega) = \left[E_z(r,k_z,\omega),\ H_z(r,k_z,\omega),\ P_e(r,k_z,\omega)\right] \qquad (2)$$

where E_z and H_z are electromagnetic field components and P_e is perturbation electron pressure. Equation (1) is solved with a Hankel transform of order zero, mapping the Laplacian into $-\lambda^2$, where λ is the Hankel transform variable. The result is the algebraic relationship:

$$\bar{\bar{C}}(\lambda,k_z,\omega)\cdot\bar{F}(\lambda,k_z,\omega) = \bar{J}_{ez}(\lambda,k_z,\omega) \text{ or } \bar{J}_{mz}(\lambda,k_z,\omega) \qquad (3)$$

where the matrix $\bar{\bar{C}}$ is constructed by adding $-\lambda^2$ along the diagonal elements of $\bar{\bar{S}}$. For regions away from the source, Eq. (3) is homogeneous, and a nontrivial solution is possible if and only if:

$$\left|\bar{\bar{C}}(\lambda,k_z,\omega)\right| = 0 \ . \qquad (4)$$

Since λ and k_z are wave numbers in the radial and z directions, respectively, Eq. (4) is recognized as a dispersion relationship. By the usual relationships between wave number and frequency, and velocity and direction-cosine, Eq. (4) may be rearranged to give a cubic polynomial in velocity squared. The roots of this polynomial correspond to the modified ordinary mode (MO), the modified extraordinary mode (MEX), and the modified plasma mode (MP) discussed by Seshadri (1964) for plane wave propagation in a compressible, anisotropic plasma.

Equation (3) is solved by inverting $\bar{\bar{C}}$ and the solution is brought into λ, z, ω space by a contour integration in the complex k_z plane. The contour is closed in the upper half-plane and the pole locations enclosed are given by the solutions to Eq. (4), since the determinant appears in the denominator of the inverse. Since Eq. (4) is also the dispersion relationship, application of Cauchy's theorem tells us that the field quantities are linear combinations of classical plane wave modes in a plasma. That is, the vector of Eq. (2) in λ, z, ω space may be written as a transformation matrix, $\bar{\bar{T}}$, operating on a vector of plane wave modal

DIPOLE RADIATION IN THE LUNAR ENVIRONMENT*

R. J. Phillips

Jet Propulsion Laboratory
California Institute of Technology
Pasadena, California 91103

Abstract. To assess the effect of the solar wind on electromagnetic sounding of the lunar subsurface, the problem of electric and magnetic dipole sources in a compressible, anisotropic plasma overlying a lossy dielectric half-space is solved. Final integrals are solved by saddle point integration involving numerical search algorithms on dispersion surfaces.

The results of recent work by Ward et al. (1968) indicate the possibility of definitive electromagnetic sounding experiments of the lunar subsurface from orbiting satellite. The present study reassesses the problem by considering the effect of finite electromagnetic sources in the solar wind plasma. That is, the lunar environment is modeled by infinitesimal electric and magnetic dipole sources embedded in a compressible anisotropic plasma overlying a lossy dielectric half-space.

Basically the task is to solve, subject to the constraints of the lunar boundary conditions, the four differential equations: 1) Faraday's law with a magnetic source term, 2) Ampere's law with an electric source term, 3) the linearized second moment of the Boltzmann-Vlasov Equation and 4) the linearized first moment combined with an adiabatic equation of state. The lower bound for efficient antenna operation is perhaps 10 kHz, and it is assumed that ion wave motion is damped out above this frequency. Therefore only electron motion is considered. The solar wind electron plasma frequency is 28.4 kHz (10/cc) and the electron plasma wave will be damped out above approximately 100 kHz and the continuum theory used here cannot account for this (Landau) damping mechanism.

The four equations may be combined into a coupled wave equation in r, k_z, ω space, modified after a procedure outlined by Chen and Cheng (1966). Here r is the radial coordinate in a cylindrical coordinate system, k_z is the Fourier transform variable from z space,

*This research was funded by NASA under Contract No. NAS 489580-26337 at the University of California, Berkeley, and under Contract No. NAS 7-100 at the Jet Propulsion Laboratory, Pasadena, California.

the normals to the dispersion surfaces are defined by the gradient of the locus of points satisfying Eq. (4). That is, for any particular mode, the dispersion surface gives the wave number $K(\lambda,k_z)$, and if ϕ is the angle, defined from the k_z axis, of a radius line to any point on the surface, then:

$$\lambda = K(\lambda,k_z)\sin\phi \ . \qquad (6)$$

Then if ψ is the normal at any point on a surface, then the gradient operation yields a relationship of the type $\psi = f(\phi)$. For the primary field, we seek a ψ that gives a straight line path from source to observer, and for the secondary field we seek a ψ for the incident mode that carries a ray to the surface, then from the surface to the point of observation. The normal on the reflected mode arises from that point(s) on the reflected mode dispersion surface with the same horizontal (λ) projection as the point on the incident surface from which ψ arises, thus satisfying Snell's law. If we could find the proper ψ for a particular problem, we would use the inverse relationship, $\phi = f^{-1}(\psi)$, and use Eq. (6) to find the saddle point(s). In practice f^{-1} is a very high order polynomial and we find the procedure difficult. Instead the forward procedure, $\psi = f(\phi)$, is used in bracketing-type search algorithms on the dispersion surfaces. For the primary field, we search for a ϕ such that the corresponding ψ is the angle between source and observer. For the half-space problem, let h be the vertical distance of the source above the ground, and r the distance of horizontal separation. Then for mode j — mode j reflection, we search for a ϕ such that $\psi = \tan^{-1}(r/2h - z)$, where z is the vertical coordinate of the point of observation. If r_1 is the horizontal distance between source and point of reflection and r_2 is the horizontal distance between point of reflection and observer, then for mode j — mode k reflection, we search for those points on the dispersion surface where $r_1 + r_2 = r$ subject to the constraint of Snell's law. This search procedure was found to be very efficient; typical computer time for the twelve saddle points for a given frequency is 2-3 seconds on a CDC 6400 computer.

By placing the source and observer well off of the interface, pole contributions may be neglected. However, the steepest descent path must be indented around branch cuts to preserve single-valuedness in the integrand, and the contribution of a branch cut is a diffracted wave traveling laterally along the lunar boundary. Using an asymptotic expansion around the branch points, similar to that given by Felsen and Rosenbaum (1967), the branch cut integrals may be evaluated to give the diffracted wave contribution. Considering only the isotropic electromagnetic field quantities, the dominant lateral wave contribution is to E_z (electric dipole source) arising in the MEX mode launched by an MP → MP reflection, the contribution being as high as 10% of the secondary field for r = 50 km. Also contributing,

solutions, and the solution in r, z, ω space is given by:

$$\left[E_z, H_z, P_e\right]' = \int_0^\infty \overline{\overline{T}}(\lambda,\omega) \cdot \left[e^{iMO_{Uz}},\ e^{iMEX_{Uz}},\ e^{iMP_{Uz}}\right]' J_o(\lambda r)\lambda d\lambda . \tag{5}$$

The reflected waves in the plasma satisfy the homogeneous form of Eq. (3) and solutions exist only for the condition in Eq. (4). This again leads to MO, MEX, and MP modal solutions. There are nine homogeneous solutions, but only three are independent. The interdependence of the solutions leads to a vector of reflected field quantities that are a matrix operation, $\overline{\overline{R}}$, on the vector of reflected modal solutions; the solution in r, z, ω space is similar to Eq. (5).

Two uncoupled, isotropic modes are transmitted into the lunar rock. For a particular source type, one mode is always associated with the isotropic field components of the source, and the other mode with the Hall components of the source. The five boundary constants are found by equating tangential $\overline{E}$ and $\overline{H}$ across the boundary of a lunar half-space, and by setting the normal component of particle velocity to zero at this boundary. The last condition follows from a postulated proton-rich sheath region at the lunar surface.

The integrals of the type in Eq. (5) are extended to $-\infty$ on the λ axis by the usual procedure, and theasymptotic form of the Hankel function is used. These integrals are then evaluated by the saddle point method. From Eq. (5) it is clear that there are three saddle point integrations for any primary field quantity, representing the three plasma modes. For the reflected field quantities, however, there are nine combinations of incident and reflected MO, MEX, and MP modes giving rise to any field quantity, representing nine saddle point integrations. These nine reflections may be easily expressed in an amplitude matrix, $\overline{\overline{A}}$, for the saddle point integrations, with an element a_{ij} representing the amplitude function for the integral representing incident mode j - reflected mode i.

Physically, the saddle point represents a wave carrying energy from the source to the observer for the primary field. For the secondary field, the saddle point represents a wave carrying energy from the source to the observer, but reflecting from, and satisfying Snell's law at the lunar surface. Mathematically, the saddle points are found by differentiating and setting to zero the argument of the exponential function in the integrand. In the present problem this can lead to polynomials in λ of at least twelfth order. We can appeal to the physical argument, taking advantage of the fact that

but insignificantly, are MEX refractions from MP-MO and MO-MP reflections. For certain points of observation, the observer passes from the propagation zone to the shadow zone as the frequency increases upward from the plasma frequency. However, the frequency band in which the observer is in the transition region; i.e., both the branch point and the saddle point expansions fail, is apparently quite narrow. From the MEX cutoff frequency (28,532 Hz) to 28,600 Hz there is an important MEX lateral contribution due to an MO-MO reflection, for r = 200 km. This is the only type of refracted wave with an important contribution to H_z, magnetic dipole source, and the band of frequencies in the transition region is reasonably wider than that of the refractions mentioned above.

The conclusions reached in this study, with regard to a remote mapping of the parameters of the lunar half-space are: 1) For approximately 1 kHz above the plasma frequency, anisotropic effects in the plasma mask the lunar subsurface parameters. These effects are mainly rapid changes in ray convergence with frequency and oscillatory effects due to constructive-destructive interference of reflected modes. 2) Above 30 kHz, H_z from the magnetic dipole source is sensitive to the electrical properties of the lunar half space. 3) Above 30 kHz, E_z is insensitive to lunar properties. This follows from the boundary condition $V_z = 0$, which essentially causes all acoustic energy to be perfectly reflected, independent of the half-space parameters. It may be shown that below 100 kHz, acoustic energy is the dominant contributor to E_z.

References

Chen, H. H. C., and D. K. Cheng (1966), Concerning lossy, compressible, magneto-ionic media — general formulation and equation decoupling, IEEE Trans. Ant. Prop. AP-14, No. 4, 497-501.

Felsen, L. B., and S. Rosenbaum (1967), Ray optics for radiation problems in anisotropic regions with boundaries. 1. Line-source excitation, Radio Sci. 2 (New Series), No. 8, 769-791.

Seshadri, S. R. (1964), Wave propagation in a compressible ionosphere, Part I, Radio Sci. J. Res. NBS 68D, No. 12, 1285-1295.

Ward, S. H., G. R. Jiracek, and W. I. Linlor (1968), Electromagnetic reflection from a plane-layered lunar model, J. Geophys. Res. 73, No. 4, 1355-1372.

VLF TRANSMITTING ANTENNAS USING FAST WAVE DIPOLES

Elwin W. Seeley

Naval Weapons Center Corona Laboratories
Corona, California

The problem of radiating high power efficiently at very low frequencies can be solved by the use of large arrays of closely spaced horizontal fast wave dipoles. The optimum antenna wave velocity is 1.1 time of that of free space. The theoretical efficiency increase of "N" dipoles over one is confirmed by measurements on a 5-dipole array constructed on Hawaiian lava. Design of a large efficient array is discussed. For ominidirectional coverage, antenna radiation directivity is required due to non-reciprocal East-West propagation attenuation.

1. ELEVATION AND AZIMUTHAL RADIATION PATTERNS

Radiation patterns are derived by summing up the current on differential lengths by integrating over the current distribution of the dipole. The resulting current moment is then used with equations for the fields radiated from a uniform current on an incremental length horizontal conductor, derived by Wait (1961), to obtain the radiated fields of the dipole. Radiation efficiency is then found by comparing these radiated fields with the field radiated in the horizontal plane by a lossless vertical monopole. The radiation efficiency of a dipole in the horizontal plane, for any resonant length, fed at a current maximum is

$$\eta = \frac{\frac{8}{3}\pi^2 f \epsilon_p \cos^2\phi}{\alpha\frac{c}{v}(\tanh\alpha\lambda\ell_{1\lambda}+\tanh\alpha\lambda\ell_{2\lambda})}\left\{\frac{\sinh\alpha\lambda\ell_{1\lambda}+j^n\cos(2\pi\ell_{1\lambda}\cos\phi)}{[\alpha\lambda+2\pi(\frac{c}{v}-\cos\phi)]\cosh\alpha\lambda\ell_{1\lambda}}+\right.$$

$$\left.\frac{\sinh\alpha\lambda\ell_{2\lambda}+j^n\cos(2\pi\ell_{2\lambda}\cos\phi)}{[\alpha\lambda+j2\pi(\frac{c}{v}+\cos\phi)]\cosh\alpha\lambda\ell_{2\lambda}}\right\}^2 \qquad (1)$$

Where Cp is antenna capacitance to ground.
ϕ is azimuthal angle from axis of long part of dipole.
θ is elevation angle from axis of long part of dipole.
σ is earth conductivity.
c/ν is ratio of free space wave velocity to that on the antenna.
$\alpha\lambda$ is attenuation constant along antenna.
λ is free space wavelength.
ℓ_1 is length of long part of dipole measured from feed.
ℓ_2 is length of short part of dipole measured from feed.
n is number of quarter wavelengths.

$$U = \sqrt{\frac{fx10^{-9}}{j18\sigma}}$$

The efficiency in the elevation plane is derived from Eq. 1, by replacing $\cos\phi$ outside the brackets with $\frac{\sin\theta}{U+\sin\theta}$ and inside the brackets ϕ is replaced by θ.

2. EFFECT OF FAST WAVE VELOCITY ON DIPOLE EFFICIENCY

The wave velocity along a conductor near the earth is usually much less than free space, c/ν is typically 1.4 for a conductor one meter above the earth. The radiation efficiency is low at this slow wave velocity (see Fig. 1). The wave velocity can be increased by inserting series capacitors into the antenna which improves the efficiency in both the horizontal and elevation planes. The optimum wave velocity for efficiency occurs when $c/\nu = 0.9$ for sky wave radiation and about $c/\nu = 1.05$ for ground wave radiation (see Fig. 1).

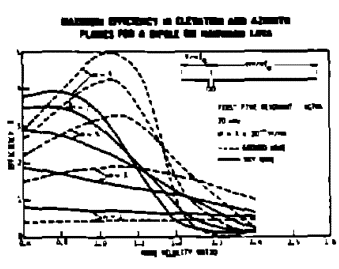

Fig. 1. Resonant Dipole Efficiency

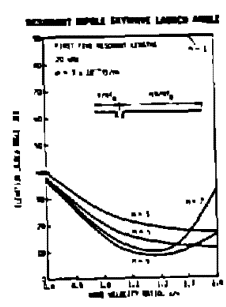

Fig. 2. Skywave Launch Angle

The sky wave launch angle can be varied over a considerable range of angles (see Fig. 2). This is important for selecting the best VLF propagation mode.

3. EFFECT OF PARALLELING DIPOLES ON THE ARRAY EFFICIENCY

A single dipole is only a few percent efficient but when "N" closely spaced parallel dipoles are connected in parallel the radiation efficiency is increased "N" folds reduced by a deteriorating factor caused by mutual resistance induced in each dipole by all the other dipoles in the array. The efficiency gain of an array of dipoles over one dipole can be calculated by summing up the inverse of the ratios of the total resistance per unit length to the self resistance per unit length of each dipole. Antenna losses have the greatest effect on efficiency when $c/\nu = 1.0$.

The ratio of mutual to self resistance is directly related to the dipole separation in skin depths. It appears that not much is gained by separating the dipoles greater than 4 skin depths. (see Fig. 3).

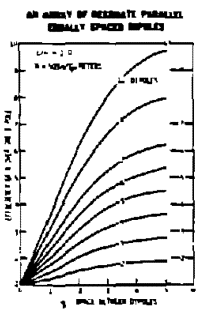

Fig. 3. Efficiency Gain

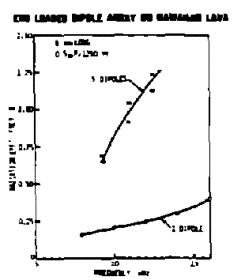

Fig. 4. Experimental Dipoles

Radiation efficiency measurements made on a five-dipole array constructed on the lava beds of Hawaii confirm the theoretical increase in efficiency (see Fig. 4). The dipoles were resonant at 11 KHz where the spacing between dipoles was 3.6 skin depths. This would indicate a theoretical increase in efficiency of 4.2 for the array over one dipole. This was approximately the measured gain.

In general the azimuth beamwidth of the array will be narrowed over that of a single dipole by the array factor. For large arrays of many dipoles the azimuth pattern is obtained by multiplying the power pattern of a single dipole (Eq. 1) by the array factor of an array of isotropic radiators.

4. LARGE EFFICIENT THEORETICAL DIPOLE ARRAY

An antenna has been designed to transmit from the lava beds of Hawaii to illustrate the radiation efficiency, power radiating capability and broad bandwidth than can be achieved with resonant fast wave dipoles. The electrical parameters needed to compute the radiation pattern (see Eq. 1) have been measured on smaller horizontal antennas above these lava beds. An array of 18 dipoles one and a half resonant, fed quarter wave from one end, are 40% efficient (-4 db) compared to a perfect vertical monopole. The mutual resistance between dipoles and the array factor have been taken into consideration in computing the radiation pattern (Figs. 5 & 6).

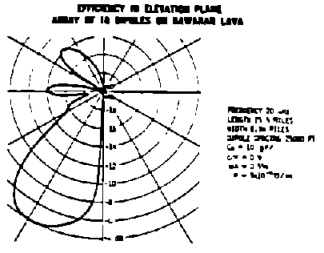

Fig. 5. Array Elevation Pattern

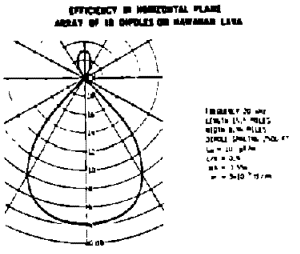

Fig. 6. Array Azimuth Pattern

The power radiating capability of this antenna greatly exceeds that of any existing transmitter. The limiting parameter is the maximum antenna voltage before onset of the corona which is 35 KV for #6 wire 20 feet above the ground. The 18 dipole array would radiate 22 megawatts. This is 14 folds greater than the most powerful VLF vertical antenna. The half power bandwidth is greater than 50%. The efficiency of this array could be increased linearly with more dipoles and approximately proportional to length. A decrease in beamwidths would result, which is desirable in the elevation plane but not the azimuth plane.

5. EFFECTS OF NON-RECIPROCAL VLF PROPAGATION

VLF propagates around the earth with less attenuation in a easterly direction than in a westerly direction. Therefore to obtain omnidirectional coverage on the earth the transmitting antenna must beam the VLF in a westerly direction.

The horizontal dipole has this shape of radiation pattern while the vertical monopole radiated equally in all directions. Also the propagation attenuation is greater over land than sea water. In addition the noise levels in some regions of the earth are much greater than others. So in order to obtain equal signal-to-noise ratios over a large area of the earth directive transmitting antennas are needed.

East-west non-reciprocal propagation has been shown theoretically to be proportional to the component of the earth's magnetic field that is horizontal and transverse to the direction of propagation. Experimental evidence (Watt & Croghan 1964) show the increase in attenuation rate of a westerly sea water path over an easterly sea water path varies from 0.5 db/mega-meter at 25KHz to 2.3 db/mega-meter at 10 KHz, at the magnetic equator. The ratio of attenuation rate off the northerly magnetic path to the rate on the north-south path varies as the sine of the azimuth angle off the northerly path. Using this evidence the required antenna radiation pattern for omnidirectional coverage at a range of 10 megameters from the transmitter over a sea water path has considerable directivity. The greatest directivity is required at the lowest frequency 10 KHz where the required half power beamwidth is 70° and the front-to-back ratio is 23 db.

6. REFERENCES

J.R. Wait, (1961). "The Electromagnetic Fields of a Horizontal Dipole in the Presence of a Conducting Half-Space." Canadian Journal of Physics, Vol. 39, pp.1017-1028 July 1961.

A.D. Watt & R.D. Croghan, (1964). "Comparison of Observed VLF Attenuation Rates and Excitation Factors with Theory." Radio Science Journal of Res.NBS, Vol. 68D, #1, pp. 1-10, January 1964.

GROUND-WAVE PROPAGATION ACROSS STRIPS AND ISLANDS ON A FLAT EARTH

R.J. King, Univ. of Wisconsin, Madison 53706
W.I. Tsukamoto, Univ. of Colorado, Boulder 80302

Abstract: Mixed path groundwave propagation over a flat earth was generalized to include the effect of arbitrary nonhomogeneous regions such as islands and peninsulas. The theory was experimentally verified to a good order of accuracy using models and microwave frequencies ($\lambda_o \simeq 7$ cm.).

The Electromagnetic Compensation theorem has been extensively applied to numerous mixed path ground-wave propagation problems by Wait and others. Following some of the earlier concepts and techniques, the formulation has been generalized to arbitrary nonhomogeneous flat surfaces [King, 1965; King and Tsukamoto, 1966].

The basic working formula for the groundwave attenuation function when both the transmitter (A) and receiver (B) are on the surface is given by

$$F'(d,Z,Z') = F(d,Z) - i\frac{d}{\lambda_o} e^{ikd} \int_S \left(\frac{Z-Z'}{\eta_o}\right) \frac{e^{-ik(R+r)}}{rR} \cdot F'(r,Z,Z')\, F(R,Z)\, \cos\delta\, dS, \qquad (1)$$

where F(d,Z) is the well-known Norton attenuation function [King, 1969a] corresponding to a homogeneous surface, $k = 2\pi/\lambda_o$ and λ_o is the free space wavelength, and $\eta_o \simeq 120\pi$. Primed quantities denote the presence of a perturbation within area S (see Fig. 1). Terms which decrease faster than r^{-1}, d^{-1}, etc., have been dropped, implying that $d \gg \lambda_o$, and that either A or B must be more than $\lambda_o/2$ away from any boundary enclosing S. The use of the surface impedance is valid if the dimensions of S are much greater than the wavelength of the medium inside S [King, 1969b].

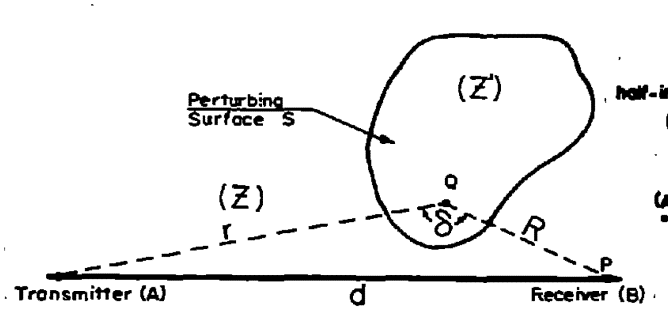

FIGURE 1. *Top view of antenna locations for propagation over a plane inhomogeneous surface.*

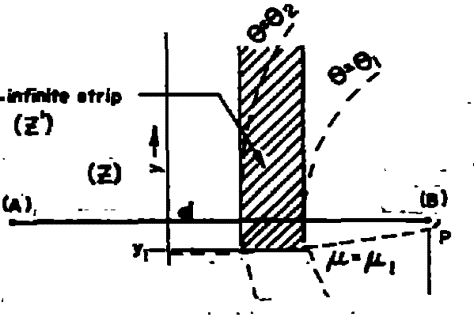

FIGURE 2. *Perpendicular propagation near a half-infinite strip*

For TE waves, one can write the dual of (1) simply by replacing impedances by admittances. In view of the results obtained earlier for a completely homogeneous surface [King, 1969a, 1969c] it is likely that (1) can also be applied to situations where the lower media can have indices of refraction referred to air which are approximately unity, provided that $|Z|^2$ and/or $|Z'|^2$ are much less than η_o^2. Problems having surface impedances which are variable with position have received little attention. These are unexplored areas which are open to further study.

In principle, (1) can be solved for very general mixed path problems, even though it may be necessary to resort to numerical methods [Christiansen and Larsen, 1967]. There is, however, an abundance of cases where (1) can be solved analytically, depending upon the geometry of S. In particular, analytic solution is possible for surface segments which coincide with elliptic-cylindrical orthogonal coordinates μ and θ as shown in Fig. 2. [King and Tsukamoto, 1966]. These results can also be approximately applied to surface segments which coincide with xyz coordinates, such as rectangular islands, peninsulas (see Fig. 2), or any straight boundary which is perpendicular to the direction of propagation. In all cases considered, the results were identical to those obtained by Wait. Calculations were made for islands and peninsulas, and compared with experimental data obtained using microwave frequency models ($\lambda_c \simeq 7$ cm.). The results were good confirming the theory and restrictions resulting from the approximations made. In the regions where the approximations were valid, the experimental and theoretical data agreed within 2-3 percent in magnitude and 1° in phase. The results clearly showed the effect of the perturbing surface S. The familiar "recovery effect" was observed when B moved across a highly conducting surface. When the perturbing surface was to the side of the direct path, reflections from S were observed, and the phase of the observed signal was quite noticeably effected.

King, R.J., (1965), Analytical and Experimental Studies of Propagation of Electromagnetic Surface Waves Across Mixed Paths, Ph.D. Thesis, University of Colorado.

King, R.J., and W.I. Tsukamoto, (1966), Groundwave Propagation Across Semi-Infinite Strips and Islands on a Flat Earth, Radio Science, 1(7), 775-787.

Christiansen, S., and T. Larsen, (1967), Numerical Application of the Compensation Theorem to Mixed-Path Propagation Problems, Radio Science, 2(12), 1471-1480.

King, R.J., (1969a), Electromagnetic Wave Propagation Over a Constant Impedance Plane, Radio Science, 4(3), 255-268.

King, R.J., (1969b), On the Surface Impedance Concept, (elsewhere in these EEAP Proceedings).

King, R.J., (1969c), EM Propagation Over a Constant Impedance Plane, (elsewhere in these EEAP Proceedings).

Wait, J. R. (1956), Mixed Path Ground Wave Propagation: 1. Short Distances, J. Res. NBS 67 (1), 1-15.

Wait, J. R. (1964), Electromagnetic Surface Waves, in Advances in Radio Research (ed. J. A. Saxton), vol. 1, 157-217 (Academic Press, London).

SOME CONSIDERATIONS ON GROUND-WAVE PROPAGATION ACROSS COASTLINES AND ISLANDS

Rayner K. Rosich

Institute for Telecommunication Sciences
Environmental Science Services Administration
Boulder, Colorado 80302

Abstract

The effect of inhomogeneities on ground-wave propagation is calculated theoretically. Sharp phase and amplitude changes occur near the boundaries between media.

1. Introduction

We shall describe the results of a study (Rosich, 1968) of the effect that inhomogeneities in the earth's surface have upon the attenuation of the surface-wave component of the ground-wave electric field at high frequencies. We shall also present some results from a recent study of the effect on the attenuation of the placement of antennas near a coastline. These results were obtained from a model (Hufford, 1952; Wait, 1956; King, 1965) where the attenuation function is given by an integral equation that is solved numerically. Computations were made for particular land-sea paths (see figure 1) to aid in the design and evaluation of the high-frequency ground-wave radar at the Naval Research Laboratory's Chesapeake Bay installation.

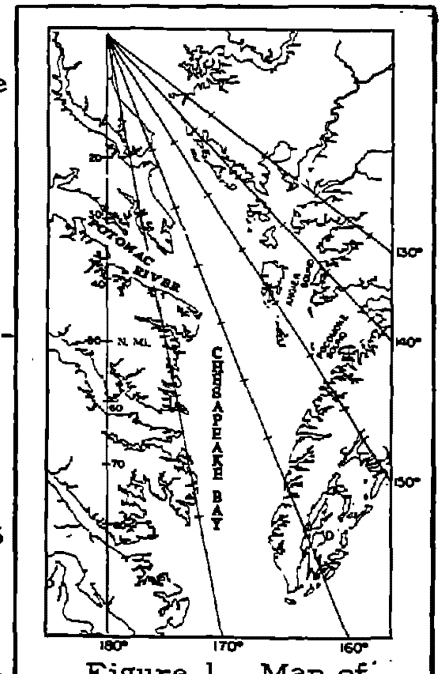

Figure 1. Map of the propagation paths.

2. Propagation Across an Island

Figures 2 (for $\Delta = 0$m) and 3 show the amplitude and phase of the attenuation function versus the distance from the transmitting antenna. The four graphs in figure 2 illustrate the frequency dependence of the attenuation in the homogeneous (all sea) and inhomogeneous cases. The inhomogeneity is a peninsula 6.85 km long (0.5 km wide) between 28.30 km and 35.15 km from the transmitter on a bearing 160° E of N (see figure 1). The dependence upon the electrical parameters of the inhomogeneity (relative to the rest of the path) is illustrated by the four graphs in figure 3. The inhomogeneity here is an island 4.32 km long (3.54 km wide) between 84.18 km and 88.50 km from the transmitter on a bearing 150° E of N (see figure 1). The values of the electrical parameters are given on each graph along with the frequency and bearing. Note that the changes in phase and amplitude are greater, the greater the difference in electrical parameters between the inhomogeneity and the rest of the path, as might be expected. Also note the

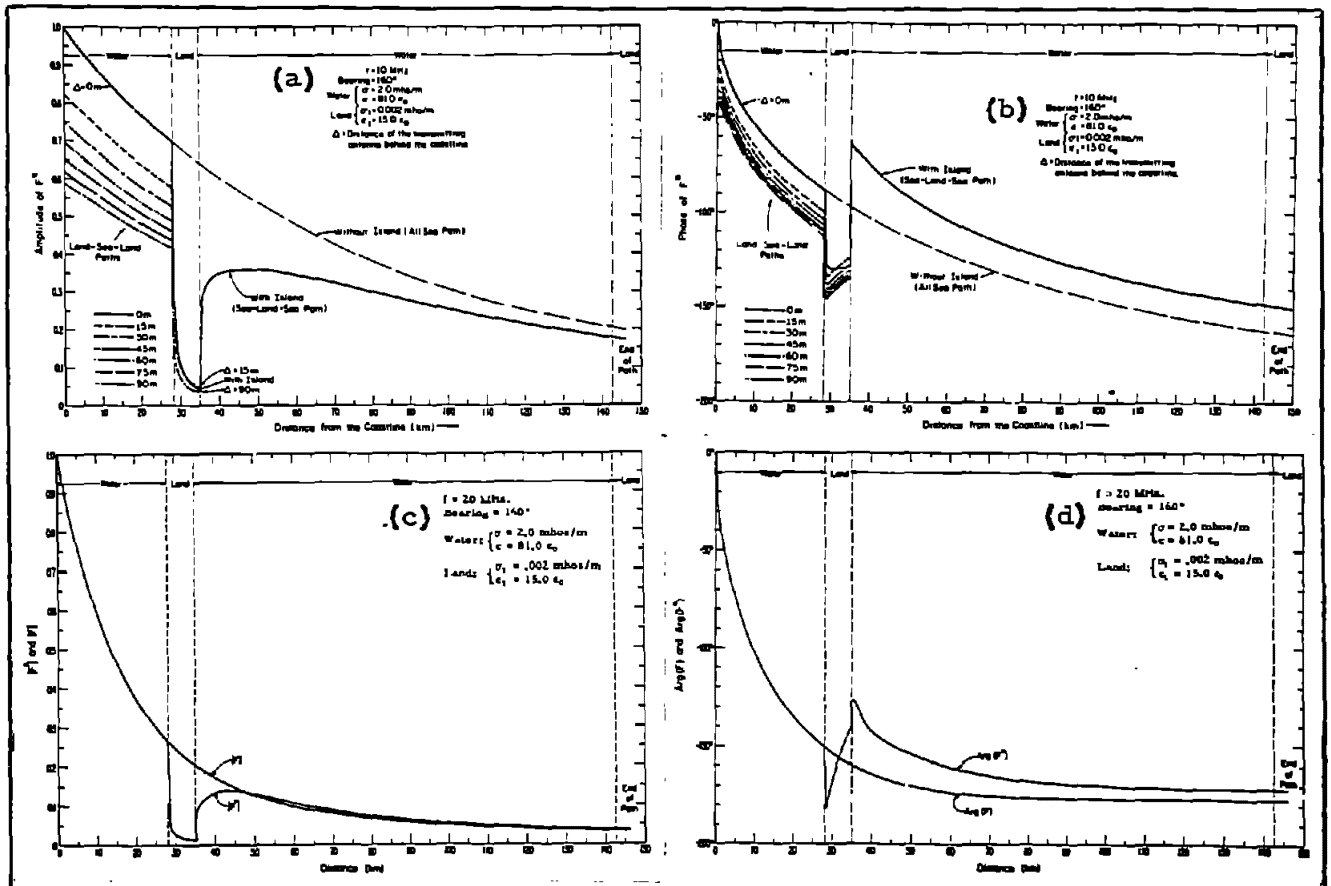

Figure 2. The frequency dependence of the attenuation function ($\Delta = 0$ m) and the effect of moving the transmitting antenna across a coastline.

"recovery" effect in the phase and amplitude immediately following the inhomogeneity. This effect was first discovered by Millington (1949 a,b) along with a fairly complete theoretical explanation of the amplitude effect. The phase effect was confirmed by Pressey et al.(1956). Elson (1949) remarks that this phenomenon is due to a vertical redistribution of energy near the boundaries between media and that it is inevitable, as the field must vary differently for different electrical parameters. Hence, the height-gain function will be different on either side of the boundaries. A rough measure of this redistribution can be seen as follows. According to Wait (1964), for low heights and sufficiently far ($>>\lambda$) from the boundaries, the height-gain function, h, has the approximate form given in figure 4. A comparison of the graphical results with the tables in figure 4 shows roughly the same trends (Rosich, 1968). This lends some support to the redistribution hypothesis.

3. Propagation Across a Coastline

At 10 MHz for the path used in figure 2, figures 2(a) and 2(b) show the effect of moving the transmitting antenna from a site over water ($\Delta = 0$ m), across a coastline, to land. The percentage changes in the amplitude and phase (relative to $\Delta = 0$) before and across the "island" of

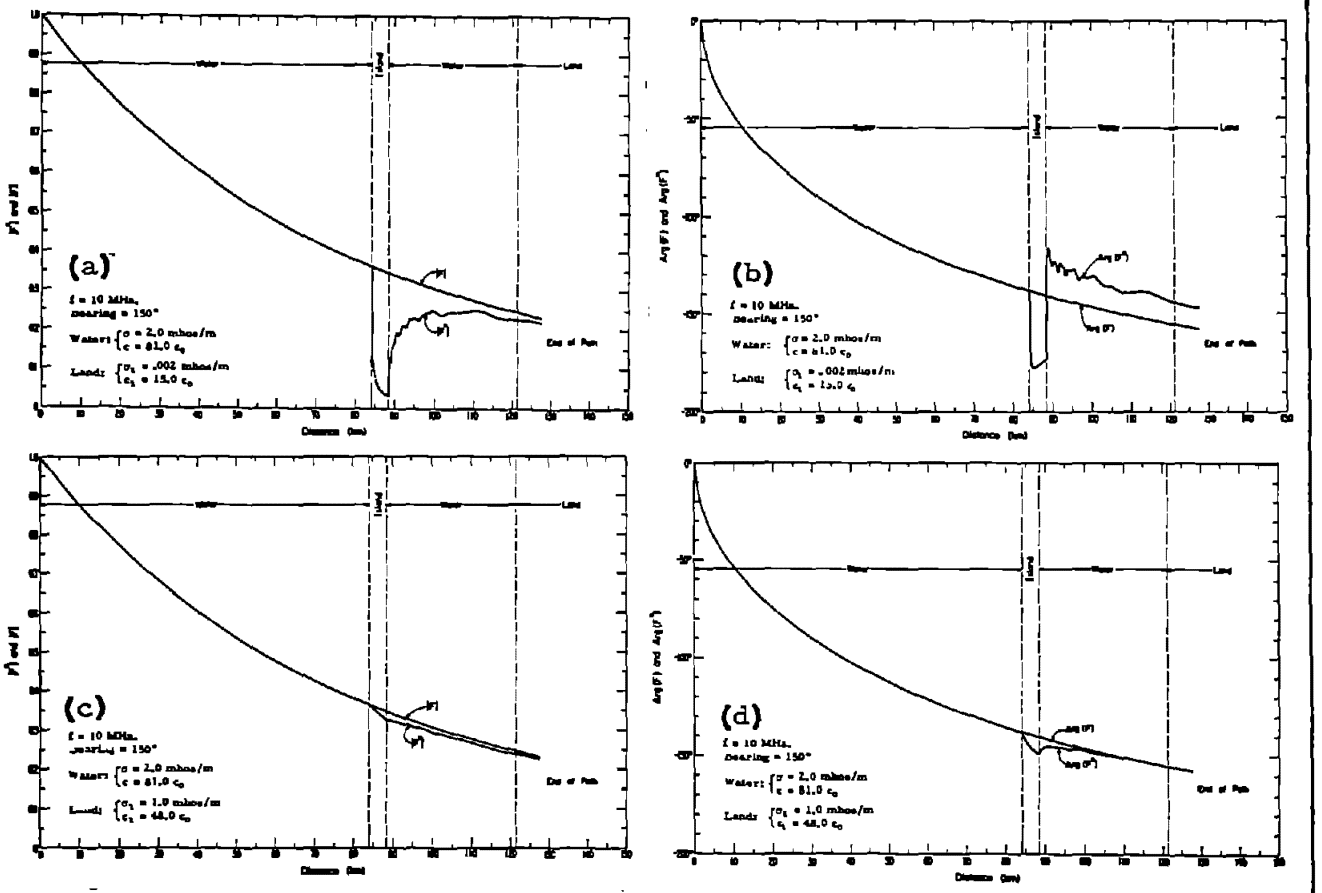

Figure 3. The dependence of the attenuation function on the electrical parameters.

inhomogeneity are shown in figure 5. The magnitudes of the changes are largest before the "island", while the percentage change is significant in both regions. For the land-sea-land paths, nothing can be said about the region following the "island", as the model only allows a three-section path. To prevent misunderstanding, a few questions should be anticipated. They are: (1) How valid are the results for $|\Delta|$ less than a few wavelengths, since the model ignores the statie and induction fields of the antennas? (2) Is the case "$\Delta = 0$" really this case, since the model ignores the land behind the coastline? In answer to (1), the results of Wait (1963) show that the results should not be altered significantly except in a region $|\Delta| << 1$ (actually a skin depth) around the coastline. The only change is the removal of a singularity (not shown in figures 2 and 3) in the field at the boundaries of the media. Thus, for

(1) $h(z) \cong 1 + ikz(Z/\eta_0)$

$Z = Re(Z) + i\,Im(Z)$

(2) $h(z) \cong (1 - kz\,Im(Z)/\eta_0) + ikz\,Re(Z)/\eta_0$

(3) *For* $|z| << 1$

$|h(z)| \cong 1 - \alpha z,$

$Arg\,(h(z)) \cong \beta z,$

where

$\alpha = k\,Im(Z)/\eta_0, \quad \beta = k\,Re(Z)/\eta_0$

(4)

FREQUENCY	ALL PATHS α	ALL PATHS β	PATHS 1 & 3 α_1	PATHS 1 & 3 β_1	PATH 2 α_1	PATH 2 β_1
10 MHz	2.4	2.5	6.3	53	3.4	3.5
15 MHz	4.5	4.6	6.4	80	6.3	6.5
20 MHz	6.8	7.1	6.4	108	9.6	10
25 MHz	9.5	10	6.5	134	13.0	14

THE VERTICAL REDISTRIBUTION OF ENERGY

Figure 4.

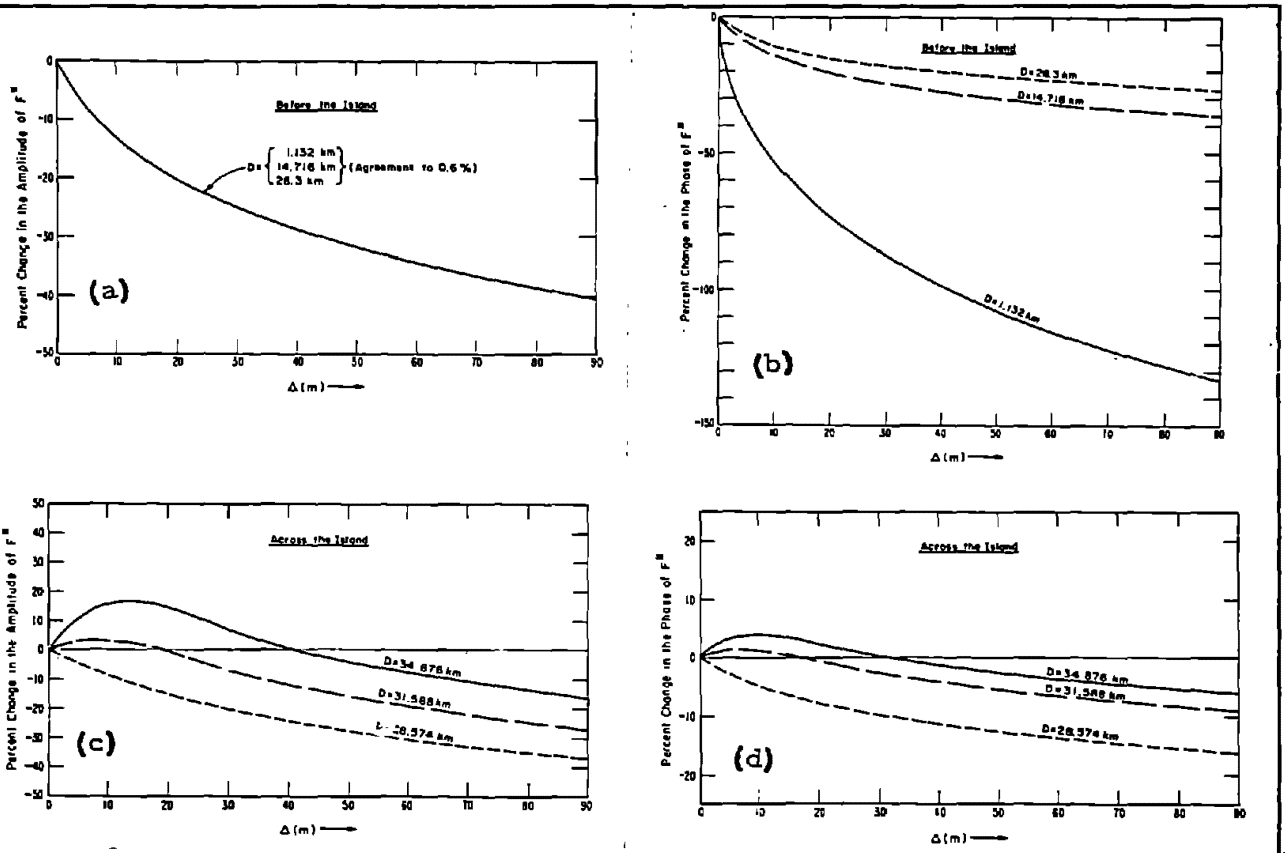

Figure 5. The percentage changes in the amplitude and phase before and across the "island" (relative to the $\Delta = 0$ values).

small values of $|\Delta|$ the results presented here are approximately correct or at least indicative of the behavior. Because of this, and the fact that the model ignores reflections from boundaries and the effect of any media not actually traversed by the wave, the case labeled "$\Delta = 0$" should be labeled "Δ slightly greater than a skin depth in front of the coastline." Since the skin depth here is between 1×10^{-5} and 1×10^{-6}m, "$\Delta = 0$" should convey the correct meaning. Also, Wait (1963) showed that the reflection effects are relatively small, thus the results are good approximations. This answers objection (2).

4. Conclusion

From these results, the utility of the model for investigating environmental effects on ground-wave propagation is clear.

5. Acknowledgments

I would like to acknowledge the invaluable advice of Messrs. J.R. Wait, A.F. Barghausen, L.A. Berry, and M.S. Lojko; also the support of the U.S. Naval Research Laboratory under Contract N00173-67-F-1503. I would also like to thank Mr. V. L. Agy for his assistance.

6. References

Elson, N. (1949), Ground-wave propagation across a land/sea boundary -- 300-m waves, Nature 164, 114-116.

Hufford, G. A. (1952), An integral equation approach to the problem of wave propagation over an irregular surface, Quart. Appl. Math. 9, 391-404.

King, R. J. (1965), Analytic and experimental studies of propagation of electromagnetic ground waves across mixed paths, Ph. D. thesis, Dept. of EE, Univ. of Colo., Boulder, Colo.

Millington, G. (1949a), Ground-wave propagation across a land/sea boundary, Nature 163, 128; 164, 114.

Millington, G. (1949b), Ground-wave propagation over an inhomogeneous smooth earth, Proc. IEE 96, Pt. 3, 53-64.

Pressey, B. G., G. E. Ashwell, and C. S. Fowler (1956), Change of phase of a low-frequency ground wave propagated across a coastline, Proc. IEE 103B, 527.

Rosich, R. K. (1968), High-frequency ground-wave attenuation over inhomogeneous paths, ESSA Tech. Memo ERLTM-ITS 137.

Wait, J. R. (1956), Mixed path ground wave propagation: 1. Short distances, NBS J. Res. 57, No. 1, 1-15.

Wait, J. R. (1963), Oblique propagation of ground waves across a coastline - Part I, NBS J. Res. 67D, No. 6, 617-624.

Wait, J. R. (1964), Electromagnetic Surface Waves, Advances in Radio Research, ed. J. A. Saxton (Academic Press, London and New York).

EFFECTIVE GROUND CONDUCTIVITY MEASUREMENTS AT RADIO FREQUENCIES USING SMALL LOOP ANTENNAS

W. L. Taylor
Institute for Telecommunication Sciences
Environmental Science Services Administration
Boulder, Colorado 80302

ABSTRACT

A new technique was developed to measure the mutual impedance of two loop antennas and was used to determine the effective conductivity of the earth's surface at frequencies of 1-3 MHz. Measurements in a four-state area revealed differences in ground conductivity exceeding 100:1.

There are several methods of determining the local RF conductivity of the ground at selected sites. These include the determination of surface impedance by measurement of the wave tilt of signals (King, 1968), the use of four-probe arrays (Wait and Conda, 1958), and the measurement of mutual impedance of two loops.

The wave tilt method is hampered by uncertainty about the effects of topography. The ground probe method is limited to sites where intimate contact between the electrodes and the earth's surface can be maintained. The two-loop mutual impedance method, free from the above limitations, requires only that the loop frame of reference must be parallel to the local site plane of the ground surface.

Earth conductivity measurements presented here were initially made to assist in the prediction of field strengths and the interpretation of data relative to MF and HF ground wave propagation.

Transmitting and receiving antennas were designed to operate between frequencies of 500 kHz and 5 MHz and at separation distances between 2 and 30 meters. The transmitting antenna was a single turn, 2.5 cm diameter tube with an overall diameter of 0.8 meters. The loop was tuned with parallel circuit condensers and adjusted to a Q of about 20. The receiving antenna was 4 turns of No. 10 insulated copper wire electrostatically shielded on a 0.7 meter square frame. Both loops were mounted such that their orientation could be readily changed for various configurations.

The only two orientations used in this work were (1) both loop planes vertical and mutually coaxial and (2) the transmitting loop axis vertical and the receiving loop axis passing through the center of the transmitting loop (perpendicular). The amplitude and phase of the receiving loop signal relative to the transmitting loop current were measured at separation distances of 5 and 10 meters for 1, 2, and 3 MHz. This gave 24 data values at each site which were ample for the present work.

Theoretical curves of the amplitude and phase of the receiver voltage relative to the transmitter current at 5 meter separation for both orientations at 1, 2, and 3 MHz are shown in the accompanying figures. Amplitude versus conductivity curves are shown in fig. 1 with the data from perpendicular and coaxial orientations at a particular site plotted on the corresponding curves. The combination data points, although plotted on the coaxial curves, represent the conductivity for which the theoretical ratio of coaxial amplitude/perpendicular amplitude was equal to the experimental ratio for each frequency. Curves of phase versus conductivity are shown in fig. 2 with data from the same site as used for the amplitude example plotted on the corresponding curves.

In this particular example, the range of conductivities extends from 4.5 to 9.0×10^{-2} with a median of 7.5×10^{-2} mhos/m. It is interesting to note that double values of conductivity are possible above certain amplitudes for the perpendicular data and above certain phase values for the coaxial data. The correct solution will, however, result in mutually consistent values of conductivity from all data of a particular site.

Conductivity was measured at 142 sites using this technique in Colorado, Wyoming, Idaho, and Washington. Individual values of measured site conductivities varied from 4×10^{-4} to 1.25×10^{-1}. Agreement was good between the median values of conductivity obtained from the loop method for large areas and the values obtained from conductivity maps of the United States based on propagation in the medium frequency broadcast band. The general agreement was excellent when median values of conductivity obtained from this method for a particular area were compared with conductivities deduced from propagation measurements from the same area.

Comparisons were made between the conductivity values from the loop induction method and the d.c. ground probe method. Agreement was very poor except for sites with very high conductivity.

Comparisons of conductivity obtained by these two methods are not expected to agree because the probe method is relevant for conductivities to great depths as a function of probe spacing, while the loop induction method indicates conductivities at depths determined by approximately the skin depth at each frequency.†

The loop induction method for determining conductivities worked well and proved to be convenient in the field. Advantages of this method include (1) the measurement of effective earth conductivity at a particular radio frequency of interest, and (2) physical contact with the ground is not required. Furthermore, the method can, in principle, be employed to measure dielectric constants (Wait, 1954).

The author is indebted to H. M. Burdick for equipment design and construction and for field operation, to R. F. May for field operation, to J. R. Johler for calculating the theoretical values of the mutual impedance of two loops above a conducting medium using the results found in Wait (1955) and Keller and Frischknecht (1966), and to D. D. Crombie and J. R. Wait for their suggestions and stimulating conversations.

Keller, G. V., and F. C. Frischknecht (1966), Electrical Methods in Geophysical Prospecting (Pergamon Press, N. Y.)

King, R. J. (1968), Crossed-dipole method of measuring wave tilt, Radio Sci. 3 (New Series), No. 4, 345-350.

Wait, J. R. (1954), Mutual coupling of loops lying on the ground, Geophys. 19, No. 2, 290-296.

Wait, J. R. (1955), Mutual electromagnetic coupling of loops over a homogeneous ground, Geophys. XX, No. 3, 630-637.

Wait, J. R., and A. M. Conda (1958), On the measurement of ground conductivity at VLF, IRE Trans. AP-6, No. 3, 273-277.

† Also, ground conductivity may itself be a strong function of frequency. (Ed.)

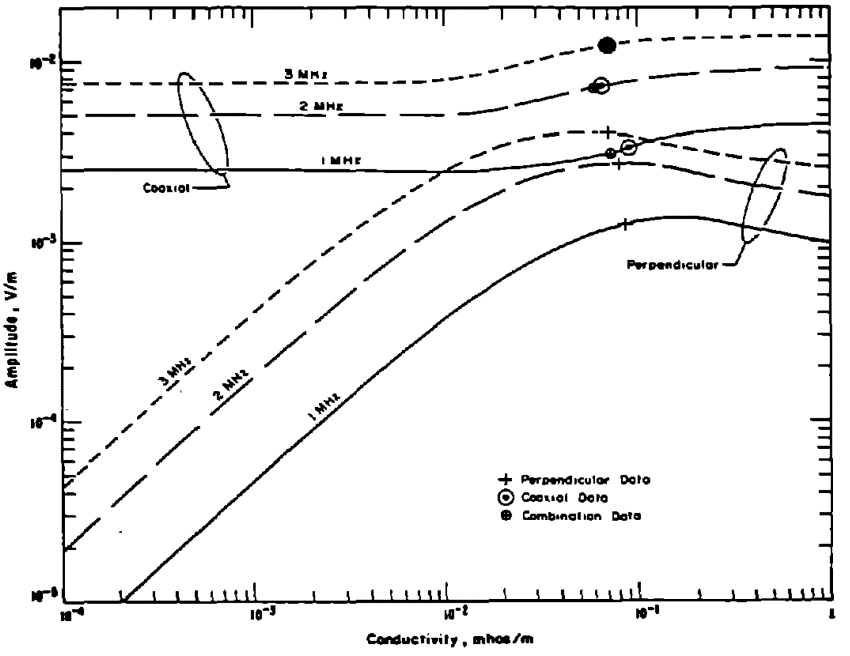

Figure 1 Amplitude versus Conductivity

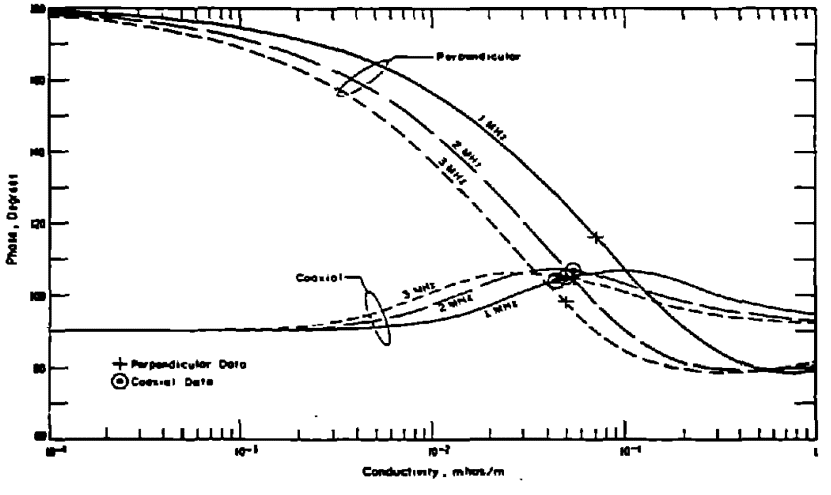

Figure 2 Phase versus Conductivity

PHASE MEASUREMENTS OF ELECTROMAGNETIC FIELD COMPONENTS

Patrick Cornille
Post Doctoral Researcher at the
University of California, Berkeley
from Lille, France

ABSTRACT

A method of phase measurement of electromagnetic field components produced by dipoles on a stratified conducting half-space is described. A symmetric process with a high frequency transmitter and two high frequency receivers is used in order to get a phase reference. This method has been applied to measure the phase of the component E_θ radiated by a horizontal electrical dipole on a stratified conducting half-space. The expression of the phase for an N-layered medium is given in the case of the quasi-static approach. A three layered model has been chosen to compute the solution in order to compare theoretical and measured results.

I. Introduction

The purpose of this paper is to describe a general method of phase measurements of electromagnetic waves in the near zone range. To measure the phase of an electromagnetic wave radiated by a dipole, we need a link between the transmitter and the receiver. A symmetric radio link has been chosen in order to avoid many technical difficulties. This method can be used for any kind of dipole over or on a layered medium and even in the case of a dipole buried in a well.

II. Description of the Process

The process uses one high frequency transmitter and two high frequency receivers (Fig. 1). The signal given by one of the high frequency receivers is amplified by a low frequency transmitter and sent in the ground. This signal is received by a low frequency receiver and amplified through one channel of a dual tuned amplifier. The signal given by the other high frequency receiver, through the other channel, gives the reference of phase for the signal picked up in the ground. The accuracy of the whole system mainly depends upon the accuracy with which the two channels are in phase.

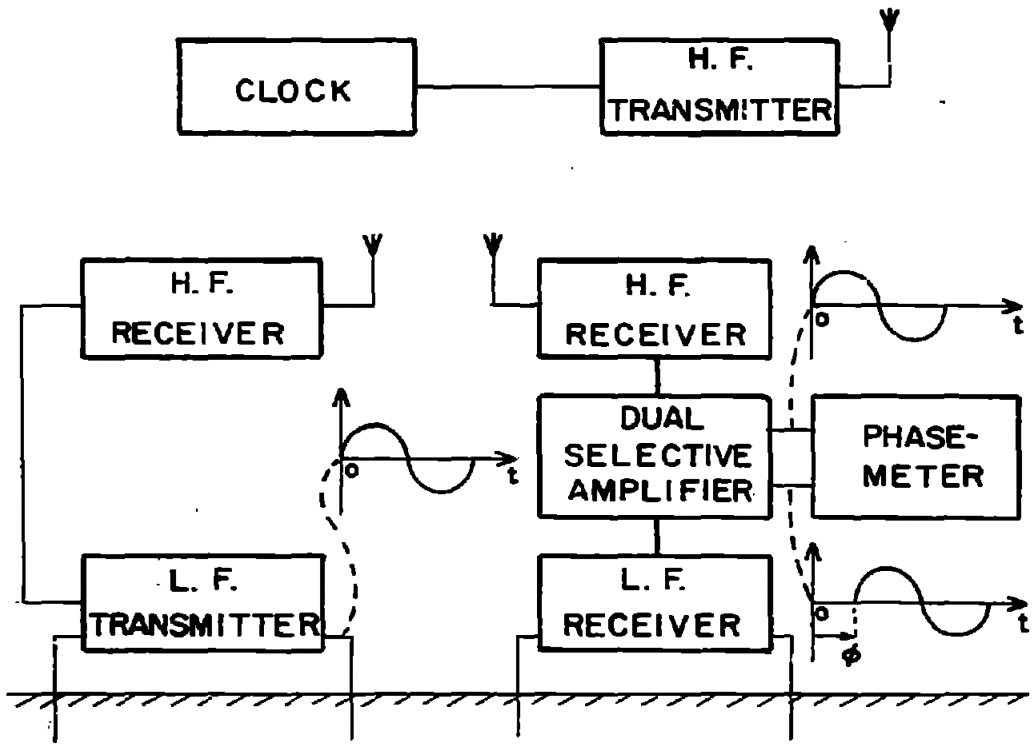

FIG. 1 PROCESS OF PHASE MEASUREMENT

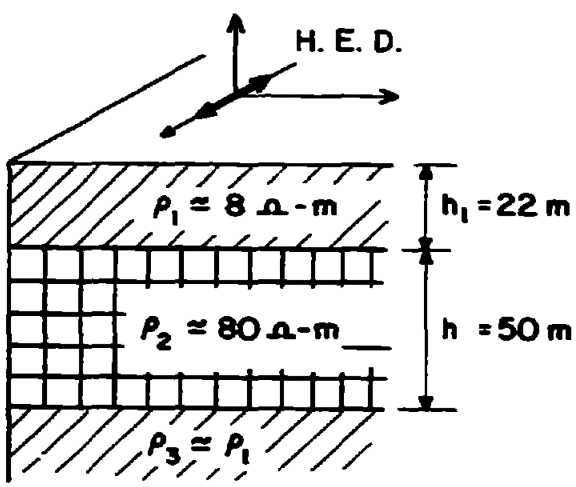

FIG. 2 THEORETICAL MODEL.

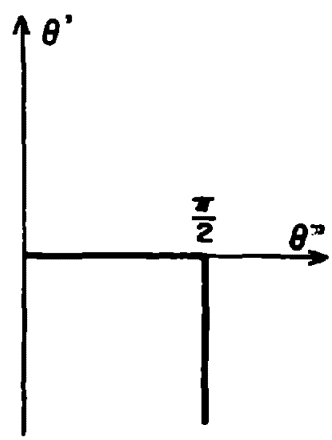

FIG. 3. λ PHASE.

III. Measurement

This process has been used with a H. E. D. to measure the phase of the electrical component E_θ. In order to compute the numerical solution, a three layered model has been chosen. The thicknesses of the first two layers have been taken on the cross section which was available (Fig. 2). Only the first two resistivities were approximately know. The resistivities of the two next layers were unknown, however these two layers were as conductive as the first one, so the same resistivity has been given to the third layer of the model. It is interesting to point out that this process has been applied to the phase measurement of the current along a long wire antenna lying on the ground. At 10 KHz for a 500 m long wire a 0.8 radian phase shift has been found at the end of the antenna.

IV. Formulation (Ref. 8)

The phase of the component E_θ of a H. E. D. can be calculated from a Hertz vector that has two components: Π_x and Π_z, which are:

$$\Pi_{xo} = p_o \left[\frac{e^{-\gamma_o R}}{R} + \int_o^\infty e^{-u_o(z+h)} R_\perp \frac{\lambda}{u_o} J_o(\lambda r)\, d\lambda \right]$$

$$\Pi_{zo} = p_o \frac{\partial}{\partial x} \int_o^\infty e^{-u_o(z+h)} \frac{R_\parallel + R_\perp}{\lambda} J_o(\lambda r)\, d\lambda$$

with

$$R_\perp = \frac{N_o - Y_1}{N_o + Y_1} \quad \text{and} \quad Y_1 = \frac{N_1}{Q_\perp^1}$$

$$R_\parallel = \frac{K_o - Z_1}{K_o + Z_1} \quad \text{and} \quad Z_1 = K_1 Q_\parallel^1$$

where the coefficients: $Q_\parallel^1$ and $Q_\perp^1$ are calculated with the recursive relations:

$$Q_\parallel^n = \frac{\gamma_n^2 u_{n+1} Q_\parallel^{n+1} + \gamma_{n+1}^2 u_n \tanh u_n h_n}{\gamma_{n+1}^2 u_n + \gamma_n^2 u_{n+1} Q_\parallel^{n+1} \tanh u_n h_n}$$

$$Q_{\perp}^{n} = \frac{u_n Q_{\perp}^{n+1} + u_{n+1} \tanh u_n h_n}{u_{n+1} + u_n Q_{\perp}^{n+1} \tanh u_n h_n}$$

For a half-space we have: $Q_{\perp}^{1} = Q_{\parallel}^{1} = 1$ and $Y_1 = N_1$ $Z_1 = K_1$. If we try to compute a half-space equivalent to the stratified medium we have: $K_e = K_1 Q_{\parallel}^{1}$ and $N_e = N_1 / Q_{\perp}^{1}$. After matching these two equations, we get:

$$\gamma_e = \frac{\gamma_1}{\sqrt{Q_{\parallel}^{1} Q_{\perp}^{1}}} \qquad (1)$$

If the coefficients $Q_{\parallel}^{1}$ and $Q_{\perp}^{1}$ do not depend upon λ, we can in the expression of the half-space set γ_e instead of γ_1 and the problem is solved. The path of integration in λ is given by Fig. 3. We can write: $\lambda = -J\gamma_o \sin\theta$, so for a real angle θ, we have:

$$\lambda = \frac{\omega}{c} \sin\theta' \quad \text{and} \quad \lambda = \frac{\omega}{c} \operatorname{ch} \theta''$$

for a complex angle.

In the quasi-static approach, we set $|\gamma_o| = \frac{\omega}{c} \sim 0$, so for a real θ, we have:

$$u_n = \sqrt{\lambda^2 + \gamma_n^2} \simeq \gamma_n$$

and, therefore,

$$Q_{\parallel}^{n} = Q_{\perp}^{n} = Q_1 = \frac{\gamma_n Q_{n+1} + \gamma_{n+1} \tanh \gamma_n h_n}{\gamma_{n+1} + \gamma_n Q_{n+1} \tanh \gamma_n h_n}$$

V. Discussion of Results (Fig. 4)

We can notice on the set of curves an important shift between the quasi-static curves and the experimental curves and the diminution of this shift with the distance 'r' and the frequency 'f'. It seems that unfortunately we cannot use the quasi-static approach for the phase in the near zone and neglect the contribution of the complex θ. This fact has been pointed out by Wait in a paper (7). In order to show this effect, the phase has been calculated in the case of an equivalent half-space with the formula (1) with λ as a constant decreasing with 'r'.

At last we get the third set of curves with the numerical solution computed without approximation.

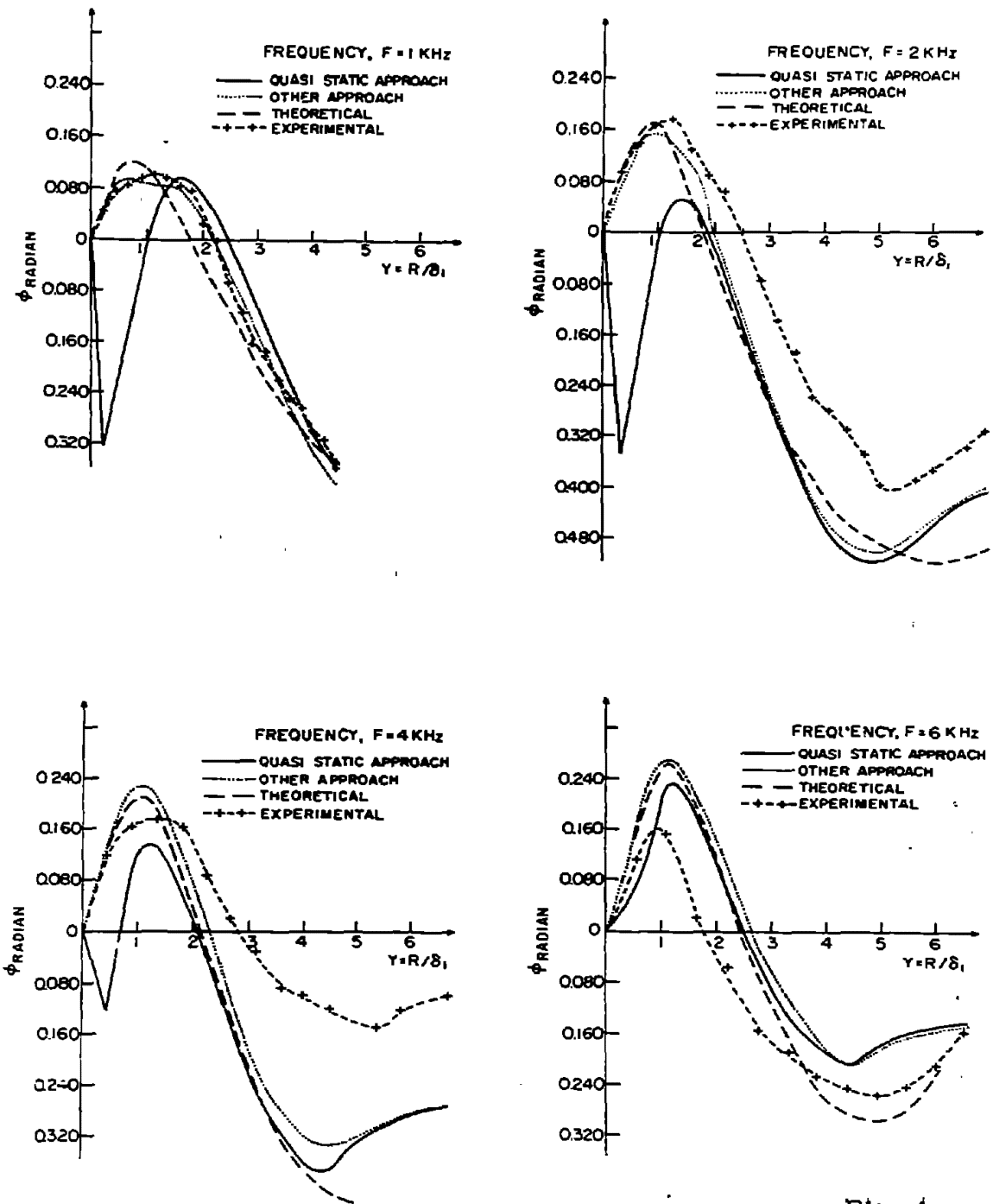
FREQUENCY, F = 1 KHz
QUASI STATIC APPROACH
OTHER APPROACH
THEORETICAL
EXPERIMENTAL
φ RADIAN
Y = R/δ1
FREQUENCY, F = 2 KHz
FREQUENCY, F = 4 KHz
FREQUENCY, F = 6 KHz

Fig. 4

VI. Acknowledgment

The experimental measurements of this work have been performed at the University of Lille, France, in the geophysical department directed by Professor Gabillard, and the theoretical research has been continued at Berkeley with a postdoctoral fellowship awarded by the research agency of the French Government (D. G. R. S. T.).

The author wishes to thank Professor S. H. Ward for accepting him as a postdoctoral researcher at Berkeley and Professor H. F. Morrison for reading and commenting on the manuscript. He is also thankful to the Computer Center of Berkeley for providing him free computer time.

VII. References

1. Baños, A., Dipole radiation in the presence of a conducting half-space, Pergamon Press, 1966.

2. Brekhovskikh, L. M., Waves in layered media, Academic Press, 1960.

3. Cornille, P., Sur une methode de mesure du dephasage d'une onde de surface se propageant le long d'un demi-milieu conducteur stratifie. Ph. D. Thesis, University of Lille, France, 1968.

4. S.E.G., Mining Geophysics, Vol. 2, Theory. Society of Exploration Geophysicists, 1967.

5. Wait, J.R., The electromagnetic fields of a horizontal dipole in the presence of a conducting half-space, Can. J. Phys. vol. 39, p. 1017-1028, 1961.

6. Wait, J.R., Electromagnetic waves in stratified media, Pergamon Press, 1962.

7. Wait, J. R., Theory of magneto-telluric fields, J. Res. NBS 66D, No. 5, 526, 1962.

8. Wait, J.R., Fields of a horizontal dipole over a stratified anisotropic half-space, IEEE Trans. vol. AP-14, No. 6, p. 790-792, 1966.

9. Watt, A.D., V.L.F. radio engineering, Pergamon Press, 1967.

RADIAL WIRE GROUND SYSTEMS FOR VERTICAL MONOPOLE ANTENNAS

S.W. Maley
University of Colorado

ABSTRACT

A vertical monopole antenna above the surface of the earth has an efficiency dependent upon the characteristics of the ground system extending out from the base of the antenna on the surface of the ground. The effects of a simple radial wire ground system on the efficiency are well understood. These effects are reviewed; also observations have been made on the possible effects of other more sophisticated ground systems.

The base impedance of a vertical monopole antenna over an imperfectly-conducting ground is given by (Wait, Pope, 1954)

$$Z = Z^{\infty} - \frac{2\pi}{I_o^2} \int_o^{\infty} H_{\phi}^{\infty}(r,o) E_r(r,o) r dr \qquad (1)$$

where Z^{∞} and $H_{\phi}^{\infty}(r,o)$ are the base impedance and magnetic field that would exist for an antenna base current I_o if the ground were perfectly conducting. $E_r(r,o)$ is the tangential electric field for the actual imperfectly conducting ground for the same antenna base current. The time dependence is $\exp(i\omega t)$ where ω is the angular frequency and $i = (-1)^{\frac{1}{2}}$. It is assumed the ground can be characterized by a surface impedance η where $E_r(r,o) = -\eta H_{\phi}(r,o) \cong -\eta H_{\phi}^{\infty}(r,o)$ and that a ground system extends from r=a out to r=b as shown in Fig. 1 then (1) can be written (Maley, King, 1964)

$$Z = Z^{\infty} + \frac{2\pi}{I_o^2} \int_a^b \eta_e \left[H_{\phi}^{\infty}(r,o)\right]^2 r dr + \frac{2\pi}{I_o^2} \int_b^{\infty} \eta_g \left[H_{\phi}^{\infty}(r,o)\right]^2 r dr \qquad (2)$$

where η_e is the surface impedance of the ground for grazing incidence with the ground system in place; it is normally a function of r. η_g is the surface impedance, for grazing incidence, of the ground without the ground system in place; it is given by

$$\eta_g = \left(\frac{i\mu_2\omega}{\sigma_2 + i\omega\varepsilon_2}\right)^{\frac{1}{2}} \left(1 - \frac{\gamma_0^2}{\gamma_2^2}\right)^{\frac{1}{2}} \cong \left(\frac{i\mu_2\omega}{\sigma_2 + i\omega\varepsilon_2}\right)^{\frac{1}{2}}$$

where γ_0 and γ_2 are the propagation constants for plane waves above and below the ground, respectively. They are given by $\gamma_0^2 = -\omega^2\mu_0\epsilon_0$ and $\gamma_2^2 = -\omega^2\mu_2\epsilon_2 + i\omega\mu_2\sigma_2$. η_e is the parallel combination of impedances consisting of η_g and η_w. η_w is the impedance of a wire grid in free space; it is given by (Wait, Pope, 1954)

$$\eta_w = \frac{i2\pi\eta_o r}{\lambda N} \log_e \frac{r}{Nc} \qquad (3)$$

where λ is the free space wave length, N is the number of radial wires, and c is the radius of the wires. The magnetic field, $H_\phi^\infty(r,o)$, for the case of a perfectly-conducting ground is well known for a sinusoidal distribution of current on the antenna (Wait, 1959); so calculations may be made from (2) for a variety of ground systems (Maley, King, Branch, 1963).

If the ground system extending from a radius of "a" out to a radius of b is a perfectly conducting disc, then $\eta_e = 0$ and (2) may be used to calculate $Z - Z^\infty = \Delta Z = \Delta R + i\Delta X$. Typical values for a quarter wave monopole with a sinusoidal current distribution are shown in Fig. 2. This figure shows ΔR is minimum for about one quarter-wave length disc radius. This is the value that would result in maximum antenna system efficiency for a disc type of ground system. For the case of a radial wire ground system, calculations may be made from (2) and (3); the results for a typical case are shown in Fig. 3 for the resistive component ΔR only. ΔR for the case of a perfectly-conducting disc (ref. Fig. 2) is also shown in Fig. 3 for comparison. It is apparent that the radial wire ground system has an effect similar to that of the radial disc, but the effect is not quite as great. If the number of wires, N, were increased without limit the curve in Fig. 3 for the radial wire ground system would approach the curve for the radial disc ground system.

In order to investigate the possibility of designing a ground system better than the radial wire ground system, it is convenient to put (2) into a slightly different form. It may be recalled that wave tilt, W is related to surface impedance. It is given by

$$W = \frac{E_r(r,o)}{E_z(r,o)}$$

where $E_z(r,o)$ is the vertical component of the electric field at the surface on the ground. The wave tilt in terms of the parameters of the earth is (Wait, 1962)

$$W = \frac{\eta_2}{\eta_0}\left(1 - \frac{\gamma_0^2}{\gamma_2^2}\right)^{\frac{1}{2}}$$

where η_2 and η_0 are the intrinsic impedance of the earth and of free-space given by

$$\eta_2 = \left(\frac{i\mu_2\omega}{\sigma_2 + i\omega\varepsilon_2}\right)^{\frac{1}{2}} \text{ and } \quad \eta_0 = \left(\frac{i\mu_0\omega}{i\omega\varepsilon_0}\right)^{\frac{1}{2}} = \left(\frac{\mu_o}{\varepsilon_o}\right)^{\frac{1}{2}}$$

Using this it is easily seen that for the case of a homogeneous earth the wave tilt can be written $W_g = \frac{\eta_g}{\eta_0}$. It is reasonable to assume that a similar relationship is valid when a ground system is in place; thus in the presence of a ground system with effective surface impedance, η the wave tilt may be written $W = \frac{\eta}{\eta_0}$

then (3) may be written

$$Z = Z^{\infty} + \frac{2\pi\eta_0}{I_0^2}\int_a^b W_e\left[H_\phi^{\infty}(r,o)\right]^2 r\,dr + \frac{2\pi\eta_0}{I_0^2}\int_b^{\infty} W_g\left[H_\phi^{\infty}(r,o)\right]^2 r\,dr \quad (4)$$

Considering the various possible ground systems it may be said that the wave tilt W_e will be maximum if there is no ground system at all. It will be less for a radial wire ground system and will result in better antenna system efficiency (for radii in the vicinity of $\lambda/4$ or less). A radial disc ground system will have a wave tilt of zero over the disc and will result in still higher efficiency. In general the less the wave tilt the higher the efficiency.

A question that naturally arises concerns the possibility of a "negative" wave tilt; (since wave tilt is a complex quantity as defined above, a "negative" wave tilt will be interpreted to mean it has a negative real part.) if such a possibility exists then the sign of the integral from a to b would change and ΔR would decrease (algebraically) making antenna system efficiency higher than for a perfectly conducting disc ground system. A ground system that causes a negative wave tilt may therefore be superior to a perfectly conducting disc. The practicability of constructing such a system is debatable. One may consider a ground system which is perfectly conducting but which is a fast wave structure on which the phase velocity of the radial current is higher than the phase velocity of the waves above the ground. Such a system

apparently would have a negative wave tilt and would improve efficiency as mentioned above. As an example, if the wave tilt were made the negative of that for the radial wire ground system of Fig. 3, the incremental resistance would be as noted for the curve labeled fast wave system in Fig. 3. It may be possible to approximate such a system by using a radial array of conductors each of which is a fast wave structure itself. Such a structure would resemble a radial wire system but fast wave structures would be used in place of the wires.

REFERENCES

Wait, J.R. and W.A. Pope (1954), The characteristics of a vertical antenna with a radial wire ground system, App. Sci. Res., B4, 177-195.

Maley, S.W. and R.J. King (1964), Impedance of a monopole antenna with a radial-wire ground system on an imperfectly conducting half-space, part II, Radio Sci., 68D, no. 2, 157-163; part III, Radio Sci., 68D, no. 3, 297-301.

Maley, S.W., R.J. King, L.R. Branch (1963), Theoretical calculations of the impedance of a monopole antenna with a radial-wire ground system on an imperfectly conducting half-space, Scientific Report No. 26, Contract AFCRL-65-583.

Maley, S.W., R.J. King (1962), The characteristics of a monopole antenna with a radial wire ground system on an imperfectly conducting half-space, part I, Radio Sci. 66D, no. 2, 175-180.

Wait, J.R. (1962), Electromagnetic waves in stratified media, (Pergamon Press, New York, London). [Revised and enlarged edition, 1969].

Wait, J.R. (1959), Electromagnetic radiation from cylindrical structures (Pergamon Press, New York).

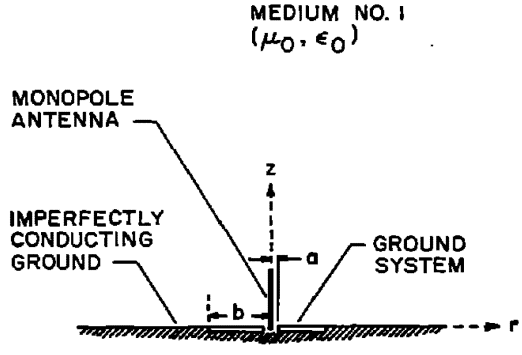

Figure 1 MONOPOLE ANTENNA SYSTEM

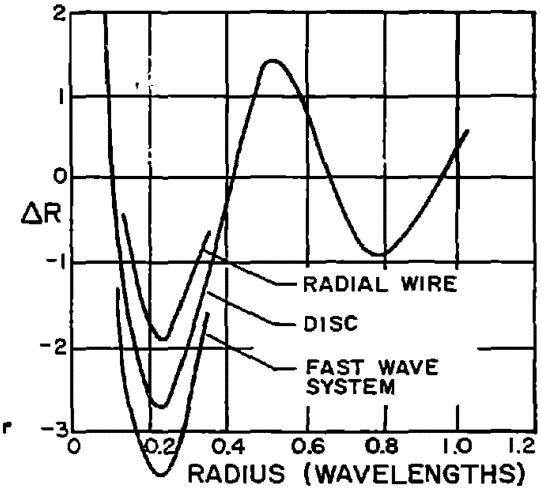

Figure 3 INCREMENTAL RESISTANCE

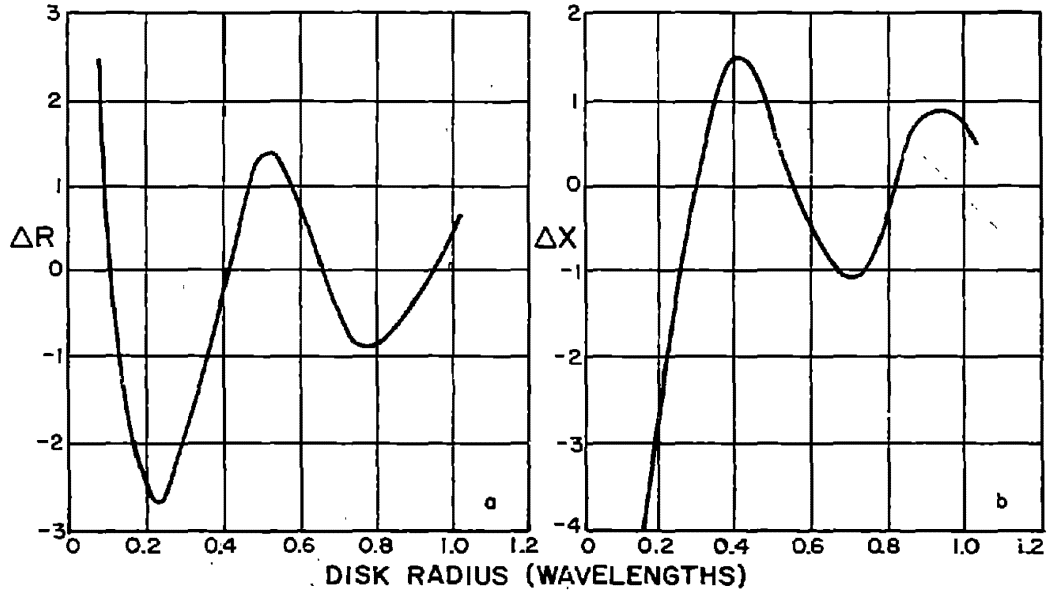

Figure 2 INCREMENTAL IMPEDANCE

SOME DESIGN CONSIDERATIONS FOR HF ANTENNA GROUND SCREENS

T. Kallszewski

General Electric Company, Syracuse, N.Y. 13201

ABSTRACT

The principle reasons for the deployment of large ground screens with high frequency antennas and some factors affecting their design are discussed. To demonstrate the combined effect of a coplanar screen-ground system the results based on the Compensation Theorem are used to compute the input resistance and the low angle radiation field for an elevated, vertically polarized Hertzian dipole. Samples of the design curves, permitting the tradeoff between the parameters of the screen and the radiated power, are presented for a set of typical ground constants. Some further problems of interest to the design optimization are identified.

1. General Remarks

Among the many factors affecting the choice and siting of large, high frequency antennas, those arising from the interaction of the radiation with the ground are of considerable importance. The input impedance of the antenna and its radiation field are critically affected by the electrical properties of the surroundings, especially in the case of vertical polarization. The properties of the ground affect also the performance of direction finding systems by introducing a siting error which, as a rule, is difficult to isolate and to estimate. Antennas must frequently be erected on sites with poor electrical and topographical features; they may also be subjected to severe climatic changes.

To insure a satisfactory performance of the antenna in such circumstances, ground screens of finite size are used. For fixed, single-element antennas the screens may consist of radial wires of adequate spacing. A square mesh is used whenever multielement structures are employed or where the phase center of the antenna varies in position with frequency. Such "imperfect" screens are effective in reducing the variable and deleterious effects of the ground and in bringing the performance of the antenna closer to the level associated with an "ideal" site.

The deployment of the ground screens is decisively affected by their enormous cost. To arrive at an economically admissible configuration some sort of tradeoff analysis must be performed. Such an analysis is currently possible for a constrained problem posed by a Hertzian dipole which is elevated above a two-component ground system. The analysis is based on the Compensation Theorem and is, in general, susceptible to further modifications.

2. The Compensation Theorem

The basis for our tradeoff analysis is the Compensation Theorem which states the following (Monteath, 1951):

$$Z'_{ab} - Z_{ab} = \left[\frac{1}{I_o^2}\right] \iint_S (\eta' - \eta)\, \bar{H}_{at} \cdot \bar{H}'_{bt}\, dS \qquad (1)$$

Here, Z_{ab}, Z'_{ab} are mutual impedances between a source dipole a and a reference b, the latter placed in the far field of a. The integration is over S, the ground surface over which the fields $\bar{H}_{at}$ and $\bar{H}'_{bt}$ are not negligible. The surface is characterized by the impedances η and η', and I_o is the dipole current.

In the application of this theorem it can be usually assumed that the unprimed quantities are known; for example, when the surface is homogeneous and, perhaps, perfectly conducting. The field $\bar{H}'_{at}$ is, however, never known a priori. A reasonable practice is to assume that the modified and unmodified fields are nearly identical. A further condition for its use pertains to the validity of the concept of surface impedance. The adequacy of that characterization usually can be tested by examining the propagation constant of the medium and the rate at which the fields change over the surface (Godzinski, 1961).

For the purposes of computing changes in the dipole's input impedance equation (1) can be reduced to

$$\Delta Z \approx \left[\frac{1}{I_o^2}\right] \iint_S \eta' \, (\bar{H}_{at})^2\, dS \qquad (2)$$

where use also has been made of the usual assumption that $\eta = 0$ (perfectly conducting reference surface).

To compute the modified far field of the dipole we note that it can be related to the unmodified field as follows

$$E'_v = E_v \left[\frac{Z'_{ab}}{Z_{ab}} \right] \tag{3}$$

The evaluation of this relation is, however, no simple matter and even for a constrained problem as discussed here requires a numerical computer solution.

3. The Effect of Finite Screen on Input Impedance

To calculate the change in the dipole's input impedance we use equation (2) and reduce it further to take advantage of the polar symmetry and of the assumption that η' = constant.

$$\Delta Z \approx \left[\frac{1}{I_o^2} \right] \eta' \int_{r=b}^{\infty} [H_\phi^\infty(r,0)]^2 \, 2\pi r \, dr \tag{4}$$

For a Hertzian dipole, $H_\phi^\infty(r, 0)$ has the following form

$$H_\phi^\infty(r, 0) = \frac{jk(I_o \ell)}{2\pi R} \left[R^2 - h^2 \right]^{1/2} \left[1 + \frac{1}{jkR} \right] e^{-jkR} \tag{5}$$

where the meaning of the variables is that shown in figure 1 and $k = 2\pi/\lambda$; $(I_o \ell)$ is a dipole moment.

The integration of equation (5) yields the following result (Monteath, 1951).

$$\Delta Z \approx \frac{\eta' k^2 \ell^2}{2\pi} \left[\frac{j}{kr_o} \left[1 - \frac{j}{2kr_o} \right] \left[1 - \frac{h^2}{2r_o^2} \right] e^{-j2kr_o} - Ei(-j2kr_o) \right] \tag{6}$$

Here r_o = hcsc Θ and Ei (-jx) is an exponential integral.

We have applied the above result to the case of an 80-ohm (free space) dipole elevated to a height of a quarter wavelength. A real part of ΔZ has been computed and is shown in figure 2. The two grounds, termed "good" and poor," are characterized by the following constants.

Poor: $\epsilon = 4.0$, $\sigma = 0.001$ mhos/meter
Good: $\epsilon = 10.0$, $\sigma = 0.01$ mhos/meter

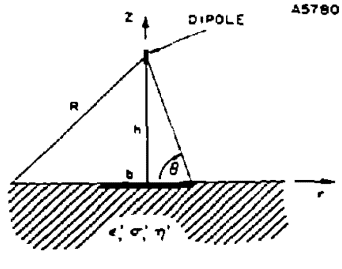

Figure 1

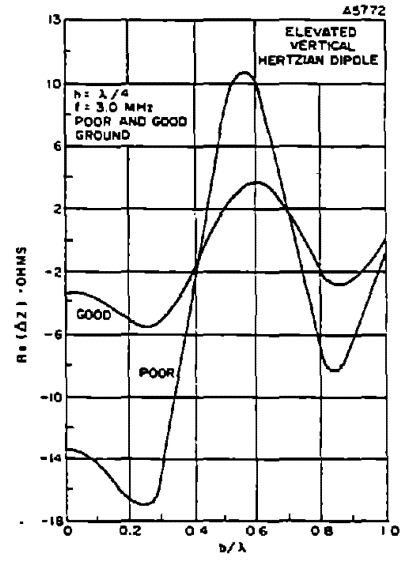

Figure 2

To compute the total input resistance of the dipole we note that the above change must be added to the resistance which the dipole has at the same height over a perfect ground,

$$\mathrm{Re}\ (Z) = \mathrm{Re}\ (Z^{\infty}) + \mathrm{Re}\ (\Delta Z) \tag{7}$$

We may note also, in passing, that the value of Re (Z^{∞}) at the height considered here is about 100 ohms.

4. The Effects of Finite Screens on a Low Angle Radiation Field

The basis for our demonstration of the effects of a finite, imperfect screen on the low angle radiation field of the probe dipole is certain results of Wait (1967), based on the Compensation Theorem and subject to the usual limitations involved in its use. In addition, the results are obtained for a constant impedance screen. This implies the use of either radial or parallel wires located upon the ground or buried within. Furthermore, the flat earth approximation restricts the validity of the results to elevation angles greater than about 2°. Within these limitations, the radiation field can be written

$$E_v \approx \frac{i\mu_o \omega_o (I_o \ell)}{2\pi R} e^{-ikR} \cos^2 \psi_o\, W' \tag{8}$$

where W' is, in general, a rather complicated function of the surface impedances of the screen and the ground, of dipole height, and of the position of the observation point. For a perfect ground W' reduces to

$$W'_{\infty} = \cos\ (kh \sin \psi_o) \tag{9}$$

and is equally simple for a homogeneous, unscreened ground,

$$W'_o = \frac{1}{2}\left[e^{ikh \sin \psi_o} + R_v\, e^{-ikh \sin \psi_o}\right] \tag{10}$$

where R_v is the Fresnel reflection coefficient. Obviously, the latter case corresponds to the usual "space" field of the dipole.

What is computed in the following is the radiated power relative to that which would prevail if the ground was perfectly conducting and infinite in extent; i.e.,

$$\text{Power loss} = 20 \log_{10} \frac{W'}{W'_{\infty}}\ (\mathrm{dB}) \tag{11}$$

The impedances are calculated as follows (Wait, 1959)

$$\eta' \approx \frac{\eta \cdot Z_g}{\eta + Z_g} \tag{12}$$

where

$$Z_g \approx \frac{i\mu_o}{\lambda} d \log_e \frac{d}{2\pi a} \tag{13}$$

and

$$\eta \approx \left[\frac{\mu_o}{\epsilon + \frac{\sigma}{i\omega}}\right]^{1/2} \tag{14}$$

where d = spacing of the wires, a = radius of the wires, ϵ' = relative dielectric constant, and σ = conductivity (mhos/meter).

The computations are for the parameters as shown in figures 3 through 6. Figures 3 and 4 demonstrate the effect of screen length; the effect of screen impedance (i.e., wire spacing) is shown in figure 5, and finally, the effect of ground parameters is shown in figure 6.

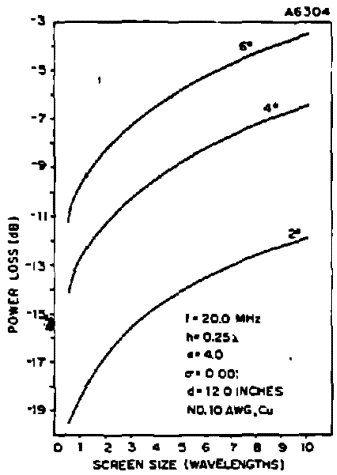

Figure 3

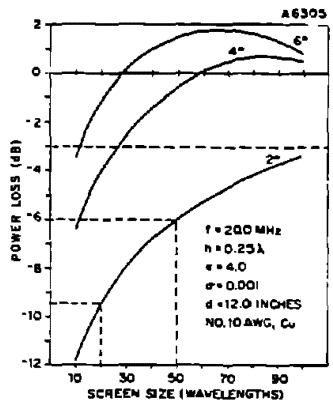

Figure 4

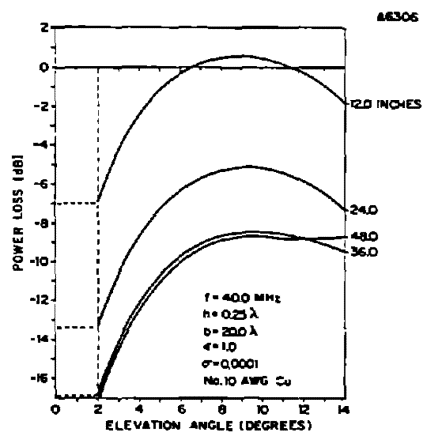

Figure 5

	A	B	C	D	E
ε	20	4	7	8	3
σ	0.1	0.01	0.001	0.0001	0.00001

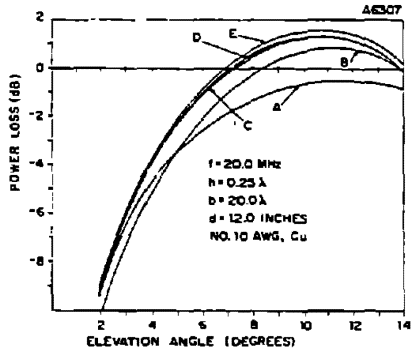

Figure 6

5. Concluding Remarks

The results presented here provide a reasonable guidance in matters pertaining to the economical design of the ground screens. Thus, given a set of ground parameters, antenna height, frequency, and a specified level of radiation field, it is possible to arrive at the basic screen design parameters, that is, its length and wire spacing. Usually, these two parameters are calculated at the lowest and highest operating frequencies, respectively.

It should be noted that the present results have been obtained for a constrained problem and extrapolations to more complex cases should not be attempted without further justification. This applies especially to screens which may present a variable surface impedance to the incident radiation (examples: elevated parallel or radial wires, wire mesh). The approach exploited here is capable of accommodating the case of a generalized screen impedance (Wait, 1967). It is also possible to extend the analysis to a multicomponent ground system such as represented by a screen, beach and sea combination (Andersen, 1963 Christiansen and Larsen, 1967). Problems connected with snow accumulation, ice coating, or vegetation appear also to be susceptible to solution; however, the Compensation Theorem does not appear to present a suitable framework for consideration of problems involving nonplanar or rough grounds.

The author would like to thank Mr. A. Waldman of the Mitre Corp. for valuable cooperation and Mr. G.R. Nelson of the General Electric Co. for permission to present this paper.

6. References

Monteath, G.D. (1951), Application of the Compensation Theorem to certain radiation and propagation problems, Proc. IEE (London), 98C, 23-30.

Godzinski, Z. (1961), The surface impedance concept and the structure of radio waves over real earth, Proc. IEE (London), 108C, 362-373.

Wait, J.R. (1959), On the theory of reflection from a wire grid parallel to an interface between homogeneous media, Part II, Appl. Sci. Research [B], 7, 355-360.

Wait, J.R. (1967), On the theory of radiation from a raised electric dipole over an inhomogeneous ground plane, Radio Science, Vol. 2, (New Series), No. 9, 997-1004.

Wait, J.R. (1967), Pattern of a linear antenna erected over a tapered ground screen, Can. J. Phys. 45, 3091-3101.

Andersen, J.B. (1963), The radiation field from a vertical dipole on an inhomogeneous ground, Electromagnetic Theory and Antennas, 1099-1112, (Pergamon Press, New York, N.Y.).

Christiansen, Soren, and Tove Larsen (1967), Numerical application of the Compensation Theorem to mixed path propagation problem, Radio Science, Vol. 2, (New Series), No. 12, 1471-1480.

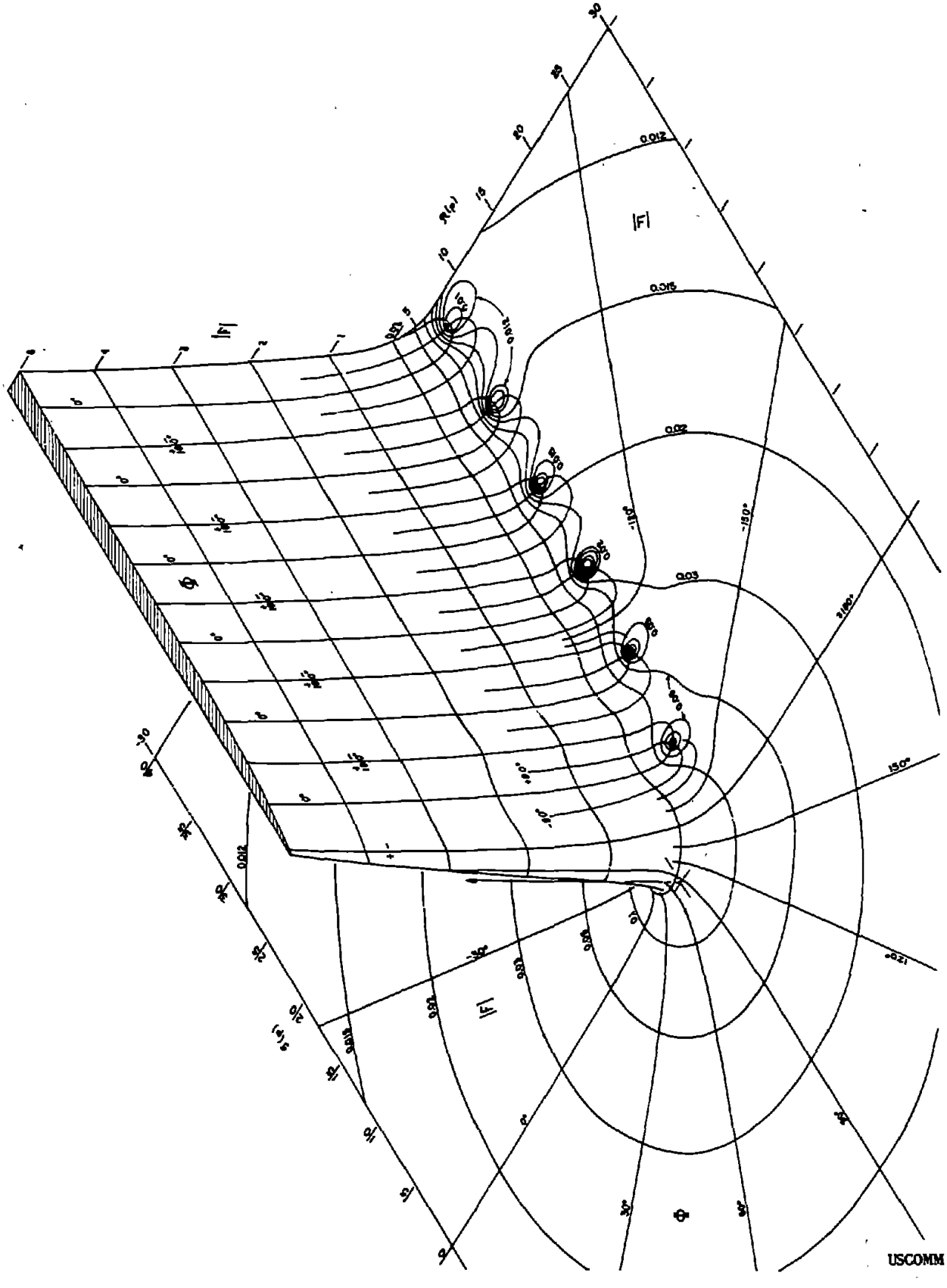
|F|
0.012
0.015
0.02
0.03
USCOMM - ERL